

Steel Centre Engineering Report No. 031 | February 2025

ALTERNATIVE DESIGN OF COLUMN WEB DOUBLER PLATES IN STEEL PIPE RACK MODULES

Hana Chaya

Ali Sadrara

Ali Imanpour

Robert G. Driver

Brett Morgan









Alternative Design of Column Web Doubler Plates in Steel Pipe Rack Modules

by

Hana Chaya

Ali Sadrara

Ali Imanpour

Robert G. Driver

Brett Morgan

Ryan Schram

Steel Centre Engineering Report No. 031

Department of Civil and Environmental Engineering
University of Alberta
Edmonton, Alberta, Canada

February 2025





ABSTRACT

Pipe rack modules are non-building structures used mostly in refineries, chemical plants, and oil sands facilities. They often consist of steel braced frames in the direction of pipes and steel moment-resisting frames in the perpendicular direction. Moment frames are designed to resist a variety of loads, which often makes their connections complex and expensive. Doubler plates are often required the in beam-to-column connection panel zone. A groove weld is typically used to weld the doubler plate to the column web. Groove welds are known to be more complex, expensive, and take more time than fillet welds.

This report proposes a new doubler plate detail involving a reduced-size plate welded to the column web, for beam-to-column moment connections in pipe rack modules, and presents a new design method to size such doubler plates under shear induced in the column panel zone. To investigate the effect of reducing the doubler plate and using fillet welds in pipe rack module connections, a full-scale experimental test setup was developed. The experimental study consisted of twelve moment connections, where each six specimens represented a different beam-to-column W-section. Six used W250×58 beams and columns and the rest used W410×60 columns and W410×100 beams. The proposed detail consisted of a reduced doubler plate fillet-welded to the column web in the panel zone area of the connection instead of a doubler plate that is groove welded. The tests showed that a reduced-size doubler plate with a fillet weld could be used in pipe rack module connections, but with certain thresholds in place. A new design method was developed to size doubler plate dimensions taking into account potential limit states and limiting shear deformation in the panel zone beyond yielding. The proposed method was validated based on the experimental results and demonstrated using two beam-to-column moment connection





examples. Furthermore, the corroborated finite element models of the connections were used to further validate the proposed method for special loading cases.

ACKNOWLEDGEMENTS

This research is funded by the Natural Sciences and Engineering Research Council (NSERC) of Canada, WF Steel and Crane Ltd., and the CISC Centre for Steel Structures Education and Research (the Steel Centre) at the University of Alberta. The first author would also like to thank NSERC for the opportunity to get a head start on this research topic through an Undergraduate Student Research Award. Lastly, the first author thanks Brian Gerbrandt Memorial and the Canadian Welding Bureau for their scholarships.

Thank you to Greg Miller and Cameron West because their guidance in the laboratory led to the success of the testing program. The discussions and constructive feedback from professors and students of the Steel Centre are also greatly appreciated.

The steel material for this project was donated by WF Steel and Crane, a Steel Centre member.





Table of Contents

A	BSTR	ACT		ii
A	CKNO	WLI	EDGEMENTS	iii
1	INT	roi	DUCTION	1
	1.1	Bac	ekground	1
	1.2	Sta	tement of Research Problem	3
	1.3	Ob	jectives	3
	1.4	Res	search Methodology	4
	1.5	Org	ganization of Report	4
2	LIT	ERA	ATURE REVIEW	5
	2.1	Des	sign of Modular Pipe Rack Systems	5
	2.2	Alt	ernative Doubler Plate Details	8
	2.2.	1	Shirsat (2011)	8
	2.2.	2	Ciutina and Dubina (2008)	9
	2.2.	3	Lee et al. (2005)	12
	2.2.	4	Reynolds and Uang (2019)	13
	2.3	Par	nel Zone Shear Deformation	14
	2.3.	1	Krawinkler (1978)	14
	2.3.	2	Skiadopoulos et al. (2021)	17
	2.4	Sur	nmary	21
3	MC	DUI	LE BEAM-TO-COLUMN CONNECTION DESIGN	22
	3.1	Gei	neral	22
	3.2	Co	nnection Design in accordance with Current Practice	23
4	TES	ST S	PECIMENS AND SETUP	33
	4.1	Pro	posed Detail	33
	4.2	Tes	st Specimens	33
	4.3	Tes	st Specimen Design	40
	4.4	Tes	st Setup	41
	4.4.	1	Column Boundary Conditions	42
	4.4.	2	Lateral Bracing System	47
	4.4.	3	Loading	50





	4.5	Insti	rumentation	52
	4.6	Anc	illary Tests	58
	4.6.	1	Mechanical Properties	58
	4.6.2	2	Residual Stress Measurement	62
5	EXF	PERI	MENTAL BEHAVIOUR AND PERFORMANCE	68
	5.1	Intro	oduction	68
	5.2	Nor	malized Force – Shear Strain Response	68
	5.3	Gen	eral Experimental Observation	71
	5.4	Pane	el Zone Local Strain Response	81
	5.5	Disc	eussion	87
	5.5.	1	Panel zone response and limit states	87
	5.5.2	2	Effect of column section size	89
	5.5.3	3	Effect of doubler plate geometry (reduced vs. standard)	89
6	DES	SIGN	RECOMMENDATIONS	91
	6.1	Desi	ign Method	91
	6.1.	1	Doubler plate interface weld	91
	6.1.2	2	Doubler plate dimensions	94
	6.1	3	Shear resistance of panel zone	97
	6.2	Desi	ign Examples	98
	6.2.	1	W250×73 beam-to-W250×73 column connection	98
	6.2.2	2	W250×58 beam-to-W250×58 column connection	100
7	FIN	ITE I	ELEMENT ANALYSIS	104
	7.1	Intro	oduction	104
	7.2	Nun	nerical Model	104
	7.3	Vali	dation of the Finite Element Model	106
	7.4	Eval	luation of the Proposed Design Method	108
	7.4.	1	Effect of combined axial force and bending in the beam	109
	7.4.2	2	Effect of column axial force	112
8	CON	NCLU	JSIONS AND RECOMMENDATIONS	121
	8.1	Sum	ımary	121
	8.2	Con	clusions	121





8.3 Limitations and Recommendations	122
REFERENCES	124
Appendix A: Material Properties	127
Appendix B: Residual Stress Measurements	136
Appendix C: Bilinear Curves	140
Appendix D: Specimen Drawings	146
LIST OF TABLES	
Table 2.1: Matrix of test specimens (Lee et al. 2005)	13
Table 2.2: Properties of test specimens (Krawinkler 1978)	
Table 3.1: Beam and column crosse section properties (subscripts b and c are used in this	10
document to introduce cross-section properties of beams and columns, respectively)	24
Table 3.2: Design forces on connection components under applied loads	
Table 4.1: W250 specimen matrix	
Table 4.2: W250 Specimen matrix (cont.).	
Table 4.3: W410 specimen matrix	
Table 4.4: W410 specimen matrix (cont.)	
Table 4.5: Measured sizes of members and stiffeners	
Table 4.6: Measured cross-sectional dimensions	
Table 4.7: Summary of test specimen design	41
Table 4.8: Mechanical properties of steel from tension coupon tests	
Table 5.1: Design load versus applied load at the beam end, and predicted shear capacity o	
panel zone versus measured panel zone shear force at yielding	
Table 6.1: Summary of proposed design for test specimens with a reduced doubler plate	
Table 7.1: Selected beam load cases.	
Table 7.2 Actual and predicted yielding shear forces	120





LIST OF FIGURES

Figure 1.1: (a) Pipe rack module in the fabrication shop; (b) Perspective view of a typical pipe
rack module; (c) Beam-to-column connection detail with standard doubler plate connected using
PJP groove welds; (d) Beam-to-column connection detail with reduced doubler plate connected
using fillet welds
Figure 2.1: Typical four-level pipe rack with eight transverse frames connected by longitudinal
struts (Drake and Walter 2010)5
Figure 2.2: Ultimate Limit State load combinations for operating conditions (Bedair 2015) 6
Figure 2.3: Bracing of vertical pipes (Bedair 2015)
Figure 2.4: Alternative doubler plate details (Shirsat 2011)
Figure 2.5: Effect of narrower doubler plate: Panel zone shear versus panel zone rotation;
Analysis case 10: No doubler plate, Analysis case 11: Full-width conventional doubler plate,
Analysis case 16: Reduced doubler plate (Shirsat 2011)9
Figure 2.6: Alternative doubler plate details (Ciutina and Dubina 2008)
Figure 2.7: Monotonic loading results (Ciutina and Dubina 2008)
Figure 2.8: Doubler plate details: (a) back-beveled fillet-welded doubler (Detail I); (b) square-cut
fillet-welded doubler (Detail II); (c) box doubler (Detail III) (Lee et al. 2005)
Figure 2.9: Test setup of a one-sided beam-to-column connection (Reynolds and Uang 2022) 14
Figure 2.10: Column panel zone shear deformation (Krawinkler 1978)
Figure 2.11: Shear force versus joint distortion (Krawinkler 1978)
Figure 2.12: Panel zone kinematics and mathematical model assumptions: (a) panel zone shear
deformation; (b) panel zone bending deformation; (c) Krawinkler trilinear model (Skiadopoulos
et al. 2021)
Figure 2.13: CJP and fillet weld details: (a) column W360×592; and (b) column W610×195
(Skiadopoulos et al. 2021)
Figure 2.14: Relative difference in average shear stresses between doubler plate and column web
versus accumulated panel zone shear distortion: (a) column W610×195; and (b) column
W360×592 (Skiadopoulos et al. 2021)
Figure 3.1: Typical pipe rack beam-to-column welded connection detail
Figure 3.2: Welded beam-to-column moment connection of a pipe rack structure (LIMCON
2006)
Figure 3.3: Free-body diagram of the beam-to-column connection under bending moment and
axial force
Figure 3.4: W250×73 column to W250×73 beam welded moment connection
Figure 4.1: Exterior beam-to-column moment connection specimen in the lab
Figure 4.2: Pipe rack structure with an exterior beam-to-column connection highlighted (WF
Steel and Crane 2021)
Figure 4.3: W250-RDP1 specimen before testing
Figure 4.4: Elevation of test specimen W250-RDP1: (a) side view, (b) front view (all dimensions
are in mm)





Figure 4.5: Column base plate: (a) plan view, (b) elevation	44
Figure 4.6: Column base plate in the laboratory during assembly	45
Figure 4.7: (a) Adapter plate front view, (b) Adapter plate elevation	
Figure 4.8: Column boundary condition: (a) Spacer W-section plan view, (b) Spacer W-section	
elevation, (c) Column top boundary in the laboratory	
Figure 4.9: Lateral bracing system of W250-RDP1 specimen	
Figure 4.10: Lateral bracing system support beam	
Figure 4.11: Loading system	52
Figure 4.12: Side view of specimen W250-RDP1 with instrumentation mounted	53
Figure 4.13: Front view of specimen W250-RDP1 with instrumentation mounted	54
Figure 4.14: Column web and doubler plate instrumentation for W250-RDP1	55
Figure 4.15: Strain rosette (45 degrees) aligned with x-y axes (efunda 2024)	56
Figure 4.16: Location of tension coupons on: (a) flange sections, (b) web sections	58
Figure 4.17: Standard tension coupons	59
Figure 4.18: Uniaxial load frame used to perform standard coupon tests	
Figure 4.19: Engineering stress–strain curves of W250 coupons	60
Figure 4.20: Engineering stress-strain curves of W410 coupons	61
Figure 4.21: Cutting locations for residual stress measurements: (a) W250×58, (b) W410×60	63
Figure 4.22: Sections for residual stress measurements after cold-sawing	64
Figure 4.23: Residual stress distribution of W250×58: (a) W250 Flange 1, (b) W250 Flange 2	2,
(c) W250 Web	66
Figure 4.24: Residual stress distribution of W410×60: (a) W410 Flange 1, (b) W410 Flange 2	2,
(c) W410 Web	67
Figure 5.1: Normalized force – shear strain responses of W250 specimens	68
Figure 5.2: Normalized force – shear strain responses of W410 specimens	69
Figure 5.3: Normalized shear force – shear strain response of the panel zone for W250 specin	nens
	70
Figure 5.4: Normalized shear force – shear strain response of the panel zone for W410 specin	
Figure 5.5: W250-NDP at the end of the test at 0.12 shear strain: (a) Deformed shape, (b) DIO	
shear strain contour (shear yielding $\gamma y = 0.007$ is shown by the boundary of purple and blue -	
red represents maximum strain)	
Figure 5.6: W410-NDP (Column web Face 2 is shown) at the end of the test at 0.12 shear stra	
(a) Deformed shape, (b) DIC shear strain contour (shear yielding $\gamma y = 0.008$ is shown by the	¥111.
boundary of purple and blue – red represents maximum strain)	72
Figure 5.7: W250-DP at the end of the test at 0.10 shear strain: (a) Deformed shape, (b) DIC	12
shear strain contour (yielding $\gamma y = 0.009$ is shown by the boundary of purple and blue – red	
represents maximum strain)	73





Figure 5.8: W410-DP: (a) Deformed shape at the end of test at 0.12 shear strain, (b) DIC shear
strain contour prior to reloading of test (yielding $\gamma y = 0.011$ is shown by the boundary of purple
and blue – red represents maximum strain)
Figure 5.9: W250-RDP1A at the end of the test at 0.10 shear strain: (a) Deformed shape, (b) DIC
shear strain contour (yielding $\gamma y = 0.008$ is shown by the boundary of purple and blue – red
represents maximum strain)
Figure 5.10: W250-RDP1B at the end of the test at 0.10 shear strain: (a) Deformed shape, (b)
DIC shear strain contour (yielding $\gamma y = 0.008$ is shown by the boundary of purple and blue – red
represents maximum strain)
Figure 5.11: W410-RDP1A at the end of the test at 0.12 shear strain: (a) Deformed shape, (b)
DIC shear strain contour (yielding $\gamma y = 0.008$ is shown by the green areas – red represents
maximum strain)
Figure 5.12: W410-RDP1B at the end of the test at 0.12 shear strain: (a) Deformed shape, (b)
DIC shear strain contour (yielding $\gamma y = 0.008$ is shown by the green areas – red represents
maximum strain)
Figure 5.13: W250-RDP2A: (a) Deformed shape at the end of the test at 0.12 shear strain, (b)
DIC shear strain contour at the end of the test at 0.12 shear strain (yielding $\gamma y = 0.008$ is shown
by the boundary of purple and blue – red represents maximum strain), (c) DIC shear strain
contour at an average shear strain of 0.008
Figure 5.14: W250-RDP2B: (a) Deformed shape at the end of the test at test at 0.12 shear strain,
(b) DIC shear strain contour at the end of the test at 0.12 shear strain (yielding $\gamma y = 0.008$ is
shown by the boundary of purple and blue – red represents maximum strain), (c) DIC shear
strain contour at an average shear strain of 0.008
Figure 5.15: W410-RDP2A: (a) Deformed shape at the end of the test at shear strain 0.10, (b)
DIC shear strain contour at the end of the test at shear strain 0.10 (yielding $\gamma y = 0.009$ is shown
by the boundary of cyan and green – red represents maximum strain), (c) DIC shear strain
contour at an average shear strain of 0.009
Figure 5.16: W410-RDP2B: (a) Deformed shape at the end of the test at shear strain 0.10, (b)
DIC shear strain contour at the end of the test at shear strain 0.10 (yielding $\gamma y = 0.009$ is shown
by the dark blue areas – red represents maximum strain), (c) DIC shear strain contour at an
average shear strain of 0.009
Figure 5.17: Local shear strain at the middle of the panel zone versus panel zone shear strain for
W250-NDP
Figure 5.18: Local shear strain at the middle of the panel zone versus panel zone shear strain for
W410-NDP 82
Figure 5.19: Local shear strain at the middle of the panel zone versus panel zone shear strain for
W250-DP
Figure 5.20: Local shear strain at the middle of the panel zone versus panel zone shear strain for
W410-DP 83





Figure 5.21: Local shear strain at the middle of the panel zone versus panel zone shear strain for W250-RDP1
Figure 5.22: Local shear strain at the middle of the panel zone versus panel zone shear strain for W410-RDP1
Figure 5.23: Local shear strain at the middle of the panel zone versus panel zone shear strain for
W250-RDP2
Figure 5.24: Local shear strain at the middle of the panel zone versus panel zone shear strain for
W410-RDP286
Figure 5.25: Panel shear force versus panel shear strain for W250-NDP
Figure 6.1: Panel zone layout and dimensions
Figure 6.2: Panel zone and panel zone components free-body diagrams (force vectors are defined
in their respective equations)
Figure 6.3: Beam-to-column moment connection force diagram
Figure 6.4: Schematic distribution of shear deformation along the panel zone height for column
panel zone with reduced DP and without DP
Figure 6.5: Bilinear shear force – shear strain responses of specimens against predicted shear
resistance of the panel zone using proposed method: (a) W250 RDP1, (b) W250 RDP2, (c)
W410 RDP1, and (d) W410 RDP2
Figure 7.1: The details of the finite element model for W410-RDP1 (a) 3D view (b) DP view.105
Figure 7.2 The schematic distribution of residual stresses in column cross-section
Figure 7.3: True stress-plastic strain curves (a) W250 specimens and (b) W410 specimens 106
Figure 7.4: Comparison of the force-displacement responses from FEA and tests (a) W250-NDP,
(b) W250-DP, (c) W250-RD1, and (d) W250-RDP2
Figure 7.5 Comparison of the force-displacement curves from FEA and tests for (a) W410-NDP,
(b) W410-DP, (c) W410-RD1, and (d) W410-RDP2
Figure 7.6: The prototype moment connection used for numerical response evaluation 109
Figure 7.7: DP shear force response: (a-d) Load Cases 1 – 4
Figure 7.8 Distribution of in-plane shear stress at the end of the analysis in DP: (a-d) Load Cases
1–4 (stress values in MPa).
Figure 7.9: (a) PZ shear force versus PZ shear strain, and (b) DP shear stress versus PZ shear
strain for W250-RDP1 under column axial force.
Figure 7.10 (a) Shear force versus shear strain of the PZ, and (b) shear stress in the DP versus the
PZ shear strain for the W250-RDP2 specimen under various column axial force
Figure 7.11 (a) Shear force versus shear strain of the PZ, and (b) shear stress in the DP versus the
PZ shear strain for the W410-RDP1 specimen under various column axial force
Figure 7.12 (a) Shear force versus shear strain of the PZ, and (b) shear stress in the DP versus the
PZ shear strain for the W410-RDP2 specimen under various column axial force
Figure 7.13 Distribution of in-plane shear strain at the onset of shear buckling: (a) W410-RDP1,
Axial Force = $0.4 F_{yc}A_{col}$ (b) W410-RDP1, Axial Force = $0.6 F_{yc}A_{col}$ (c) W410-RDP2, Axial
Force = $0.4 F_{yc}A_{col}(d)$ W410-RDP2, Axial Force = $0.6 F_{yc}A_{col}$





LIST OF SYMBOLS

 A_s = Total cross-sectional area of stiffeners

 $A_{\rm w}$ = Area of fillet weld

 $b_{\rm f}$ = Flange width

 $b_{\rm bf}$ = Beam flange width

 $b_{\rm cf}$ = Column flange width

 $b_{\rm s}$ = Width of stiffener

 $b_{\rm se}$ = Effective width of stiffener

 $C_{\text{y,web}}$ = Column web axial yield strength

 $C_{y,fl}$ = Column flange axial yield strength

 $C_{\rm f}$ = Column web axial force

 C_{f-bf} = Axial compression in the beam flanges

 C_{f-bw} = Axial compression in the beam web

 C_{f-s} = Stiffener design compression force

 C_{r-wc} = Factored column web crippling strength

 C_{r-wb} = Factored column web buckling strength

 $C_{\rm v}$ = Column axial yield strength, which is equal to the column yield

strength multiplied by the area of the column web

 C_{r-sb} = Transverse stiffener buckling strength

D = Fillet weld leg size

d = W-section depth

 $d_{\rm b}$ = Beam depth

 $d_{\rm c}$ = Column depth

E = Modulus of elasticity of steel

 $F_{\rm v}$ = Specified yield strength

 F_{v-m} = Measured yield stress

 F_{y-n} = Nominal yield stress





 $F_{\rm vc}$ = Column yield stress

 $F_{y,DP}$ = Doubler plate yield stress

 $F_{y,fl}$ = Flange yield stress

 $F_{y,web}$ = Web yield stress

 F_{ys} = Stiffener yield stress

G = Shear modulus of elasticity of steel

 $H_{\rm DP}$ = Doubler plate height

 H_{PZ} = Panel zone height

 H_1 = Doubler plate reduction in the vertical direction

h = The clear distance between flanges minus the fillet or corner radius

for rolled shapes

 $h_{\rm o}$ = Distance between flange centroids

 $I_{\rm s}$ = Moment of inertia of stiffener

K = Effective length factor

 $K_{\rm e}$ = Elastic stiffness

 K_{p} = Post-elastic stiffness

k = The distance from the outside face of the column flange to the web

toe of the flange-to-web fillet

 $k_{\rm v}$ = shear buckling coefficient

 $l_{\rm b}$ = Bearing length

 $L_{\rm DP}$ = Doubler plate length

 $L_{\rm PZ}$ = Panel zone length

 L_1 = Doubler plate reduction in the horizontal direction

 $l_{\rm s}$ = length of stiffener

 $l_{\rm w}$ = Fillet weld length

 $M_{\rm b-R}$ = Beams' right moment at the column face

 $M_{\rm h-L}$ = Beams' left moment at the column face

 $M_{\rm fy-b}$ = Beam strong-axis moment

 $M_{\rm fx-b}$ = Beam weak-axis moment

 $M_{\rm f-bw}$ = Connection design moment





 $N_{\rm f-b}$ = Beam axial force

N = Axial force

 $P_{\rm br}$ = Required strength of end or intermediate point brace

 $P_{\rm Vp-m}$ = Applied load at the beam end

 P_{Vp-n} = Design load at beam end

 $Q_{\rm f}$ = Chord-stress interaction parameter

r = Radius of gyration

 S_{x-b} = Beam elastic section modulus

 S_{x-hw} = Beam web elastic section modulus

 T_{f-bf} = Axial tension in the beam flanges

 T_{f-bw} = Axial tension in the beam web

 T_{f-s} = Stiffener design tension force

 $T_{\text{r-cfb}}$ = Factored flange local bending strength

 T_{r-cwv} = Factored local web yielding strength

 T_{r-syt} = Transverse stiffener factored yield strength at the beam tension

flange

 T_{r-syc} = Transverse stiffener factored yield strength at the beam

compression flange

 t_w = Web thickness

 $t_{\rm hf}$ = Beam flange thickness

 $t_{\rm bw}$ = Beam web thickness

 $t_{\rm cf}$ = Column flange thickness

 $t_{\rm cw}$ = Column web thickness

 $t_{\rm dp}$ = Doubler plate thickness

 t_{pz} = Panel zone thickness

 t_s = Stiffener thickness

 V_{ij} = Ultimate shear strength

 $V_{\rm v}$ = Yield shear strength

 V_{f-cw} = Column web panel shear

 V_{f-h} = Connection design shear





 V_{r-fw} = Beam flange factored weld resistance for direct shear and tensioninduced shear V_{r-ww} = Beam web factored weld resistance for direct shear and tensioninduced shear $V_{\rm r-ws}$ = Factored shear strength of the column panel zone without a doubler plate = Factored shear strength of the column panel zone with a doubler $V_{\rm r-PZ}$ V_{r-es} = Stiffener end factored weld resistance V_{r-ss} = Stiffener side factored weld resistance = Column shear force above the connection $V_{\rm col-T}$ = Column shear force below the connection $V_{\rm col-B}$ = Measured panel zone shear force at yield $V_{\rm p-m}$ = Predicted shear capacity of the panel zone $V_{\rm p-n}$ $V_{\rm PZH.d}$ = Horizontal shear force demand of the panel zone V_{PZV} = Vertical shear force of the panel zone V_3 = Horizontal shear force in part C V_4 = Horizontal shear forces induced in the unreinforced areas A and B V_5 = Vertical shear force imposed on H V_6 = Vertical shear forces induced in the unreinforced areas E and F V_{r-w} = Shear capacity of the fillet weld of the doubler plate $V_{\rm DPH}$ = Horizontal shear force of the panel zone transferred by the column web = Weld design force V_{f-w} = Nominal shear strength of the panel zone with a doubler plate $V_{\rm n}$ $V_{\rm r}$ = Factored shear resistance of the column panel zone with a reduced doubler plate $W_{\rm ext}$ = External work $W_{\rm int}$ = Internal work



= Internal work in the web

 $W_{\rm int,web}$



 $W_{\text{int.DP}}$ = Internal work in the doubler plate

 $X_{\rm u}$ = Weld ultimate tensile strength

 Z_{x-b} = Beam plastic section modulus

 α = Shear strain ratio

 α_c = Member slenderness reduction factor

 Δ = Total shear deformation of the panel zone

 ε_a = Strain measured from strain rosette at 0°

 $\varepsilon_{\rm b}$ = Strain measured from strain rosette at 45°

 $\varepsilon_{\rm c}$ = Strain measured from strain rosette at 90°

 $\varepsilon_{\mathbf{x}}$ = Normal Strain in x-direction

 ε_{v} = Normal Strain in y-direction

 ε_{xy} = Normal Strain in xy-direction

 γ_{ave} = Average yield shear strain

 γ_{xy} = Shear strain

 γ_v = Yield shear strain

 $\gamma_{y,web}$ = Column web yield shear strain

 λ = Slenderness parameter

 θ = Angle of the weld segment axis with respect to the line of action of

the applied force

 φ = Resistance factor

 σ_{VM} = Von Mises stress

 σ_x = Normal stress in x-direction

 σ_{v} = Normal stress in y-direction

 σ_{vs} = Yield stress

 τ_{xy} = Shear stress

 τ_y = Yield shear stress

v = Poisson's ratio





1 INTRODUCTION

1.1 Background

Pipe-supporting structures, commonly referred to as pipe racks, are heavy steel structures used extensively in refineries, chemical plants, oil sands, and recently in carbon capture utilization and storage facilities in Canada. Due to similar loading conditions along the network, they are often broken into repetitive volumetric modules that can be prefabricated off-site and shipped to the construction site for assembly. Modularization can reduce the fabrication and construction costs even though the tonnage typically increases by about 30% (Bedair 2015). Figure 1.1a shows an example of a pipe rack module being fabricated at a fabrication shop. The beams and columns of the modules are often made of wide-flange shapes, e.g., W250, W310, and W360. and their braces typically consist of double angles as shown in Figure 1.1a. The beams and columns carry the anticipated vertical and horizontal loads using a combination of steel concentrically braced frames and moment-resisting frames. The connections between beams and columns are often designed as moment-resisting connections in the transverse (short) direction of the pipe rack and as simple connections in the longitudinal direction where the beams are framing into the column web, as shown in Figure 1.1b. As opposed to building applications, beam-to-column moment connections in pipe rack modules often involve multiple stiffeners designed to resist complex combinations of torsion, axial forces and both strong- and weak-axis moments, in addition to serving as the connection points for attachments. This complexity tends to lead to expensive connection details and labor-intensive tasks that can significantly impact fabrication costs and scheduling. The web of the column in the plane of the moment-resisting frame bounded by beam and column flanges is called the panel zone, which is primarily subjected to in-plane shear due to flexural moments applied by the beams and being transferred into the columns through the panel zone. Web doubler plates are often required in the panel zone area to increase the shear capacity of the column web, which is often not sufficient in typical rolled shapes (e.g., W250 and W310) to carry relatively high shear being produced by force couples in the connection. Complete- or partial-joint penetration (CJP or PJP) groove welds are typically used to attach web doubler plates to the column radius in the connection region (see Fig. 1.1c) (Morgan 2021). However, the fabrication of such connections with doubler plates connected using PJP groove welds pose several challenges due to the presence of several stiffeners and other fixtures in the connection area. Additionally, PJP welds





require surface preparation, advanced manufacturing technology and inspection, which all require skilled workers, leading to increased fabrication time and costs of already-costly connections. As such, reduced doubler plates connected to the column web using fillet welds (see Figure 1.1d) would present a desirable alternative to PJP or CJP welds for fabrication of steel moment connections in pipe rack structures. However, the structural performance and load-carrying capacity of the alternative (reduced doubler plate) detail has not been verified yet and no design method is currently available to select such doubler plates and their welds.

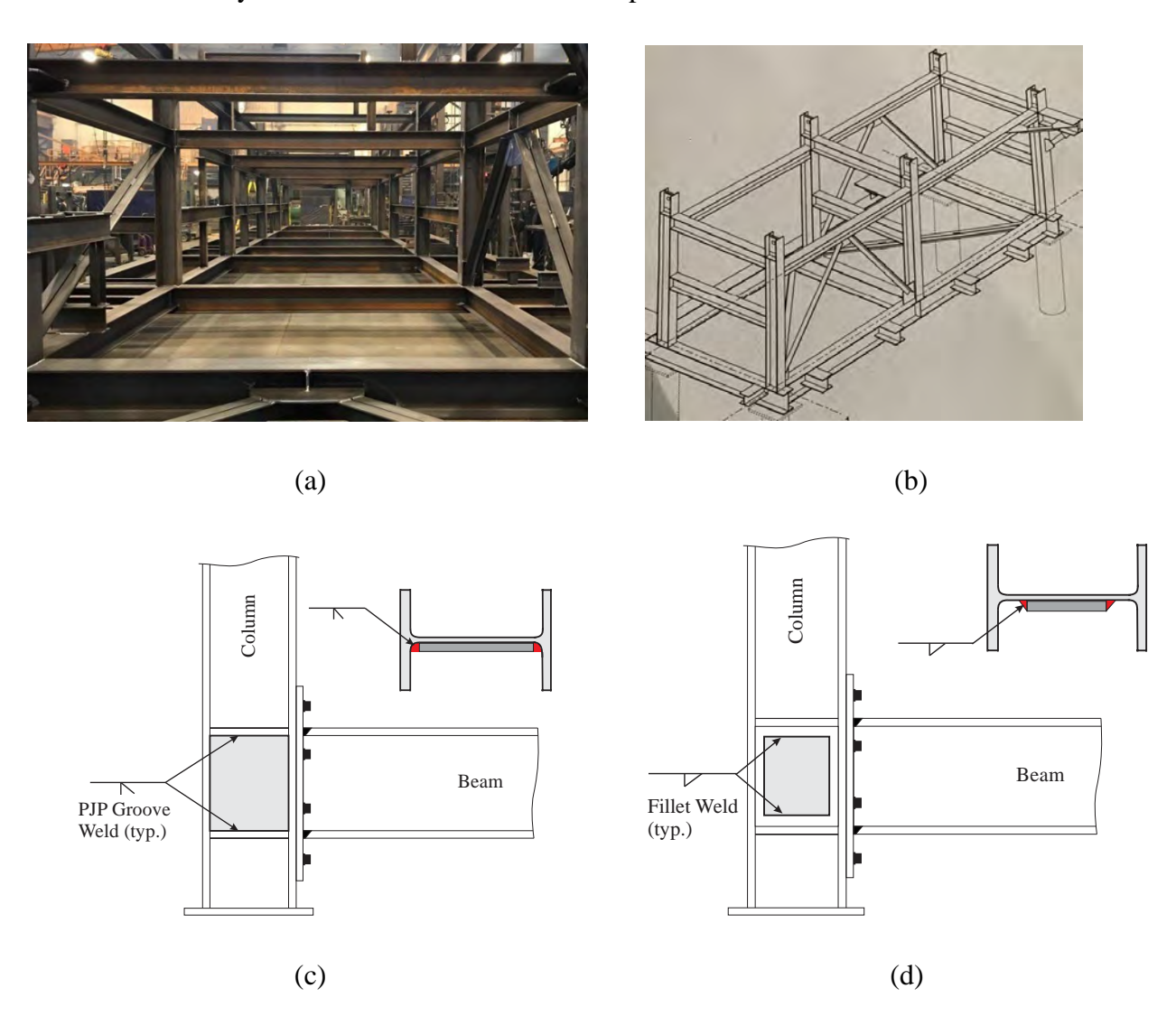


Figure 1.1: (a) Pipe rack module in the fabrication shop; (b) Perspective view of a typical pipe rack module; (c) Beam-to-column connection detail with standard doubler plate connected using PJP groove welds; (d) Beam-to-column connection detail with reduced doubler plate connected using fillet welds





1.2 Statement of Research Problem

Despite the extensive use of heavy pipe-supporting structures in Canada, particularly in natural resource development regions, limited information and guidelines are available in practice for design and detailing of their connections (Drake and Walter 2010). In lieu of a unified design procedure, steel fabricators typically develop their own design manuals and spreadsheets, which may lead to prohibitively expensive and complex details with uneconomical fabrication processes (Bedair 2015). The fabrication of steel pipe racks involves labor-intensive tasks, such as cutting, drilling, fitting, welding, crane operations, and assembly. Additionally, complex connections are expected in such structures to resist permanent loads such as gravity, transient loads such as hydraulic and wind loads, plus other potential loading scenarios that could arise during the life of the structure. Other loads that factor into the design of pipe racks' connections include thermal loads resulting from contraction or expansion due to the changes in ambient temperature during operation, anchor loads that arise from the restraints to displacements or rotations imposed during operating conditions, friction loads, which can result from sliding pipes, erection loads, and impact loads (Bedair 2015). As such, stiffeners and complex welding details are used in the connection of modules, leading to substantial added costs to the fabrication of pipe racks. CJP or PJP groove welds are typically used to attach web doubler plates to the column radius in the connection region since the structural performance and load-carrying capacity of an alternative detail has not been verified yet and no design method is currently available to select a reduced doubler plate with a fillet weld. This research will address the following problems:

- **P1**) inefficient and costly PJP weld detail for doubler plates in pipe racks, and
- **P2**) absence of a design method for an alternative reduced doubler plate.

1.3 Objectives

The general objective of this M.Sc. research project is to develop an efficient, economical, and structurally safe steel beam-to-column connection for pipe-supporting modules with the focus on an alternative doubler plate design. This alternative detail is designed to avoid the use of groove welds in the column panel zone area to facilitate the fabrication process and reduce fabrication costs. The specific objectives of this study are as follows:

O1) develop and verify using laboratory testing a new doubler plate detail for pipe rack beam-to-column connections,





- **O2**) propose and validate design guidelines and fabrication recommendations for the improved doubler plate detail, and
- Q3) produce full-scale experimental test data on beam-to-column moment connections under monotonic loading.

1.4 Research Methodology

To accomplish the goals of this project, the following steps are performed:

- **M1**) literature review on steel moment connections and pipe rack structures and current industry practice for the design of steel module connections,
- M2) test program development,
- M3) full-scale laboratory testing of beam-to-column connections,
- M4) development of design method in the framework of Canadian steel design standard, and
- M5) demonstration of the proposed method via design examples
- M6) validation of the proposed method for special cases using finite element analyses

1.5 Organization of Report

This report consists of seven chapters. Chapter 1 presents the scope of the project, problem statement and objectives. Chapter 2 provides a summary of past research conducted on steel moment connections, pipe rack modules and doubler plate details. The design of pipe rack moment connections consistent with the current practice is outlined in Chapter 3, through a design example. In Chapter 4, the design of experimental specimens and test setup, plus ancillary tests, loading scheme and instrumentation are presented. Chapter 5 includes test results with discussions regarding the performance of connections with the proposed detail and how they compare to conventional connections. In Chapter 6, a design method is proposed to size beam-to-column connections with proposed (reduced) doubler plate detail. Chapter 7 presents the details of finite element model and the parametric study performed to further validate the proposed design method. A summary and key findings of the project are described in Chapter 8.





2 LITERATURE REVIEW

This chapter presents an overview of the design of steel pipe rack module connections and summarizes past studies performed on doubler plate details and behaviour of column panel zones of steel beam-to-column moment connections.

2.1 Design of Modular Pipe Rack Systems

Pipe racks are non-building structures that have similarities to structural steel buildings with additional loads and design considerations. Figure 2.1 shows a typical pipe rack consisting of eight transverse frames connected by longitudinal struts. Design specifications outlined in the building codes lack clarity regarding their application to pipe racks. Various industry resources are available to assist designers in interpreting the code's intent while following standard engineering practices (Drake and Walter 2010).



Figure 2.1: Typical four-level pipe rack with eight transverse frames connected by longitudinal struts (Drake and Walter 2010)

Due to the complexity in the design of pipe racks, Bedair (2015) found that modularizing these structures minimizes cost and construction errors. Modularization is particularly economical for pipe rack structures located in remote sites with harsh weather conditions. Modularized pipe racks are fabricated off-site and transported to construction sites using public roads, which imposes constraints on the size and weight of each module. If a module does not meet the transportation





standards, it can be further divided into submodules that are assembled on site. When designing pipe racks, the following loads must be considered: dead loads, live loads, thermal loads, anchor loads arising from restraints to displacements or rotations during operating conditions, friction loads resulting from sliding pipes, wind loads, snow loads, erection loads, and impact loads that mimic transportation loads and are applied at the centre of gravity of the assembled modules (Bedair 2015). Figure 2.2 shows the load combinations considered to determine the most critical case for operating, testing, transportation, and erection conditions, which is from the Process Industry Practices (PIP 2004).

Principal loads	Companion loads						
1.4DL	-						
$1.25(DL_p + DL_O + TL + AL + FL) + 1.5LL_3$	0.5SL						
$1.25(DL_p + DL_O + TL + AL + FL) + 1.5SL$	0.5LL ₃						
$1.25(DL_p + DL_O + TL + AL + FL) + 1.5LL_3$	±0.4(WL) EW						
$1.25(DL_p + DL_O + TL + AL + FL) + 1.5SL$	±0.4(WL) EW						
$1.25(DL_p + DL_O + TL + AL + FL) + 1.5LL_3$	±0.4(WL) sn						
$1.25(DL_p + DL_O + TL + AL + FL) + 1.5LL$	±0.4(WL) sn						
$1.25(DL_p + DL_O + TL + AL + FL) \pm 1.4(WL)_{EW}$	0.5LL ₃						
$1.25(DL_p + DL_O + TL + AL + FL) \pm 1.4(WL)_{EW}$	0.5SL						
$1.25(DL_p + DL_O + TL + AL + FL) \pm 1.4(WL)_{SN}$	0.5LL ₃						
$1.25(DL_p + DL_O + TL + AL + FL) \pm 1.4(WL)_{SN}$	0.5SL						
Note: EW = east–west wind direction; SN = south–north wind direction.							

Figure 2.2: Ultimate Limit State load combinations for operating conditions (Bedair 2015)

Bedair (2015) also outlines design considerations to help practicing engineers achieve an efficient and effective design of pipe racks. The considerations are as follows:

- Placing steel shoes on the pipe rack beams to allow pipes to expand and contract freely
 without creating additional stresses in addition to imposing displacement limitations on
 structural members affected by pipe movements.
- Checking for lateral displacement, in the direction parallel to the axis of the pipes, for beams supporting pipe anchors or guides to check if horizontal bracing is required to





- achieve the strength and stiffness needed to resist resulting restraining forces. Pipe anchors and guides are usually used to restrict pipe movements at certain locations.
- Providing vertical bracings should to limit the horizontal displacement as shown in Figure 2.3. Intermediate horizontal supports, shown in dashed lines, can also be used to reduce the effective length of the inclined bracings. Additionally, horizontal bracings are required to limit horizontal displacements of the restraining box that is shown in Section B-B in Figure 2.3.
- Applying horizontal piping loads through the shear centre of the beams supporting the pipes to avoid inducing torsional loading.
- Avoiding steel supports that restrain pipe rotations at the top elevation of the pipe rack due
 to the high costs associated with providing structural members that would satisfy the
 torsional strength and stiffness needs at these locations.

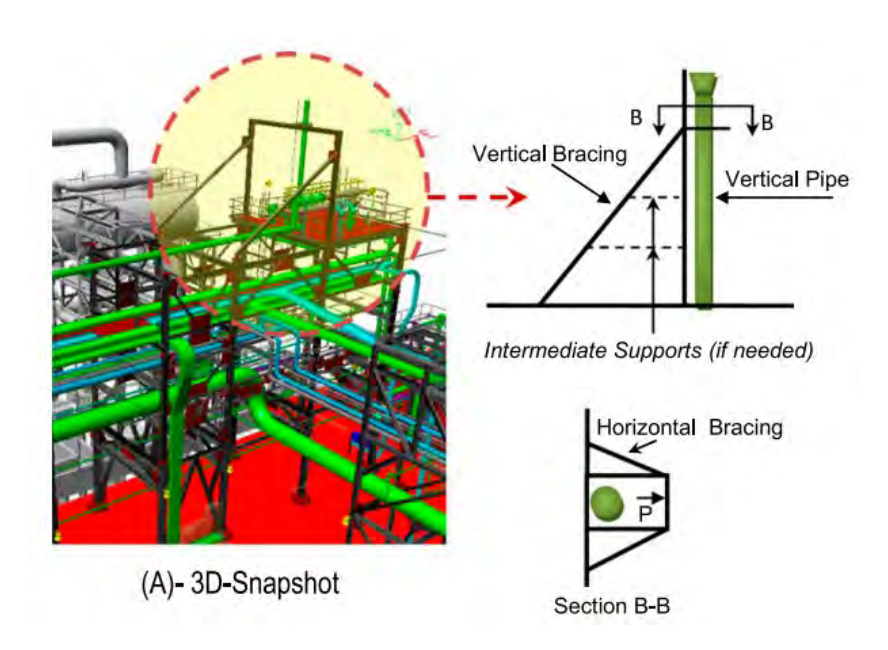


Figure 2.3: Bracing of vertical pipes (Bedair 2015)





2.2 Alternative Doubler Plate Details

Limited attention has been given to identifying cost-effective and structurally efficient methods for doubler plate details in moment connections. In this section, different doubler plate details that have been studied are discussed.

2.2.1 Shirsat (2011)

Shirsat (2011) performed a set of numerical analyses to investigate twenty-one cases, each featuring distinct doubler plate configurations. The different details, shown in Figure 2.4, included welding different edges of the doubler plate to the column: welding the vertical edges only, as seen in 2.4a; horizontal welds only, as in 2.4b; or all sides, as in 2.4c. Other details included using two thinner doubler plates on both sides of the column web instead of a single thick doubler plate, as shown in Figure 2.4d; extending the doubler plate beyond the panel zone region, as shown in Figure 2.4e; or using a narrower doubler plate, as in 2.4f.

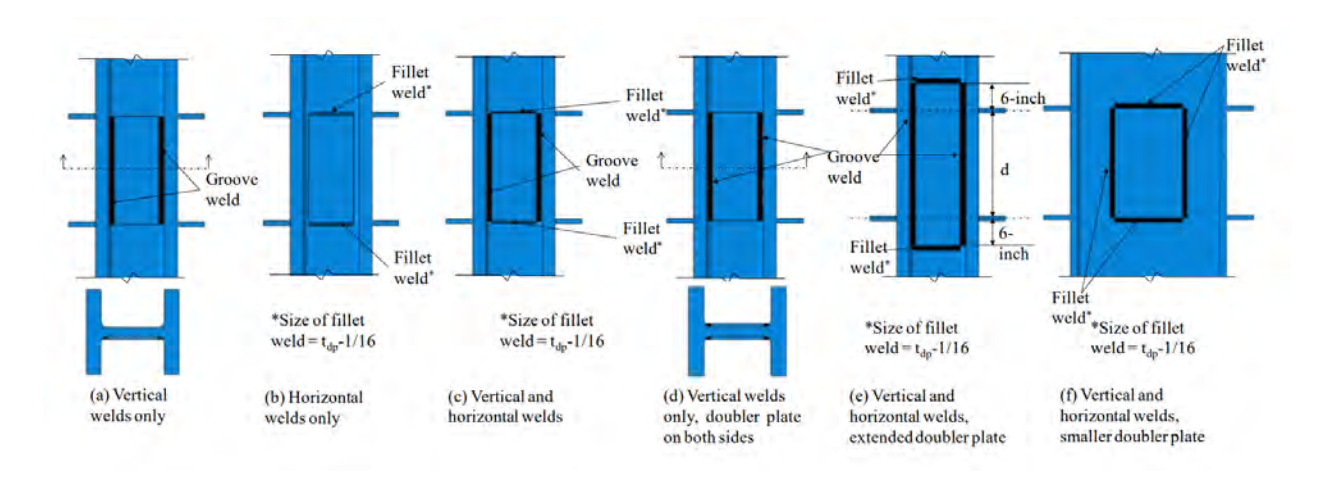


Figure 2.4: Alternative doubler plate details (Shirsat 2011)

The conclusions of the analyses performed under monotonic loading are as follows:

When the doubler plate was groove welded along its vertical edges, the full strength of the doubler plate was developed. Additionally, welding the horizontal edges added very little advantage to the detail, other than helping to restrain buckling of thinner plates. Extending the doubler plate beyond the panel zone region resulted in a small increase in panel zone stiffness and strength, whereas narrowing the doubler plate resulted in a reduction in panel zone stiffness and strength when





compared to the full width doubler plate (Figure 2.5) since a significant amount of shear deformation is contributed by the unreinforced part of the column. Lastly, utilizing two thin doubler plates, one on each side of the column web, rather than a one-sided thick doubler plate, resulted in essentially no change in stiffness and strength. According to Shirsat's (2011) research, Analysis case 10 represented the no doubler plate case and Analysis case 11 represented the full-width conventional doubler plate. Analysis case 16 showed the results of the narrower doubler plate case, which demonstrated a reduction in panel zone stiffness and strength with respect to Analysis case 11.

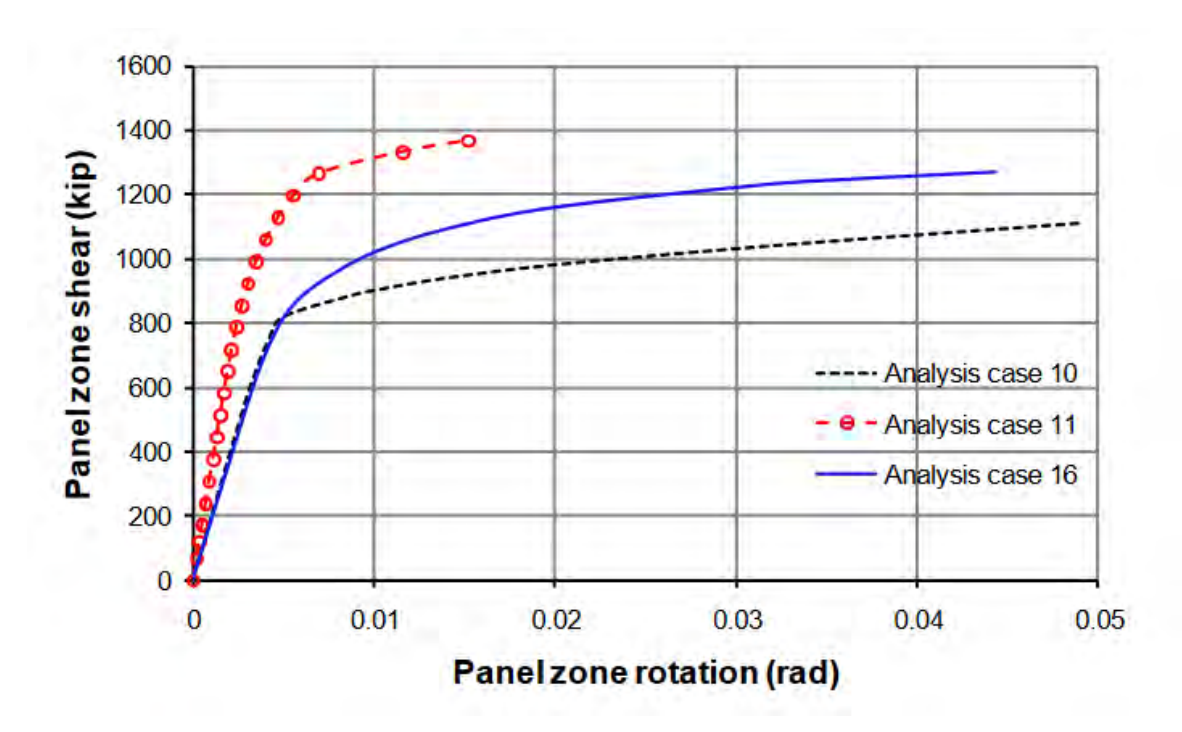


Figure 2.5: Effect of narrower doubler plate: Panel zone shear versus panel zone rotation;

Analysis case 10: No doubler plate, Analysis case 11: Full-width conventional doubler plate,

Analysis case 16: Reduced doubler plate (Shirsat 2011)

2.2.2 Ciutina and Dubina (2008)

Ciutina and Dubina (2008) investigated the effect of different doubler plate details by performing experimental testing. The different cases tested are shown in Figure 2.6. Specimen CP-IP consisted of a doubler plate narrower than the conventional one and was fillet welded on all four sides. CP-IIP had two narrow doubler plates on either side of the column web, whereas specimen CP-IIPL had doubler plates on both sides that are extended to the root fillet of the column and





welded using full penetration welds to the column flanges. In specimen CP-IIPD, two doubler plates, offset from the column web on either side, were fillet welded to the column flanges. Lastly, specimen CP-C used reinforced concrete to stiffen the column web (Ciutina and Dubina 2008). All the doubler plates used were 10 mm thick. Two loading scenarios were considered for each test specimen: monotonic loading and cyclic loading.

Test reference	Reinforcing type	Sketch	Width of the doubler plates	Loading type
CP-R-M CP-R-C	None			Monotonic Cyclic - ECCS
CP-C-M CP-C-C	Concrete			Monotonic Cyclic - ECCS
CP-IP-M CP-IP-C	Doubler plates		150 mm	Monotonic Cyclic - ECCS
CP-IIP-M CP-IIP-C	Doubler plates	***************************************	150 mm	Monotonic Cyclic - ECCS
CP-IIPL-M CP-IIPL-C	Doubler plates		220 mm	Monotonic Cyclic - ECCS
CP-IIPD-M CP-IIPD-C	Doubler plates		260 mm	Monotonic Cyclic - ECCS

Figure 2.6: Alternative doubler plate details (Ciutina and Dubina 2008)

From the results of the experiments conducted, Ciutina and Dubina (2008) drew a conclusion that test specimen CP-IIPD, which is the specimen with the offset doubler plates, was the most effective





detail in terms of panel zone strength followed by CP-IIPL, then CP-IIP, then CP-IP, and lastly CP-C. The results are shown in Figure 2.7, which illustrates moment versus shear distortion for all the test specimens. Both loading scenarios yielded the same conclusion, being that the CP-IIPD test specimen performed better than the rest of the specimens since it reached the highest moment before yield.

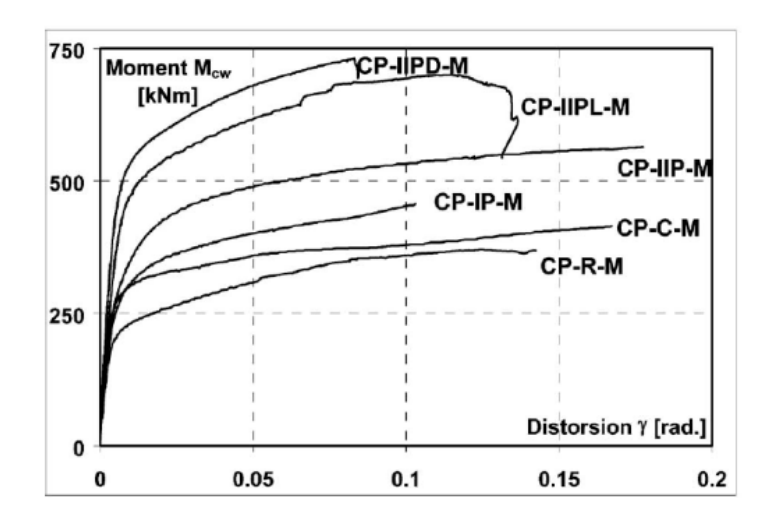


Figure 2.7: Monotonic loading results (Ciutina and Dubina 2008)

The detail in specimen CP-IIPD was not evaluated for the purpose of the current research, since in pipe rack modules it is very likely that other members are connected to the column web, and having an offset doubler plate on both sides of the column would not be a practical solution. The detail with two narrow doubler plates was also not tested since the goal was to reduce the amount of welding to be performed, especially since the use of two doubler plates yielded the same result as using one doubler plate of the same combined thickness according to Shirsat's research (2011). According to Figure 2.7, specimen CP-IP performed significantly better than the no doubler plate case, indicating that even the addition of a narrow doubler plate produced a significant amount of strength and stiffness to the panel zone.





2.2.3 Lee et al. (2005)

This research involved both experimental and computational work, investigating various details for attaching doubler plates and continuity plates to the column. The three details shown in Figure 2.8 were developed to avoid welding in the k-area of the column (Lee et al. 2005). In Details I and II, fillet welds were used between the doubler plate and the column flanges, whereas in Detail III, complete joint penetration groove welds were used. Detail I consists of two doubler plates that are back-beveled at 45 degrees to minimize the interference with the k-region of the column, allowing the doubler plate to be flush against the column web and welded to the column flanges. Detail II was considered due to the increased k-values for W-sections in recent years, which would not allow the doubler plate to be placed flush with the column web without making the doubler plate unrealistically thick or leaving a gap between the column web and the plate. Hence, Detail II consists of doublers cut to the width between the column flanges, then fillet-welded to the latter on either side. The third detail is referred to as the box doubler and is shown in Figure 2.8c. In this detail, the doubler plates serve as both doubler plates and continuity plates since they were welded at a distance from the column web, which is economically desirable.

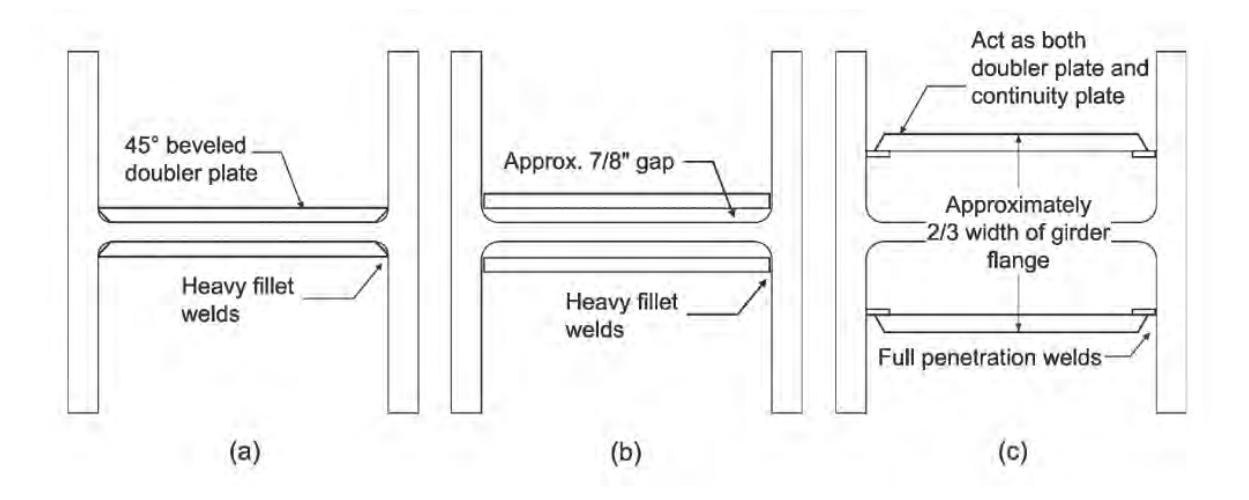


Figure 2.8: Doubler plate details: (a) back-beveled fillet-welded doubler (Detail I); (b) square-cut fillet-welded doubler (Detail II); (c) box doubler (Detail III) (Lee et al. 2005)

It was concluded that these details can perform well under seismic and non-seismic loads, i.e. withstand the loads applied, but further research is required to prove the viability of these details. Table 2.1 shows the five different specimens tested. All specimens failed due to low-cycle fatigue crack growth that led to the rupture of the girder-flange-to-column-flange complete joint





penetration (CJP) groove welds. The three details showed no cracks or distortions in the welds connecting the doubler plates to the column flanges before the failure of the CJP welds. No cracking was observed in the k-area of the columns. Additionally, the doubler plates in Detail III (box doubler) were found to perform effectively as continuity plates, in addition to serving as column web doubler plates.

Table 2.1: Matrix of test specimens (Lee et al. 2005)

	CR1	CR2	CR3	CR4 and CR4R	CR5
Girder	W610×140	W610×140	W610×140	W610×140	W610×140
Column	W360×421	W360×287	W360×262	W360×262	W360×216
Doubler	None	Detail II	Detail II	Detail III Box	Detail I
Plate (DP)				(Offset)	
DP	NA	15.9 mm	2 @ 12.7 mm	2 @ 19.1 mm	2 @ 15.9 mm
thickness					
Continuity	None	None	Fillet-welded	None	None
Plate (CP)					
CP	NA	NA	12.7 mm	NA	NA
thickness					

2.2.4 *Reynolds and Uang* (2019)

Reynolds and Uang (2019) explored alternative weld details by conducting ten full-scale cyclic tests on steel moment frame connections. The focus was on the design of continuity plates and doubler plates for applications in special and intermediate moment frames. The test setup used in this research aided in creating the test setup detailed in Chapter 4. Figure 2.9 shows one of the test setups of an exterior beam-to-column moment connection. The column boundary conditions are depicted using W-shaped hinges. The inflection points were assumed to be at the mid-height of each story. The length of the beam is half the bay width with an inflection point at midspan. The free end of the beam was used to load the specimen using a hydraulic actuator affixed to the beam through a bolted loading corbel. Lateral bracing was also provided to restrain the out-of-plane movement of the beam using two HSS sections (Reynolds and Uang 2019).





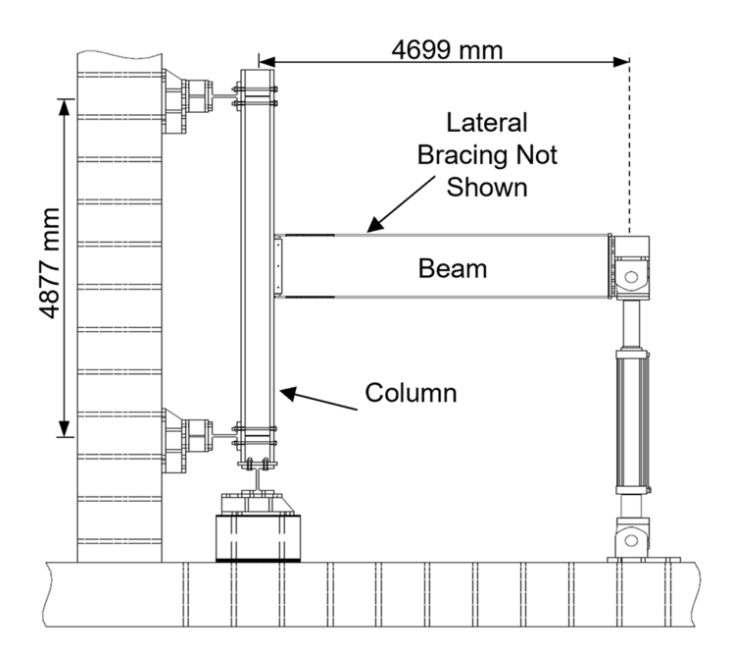


Figure 2.9: Test setup of a one-sided beam-to-column connection (Reynolds and Uang 2022)

2.3 Panel Zone Shear Deformation

2.3.1 Krawinkler (1978)

This research investigated the effects of shear in a beam-to-column joint on the strength, stiffness, and ductility of moment resisting frames under seismic loads. Figure 2.10 shows the panel zone of an interior joint and its deformation under lateral loading. When exposed to lateral loading, the panel zone experiences the maximum shearing stresses at its centre, gradually decreasing towards the corners. When stress exceeds the elastic limit, yielding begins at the centre and spreads towards the beam flanges. These series of actions are reflected in the load deformational behaviour of joints, showing an initial elastic phase, followed by a gradual decrease in stiffness, then a stabilization to a relatively constant stiffness over a wide range of deformation which is mostly due to strain-hardening in the material. This transition is mainly caused by the fact that the elements surrounding the panel zone also contribute to the resistance of the shear induced. Hence, the post-yield strength and stiffness of joints depends heavily on the flexural stiffness of the column flanges and the aspect ratio d_b/d_c , in addition to the stiffness of the beams and column outside the panel zone, where d_b and d_c are the beam and column depths, respectively. It was seen that with the increase in column flange thickness and the decrease in the aspect ratio, d_b/d_c , inelastic deformations decreased.





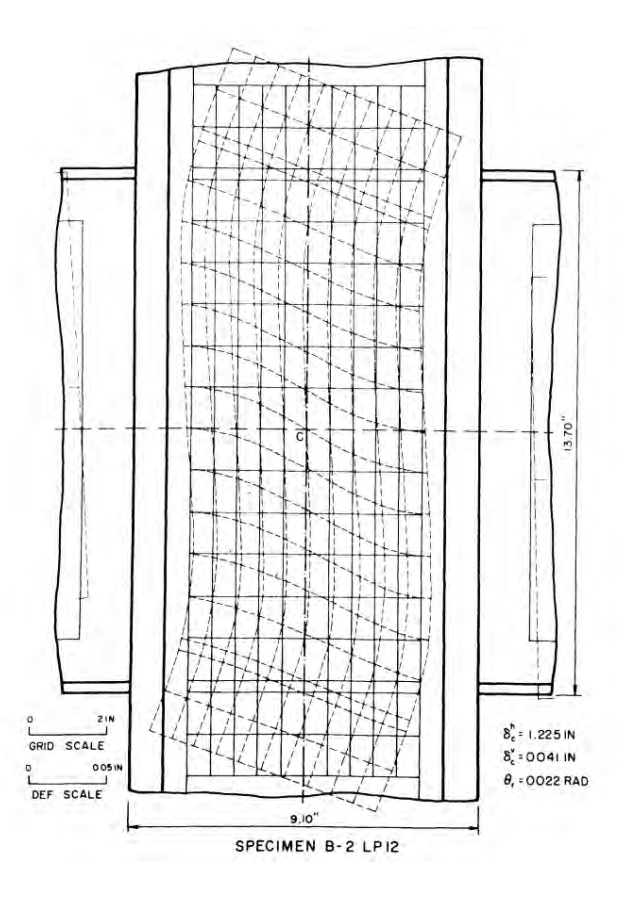


Figure 2.10: Column panel zone shear deformation (Krawinkler 1978)

Table 2.2 presents the properties of the test specimens used in Krawinkler's paper. Figure 2.11 shows the results from the three specimens in Table 2.2, where the shear force and strain values were normalized by the AISC (1973) plastic design strength, V_y , and the corresponding yield strain, γ_y . Based on Figure 2.11, the AISC (1973) equation for calculating maximum shear force in the plastic range is conservative, since it predicts a much lower ultimate shear strength of the joints than what is actually measured during the tests. The AISC (1973) equation is given by:

$$V_u = 0.55 F_{yc} d_c t_{cw}$$





Table 2.2: Properties of test specimens (Krawinkler 1978)

Specimen	d_c	t_{cw}	$t_{ m cf}$	$b_{ m cf}$	d_b	$F_{ m y,web}$	$F_{ m y,fl}$	$\frac{C}{C}$	С	Web	Horiz.
Specimen	mm	mm	mm	mm	mm	MPa	MPa	$\mathcal{L}_{ ext{y,web}}$	$C_{ m y,fl}$	Reinf.	Stiff.
A-2*	204	6.48	10.0	147	254	283	279	0.32	0.33	No	Yes
B-2**	231	15.9	23.1	207	348	324	293	0.37	0.41	No	No
B-3**	231	15.9	23.1	207	302	324	-	0.37	-	No	No

^{*}Column is W200×35.9 section with flanges milled to simulate W360×101 prototype.

where $F_{y,\text{web}}$ is the yield strength of the column web, $F_{y,\text{fl}}$ is the yield strength of the column flange, C is the is the axial column load at the design level, and C_y is the yield axial load.

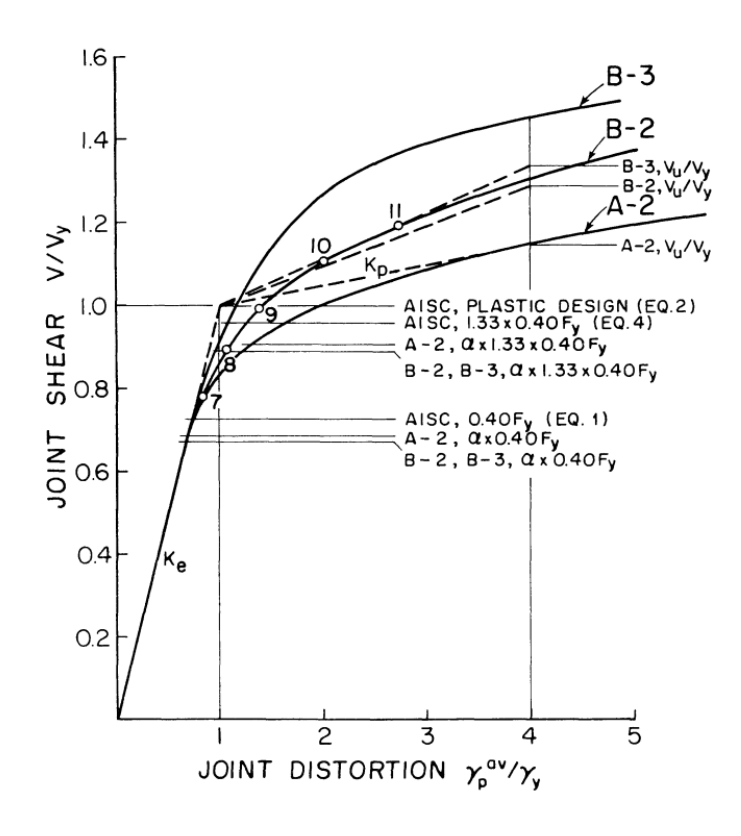


Figure 2.11: Shear force versus joint distortion (Krawinkler 1978).



^{**}Column is W200×100 section simulating W360×342 prototype.



Krawinkler (1978) suggests that the total angle of shear distortion is equal to four times the angle of shear distortion at yielding, γ_y , since the ultimate shear force was attained when the joint distortions were equal to or less than $4\gamma_y$, as shown in Figure 2.11. It is assumed that strain hardening stiffness is valid up to $4\gamma_y$. The design model proposed consists of an elastic perfectly plastic shear panel where K_e represents the elastic stiffness. The panel zone is surrounded by rigid boundaries with the corners considered as four springs that contribute to the post-elastic stiffness of the joint K_p . This model was referred to as Krawinkler's trilinear model. If all the joints are designed for the maximum ultimate shear force calculated using the equation proposed by Krawinkler, which was derived based on the previous assumptions, the maximum stiffness and strength of the frames will be reached. The equation used for the ultimate shear strength is the following:

$$V_u = V_y \left(1 + \frac{3K_p}{K_e} \right) = 0.55 F_{yc} d_c t_{cw} \left(1 + \frac{3.45 b_{cf} t_{cf}^2}{d_b d_c t_{cw}} \right)$$

where $V_y = 0.55 F_y d_c t_{cw}$, F_{yc} is the yield strength of the column, d_c is the depth of the column, t_{cw} is the thickness of the column web, b_{cf} is the width of the column flange, t_{cf} is the thickness of the column flanges, and d_b is the depth of the beam.

Lastly, it was found that when reinforcement is present at the column web, larger distortions were seen in the web rather than the doubler plates. Web stiffeners do not affect the post-elastic stiffness, K_p , derived. Therefore, the ultimate shear strength of the joint with a doubler plate is:

$$V_u = 0.55 F_{yc} d_c t_{cw} \left(1 + \frac{3.45 b_{cf} t_{cf}^2}{d_b d_c t_{cw}} \right) + \frac{F_y}{\sqrt{3}} (d_c - t_{cf}) t_{DP}$$

where t_{DP} is the thickness of the doubler plate.

2.3.2 *Skiadopoulos et al.* (2021)

The research by Skiadopoulos et al. (2021) builds on Krawinkler's (1978) work. The main goal was to develop a mechanics-based model for the design of beam-to-column panel zone connections in steel moment-frames under seismic loads. Figure 2.12, and specifically 2.12c, shows the phases of the trilinear mode, which consists of an elastic stiffness, K_e , dominated by shear stress extending





up to the yield shear strength, V_y . The post-yield behaviour of the panel zone is defined by an inelastic hardening region with post-yielding stiffness, K_p , extending to a shear strength, V_p , which occurs at $4\gamma_y$. This strength includes the contributions from surrounding elements such as continuity plates and column flanges (Krawinkler 1978). The continuum finite element (CFE) simulations proved that assuming uniform shear yielding in the panel zone is only acceptable in panel zones of stocky and shallow column sections, regardless of the level of inelastic shear strain, since the column flanges' contribution to shear yielding is significant in these sections (the area of flanges outweighs that of the web). In contrast, this assumption is not valid for slender columns (Skiadopoulos et al. 2021).

Figure 2.12a shows the kinking locations of the column flanges that contribute to the plastic moment resistance. The third phase on the plot in Figure 2.12c accounts for the shear strength stabilization, which is represented by a post- γ_p slope that is expressed as a percentage of the elastic stiffness (Skiadopoulos et al. 2021). The panel zone bending deformation shown in Figure 2.12b was neglected in the Krawinkler (1978) model, whereas the proposed model by Skiadopulos, based on the CFE analyses, considers both shear and bending deformations. This led to the proposition of a new equation for predicting panel zone stiffness and shear strength, with the shear strength at yield being the same as the Krawinkler's (1978) model for panel zones dominated by shear deformations, and an additional benefit of predicting strength when bending deformation is significant. The following equation of the panel zone shear strength is given by:

$$V_y = \frac{F_y}{\sqrt{3}} a_y (d_c - t_{cf}) t_{PZ}$$

where $a_y = 0.9$ and 1.0 for slender and stocky panel zones, respectively, and $t_{PZ} = t_{cw} + t_{DP}$.





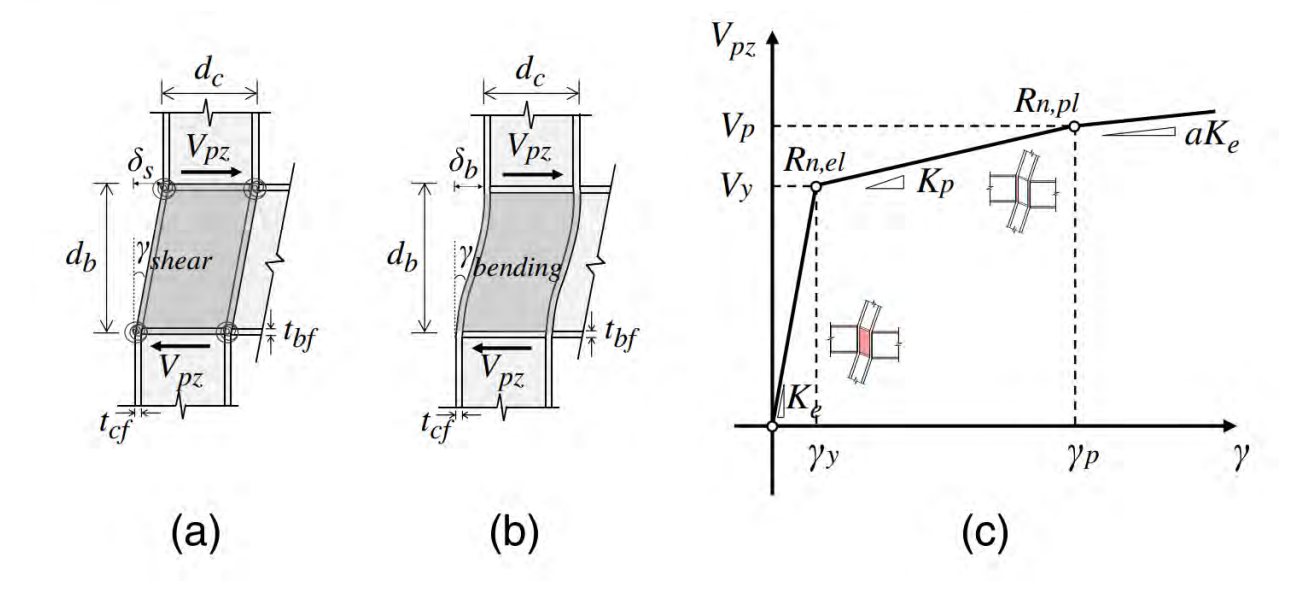


Figure 2.12: Panel zone kinematics and mathematical model assumptions: (a) panel zone shear deformation; (b) panel zone bending deformation; (c) Krawinkler trilinear model (Skiadopoulos et al. 2021).

The effect of doubler plates and their influence on the proposed model were also outlined. Two column sections were used for the CFE simulations: the first is a shallow and stocky (W360×592) column section, shown in Figure 2.13a and the second is a deep (W610×195) section, as shown in Figure 2.13b, both having a doubler plate on one side. The doubler plate used is thick, with $t_{\rm DP} > 40$ mm, since it was determined by avoiding welding in the k-area of the column as suggested by Lee et al. (2005). The doubler plates were only welded along their vertical edges. It was concluded that the doubler plate to column web shear stress incompatibility is not a concern for moment connections when they follow seismic provisions and detailing standards based on 2022 AISC Seismic Provisions for Structural Steel Buildings, AISC 341 (2022) and the American Welding Society (AWS 2016), as it was recorded that after yielding of both the column web and doubler plate, the relative difference in their shear stress demand is 10% or lower. The relative difference in shear stress is calculated as follows:

$$(\bar{\tau}_{cw} - \bar{\tau}_{DP})/\bar{\tau}_{DP}$$

where $\bar{\tau}_{cw}$ and $\bar{\tau}_{DP}$ are the average shear stresses in the column web and the doubler plate, respectively.





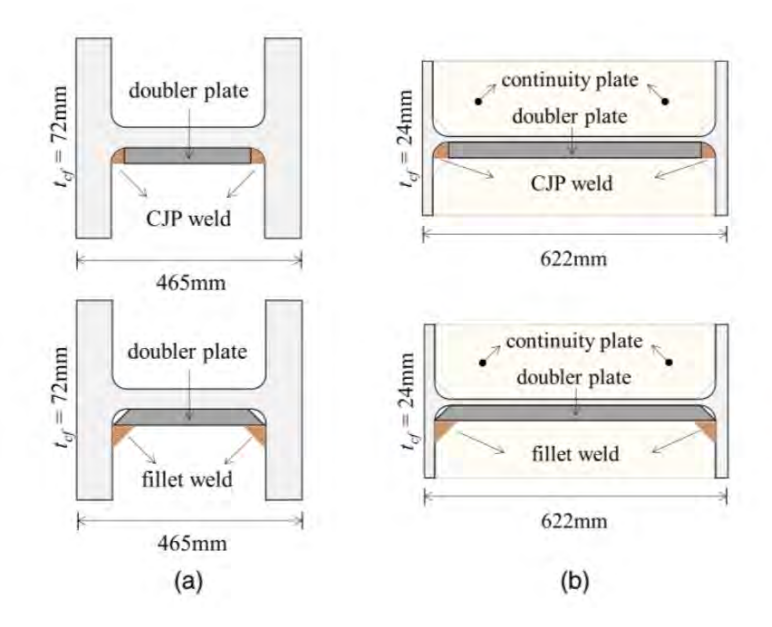


Figure 2.13: CJP and fillet weld details: (a) column W360×592; and (b) column W610×195 (Skiadopoulos et al. 2021).

The relative difference in average shear stresses between doubler plate and column web versus the accumulated panel zone shear distortion plots for the specimens in Figure 2.13 are illustrated in Figure 2.14. Stocky and shallow columns were observed to have a lower stress compatibility than deep columns in the initial stages, but after panel zone yielding the relative difference in shear stress decreased, as shown in Figure 2.14. Additionally, it was found that CJP welds provided a higher shear stress compatibility compared to fillet welds, but this difference is mostly due to the uncertainty of the welding material and the weld specifications used at that time.





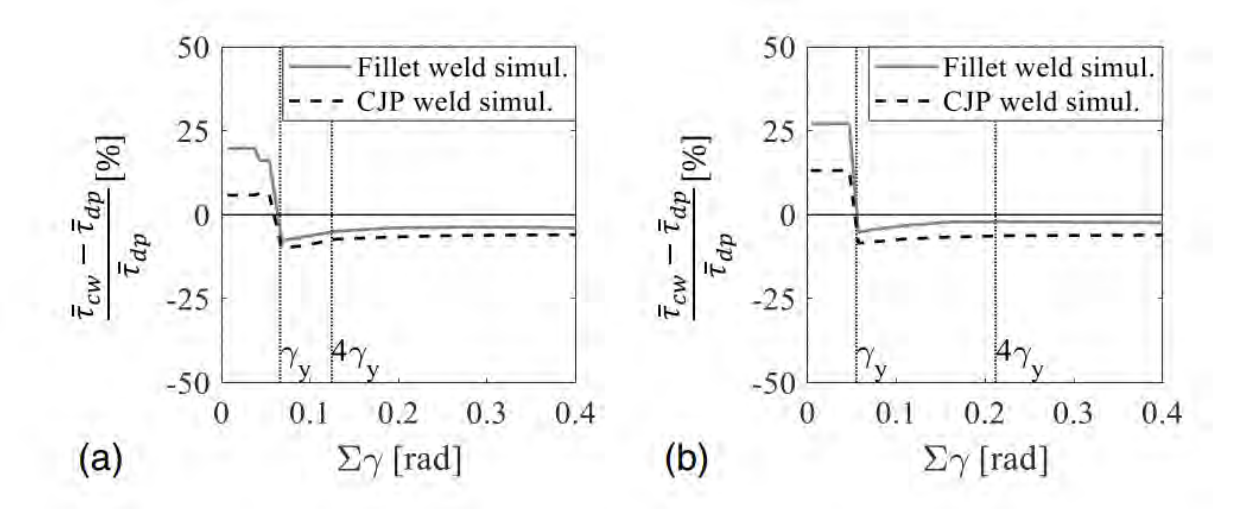


Figure 2.14: Relative difference in average shear stresses between doubler plate and column web versus accumulated panel zone shear distortion: (a) column W610×195; and (b) column W360×592 (Skiadopoulos et al. 2021)

2.4 Summary

The literature review presented in this chapter confirmed that narrower doubler plates have the potential to be used in steel moment connections with wide flange columns, but further investigation is required to ensure the viability of this option since it may lead to the reduction of panel zone stiffness and strength. The resultation of the experimental evaluation of other doubler plate details, e.g., offset doubler plates, column flange fillet welded doubler plate, and extended doubler plates, in building structures showed that they could be viable options in the design of pipe rack moment connections to avoid complete joint penetration welds. However, such details often lack design methods consistent with the Canadian practice.





3 MODULE BEAM-TO-COLUMN CONNECTION DESIGN

3.1 General

To transfer the demands, including bending, axial force, and shear, from beams to the column in pipe racks, welded or end-plate beam-to-column moment connections are typically used. Figure 3.1 shows an example of a welded beam-to-column moment connection. Web doubler plates are often used to strengthen the column web when its thickness is not sufficient to transfer the beam moment through shear to the column, and in the case of a slender panel zone to reduce its h/t_{cw} , where h is the web depth and t_{cw} is the web thickness. Groove welds are typically used to attach the web doubler plates to the column radius in the connection region, as shown in Figure 3.1 (Section A-A). The detail and type of weld can vary from fabricator to fabricator because of the challenges associated with the implementation of such welds in the k-region of the column section and along the column web stiffeners. An example of such beam-to-column connection details is shown in Figure 3.1 where a PJP weld is used to connect the doubler plate to the column web due to the available welding position and the inherent difficulty with surface preparation and inspection.

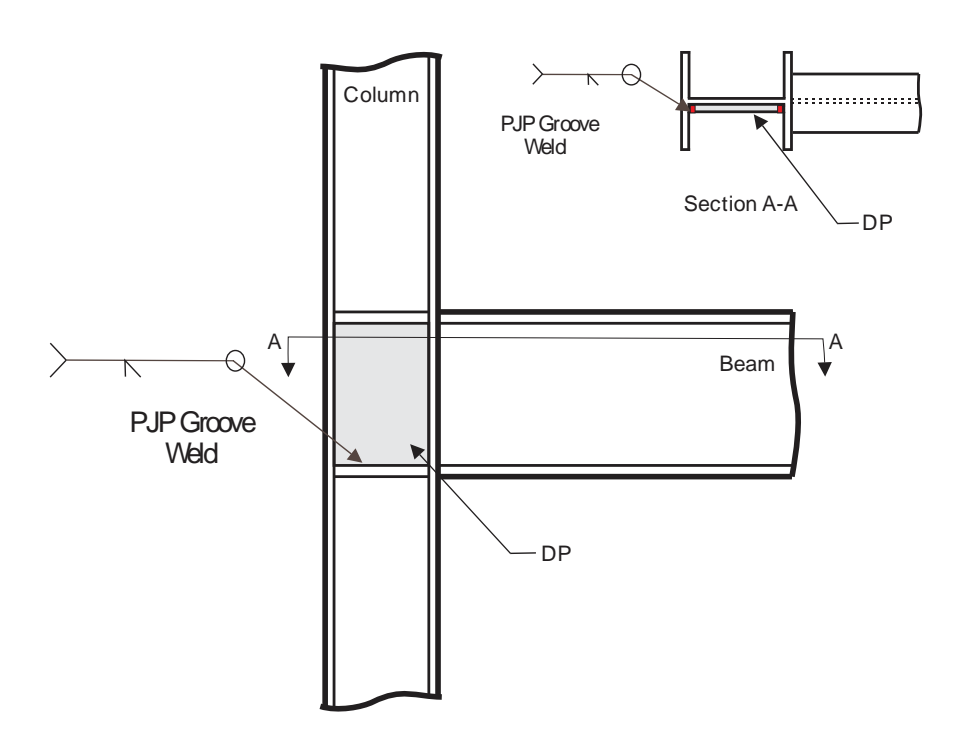


Figure 3.1: Typical pipe rack beam-to-column welded connection detail





3.2 Connection Design in accordance with Current Practice

The structural design of the pipe rack moment connection shown in Figure 3.2 is illustrated here. Figure 3.2 presents a baseline welded moment connection representing the current practice, which consists of a full-sized (or standard) doubler plate attached to the column web using PJP welds. The design is performed in accordance with the provisions of the Canadian steel design standard, CSA S16 (CSA 2024) and the American Institute of Steel Construction Specification for Structural Steel Buildings, AISC 360 (2022). It should be noted that for ease of explanation, CSA S16 terminology and variables are used in the design steps below. The beam and column consist of wide-flange sections conforming to 350W steel with the specified yield strength $F_y = 350$ MPa. The same W250×73 was selected for the beam and column. Table 3.1 shows the cross-section properties for the beam and column.

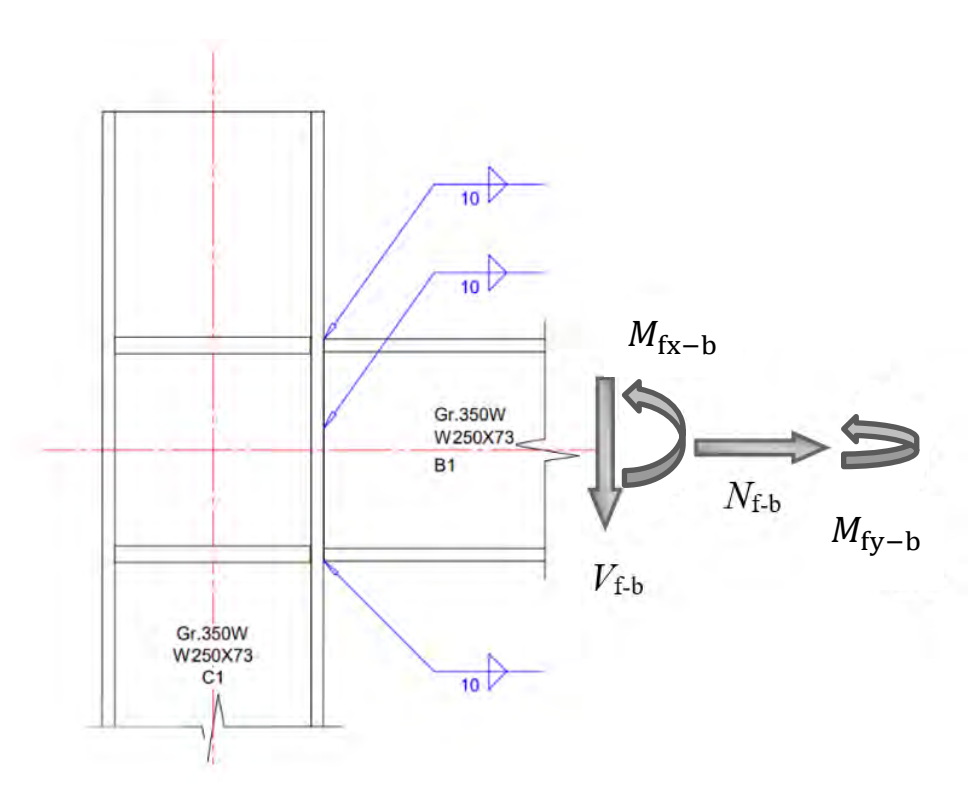


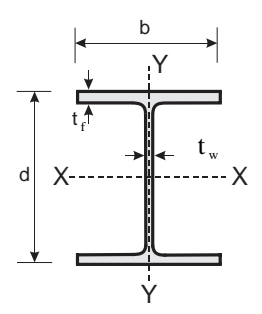
Figure 3.2: Welded beam-to-column moment connection of a pipe rack structure (LIMCON 2006)





Table 3.1: Beam and column crosse section properties (subscripts b and c are used in this document to introduce cross-section properties of beams and columns, respectively)

Section	W250×73		I_{x}	113×10^6	mm^4
b	254	mm	$I_{ m y}$	38.9×10^{6}	mm^4
t_f	14.2	mm	Z_{x}	990×10^3	mm^3
d	254	mm	Z_{y}	464×10^3	mm^3
t_{w}	8.64	mm	$S_{\rm x}$	895×10^3	mm^3
A	9290	mm^2	S_{y}	306×10^3	mm^3
r_{x}	110.0	mm	J	579×10^3	mm^4
$r_{ m y}$	64.5	mm	$C_{ m w}$	556×10^9	mm^6



Various loading conditions were evaluated and the design under the most critical load case are presented. The load case includes a strong-axis moment $M_{\rm fx-b}$, a weak-axis moment $M_{\rm fy-b}$, a shear force $V_{\rm f-b}$, and an axial force, $N_{\rm f-b}$, applied at the face of the column, as shown in Figure 3.2. The connection design forces due to the factored applied loads are presented in Table 3.2.





Table 3.2: Design forces on connection components under applied loads

Connection Component	Force or Moment
Beam strong-axis moment, M_{fx-b}	160 kN-m
Beam weak-axis moment, $M_{\rm fy-b}$	0 kN-m
Beam shear force, V_{f-b}	230 kN
Beam axial force, N_{f-b}	250 kN
Column web axial force, C_f	230 kN
Axial tension in the beam flanges, T_{f-bf}	792 kN
Axial tension in the beam web, T_{f-bw}	0 kN
Axial compression in the beam flanges, C_{f-bf}	542 kN
Axial compression in the beam web, C_{f-bw}	0 kN
Beam web bending moment, M_{f-bw}	13 kN-m
Column web panel shear, V_{f-cw}	792 kN
Stiffener tension, T_{f-s}	395 kN
Stiffener compression, C_{f-s}	542 kN

The factored design forces are obtained as follows based on Figure 3.3. The axial tension force, T_{f-bf} , in the beam flanges is:

$$T_{\text{f-bf}} = \frac{M_{\text{fx-b}}}{d_b - t_{bf}} + \frac{N_{\text{f-b}}}{2} = 792 \text{ kN}$$
 (3-1)

where $d_b = 254$ mm is the beam depth and $t_{bf} = 14.2$ mm is the beam flange thickness.

The axial tension force in the beam web, T_{f-bw} , is:

$$T_{f-bw} = 0 (3-2)$$

The axial compression force in the beam flanges, C_{f-bf} , is:

$$C_{\text{f-bf}} = \frac{M_{\text{fx-b}}}{d_b - t_{bf}} - \frac{N_{\text{f-b}}}{2} = 542 \text{ kN}$$
 (3-3)





The beam web bending moment, M_{f-bw} , is:

$$M_{\text{f-bw}} = M_{\text{fx-b}} \times \frac{S_{x-bw}}{S_{x-b}} = 13 \text{ kNm}$$
(3-4)

where $S_{\text{x-bw}} = \frac{(d_b - 2t_{bf})^2 \times t_{bw}}{6} = 73 \times 10^3 \text{ mm}^3$ is the beam web elastic section modulus, $t_{bw} = 8.6 \text{ mm}$ is the beam web thickness, and $S_{\text{x-b}} = 895 \times 10^3 \text{ mm}^3$ is the beam elastic section modulus.

The column web panel shear, V_{f-cw} , is:

$$V_{\text{f-cw}} = T_{\text{f-bf}} = 792 \text{ kN}$$
 (3-5)

where the resulting axial tension in the beam flanges is transferred to the column through column web panel shear.

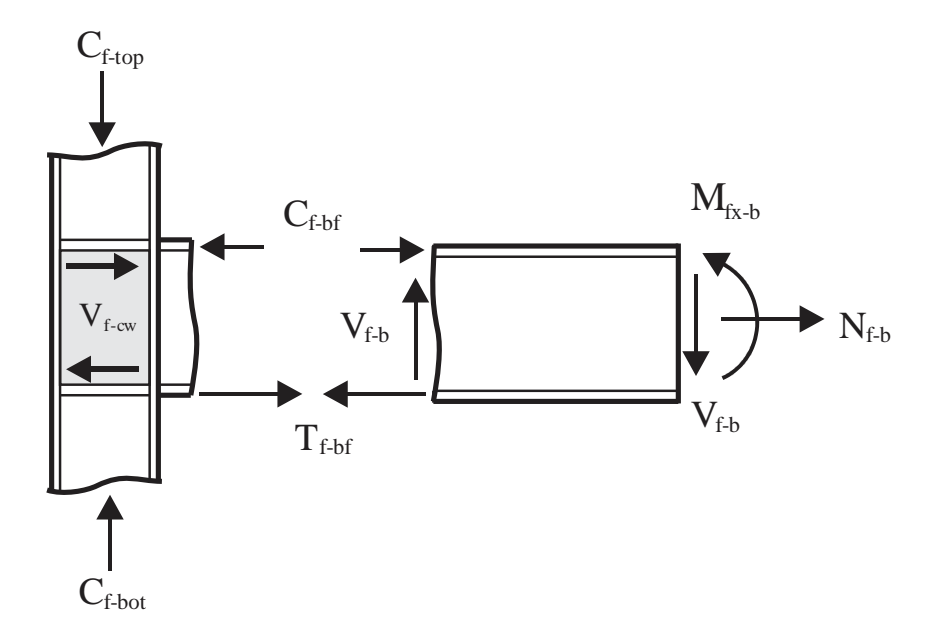


Figure 3.3: Free-body diagram of the beam-to-column connection under bending moment and axial force

The design steps for the connection presented in Figure 3.2 are as follows:





Step 1) Design the beam flange fillet weld following S16 Clause 13.13.2.2:

$$V_{r-fw} = 0.67 \phi_w A_w X_u (1.00 + 0.5 \sin^{1.5} \theta)$$

$$V_{r-fw} = 1165 \text{ kN} > T_{f-bf} = 792 \text{ kN}$$
(3-6)

where $V_{\rm r-fw}$ is the beam flange factored weld resistance for direct shear and tension-induced shear, $A_{\rm w}$ is the area of the fillet weld where $A_{\rm w}=0.707\times l_{\rm w}\times D=3531~{\rm mm^2}$, $l_{\rm w}=499~{\rm mm}$ is the fillet weld length, 2b- $t_{\rm w}$, and $D=10~{\rm mm}$ is the weld leg size, $X_{\rm u}=490~{\rm MPa}$ is the ultimate tensile strength of the matching electrode, and θ is the angle of the weld segment axis with respect to the line of action of the applied force and is equal to 90° .

Step 2) Design the beam web fillet following S16 Clause 13.13.2.2:

$$V_{\text{r-ww}} = 0.67 \phi_w A_w X_u (1.00 + 0.5 \sin^{1.5} \theta)$$

$$V_{\text{r-ww}} = 1.56 \text{ kN/mm} > 1.19 \text{ kN/mm}$$
(3-6)

where $1.56 \,\mathrm{kN/mm}$ is the weld strength, $A_w = 0.707 \times l_w \times D$, $D = 10 \,\mathrm{mm}$, $l_w = 193 \,\mathrm{mm}$ is the fillet weld length, θ is equal to 0°, and $1.19 \,\mathrm{kN/mm}$ is the resultant of the demands induced onto the web weld due to the shear, axial, and moment applied as follows:

- Shear force/length of weld: $\frac{V_{\text{f-b}}}{2l_w} = \frac{230 \times 10^3}{2(193)} = 0.60 \text{ kN/mm}$
- Axial force/length of weld: $\frac{T_{\text{f-bw}}}{2l_w} = \frac{0 \times 10^3}{2(193)} = 0 \text{ kN/mm}$
- Moment force/length of weld: $\frac{4 \times M_{f-bw}}{(d_b 2t_{hf})^2} = \frac{4(13 \times 10^3)}{(254 2(14.2))^2} = 1.03 \text{ kN/mm}$
- Resultant force/length of weld: $\sqrt{(0 + 1.03)^2 + (0.60)^2} = 1.19 \text{ kN/mm}$

where $d_b = 254$ mm is the beam's depth and $t_{\rm bf} = 14.2$ mm is the beam flange thickness.

Step 3) Check the unstiffened column flange bending at beam tension flange under the applied tension load in the flange following AISC 360, Section J10-1:

$$T_{\text{r-cfb}} = 0.9 \times 6.25 F_{yc} t_{cf}^2$$
 (3-7)
 $T_{\text{r-cfb}} = 397 \text{ kN} < T_{\text{f-bf}} = 792 \text{ kN}$





where $T_{\rm r-cfb}$ is the factored flange local bending strength, $t_{\rm cf} = 14.2$ mm is the column flange thickness, $F_{\rm yc}$ is the specified yield strength of the column, 350 MPa. Step 3) fails showing that a stiffener is required at the beam tension flange.

Steps 4 & 5) Check the unstiffened column web yielding at both beam tension and compression flanges under the applied tension load in the flange, following AISC 360 J10-2:

$$T_{\text{r-cwy}} = F_{yc}t_{cw}(5k + l_b)$$
 (3-8)
 $T_{\text{r-cwy}} = 562 \text{ kN} < T_{\text{f-bf}} = 792 \text{ kN}$
 $T_{\text{r-cwy}} = 562 \text{ kN} > C_{\text{f-bf}} = 542 \text{ kN}$

where $T_{\rm r-cwy}$ is the factored local web yielding strength, $t_{\rm cw}=8.6\,{\rm mm}$ is the column web thickness, $k=30.5\,{\rm mm}$ is the distance from the outside face of the column flange to the web toe of the flange-to-web fillet, and $l_{\rm b}$ is the bearing length $l_b=t_{bf}+2(10)=34\,{\rm mm}$. Step 4) fails indicating the need for a stiffener at the beam tension flange.

Step 6) Check local web crippling under the applied compression load in the beam flange as per AISC 360 Section J10-4:

$$C_{\text{r-wc}} = 0.75 \times 0.8t_{cw}^{2} \left[1 + 3 \left(\frac{l_b}{d_c} \right) \left(\frac{t_{cw}}{t_{cf}} \right)^{1.5} \right] \sqrt{\frac{EF_{yc}t_{cf}}{t_{cw}}} Q_f$$

$$C_{\text{r-wc}} = 568 \text{ kN} > C_{\text{f-bf}} = 542 \text{ kN}$$
(3-9)

where $C_{\rm r-wc}$ is the factored column web crippling strength, E=200 GPa is the modulus of elasticity of steel, $Q_{\rm f}$ is the chord-stress interaction parameter that is equal to 1 for wide flange sections, and $d_{\rm c}=254$ mm is the depth of the column.

Step 7) Check column web buckling following AISC 360, Section J10-8:

$$C_{\text{r-wb}} = 0.9 \times \left(\frac{24t_{cw}^3 \sqrt{EF_{yc}}}{h}\right) Q_f$$
 (3-10)
 $C_{\text{r-wb}} = 596 \text{ kN} > C_{\text{f-bf}} = 542 \text{ kN}$





where C_{r-wb} is the factored column web buckling strength and h is the clear distance between flanges minus the fillets or corner radii for rolled shapes ($h = d_c - 2k = 193$ mm).

Step 8) Check the unstiffened column web panel in shear, including the contributions from column flanges, as per AISC 360 J10-11, J10-12 assuming inelastic panel zone deformation:

$$V_{r-ws} = \begin{cases} 0.9 \times 0.6 F_{yc} d_c t_{cw} \left(1 + \frac{3 b_{cf} t_{cf}^2}{d_b d_c t_{cw}} \right) & \alpha C_f \le 0.75 C_y \\ 0.9 \times 0.6 F_{yc} d_c t_{cw} \left(1 + \frac{3 b_{cf} t_{cf}^2}{d_b d_c t_{cw}} \right) \left(1.9 - \frac{1.2 \alpha P_r}{P_y} \right) & \alpha C_f > 0.75 C_y \end{cases}$$

$$V_{r-ws} = 527 \text{ kN} < V_{f-cw} = 792 \text{ kN}$$

where $V_{\rm r-ws}$ is the factored shear strength of the column panel zone without a doubler plate, $C_{\rm f}$ = 230 kN is the factored axial force of the column, and $C_{\rm y}$ = 768 kN is the column axial yield strength, which is equal to the column yield strength multiplied by the area of the column web, $b_{\rm cf}$ = 254 mm is the width of the column flange, $d_{\rm b}$ = 254 mm is the depth of the beam, $d_{\rm c}$ = 254 mm is the depth of the column, $t_{\rm cf}$ = 14.2 mm is the thickness of the column flange, $t_{\rm cw}$ = 8.6 mm is the thickness of the column web, and α = 1.0. Step 8) fails, showing that a doubler plate is required at the column web. A 10 mm doubler plate is designed on one side of the column as follows:

$$V_{r-PZ} = 0.9 \left(1 + \frac{3 b_{cf} t_{cf}^2}{d_b d_c (t_{cw} + t_{DP})} \right) \left[0.6 F_{yc} d_c t_{cw} + 0.6 F_{y,DP} L_{DP} t_{DP} \right]$$

$$V_{r-PZ} = 894 \text{ kN} > V_{f-cw} = 792 \text{ kN}$$
(3-12)

where V_{r-PZ} is the factored shear strength of the column panel zone with a doubler plate, $t_{DP} = 10 \text{ mm}$ is the DP thickness, $F_{y,DP} = 300 \text{ MPa}$ is the doubler plate yield strength, and $L_{DP} = 201 \text{ mm}$ is the length of the doubler plate.

Using S16, the factored shear strength of the column panel zone with a doubler plate (excluding the effect of the flanges) can be computed as follows:

$$V_{r-PZ} = 0.9[0.66F_{y,DP}L_{DP}t_{DP} + 0.66F_{yc}d_ct_w]$$

$$V_{r-PZ} = 812 \text{ kN} > V_{f-cw} = 792 \text{ kN}$$
(3-13)





Due to the failure of the two checks in Steps 3) and 4), transverse stiffeners with a thickness of 19.05 mm and a yield stress of 300 MPa are added.

Step 9) Check the transverse stiffener yielding at the beam tension flange following S16 Clause 13.2:

$$T_{\text{r-syt}} = 0.9A_s F_{ys}$$
 (3-14)
 $T_{\text{r-syt}} = 1090 \text{ kN} > T_{\text{f-s}} = T_{\text{f-bf}} - T_{\text{r-fb}} = 395 \text{ kN}$

where $T_{\rm r-syt}$ is the stiffener's factored yield strength at the beam tension flange, $A_{\rm s}=2(b_{se}\times t_s)=4039~{\rm mm^2}$ is the total cross-sectional area of stiffeners, $b_{\rm se}=106~{\rm mm}$ is the effective width of the stiffeners, $t_{\rm s}=19.05~{\rm mm}$ is the thickness of the stiffener, and $F_{\rm ys}=300~{\rm MPa}$ is the yield strength of the stiffener. $T_{\rm r-fb}=397~{\rm kN}$ calculated in Step 3) is the flange local bending strength.

To ensure the fillet welds used to connect the stiffeners to the column web and flange are adequate using Equation (3-6), the weld strength is taken to be the minimum between the base metal and the weld metal.

End welds (welds connecting stiffeners to column flanges):

$$V_{\text{r-es}} = min \begin{pmatrix} 0.67 \phi_w A_w X_u (1.00 + 0.5 \sin^{1.5} \theta) = 793 \text{ kN} \\ 0.67 \phi_w A_m F_u = 687 \text{ kN} \end{pmatrix} = 687 \text{ kN} > T_{\text{f-s}} = 395 \text{ kN}$$

Where $A_w = l_w D_s$ is the fillet weld effective area, $l_w = 425$ mm is the length of the fillet, and $D_s = 8$ mm is the size of the fillet weld. $X_u = 490$ MPa, $\theta = 90^\circ$, $F_u = 450$ MPa, and $A_m = 3399$ mm² is the shear area of the effective fusion face.

Side welds (welds connecting stiffeners to column web):

$$V_{\rm r-ss} = min \begin{pmatrix} 0.67\phi_w A_w X_u (1.00 + 0.5 \sin^{1.5}\theta) = 966 \text{ kN} \\ 0.67\phi_w A_m F_u = 1255 \text{ kN} \end{pmatrix} = 966 \text{ kN} > T_{\rm f-s} = 395 \text{ kN}$$

where $l_w = 776 \text{ mm}$, $D_s = 8 \text{ mm}$, $X_u = 490 \text{ MPa}$, $\theta = 0^\circ$, $F_u = 450 \text{ MPa}$, and $A_m = 6211 \text{ mm}^2$.





Step 10) Check the transverse stiffener yielding and buckling at the beam compression flange following S16 Clauses 13.2 and 13.3.1.1:

Yielding:
$$T_{r-syc} = T_{r-cwy} + 0.9A_s f_{ys}$$
 (3-15)
 $T_{r-syc} = 1652 \text{ kN} > C_{f-s} = C_{f-bf} = 542 \text{ kN}$

Stability:
$$C_{r-sb} = \frac{0.9A_s F_{ys}}{(1 + \lambda^{2n})^{\frac{1}{n}}}$$

$$\lambda = \frac{Kl_s}{r} \sqrt{\frac{F_{ys}}{\pi^2 E}} = 0.52$$

$$C_{r-sb} = 1124 \text{ kN} > C_{f-s} = 542 \text{ kN}$$
(3-16)

where $T_{\rm r-syc}$ is the factored yield strength at beam compression flange, $T_{\rm r-cwy}=562$ kN is the unstiffened column web yield strength obtained in Step 5), $C_{\rm r-sb}$ is the transverse stiffener buckling strength, λ is a slenderness parameter, $\frac{Kl_s}{r}$ is the effective slenderness ratio, K=1 is the effective length factor, $l_s=225$ mm is the length of the stiffener, $r=\sqrt{\frac{l_s}{A_s}}=5$ mm is the radius of gyration of the stiffener plate, $I_s=\frac{2b_st_s^3}{12}=1.4\times10^5$ mm³ is its moment of inertia about its weak axis, $b_s=122$ mm is the width of the stiffener, and n=1.34 is the residual stress factor used for hot-rolled and hollow structural sections.

The critical limit state among the 10 checks performed here is the column web panel shear strength with a utilization ratio of 97%. Figure 3.4 summarizes the dimensions and weld sizes of the plates and stiffeners of the connection presented in Figure 3.2.





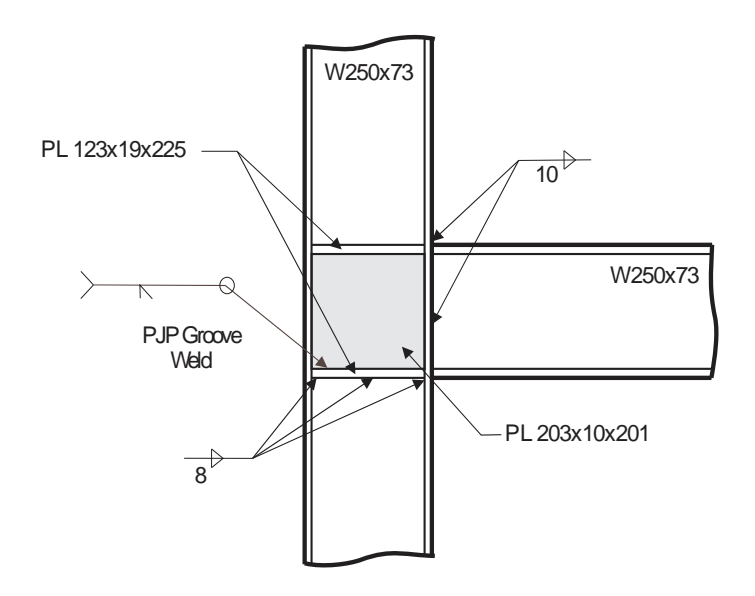


Figure 3.4: W250×73 column to W250×73 beam welded moment connection





4 TEST SPECIMENS AND SETUP

A total of 12 full-scale moment-resisting frame joints were tested to examine the behaviour of steel beam-to-column connections used in pipe rack structures with the focus on column web doubler plates. Testing was conducted at the I.F. Morrison Structural Engineering Laboratory of the University of Alberta. The test specimens and test setup, including test fixtures, loading and instrumentation, and ancillary tests are presented in this chapter.

4.1 Proposed Detail

Due to the challenges associated with the conventional doubler plate detail shown in Figure 1.1c, a new doubler plate attachment detail using fillet welds is proposed here (see Figure 1.1d). This detail involves a doubler plate with reduced dimensions, named the reduced doubler plate as shown schematically in Figure 1.1d. To study the behaviour of the reduced doubler plate, two different reductions are used: 1) a doubler plate that is reduced by one D on all sides with respect to the dimensions used in the current practice (Figure 1.1c), and 2) a doubler plate that is reduced by 2D on all sides with respect to the dimensions used in the current practice (Figure 1.1c), where D is the fillet weld size used to attach the doubler plate to the column web. The reduction is measured in the horizontal direction, between the column web toe and the doubler plate edge, and the same reduction is applied in the vertical direction above and below the doubler plate, between the column web stiffener fillet weld and the double plate edge. It is expected that the new doubler plate detail helps reduce costs and labour time associated with performing groove welds while meeting strength requirements. Table 4.1 shows the proposed detail versus the regular and no doubler plate cases.

4.2 Test Specimens

The test program includes 12 tests. The test specimens shown in Figure 4.1 represent an exterior beam-to-column moment connection taken out of pipe rack structures, as shown in Figure 4.2. The length of the beam was determined by ensuring the moment and shear combination at the face of the column cause first shear yielding in the panel zone area, while meeting laboratory constraints. Stiffeners are located in the beam web along the direction of loading and at the top of the column to help resist the concentrated forces induced at these locations. Additionally, horizontal stiffeners are added in the column panel zone on either side. The connections tested either consist of a W250×58 beam and column or a W410×60 column connected to a W410×100 beam.





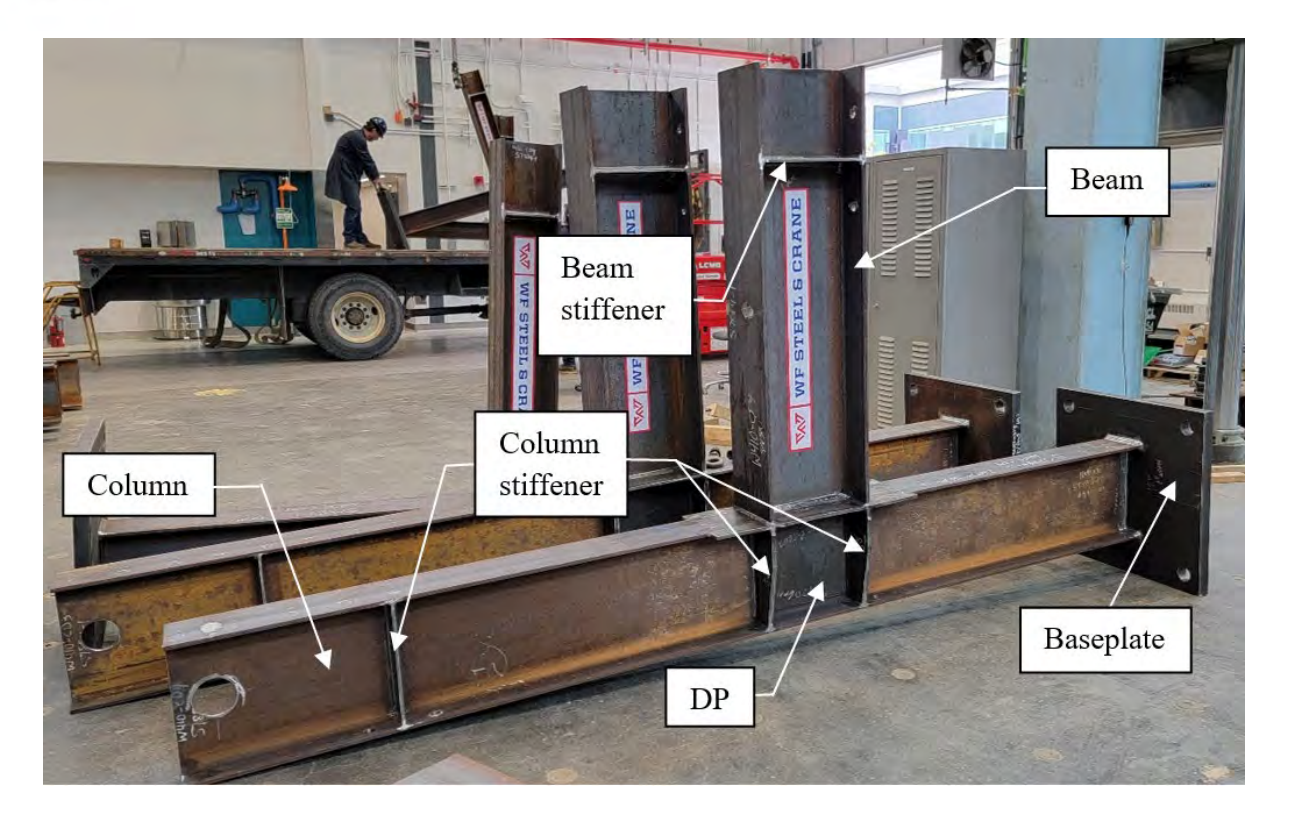


Figure 4.1: Exterior beam-to-column moment connection specimen in the lab



Figure 4.2: Pipe rack structure with an exterior beam-to-column connection highlighted (WF Steel and Crane 2021)





The experimental program consists of six connection details that use a W250×58 section for both the beam and column of the specimen (W250 specimens) and six connections that use a W410×100 beam with a W410×60 column (W410 specimens). Tables 4.1 and 4.2 give the details of each W250 and W410 specimen, respectively. W250-NDP and W410-NDP specimens were designed without column web doubler plate (NDP). W250-DP and W410-DP specimens consist of the standard doubler plate case (DP), as shown in Figure 1.1c. In this detail, the doubler plate covers the entire web on one side of the column and is welded to the column web using a partial joint penetration groove weld. W250-RDP1 and W410-RDP1 specimens were designed with a reduced doubler plate detail using fillet welds and consist of two identical specimens each (RDP1A and RDP1B). W250-RDP2 and W410-RDP2 specimens consist of a further reduced doubler plate fillet welded to the web. Two identical specimens were tested for each (RDP2A and RDP2B). Table 4.3 presents the measured member sizes and stiffener, or continuity plates (CP), details of each specimen set. Table 4.4 outlines their measured cross-sectional dimensions, which were obtained by measuring the dimensions of each specimen in the laboratory then averaging the values of each component. For more information on the specimens, see Appendix D for the specimen drawings.





Table 4.1: W250 specimen matrix

Specimen	Specimen	Doubler Plate	Connection Detail
Number	ID	Dimensions	
		(mm)	
1	W250-	No doubler	
	NDP	plate	CJPGW CJPGW CJPGW CJPGW
2	W250- DP	184×8×207	20.5 184.0 20.5 CJPGW CJPGW CJPGW CJPGW DP 184x8x207



Table 4.2: W250 Specimen matrix (cont.).

3	W250-	168×8×191	
	RDP1A		
			⟨CJPGW
			28.5 168.0 28.5
			E 0 8V
			5. C1bCm) ⁶ 8 8
4	W250-	168×8×191	4 2 000
	RDP1B		
			121
			CJPGW
			Тур.
			DP 168x8x191
5	W250-	152×8×175	
	RDP2A		
			CJPGW
			36.5 152.0 36.5
			7
			CJPGW> 6 CJPGW>
6	W250-	152×8×175	4. 8h
	RDP2B		
			£ 1
			< CJPGW
			Typ. 6 DP 152x8x175





Table 4.3: W410 specimen matrix

Specimen	Specimen	Doubler	Connection Detail	
Number	ID	Plate		
		Dimensions		
		(mm)		
7	W410-	No doubler	/ CJPGW	
	NDP	plate	12	
			1.60	
			CJPGW>—R	
			66	
			(a)	
			2 CJPGW	
			Тур. 6	
8	W/410	229,7,260		
8	W410- DP	338×6×360	CJPGW	
	DF		21.2 338.0 21.2 / 12	
			06	
			CJPGW CJPGW	
			60	
			0.8	
			ē; CJPGW	
			Typ. 6 DP 338x6x360	



Table 4.4: W410 specimen matrix (cont.)

		_	
9	W410-	326×6×348	/ CJPGW
	RDP1A		27.2 326.0 27.2
			5 1 12 12 12 12 12 12 12 12 12 12 12 12 1
			115.0
			DP 326x6x348
10	W410-	326×6×348	CJPGW> 6D
10		320~0~348	, G 6V
	RDP1B		15.0
			56
			CJPGW
			тур6
11	W410-	314×6×336	CJPGW
	RDP2A		33.2 314.0 33.2
			26
			21.0
			DP 314x6x336
12	W/410	314×6×336	CJPGW> 6 P
12	W410-	314×0×330	6
	RDP2B		51.0
			5.61
			CJPGW
			Тур. 6
			134.60





Table 4.5: Measured sizes of members and stiffeners

Specimen	Beam	Column	CP thickness (mm)	DP thickness (mm)
Group				
W250	W250×58	W250×58	12.7	8.0
W410	W410×100	W410×60	19.1	6.0

Table 4.6: Measured cross-sectional dimensions

Member	d (mm)	t _w (mm)	b_f (mm)	t_f (mm)
W250×58	251	8.3	204	13.7
W410×60	405	8.2	179	12.5
W410×100	413	10.2	259	16.6

4.3 Test Specimen Design

The doubler plate dimensions in Tables 4.1 and 4.2 are obtained by following the design steps described in Chapter 3 for each connection assuming an applied shear at the tip of the beam sufficient to fail the panel zone in shear before any limit states in the connection and members. For the sake of specimen design and test setup, the resistance factors used in design are all set to 1.0. Additionally, to ensure that the first mode of failure to occur is doubler plate yielding in shear, the resulting shear from Step 7 was used to back calculate the required shear force that should be reached to yield the column panel first. In all the connections, yielding of the doubler plate is the governing limit state. The checks performed for all the specimens are summarized in Table 4.7, following the same steps in Chapter 3.





Table 4.7: Summary of test specimen design

Step 1)	Beam flange-to-column flange weld
Step 2)	Beam web-to-column flange weld
Step 3)	Unstiffened column flange bending at beam
	tension flange
Step 4)	Unstiffened column web yielding at beam
	tension flanges
Step 5)	Unstiffened column web yielding at beam
	compression flange
Step 6)	Local web crippling
Step 7)	Column web yielding/buckling
Step 8)	Unstiffened column web panel in shear
Step 9)	Transverse stiffener yielding at the beam
	tension flange
Step 10)	Transverse stiffener yielding and buckling at
	the beam compression flange

4.4 Test Setup

The experimental test setup including specimen W250-RDP1 is shown in Figure 4.3. As shown, the specimen consists of the beam-to-column moment connection with a column fixed at its base and pinned at its top end. At the column base all degrees of freedom are fixed to avoid rotation, vertical, and horizontal translations, whereas at the column top, rotation is allowed but vertical and horizontal translations are restricted. At 1.2 m away from the column face an actuator is connected to the bottom flange of the beam to apply the required loads (see Figure 4.3). The support allows movement of the beam in Y-direction since loading will be applied along that direction. Additionally, a lateral bracing system to prevent the beam from out-of-plane movement is added. The rest of the specimens use the same test setup as W250-RDP1.





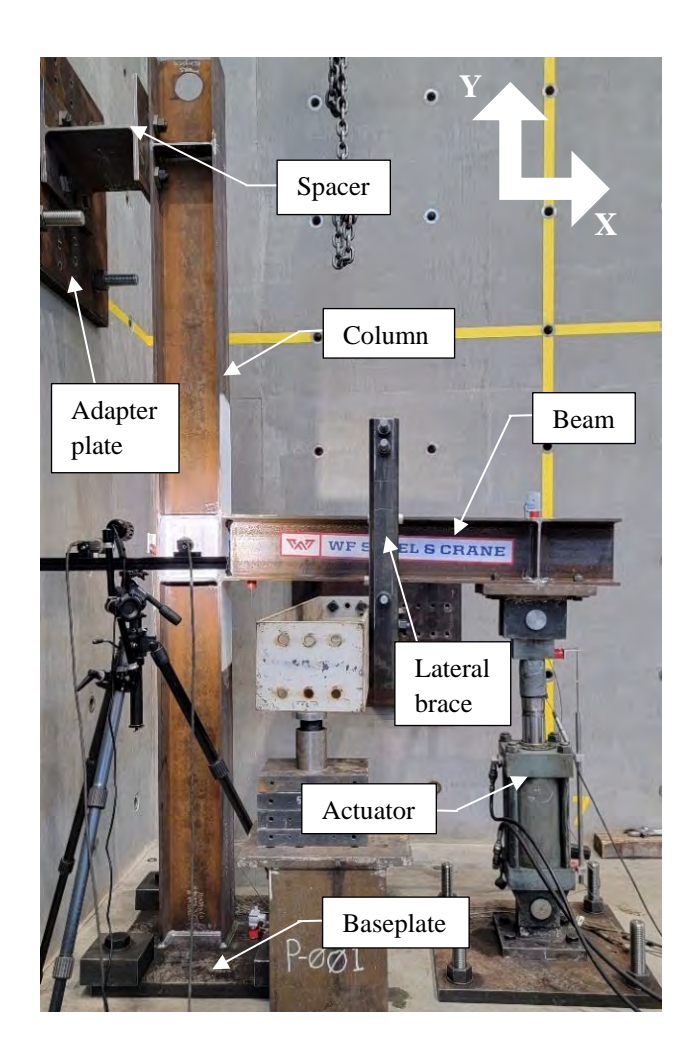


Figure 4.3: W250-RDP1 specimen before testing

4.4.1 Column Boundary Conditions

A column base plate, 760×760×50.8 mm, is welded to the column base using a 12 mm fillet weld, as shown in Figure 4.4. The location of the column on the base plate is controlled by the depth of the column and length of the beam to ensure enough distance away from the actuator. The length and width of the plate, as well as the hole diameter, were defined by the strong floor's hole pattern. As shown in Figures 4.5 and 4.6, four 2-inch diameter bolts were used to connect the plate to the strong floor using 88.9 mm thick plate washers since the bolt length available in the lab was 8-inch. The baseplate is designed to resist the maximum moment, shear, and axial forces induced after yielding and strain-hardening of the doubler plate to ensure the base plate resists the expected forces. The design demands were obtained using a numerical model created in the ABAQUS finite element program (Simula 2023), as described in Chapter 7. In the finite element analysis, an ultimate vertical displacement of 190 mm was applied to the beam tip to obtain force demands. As





a result, a maximum of 537 kN axial force, 329 kN shear force, and 398 kN-m moment were induced at the column base, including a 1.25 factor of safety.

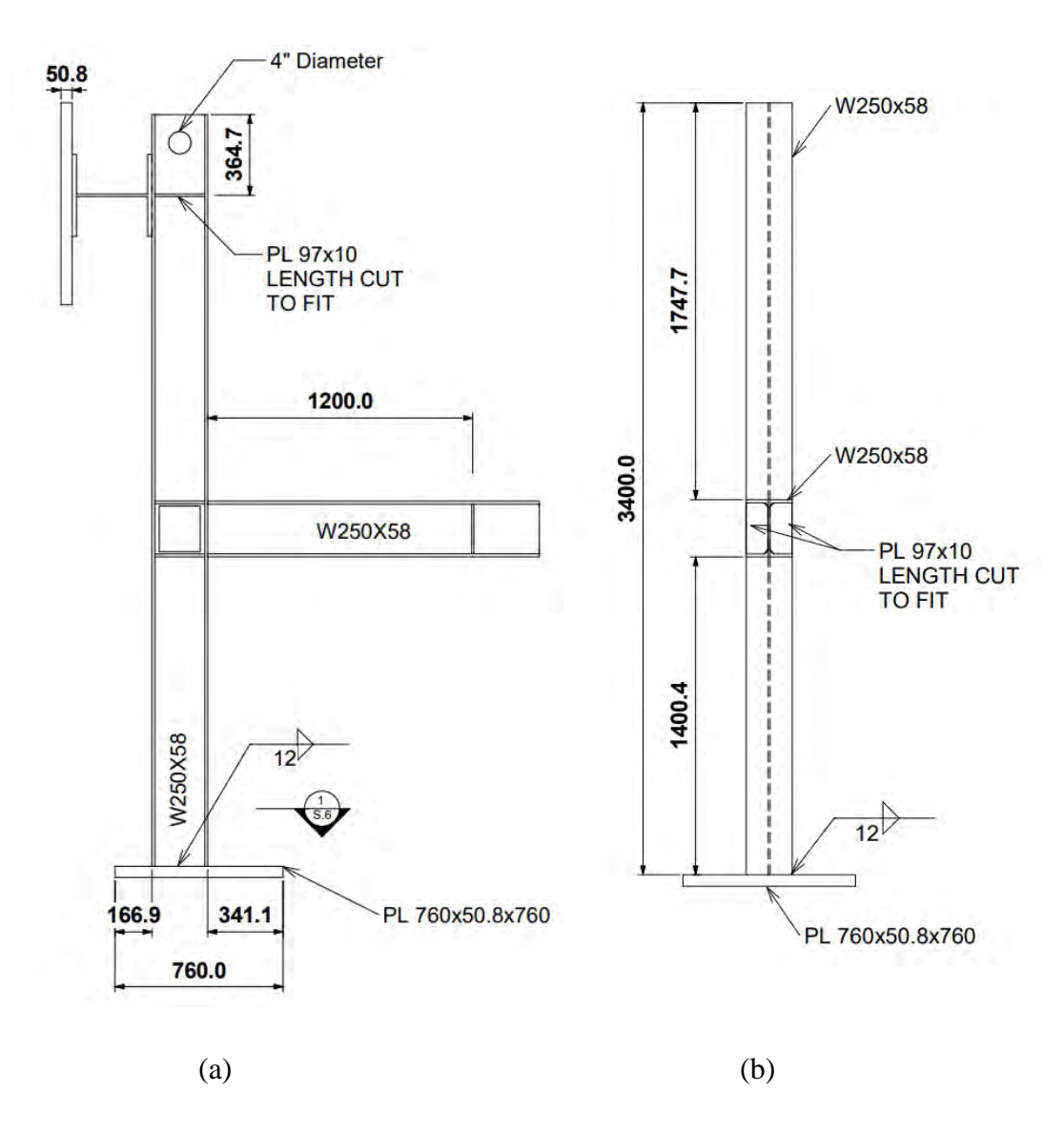
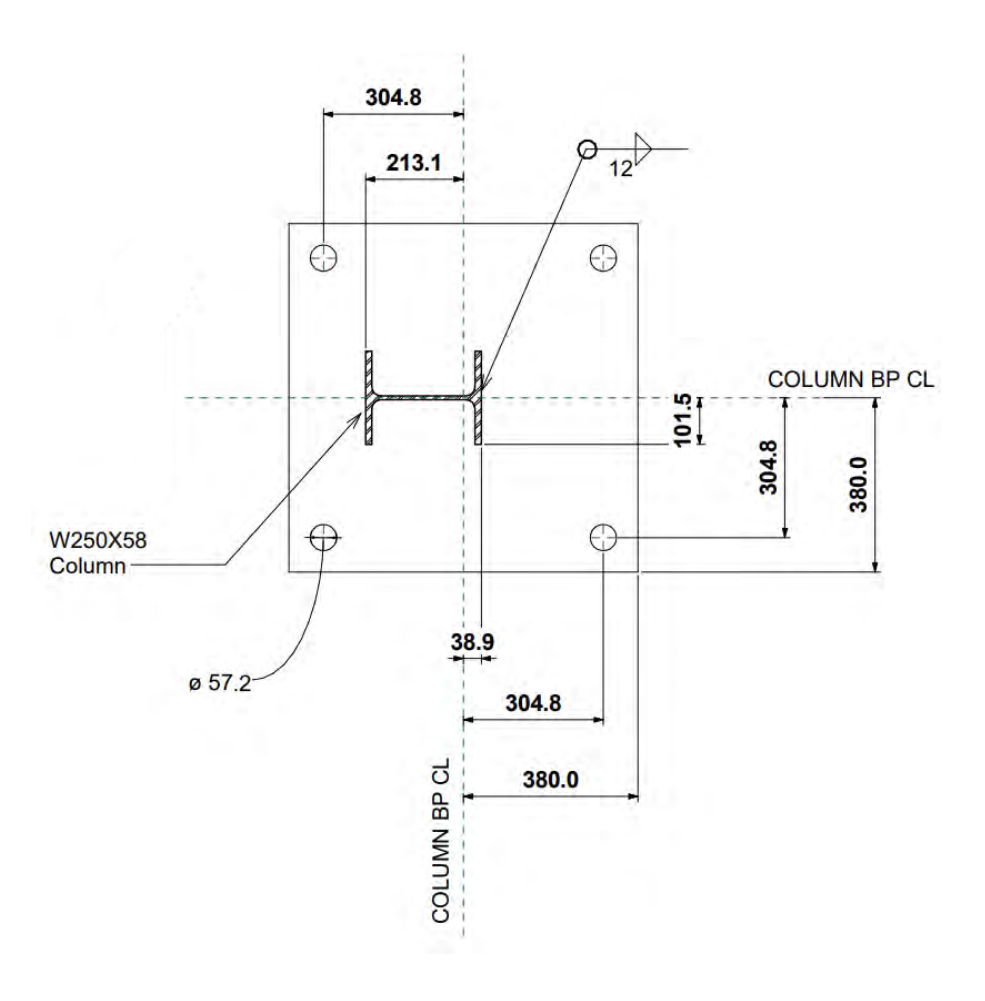


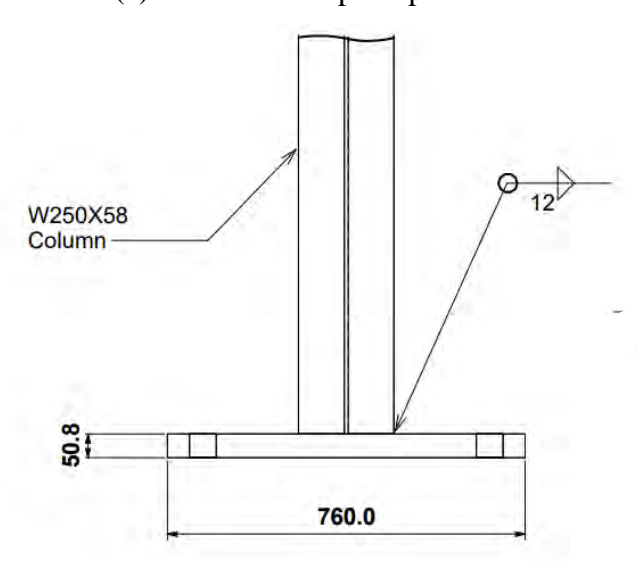
Figure 4.4: Elevation of test specimen W250-RDP1: (a) side view, (b) front view (all dimensions are in mm)







(a) Column base plate plan view



(b) Column base plate elevation

Figure 4.5: Column base plate: (a) plan view, (b) elevation





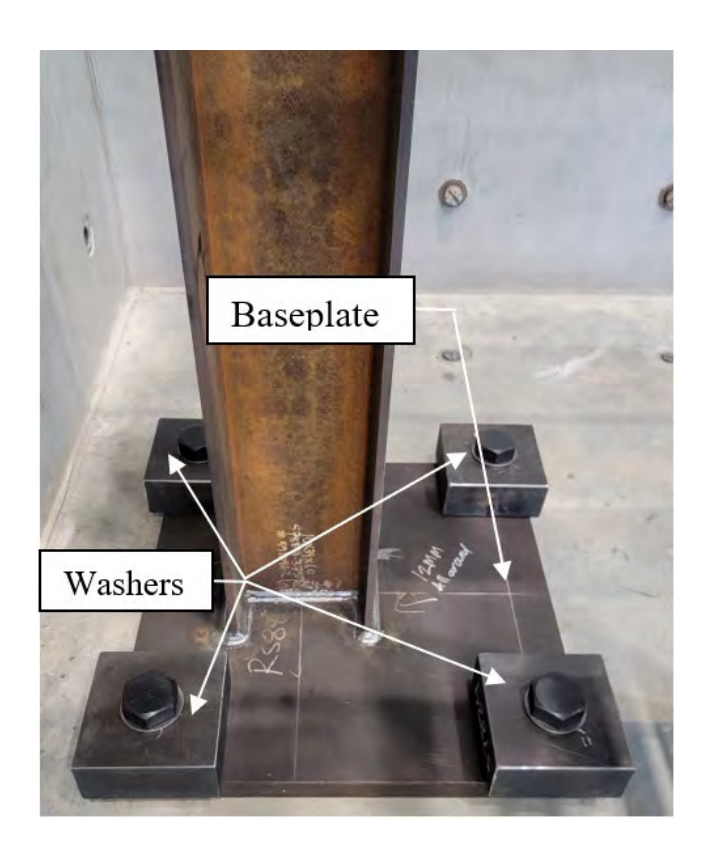


Figure 4.6: Column base plate in the laboratory during assembly

The adapter plate shown in Figure 4.7, along with the W-shape spacer in Figures 4.8a and 4.8b, are used to connect the column top to the strong wall. The photograph of the column top adapter plate and spacer is shown in Figure 4.8c. Two identical adapter plates are fabricated, one is used for the column top connection, whereas the next adapter plate is used for the lateral bracing system. The adapter plate has a thickness of 50.8 mm (2-inch) with 22 threaded holes at a grid spacing of 6×3 inches. The threaded holes have a diameter of 1-inch, and the through holes have a diameter of 2-inches to match the strong wall's grid.

The spacer is a W360×147 section that is designed to resist the maximum tensile force (~330 kN) induced at the column top without local yielding and crippling of the section, as well as prying and bending of the flange. The column shear force is extracted from the model and translated to a tensile force at the column top. The spacer has a different bolt hole spacing on either flange, as shown in Figure 4.8a and 4.8b, to accommodate the edge spacing requirements on the side





connected to the column flange of the specimen. The other flange has four 1-inch bolt holes with the same hole pattern as the adapter plate.

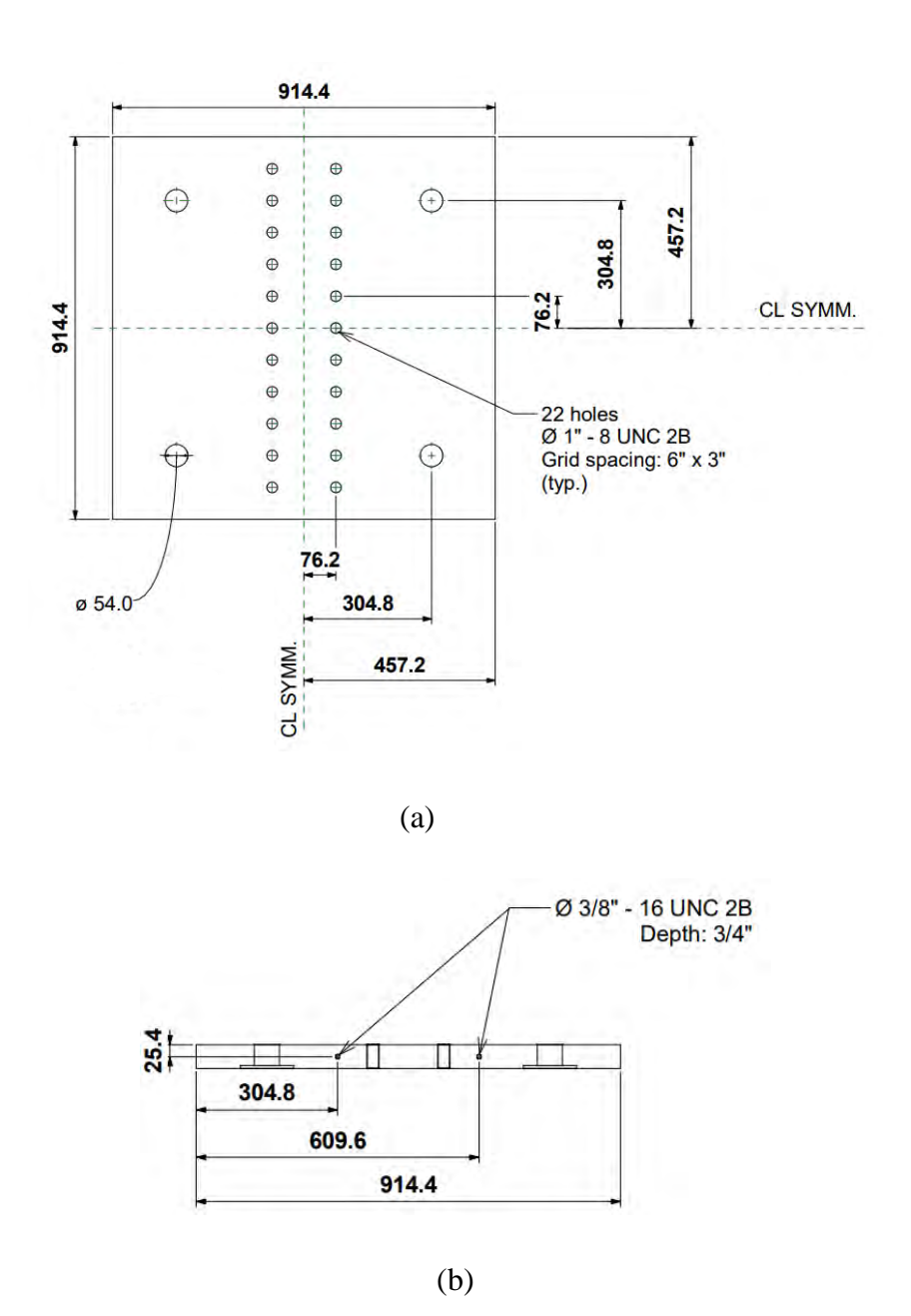


Figure 4.7: (a) Adapter plate front view, (b) Adapter plate elevation





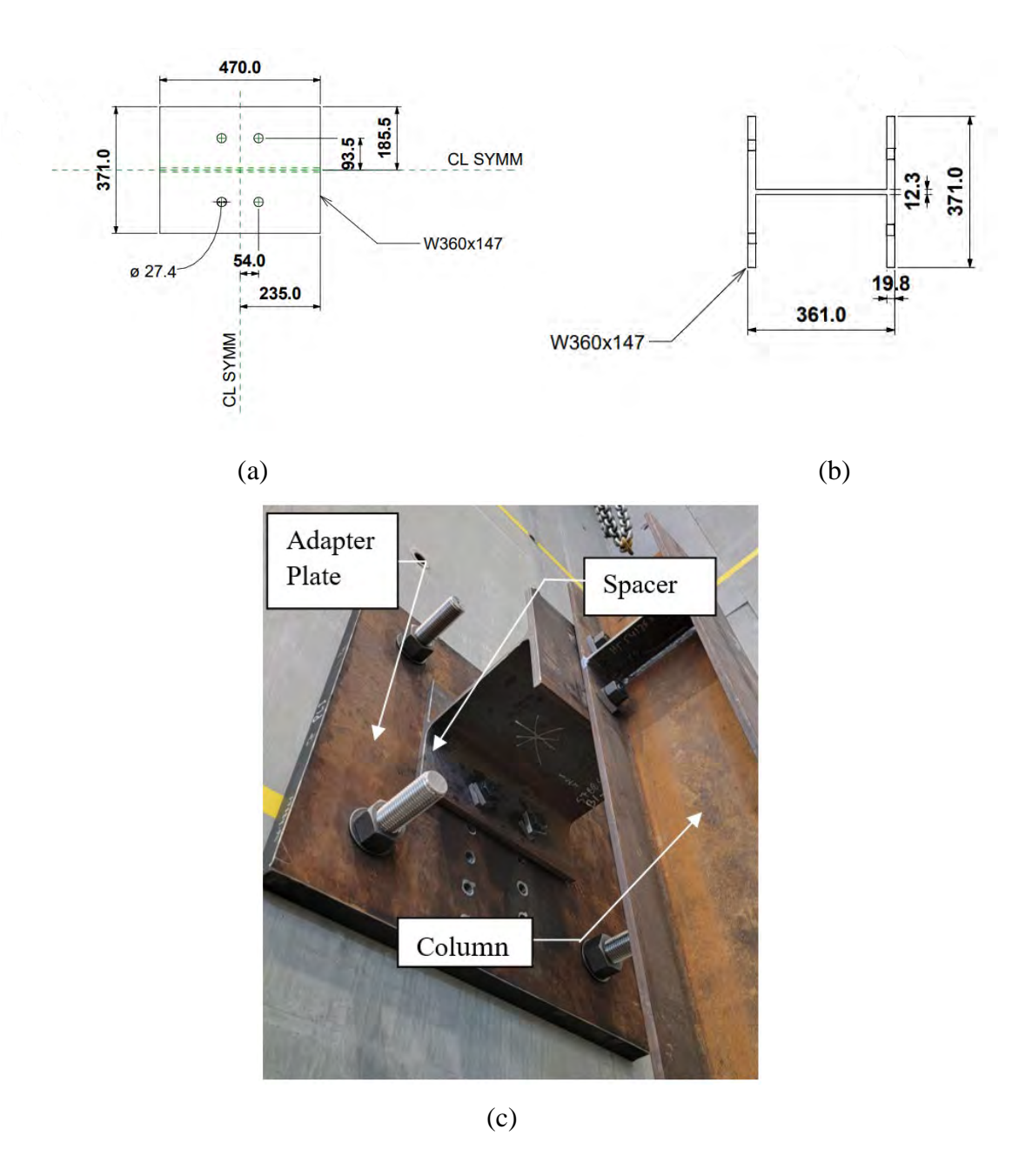


Figure 4.8: Column boundary condition: (a) Spacer W-section plan view, (b) Spacer W-section elevation, (c) Column top boundary in the laboratory

4.4.2 Lateral Bracing System

To avoid lateral out-of-plane movement of the beam during loading, a lateral bracing system that consists of a set of hollow structural sections (HSSs) is used, which involves two HSS $101.6\times101.6\times12.7$ that are 914 mm (3 ft) long on the outside and another two HSS $76.2\times76.2\times6.4$ on the inside that are 610 mm (2 ft) long, as shown in Figure 4.9a. The inner HSS move slightly





outwards to accommodate the W410 specimens since the W410×100 beam has a wider flange, 259 mm, as opposed to the W250 specimens that have a 203 mm flange width. Figure 4.9b shows the bracing system on the W250-RDP1 specimen. The HSS sections are connected using 1-inch rods, with one rod running across the top and four shorter rods to accommodate the movement of the HSS at two locations. The length of the rods is chosen according to the width of the HSS, the thickness and number of both the nuts and washers, and a 38.1 mm (1.5-inch) extension on either end of the HSS's outer faces. Additionally, an extra 50.8 mm (2-inch) is left to ensure there's room to move the HSS between different specimens.

Local yielding, local buckling and flexural stiffness of the system are checked to ensure the brace will carry the applied loads in the case of beam out-of-plane movement. The lateral load is calculated using the following equation as per Section A-6-7 of AISC 360:

$$P_{br} = 0.02 \frac{M_r C_d}{h_o}$$

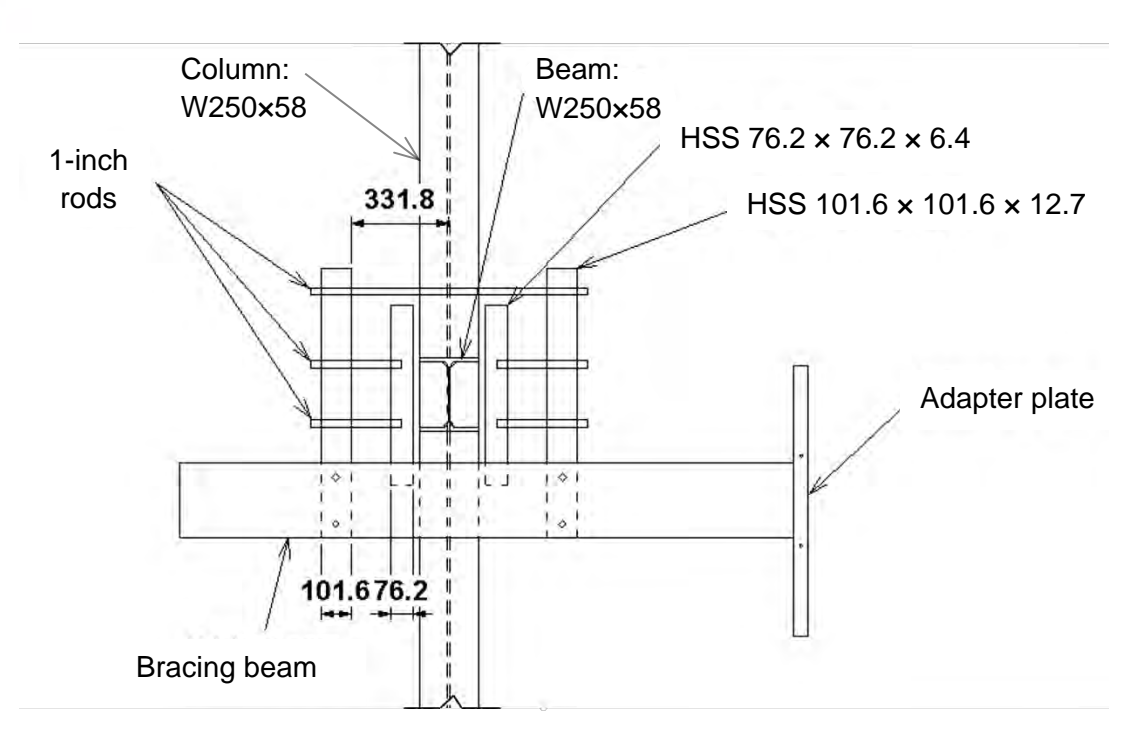
$$P_{br} = 36 \text{ kN}$$
(4-1)

where $M_{\rm r}=M_{\rm p}=746\,{\rm kN}$ is the required flexural strength of the beam within the unbraced lengths adjacent to the point brace, $C_{\rm d}=1$, and $h_{\rm o}=414\,{\rm mm}$ is the distance between flange centroids.

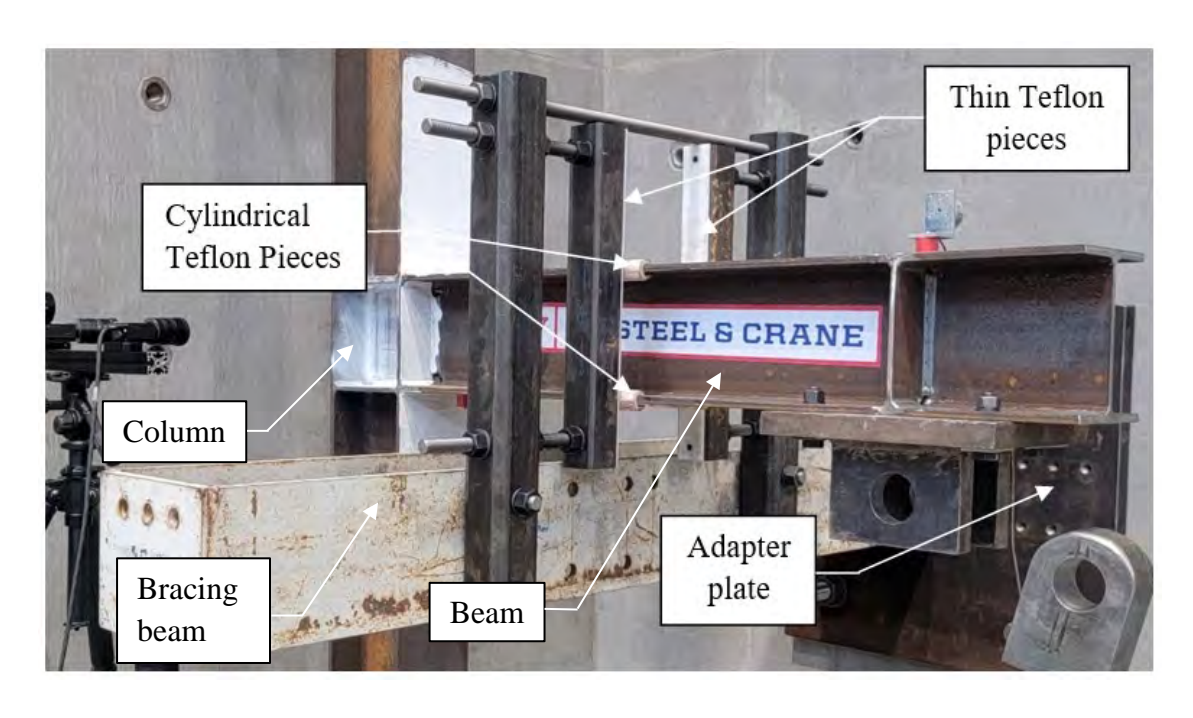
To greatly reduce any sources of friction in the bracing system, AcetalTM is used on both surfaces of contact. Acetal is a mixture of Polytetrafluorethylene (PTFE), commonly referred to as TeflonTM, which has a very low coefficient of friction. Hence, a cylindrical Teflon piece is added to the flanges of the beam and a thin sheet of Teflon is attached to the moving HSS at the point of contact, as shown in Figure 4.9b. This creates a Teflon-on-Teflon action, which minimizes the effect of friction. Both pieces of Teflon are also coated with a layer of grease.







(a) Lateral bracing system front view



(b) Lateral bracing system in the laboratory (Specimen W250-RDP1)

Figure 4.9: Lateral bracing system of W250-RDP1 specimen





An adapter plate identical to the one used at the column top boundary condition is used as a fixture for the lateral brace with the bolt holes aligned horizontally, as shown in Figure 4.9b. A 177.8 mm (7 ft) long beam is attached to the adapter plate using four 1-inch bolts, at the third bolt column of the adapter plate for the W250 specimens and the fifth bolt column for the W410 specimens, to ensure the brace point on the beam is almost halfway between the face of the column and the loading point in both W250 and W410 specimens. Additionally, the bolts connecting the HSS to the bracing beam are pretensioned to avoid any slip that might occur. To ensure that the bracing beam stays level before and during the test, a support is added to its other end. The bracing beam support is shown in Figure 4.10, and it consists of a pedestal, four 50.8 mm (2-inch) plates, and a cylindrical beam support.

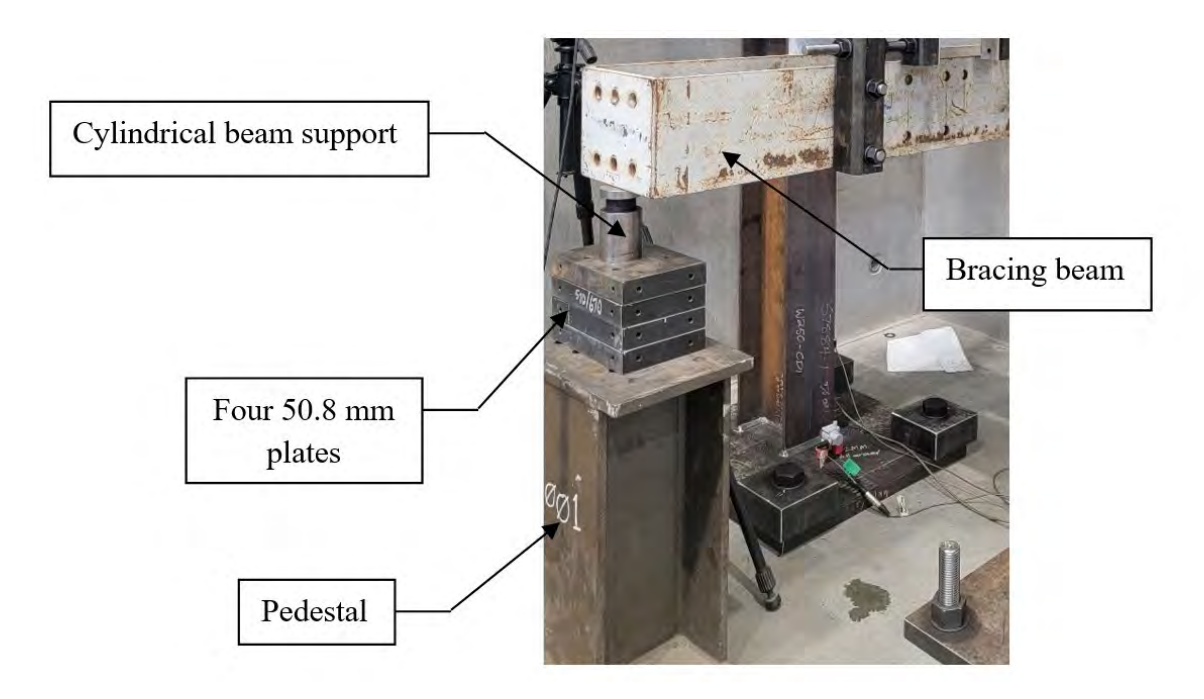


Figure 4.10: Lateral bracing system support beam

4.4.3 Loading

As discussed before, pipe racks are exposed to various loads inducing strong and weak axis moments, axial forces, and shear forces at the face of the column. In order to simplify the test setup, only shear and strong-axis moment are induced in the laboratory. The beam is loaded by pulling downwards at a distance 1.2 m away from the face of the column (Figure 4.4) using a 200 mm (8-inch) stroke hydraulic actuator. The hydraulic actuator shown in Figure 4.11a is used



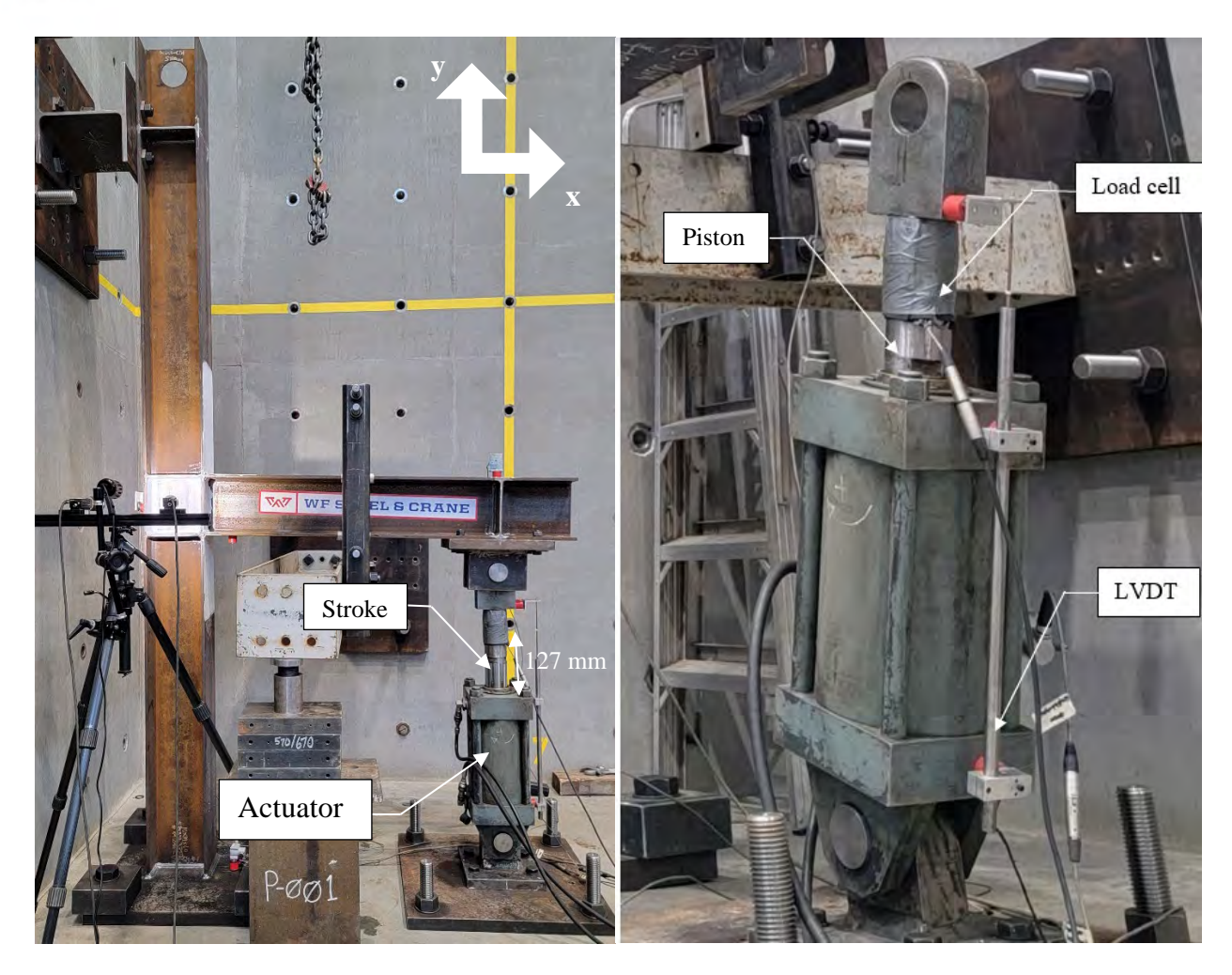


to perform the test. The actuator is pinned on both ends and sits on a 44 mm (1.75-inch) thick plate that is connected to the strong floor using four 2-inch threaded rods, as shown in Figure 4.11b. The retracting capacity of this actuator is 889 kN in tension (pulling downward) but the maximum allowable operating pump pressure is 21 MPa (3000 psi) which limits the actuator to a maximum pulling capacity of about 530 kN. The maximum expected pull load during the experiments is 423 kN. This load is obtained from a finite element model of the specimens by applying a downward displacement of 190 mm (7.5-inch) to all 12 specimens then choosing the ultimate post-yield load that the connection experiences.

The test setup is designed to ensure at least 127 mm of stroke are allowed when the hydraulic actuator is fully extended to the beam's bottom flange, as shown in Figure 4.11a. This was the determining factor when deciding where the beam should be connected to the column in the test specimen. Five inches of downward displacement applied at the loading point are sufficient to yield the doubler plate and observe post-yielding behaviour. The tests were performed in a displacement control mode with a loading rate of 1 mm/minute for the first 50 mm of displacement to ensure the elastic region and initiation of yielding are captured accurately, followed by a 2 mm/minute rate for the next 10 mm of displacement (i.e., strain hardening range), and a 5 mm/minute towards the end of the test. The loading rate was increased gradually to avoid spikes in the data. The displacement applied induces a shear force and a moment at the face of the column, which then creates shear in the doubler plate.







(a) Hydraulic actuator in the test-setup

(b) Hydraulic actuator

Figure 4.11: Loading system

4.5 Instrumentation

Instrumentation is designed and set-up to measure and record specimen response parameters during the experiment. The data collected includes the strains, displacements, rotations, and forces throughout each test. Figures 4.12 and 4.13 show the instrumentation mounted on W250-RDP1. The same instrumentation setup is used for other specimens. A 1200 kN load cell is attached to the end of the actuator to record the corresponding loads during the test. Additionally, a linear variable differential transformer (LVDT) is mounted onto the actuator to measure the linear displacement at the loading point. A combination of displacement transducers, strain gauge rosettes, clinometers, and digital image correlation (DIC) system were used to measure both global and local deformation and rotation responses. The two cable transducers are placed on the beam's bottom





flange, 100 mm and 1200 mm away from the column face. A strain gauge is placed on the column web side of the panel zone, as shown in Figure 4.14a, whereas DIC is used on the doubler plate side as shown in 4.14b. Both instruments were used on opposite sides of the column web/doubler plate for certain specimens.

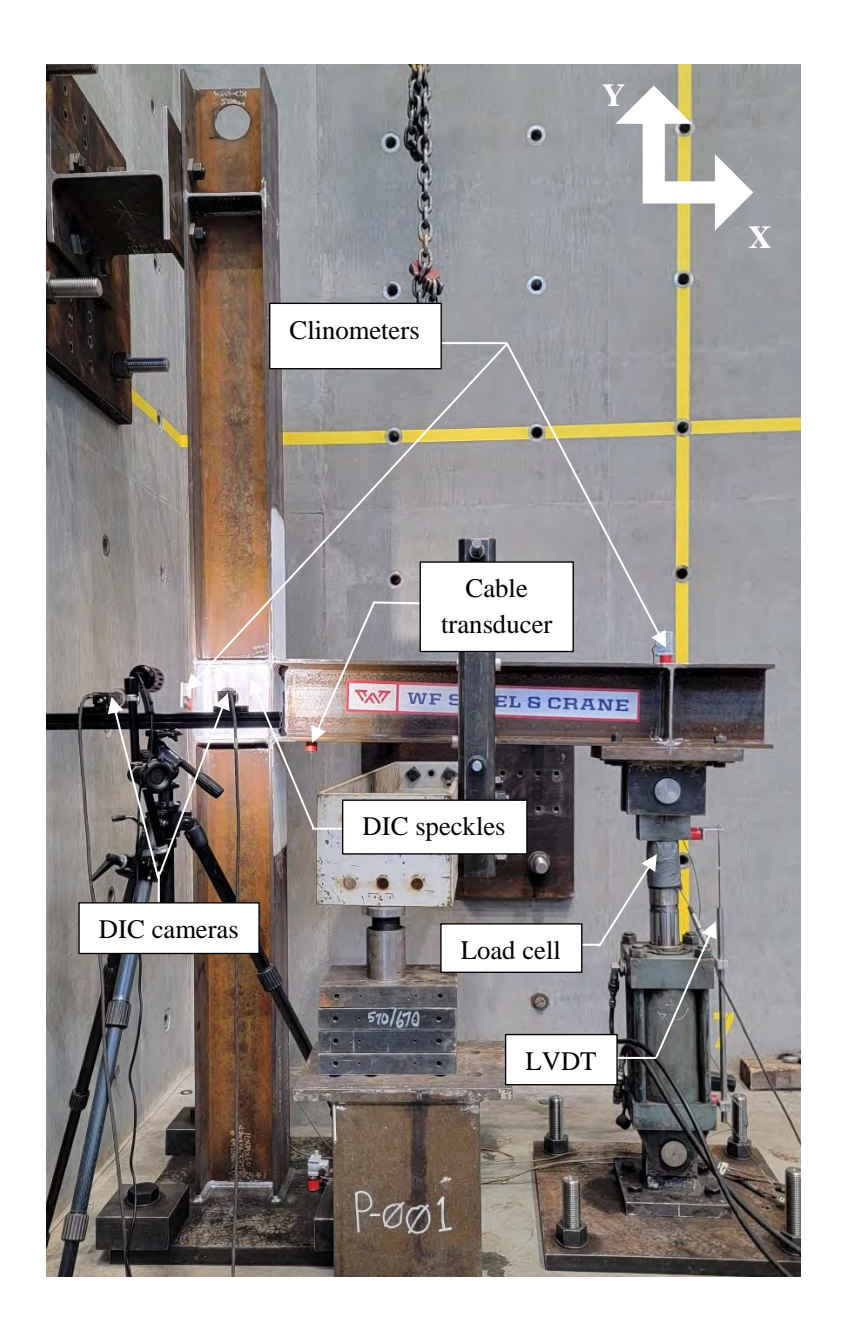


Figure 4.12: Side view of specimen W250-RDP1 with instrumentation mounted





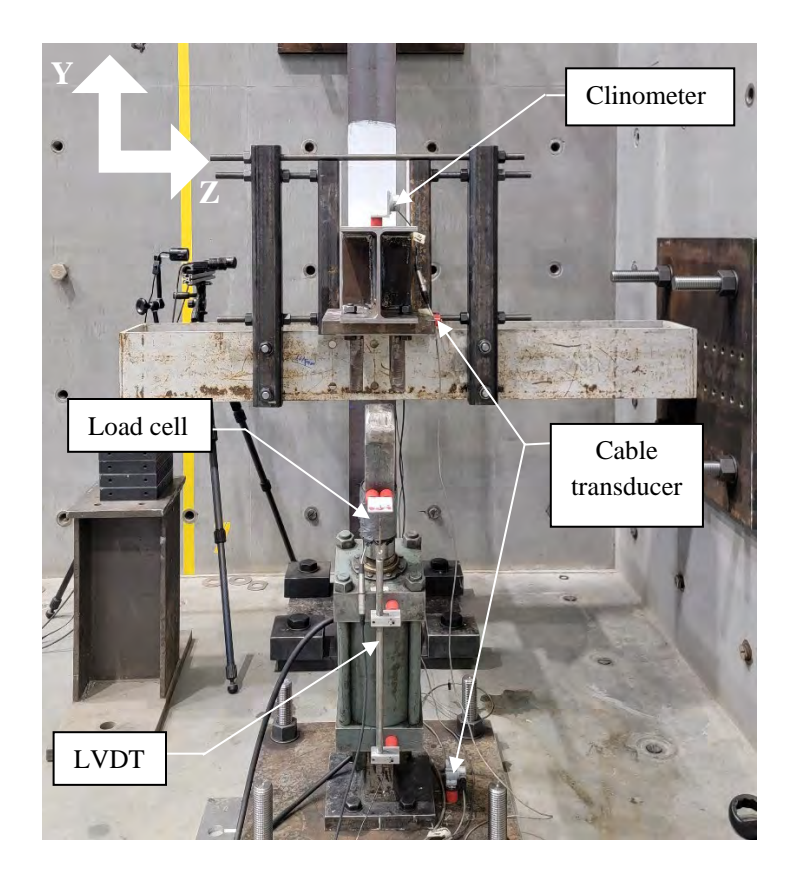
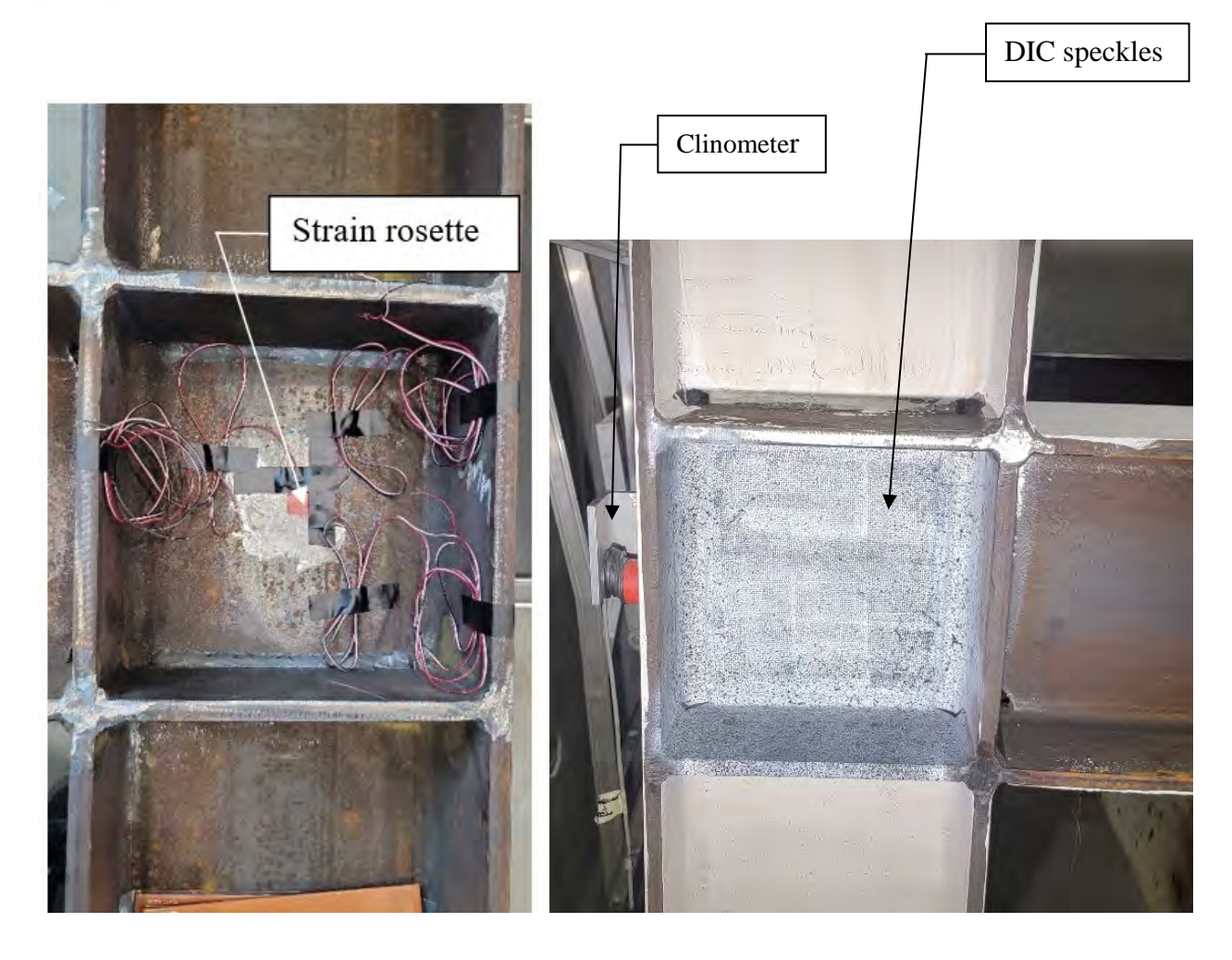


Figure 4.13: Front view of specimen W250-RDP1 with instrumentation mounted







(a) Strain gauge on the column web

(b) DIC speckles on the doubler plate

Figure 4.14: Column web and doubler plate instrumentation for W250-RDP1

In all specimens, the force at the loading point is recorded using a load cell that is attached to the actuator and the corresponding displacement is recorded using an LVDT, as shown in Figures 4.12 and 4.13. Additionally, one strain rosette is placed on the column web side in the centre of the panel zone, as shown in Figure 4.14a. Strain rosettes measure strain in a local area over three directions, 0° , 45° , & 90° . Strain at 0° is represented by ϵ_c , strain at 45° is represented by ϵ_b , and that at 90° is represented by ϵ_a as shown in Figure 4.15. These strains are recorded during the test using a data acquisition unit, then used to calculate ϵ_x , ϵ_y , and ϵ_{xy} as:

$$\varepsilon_{x} = \varepsilon_{a} \tag{4-2}$$





$$\varepsilon_{\nu} = \varepsilon_{c}$$
 (4-3)

$$\varepsilon_{xy} = \varepsilon_b - \frac{\varepsilon_a + \varepsilon_c}{2} \tag{4-4}$$

where ε_x , ε_y , and ε_{xy} are the normal strains in the x-, y-, and xy- directions, respectively, and are local rosette axes. ε_a , ε_b , and ε_c are the strains measured in the strain rosette as shown in Figure 4.15.

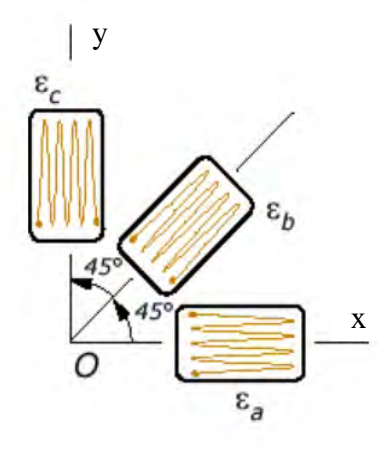


Figure 4.15: Strain rosette (45 degrees) aligned with x-y axes (efunda 2024)

Shear strain, γ_{xy} , is obtained by multiplying ε_{xy} by 2, since ε_{xy} obtained above is the local strain measured and not the engineering shear strain, γ_{xy} . Knowing the normal and shear strains, the normal stresses in the column panel zone are obtained by assuming a plane state of stress in the elastic region using the following matrix:

$$\begin{cases}
\sigma_{x} \\
\sigma_{y} \\
\tau_{xy}
\end{cases} = \frac{E}{(1+v)(1-2v)} \begin{bmatrix}
1-v-\frac{v^{2}}{v-1} & v-\frac{v^{2}}{1-v} & 0 \\
v-\frac{v^{2}}{1-v} & 1-v-\frac{v^{2}}{v-1} & 0 \\
0 & 0 & \frac{1-2v}{2}
\end{bmatrix} \begin{cases}
\varepsilon_{x} \\
\varepsilon_{y} \\
\gamma_{xy}
\end{cases}$$
(4-5)

where σ_x is the stress in the x-direction, σ_y is the stress in the y-direction, τ_{xy} is the shear stress, E is the modulus of electricity, and v is Poisson's ratio taken as 0.3 for steel.





von-Mises stress is then calculated using the following equation in the elastic range when $\sigma_{VM} \leq \sigma_{vs}$:

$$\sigma_{VM} = \frac{1}{\sqrt{2}} \left[\left(\sigma_x - \sigma_y \right)^2 + \left(\sigma_y \right)^2 + (\sigma_x)^2 + 6 \left(\tau_{xy} \right)^2 \right]^{0.5} \tag{4-6}$$

where σ_{vs} is the normal yield stress.

Beyond plate yielding, when $\sigma_{VM} > \sigma_{ys}$, a state of pure shear stress is assumed, and strain hardening is neglected. This assumption is based on the observation of very low stresses in both x and y directions and von-Mises stress is set as:

$$\sigma_{VM} = \sqrt{3}\tau_{rv} \tag{4-7}$$

The DIC system is used on the other side of the column web in the connection area, as shown in Figure 4.12, where the doubler plate is attached. Figure 4.14b shows a closeup view of the DIC speckles on W250-RDP1. The mill scale is ground off the area where the DIC is located, and then the area of interest is sprayed with three coats of white paint. After the paint is dry, black speckles are sprayed or rolled onto the surface. A camera system that views the panel zone from two angles is set up, with a light that shines onto the panel zone for improved calibration. The cameras connect to a computer with a software called Vic-3D9, which analyzes the area of interest using the images taken during the test to obtain the strains at each point over the speckled area. The software traces the movement of the speckles based on the images taken during the experiment, then converts the movements into displacements which, in turn, are converted to strains.

Whitewash, which is a mixture of lime and water, is used to paint in the joint outside the panel zone area, i.e., above and below the column stiffeners, on both sides. Additionally, the column back flange and beam flanges are also painted. As steel deforms in the plastic range, the whitewash flakes off indicating yielding of the material.

As shown in Figure 4.14b, a clinometer located at the back flange of the column is used to measure the column rotation. Another clinometer is positioned at the beam's top flange at the location of loading, as shown in Figure 4.12, to measure the beam rotation. At that same location, a cable transducer is added to measure the vertical deflection of the beam at the point of load application. A second cable transducer (Figure 4.12) is located on the beam's bottom flange 100 mm away





from the column face. This cable transducer is meant to measure the vertical deflection of the beam, at a second point, to ensure the rotation recorded from the beam's clinometer is not contaminated by any joint or column rotations.

4.6 Ancillary Tests

4.6.1 Mechanical Properties

To obtain the material properties of the column and doubler plates used in this experiment, tensile coupon tests are performed. Three dog-bone specimens are cut out from each flat plate creating 9 dog-bones per each column profile and 3 dog-bones per each doubler plate size, as shown in Figure 4.16. In total, 24 coupon specimens were tested as shown in Figure 4.17a. Figure 4.17b shows the specimens after the tensile tests. All plates used in the tests conformed to the sheet-type specimens with 50 mm gauge lengths as per ASTM A370-23 (ASTM International 2023). To find the cross-sectional area of each of the coupons, the widths and thicknesses of the reduced areas are measured using calipers and recorded to obtain the stresses after conducting the tests.

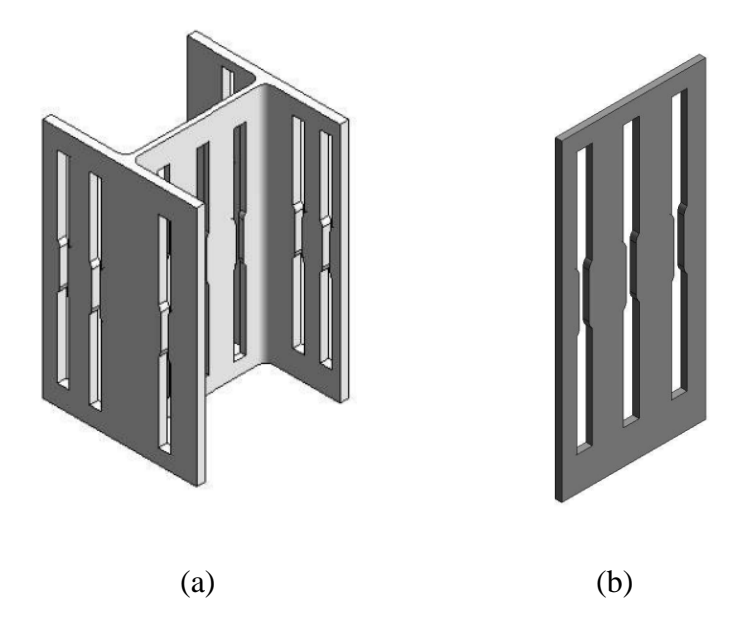


Figure 4.16: Location of tension coupons on: (a) flange sections, (b) web sections









(a) Coupon specimens before testing

(b) Coupon specimens after testing

Figure 4.17: Standard tension coupons

Mechanical properties are obtained based on the standard coupon test (ASTM International 2023). The tension coupons are tested in a uniaxial load frame as shown in Figure 4.18, where a tensile strain rate of 0.5 mm/min is exerted when the coupons are in the elastic region, which is then increased gradually to 6 mm/min after taking the static yield stress measurements. An average value of the static yield stress is obtained using three to four readings taken on the yield plateau. The static ultimate stress is recorded at the approximate maximum stress for each coupon. To obtain the modulus of elasticity, *E*, the stress strain curve is plotted and the slope in the elastic region is calculated. The results for each of the plates, webs, flanges, and doubler plates, are shown in Table 4.6. The values in the table are obtained by averaging the results of the yield stress, ultimate stress, and modulus of elasticity from all the coupons corresponding to the same plate. The engineering stress strain curves for one coupon from each wide flange profile are shown in Figures 4.19 and 4.20 for W250×58 and W410×60 profiles, respectively. The remaining coupon test results are presented in Appendix A.







Figure 4.18: Uniaxial load frame used to perform standard coupon tests

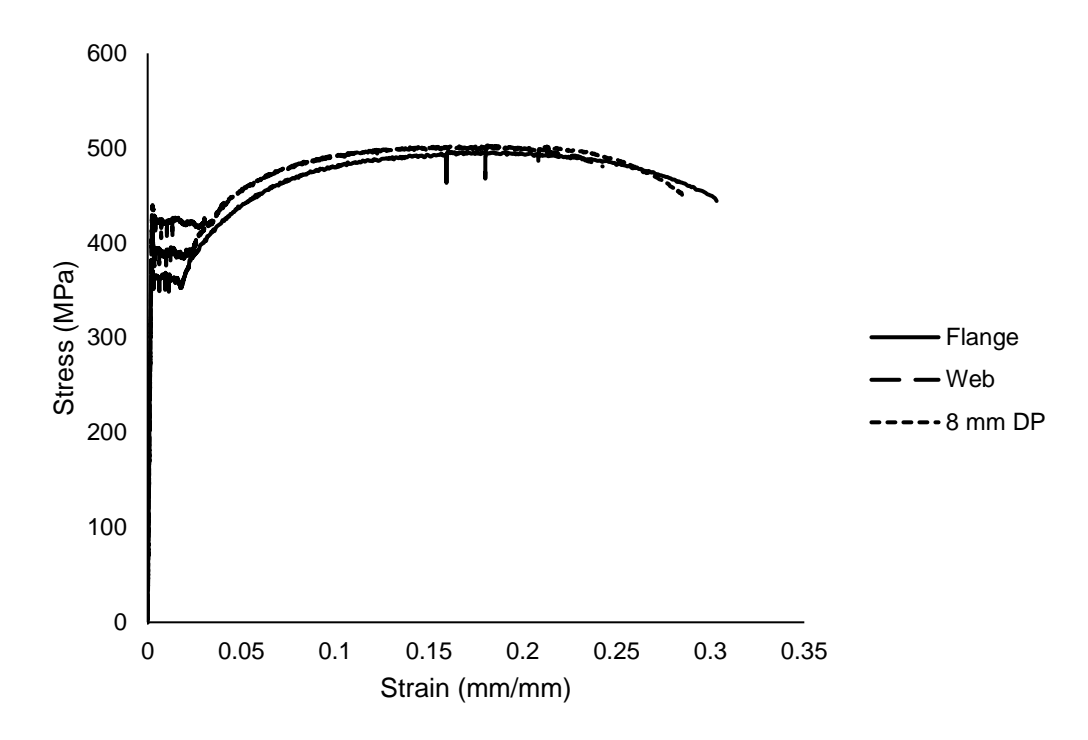


Figure 4.19: Engineering stress-strain curves of W250 coupons





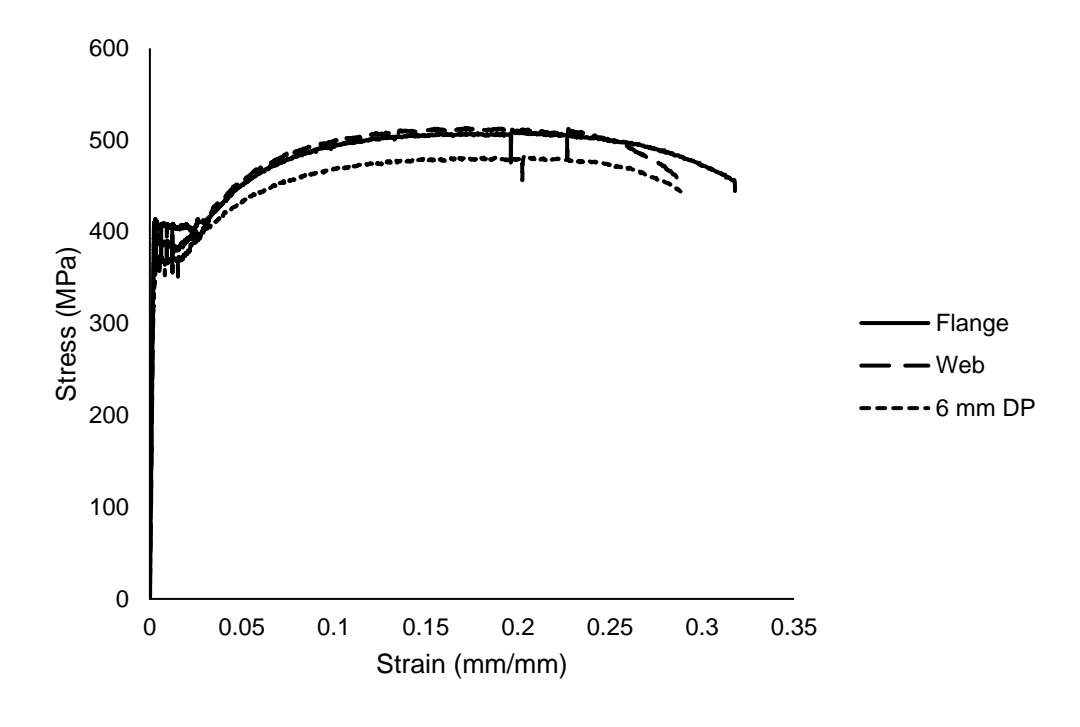


Figure 4.20: Engineering stress-strain curves of W410 coupons

Table 4.8: Mechanical properties of steel from tension coupon tests

Component	Mean Measured	Mean Measured	Modulus of Elasticity,		
	Yield Stress, F _{y-m}	Ultimate Stress, F _{u-m}	E		
	(MPa)	(MPa)	(MPa)		
W250×58 Flange	351	477	200,000		
W250×58 Web	378	479	200,000		
8 mm DP	406	478	203,333		
W410×60 Flange	369	483	201,167		
W410×60 Web	391	479	198,750		
6 mm DP	353	456	200,000		

The results of the tension coupon tests show that the flange yield stresses were found to be consistently lower than the web yield stresses in both profiles, with values rarely falling below the minimum specified yield stress for CSA G40.21 350W steel. The ultimate stress, $F_{\text{u-m}}$, was found





to be higher than the minimum specified value of 450 MPa, with averages of 478 MPa and 481 MPa for W250×58 and W410×60 profiles, respectively. The mean of all web and flange yield strengths, F_{y-m} , is 364 MPa for the W250×58 section and 380 MPa for the W410×60 section, which both are higher than the nominal value of 350 MPa.

The doubler plate coupon test results showed a much higher yield stress (406 and 353 MPa for 8-mm and 6-mm thick plates) than the minimum specified yield stress for CSA G40.21 300W steel. The ultimate stress, $F_{\text{u-m}}$, was also found to be higher than the minimum specified value of 450 MPa, as shown in Table 4.6.

4.6.2 Residual Stress Measurement

Residual stress measurements were performed for both column profiles, W250×58 and W410×60, using the method of sectioning described by Ziemian (2010). This method determines the residual stresses through the thickness of the specimen by marking up the ancillary section into strips. If the specimen is cold sawed, which is the case here, the specimen piece used for the residual stress measurements should be cut to a minimum length of three times the largest transverse dimension, plus the gauge length, plus 50 mm to minimize the possibility of disturbing the residual stress pattern that is in the central portion of the specimen. Thus, for the W-sections being tested with a gauge length of 200 mm, the required lengths for a residual stress specimen are 904 and 1380 mm for W250×58 and W410x60, respectively, which are both less than provided residual stress pieces, 1200 mm piece of W250×58 and 1500 mm piece of W410×60.

The first step of the sectioning method is to define the slices prior to cutting, as shown in Figure 4.21. The flanges and webs of the residual stress sections are defined into 20×300 mm strips. For the W250×58 specimen, eight strips are taken from each flange and web, whereas for the W410×60 specimen, six strips are taken from each flange and sixteen strips are taken from the web. The fillets, the juncture between the web and the flanges, are not included in the sectioning method since the digital measuring device would not provide an accurate reading in that area. These areas are known to possess a high tensile residual stress in the flanges, which helps estimate the residual stresses in that area after calculating the rest of the stresses.





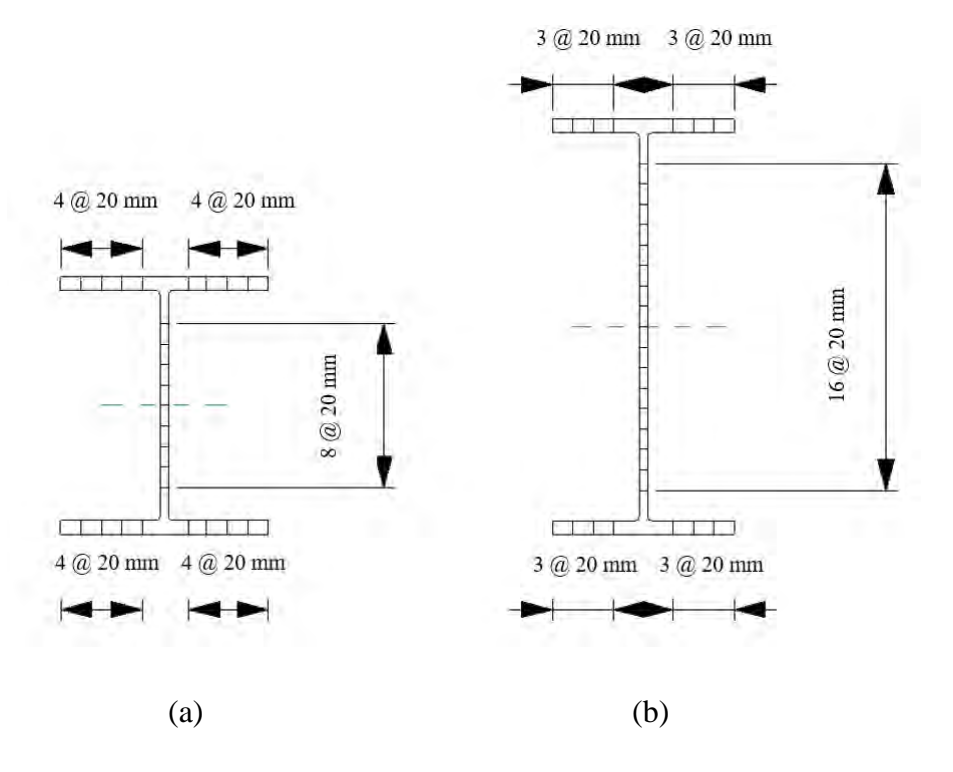


Figure 4.21: Cutting locations for residual stress measurements: (a) W250×58, (b) W410×60

The slices, before cutting, are scribed at mid-width all the way through, then punched slightly at 200 mm gauge length. Since the punch marks leave a shallow and wide diameter hole, a drill is then used to create deeper holes with a 1.5875 mm (0.0625-inch) diameter drill bit. The punch marks are used to guide the location for placing the handheld drill. Drilling is performed by ensuring the drill is held perpendicular to the surface of the plates. Using a digital demec, with a gauge length of 200 mm, the initial gauge length between the drilled holes is measured three times to make sure the measurement is consistent and the largest difference between the three measurements is within one or two dial indicator units. Before measuring the longitudinal distances, the demec is zeroed on a reference bar, then the three readings are recorded to get a mean value for each strip. According to the data recorded, the measurements taken by the demec on the drilled holes gave repeatable values for each of the three measurements.

The marked-up W-sections are cold sawn into 20×300 mm strips as shown in Figure 4.22. After cutting, one measurement of the longitudinal distance between the drilled holes is recorded using the same demec. To calculate the value of residual strain in each strip, the change in gauge length





after cutting is divided by the initial gauge length measurement on each side of the strip and the mean value is taken to be the residual strain present in that strip, which negates the need to correct for curvature in the strip caused by cutting. Additionally, the temperature during both the initial and final measurements was recorded to be around 18 degrees Celsius, and therefore the effect of temperature on the change in length is ignored. The residual strains obtained are converted to stresses using the average modulus of elasticity corresponding to each case; 200 GPa for both W250×58 and W410×60. The compressive and tensile forces are then obtained by multiplying the residual stresses by the cross-sectional area measured prior to the ancillary test.



Figure 4.22: Sections for residual stress measurements after cold sawing

The same process is repeated for the 100 mm gauge length using a different digital demec. However, the results from using the 100 mm gauge length were deemed unreliable since they resulted in residual stress distribution pattern that does not align with the expected trend in a W-section. Additionally, the summation of compressive and tensile forces was not equal to or close to zero, meaning that equilibrium was not satisfied.

The residual stress distribution resulting from the measurements using the 200 mm gauge are plotted in Figure 4.23 for W250×58 and in Figure 4.24 for W410×60. Compression is represented by negative values and tension is shown as positive. For W250×58, the web experiences a maximum of 142 MPa $(0.38F_{y-m})$ compressive residual stress at the middle and 80 MPa $(0.21F_{y-m})$ tensile residual stress at the web-flange junction. The flanges experience compressive





stresses at the tips with a maximum of 60 MPa $(0.17F_{y-m})$ and a maximum tensile residual stress of 99 MPa $(0.28F_{y-m})$ towards the middle of the flange, at the web-flange junction. The change in curvature of the residual stress curve in the flanges could be due to cold straightening of the steel or measurement errors. In the W410×60 case (Figure 4.24), the web experiences a maximum compressive residual stress of 258 MPa $(0.66F_{y-m})$ at the middle and a maximum tensile residual stress of 172 MPa $(0.44F_{y-m})$ at the web-flange junction. The W410 flanges also exhibit a maximum tensile residual stress of 172 MPa $(0.47F_{y-m})$. The compressive residual stresses in the tips of the flanges were not as prominent, reaching only a maximum of 15 MPa $(0.04F_{y-m})$.

To obtain the estimated stresses in the fillet areas, it is assumed that the stress at web-flange junction is the same in the web and flanges. This assumption helps calculate the tensile force in this area, which is also used to obtain the residual forces in the cross-section attributed to inaccurate widths of strips (e.g., $20 \text{ mm} \pm 1 \text{ mm}$) after cold-sawing or an overestimation of the area at the web-flange junction (fillets). The residual forces are found to be approximately 40 kN for both sections.





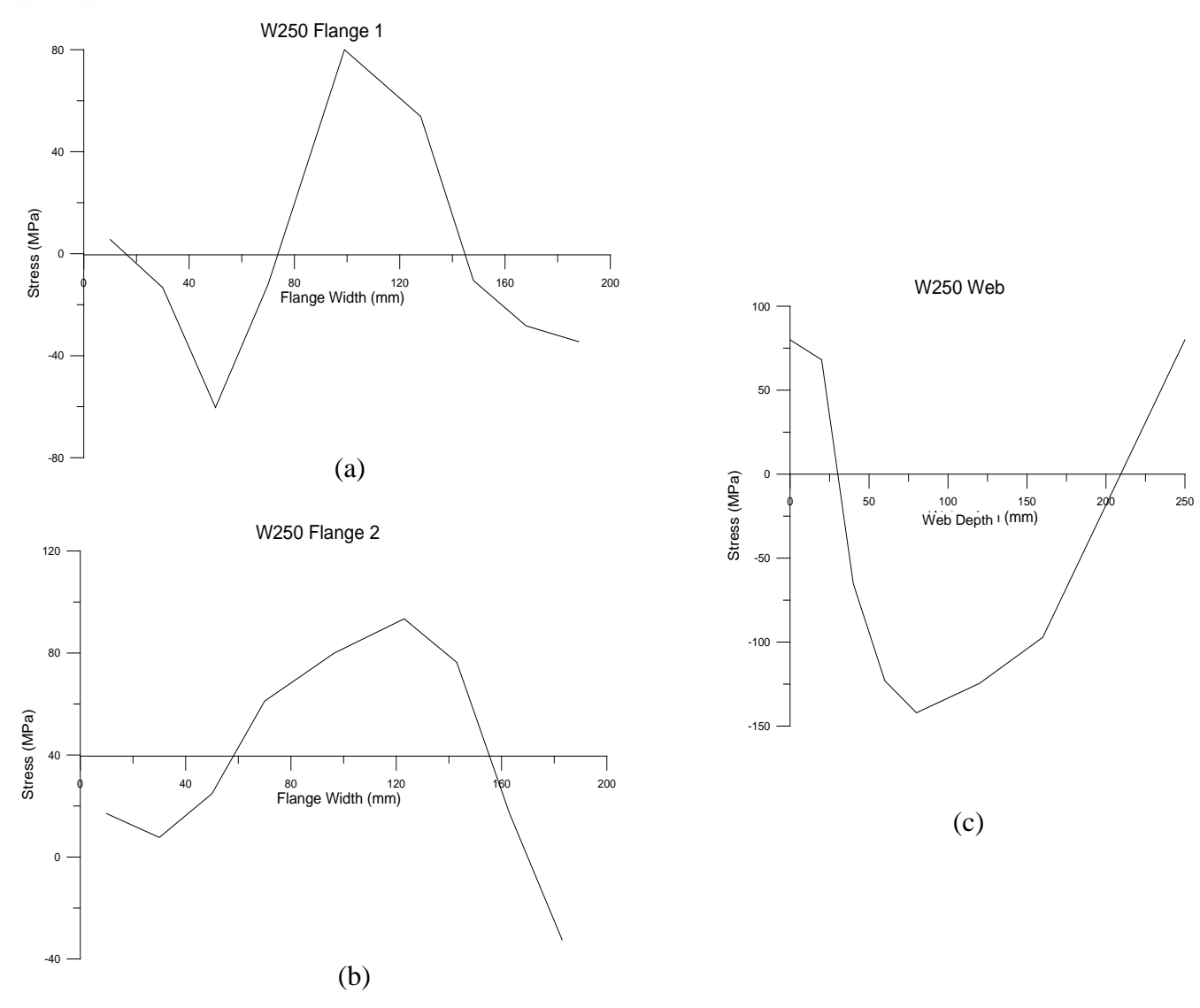


Figure 4.23: Residual stress distribution of W250×58: (a) W250 Flange 1, (b) W250 Flange 2, (c) W250 Web





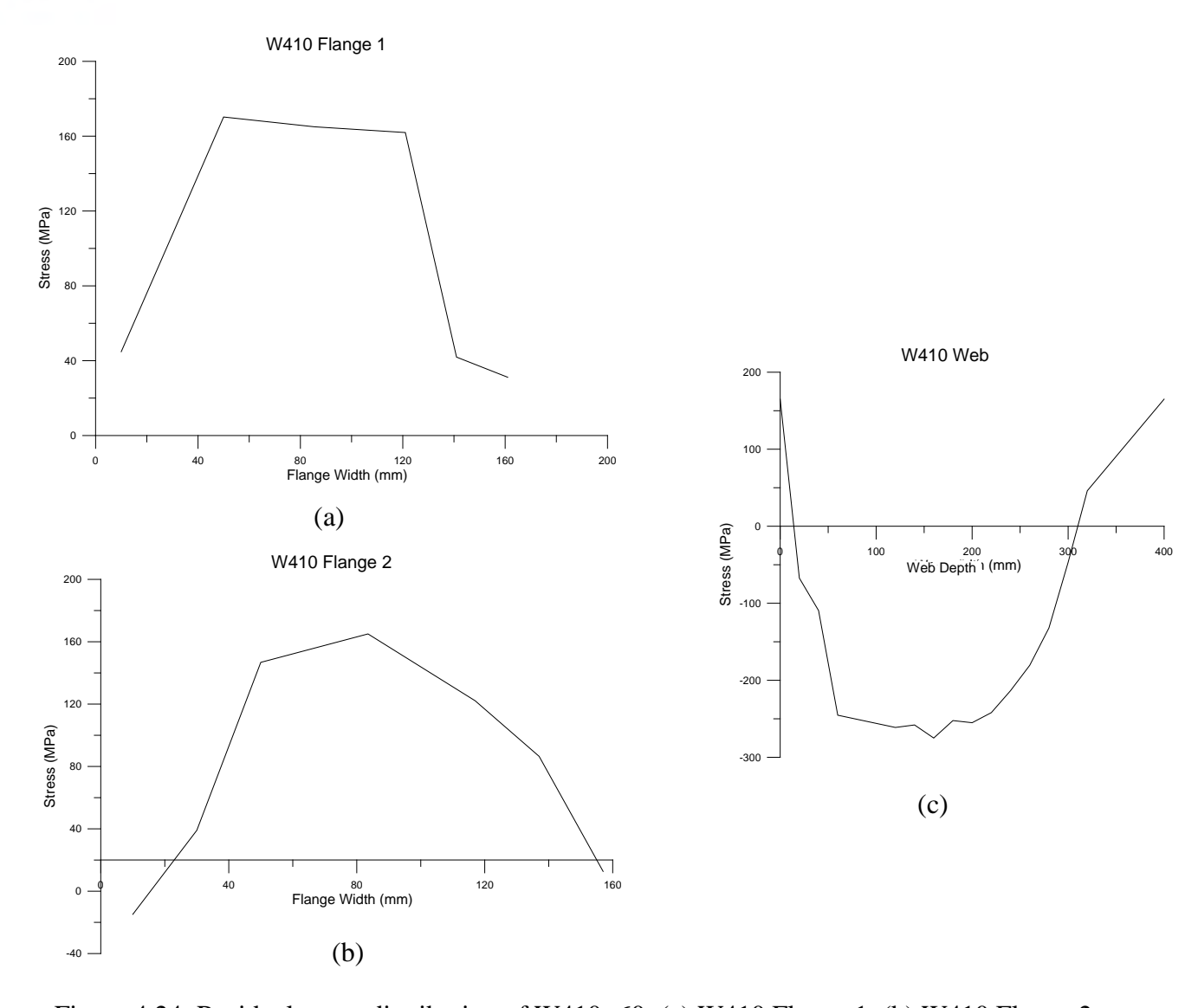


Figure 4.24: Residual stress distribution of W410×60: (a) W410 Flange 1, (b) W410 Flange 2, (c) W410 Web





5 EXPERIMENTAL BEHAVIOUR AND PERFORMANCE

5.1 Introduction

The results of the twelve full-scale tests are presented in this chapter.

5.2 Normalized Force – Shear Strain Response

During the tests, a displacement is applied to the beam end, 1200 mm away from the column face (Figure 4.4). Figures 5.1 and 5.2 show the normalized force – average shear strain response of W250 and W410 specimens, respectively. Note that specimens W250-NDP and W410-NDP were tested to study the behaviour of connections lacking the required doubler plate. The vertical axis of these plots shows the ratio of the load applied at the beam end to the connection design force. For each specimen, the applied load is obtained from the actuator load and the connection design force is back calculated from Equation (3-11) when the column panel zone reaches its nominal shear capacity in yielding, i.e., the expected limit state of the connection. The horizontal axis of the plots in Figures 5.1 and 5.2 gives shear strain, which is the average shear strain in the column panel zone (web or doubler plate) and obtained from the DIC system data. The strain data from the DIC system are not contaminated by the elastic deformation of the column and beam.

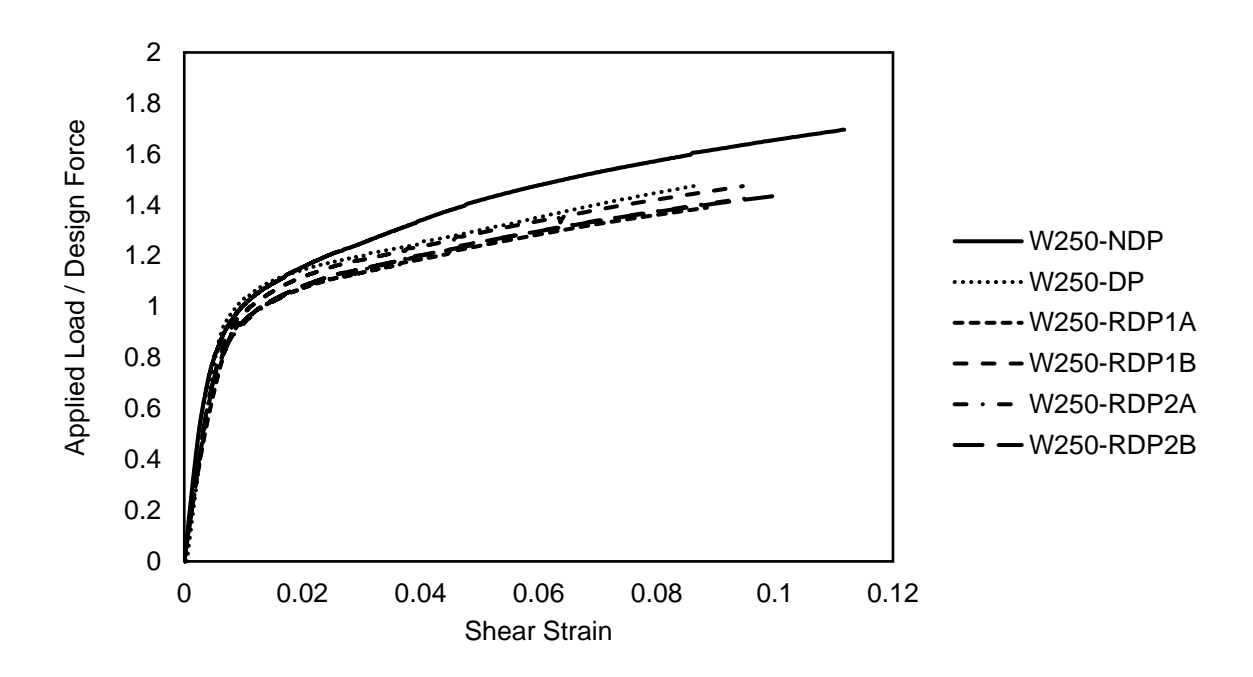


Figure 5.1: Normalized force – shear strain responses of W250 specimens





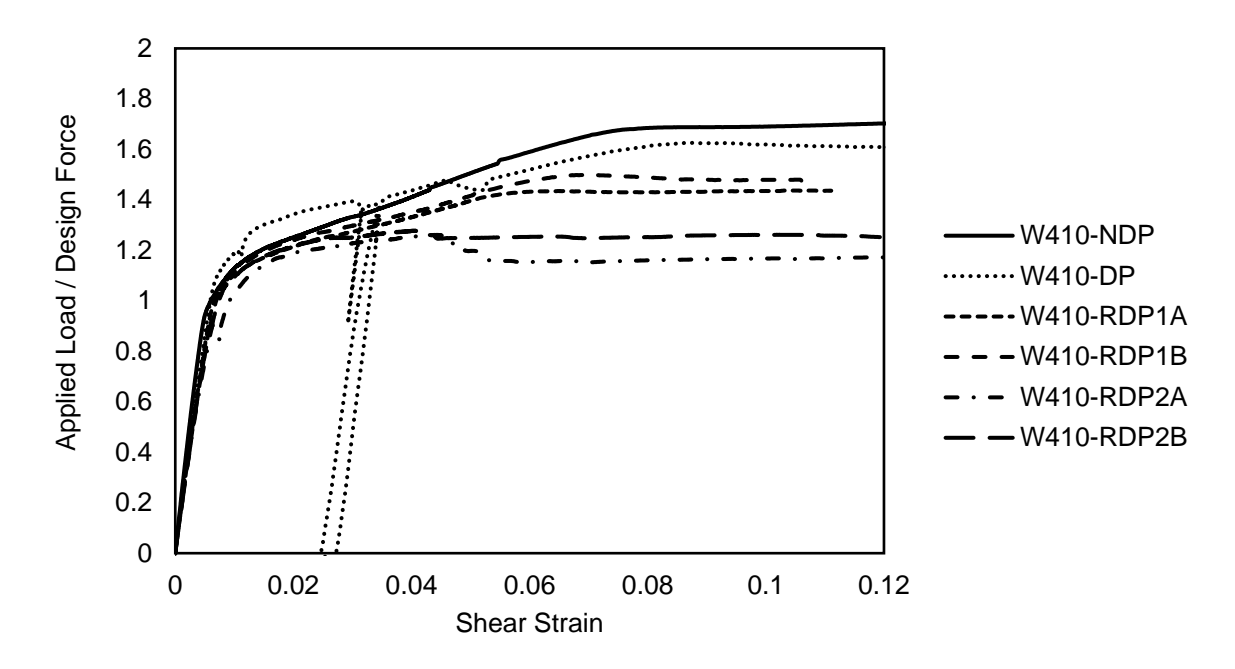


Figure 5.2: Normalized force – shear strain responses of W410 specimens

As shown in Figures 5.1 and 5.2, panel zone yielding occurred at average shear strains of 0.007 and 0.009 for W250-NDP and W410-NDP, respectively. At 0.009 strain, W250-DP experienced column web and doubler plate yielding, whereas W410-DP showed shear yielding at 0.011. The drops associated with the force – rotation response of W410-DP in Figure 5.2 are due to the malfunctioning of the hydraulic pump. To examine the behaviour of this specimen after the sudden pressure drop, the pump was replaced, and the specimen was reloaded.

Referring to Figure 5.1, W250-RDP1A and W250-RDP1B experienced shear yielding in the doubler plate and column web at a shear strain of 0.008. Panel zone yielding in W410-RDP1A and W410-RDP1B occurred at 0.008 shear strain as well.

W250-RDP2A and W250-RDP2B experienced panel zone shear yielding at 0.008 shear strain, whereas in W410-RDP2A and W410-RDP2B both the doubler plate and column web yielded at 0.009 shear strain. The force – rotation responses of the W410-RDP2A and W410-RDP2B drops at 0.047 and 0.046 strain, respectively. This is due to weld rupture in the panel zone, which led to the separation of the doubler plate from the column web degrading the load-carrying capacity of the connection. No weld fracture was observed in W410-RDP1 (Figure 5.2).





Figures 5.3 and 5.4 show column panel zone shear force versus the average shear strain. The average shear strain in Figures 5.3 and 5.4 is obtained from the data measured by the DIC system positioned on the column's doubler plate side. The column panel zone shear force is divided by the minimum value of all the limit states calculated in Section 3.2, i.e., panel zone shear yielding, and is used as the vertical axis. For all the specimens, the deformation is minimal in the elastic region with a maximum of ~0.01 strain. As the applied force increases, the deformation increases, which leads to plastic deformation post-yielding. Beyond panel zone yielding, strain hardening in shear is observed as the plastic deformation increases as shown in Figures 5.3 and 5.4. W410-NDP experienced shear buckling that isn't reflected in the shear force – shear strain response, but evident in the shear strains shown later (Figure 5.18). In W410-DP, a small drop in the shear force – shear strain response at 0.052 shear strain occurred indicating shear buckling followed by a plateau, whereas in both specimens W410-RDP2A and W410-RDP2B a load degradation is recorded after yielding due to the DP fillet weld fracture accompanied by shear buckling at 0.044 and 0.043 shear strain, respectively. W410-RDP1A and W410-RDP1B experienced moderate shear buckling beyond yielding, but this was not evident in the shear force – shear strain responses due to almost negligible amplitude of buckling.

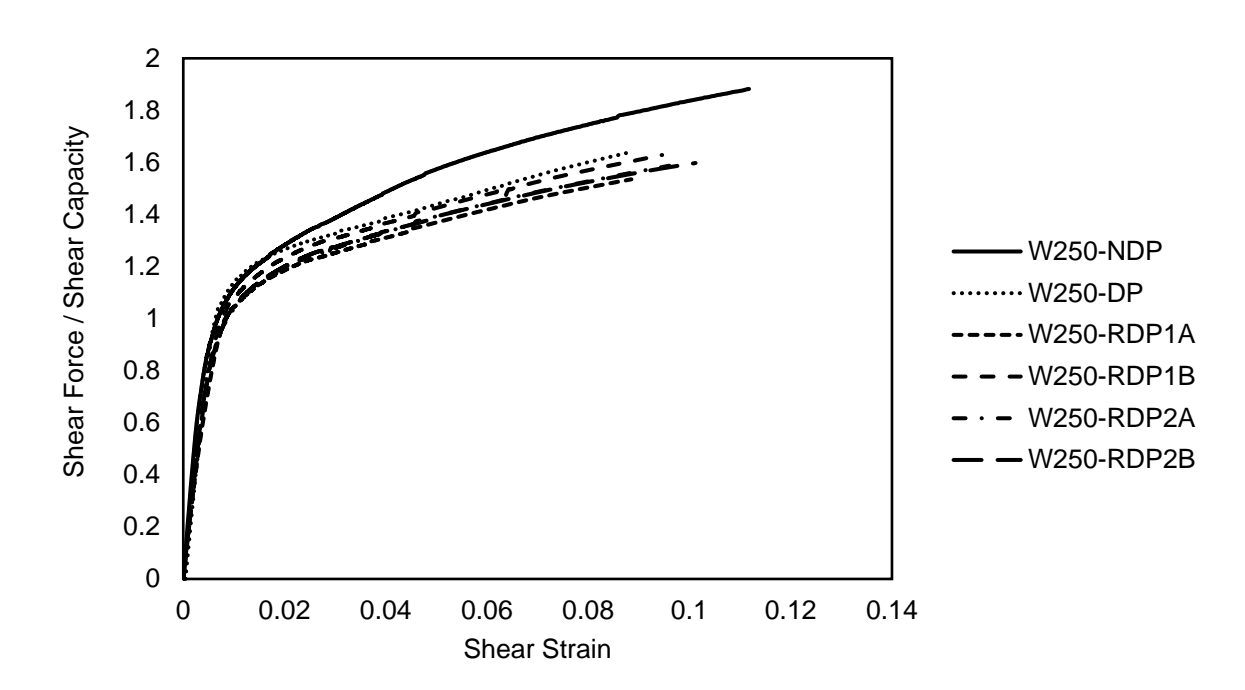


Figure 5.3: Normalized shear force – shear strain response of the panel zone for W250 specimens





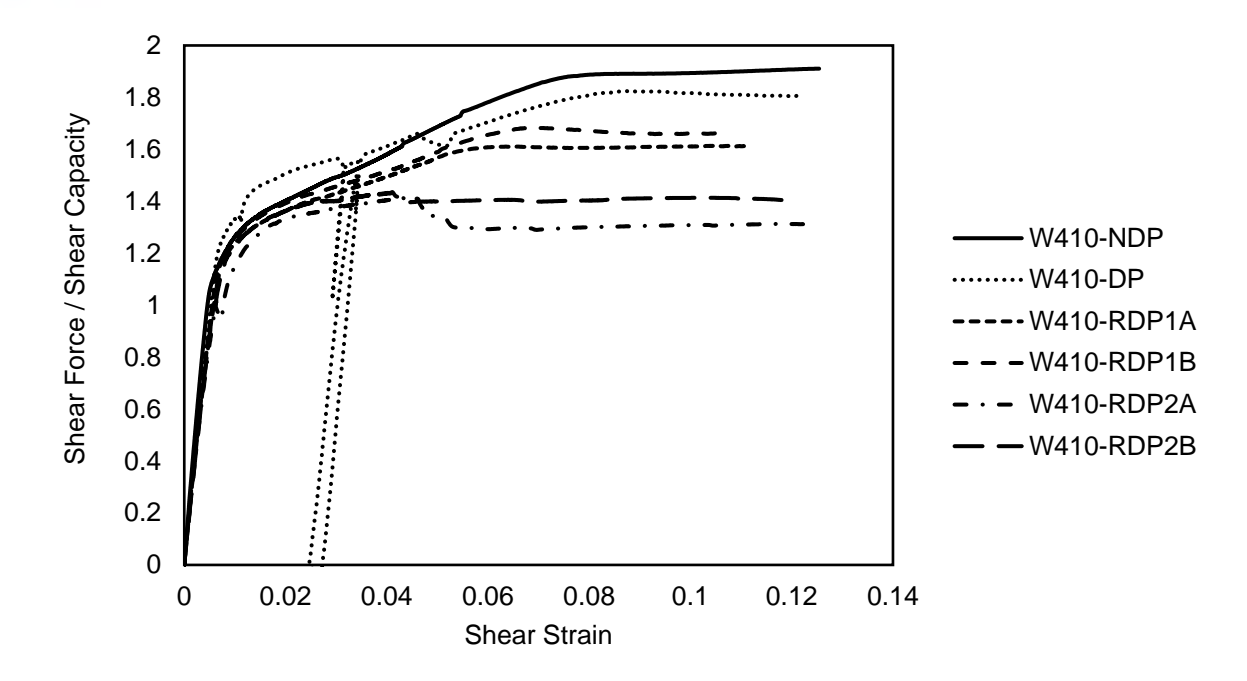


Figure 5.4: Normalized shear force – shear strain response of the panel zone for W410 specimens

5.3 General Experimental Observation

Figures 5.5a and 5.5b show W250-NDP deformed-shape in the panel zone area and shear strain contour on the column web at the end of the test (0.12 shear strain), respectively. The same set of photographs are provided at the end of the test (0.12 shear strain) for W410-NDP in Figures 5.6a and 5.6b, respectively. W250-NDP failed by yielding in the panel zone area (0.007 shear strain), while the failure mode of W410-NDP involved column web yielding at 0.008 shear strain accompanied by shear buckling of the column web in the panel zone at 0.06 shear strain, which eventually resulted in bulging of the column web at the end of the test, as shown in Figure 5.6a.





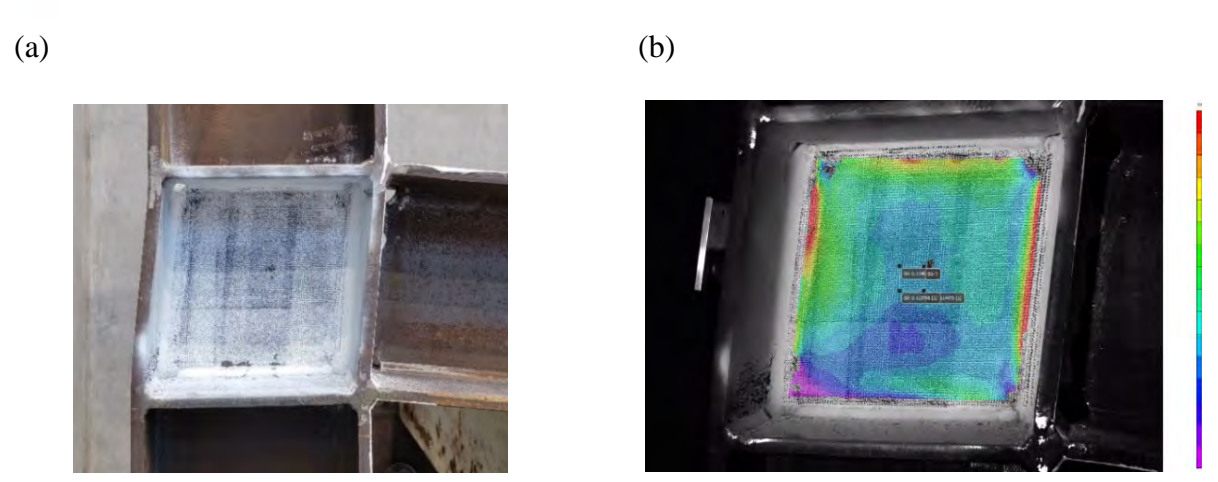


Figure 5.5: W250-NDP at the end of the test at 0.12 shear strain: (a) Deformed shape, (b) DIC shear strain contour (shear yielding $\gamma_y = 0.007$ is shown by the boundary of purple and blue – red represents maximum strain)

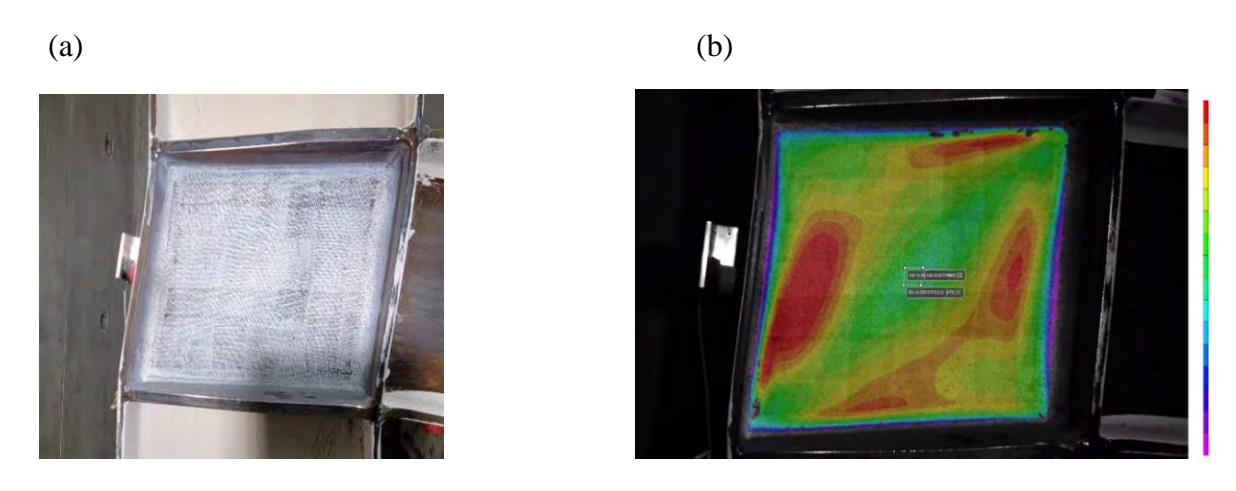


Figure 5.6: W410-NDP (Column web Face 2 is shown) at the end of the test at 0.12 shear strain: (a) Deformed shape, (b) DIC shear strain contour (shear yielding $\gamma_y = 0.008$ is shown by the boundary of purple and blue – red represents maximum strain)

Panel zone deformed shape and shear strain distribution of the doubler plate for W250-DP, with standard doubler plate detail, at the end of the test (0.10 shear strain) are shown in Figures 5.7a and 5.7b, respectively. The first failure mode observed in specimens W250-DP and W410-DP was shear yielding in the panel zone area at 0.009 and 0.011 shear strain, respectively, while shear yielding in W410-DP (see Figures 5.8a and 5.8b) was followed by shear buckling at 0.052 shear





strain due to a more slender column web panel zone ($h/t_{\rm cw}$ = 46.3 vs. 26.9). Shear buckling in this specimen was not captured by DIC, since unloading occurred while conducting this test due to the pump pressure limit, but bulging in the panel zone area was recorded. Shear buckling was observed after reloading.

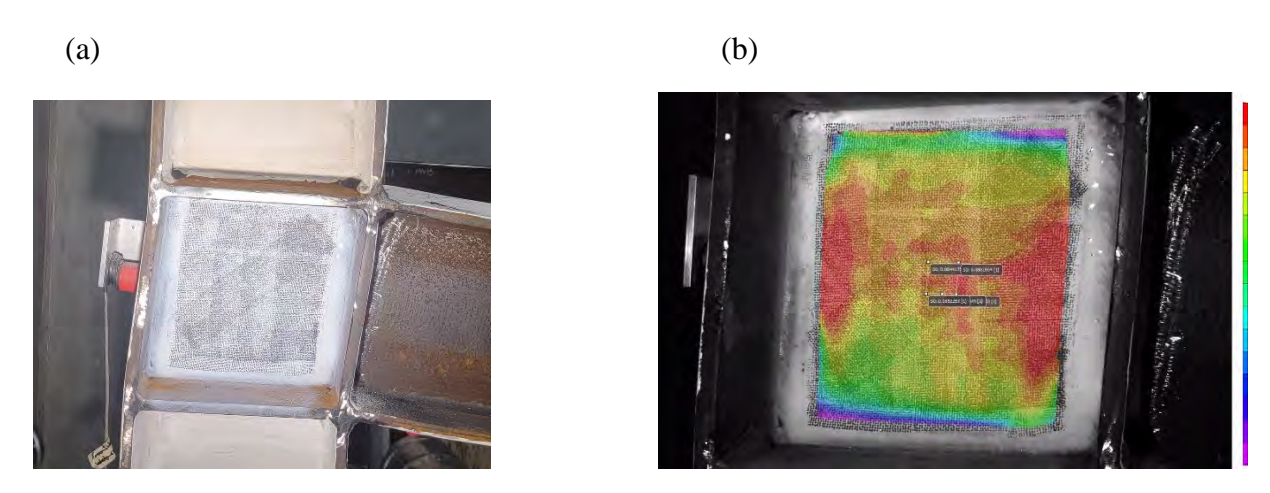


Figure 5.7: W250-DP at the end of the test at 0.10 shear strain: (a) Deformed shape, (b) DIC shear strain contour (yielding $\gamma_y = 0.009$ is shown by the boundary of purple and blue – red represents maximum strain)

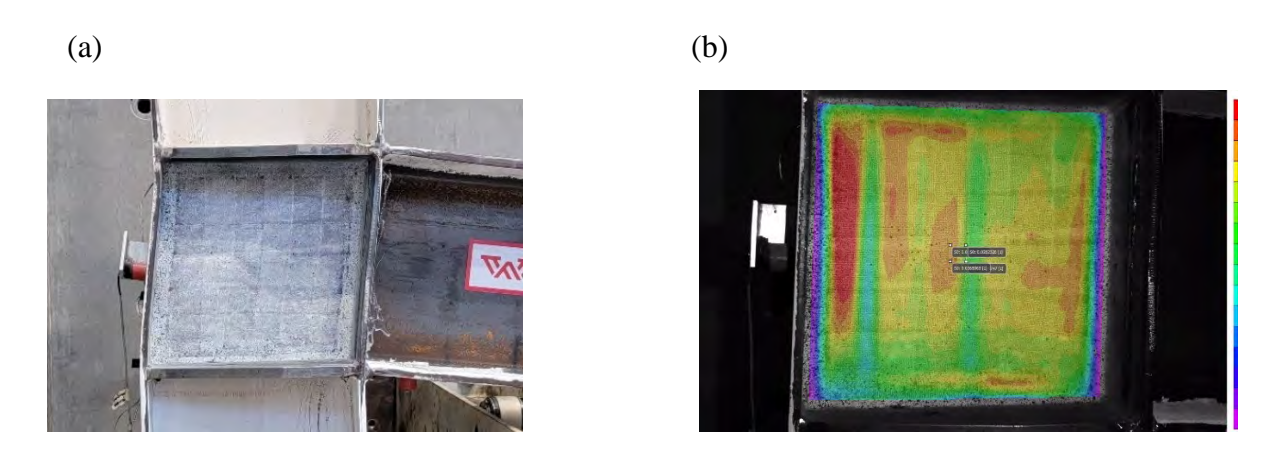


Figure 5.8: W410-DP: (a) Deformed shape at the end of test at 0.12 shear strain, (b) DIC shear strain contour prior to reloading of test (yielding $\gamma_y = 0.011$ is shown by the boundary of purple and blue – red represents maximum strain)





The specimens involving the proposed doubler plate detail are RDP1, where the doubler plate is reduced by the weld leg size on all four sides or two times D in each direction, and RDP2, where the doubler plate is reduced by two times the weld leg size on all sides or four times D in each direction (D is the fillet weld leg size used to connect the double plate to the column web). Figures 5.9a and 5.9b show the deformed shape and strain contour of W250-RDP1 at the end of the test (0.10 shear strain), respectively. Yielding in the panel zone occurred at 0.008 strain in W250-RDP1A and W250-RDP1B (Figure 5.10).

Figures 5.11a and 5.11b show the deformed specimen and strain contour on the doubler plate for W410-RDP1A at the end of the test (0.12 shear strain). Yielding in the panel zone occurred at 0.08 in W410-RDP1A and W410-RDP1B (Figures 5.12). Shear buckling of the column web and doubler plate occurred at a shear strain of 0.044 in W410-RDP1A and 0.043 in W410-RDP1B, which resulted in bulging in the panel zone at the end of the test.

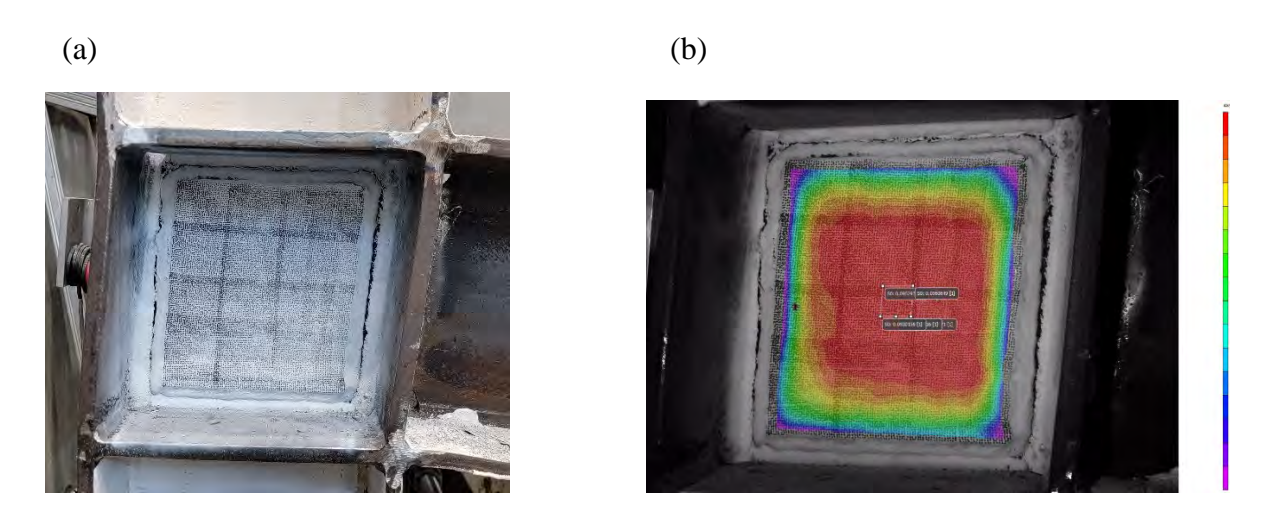


Figure 5.9: W250-RDP1A at the end of the test at 0.10 shear strain: (a) Deformed shape, (b) DIC shear strain contour (yielding $\gamma_y = 0.008$ is shown by the boundary of purple and blue – red represents maximum strain)





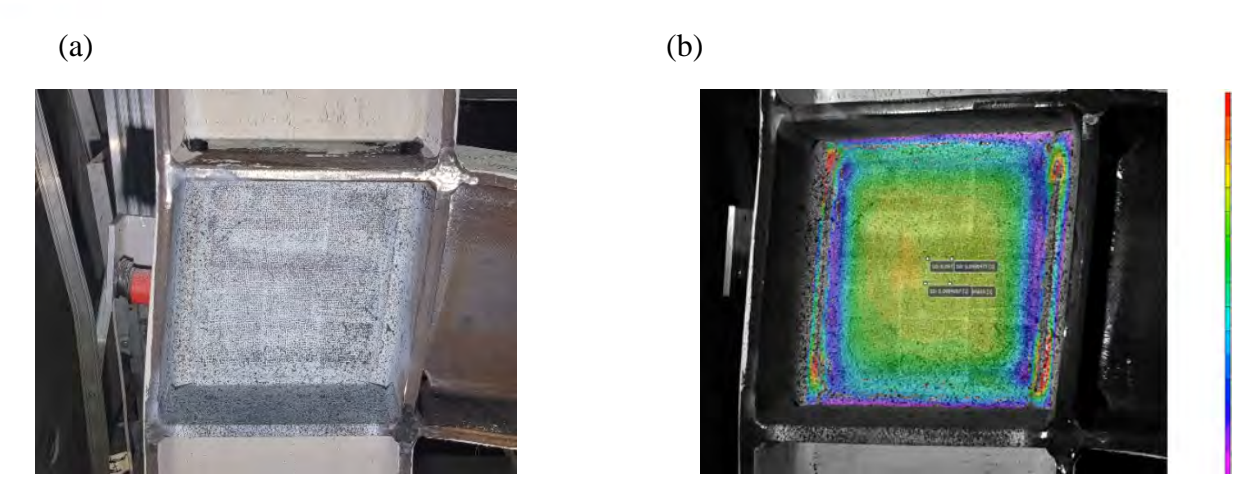


Figure 5.10: W250-RDP1B at the end of the test at 0.10 shear strain: (a) Deformed shape, (b) DIC shear strain contour (yielding $\gamma_y = 0.008$ is shown by the boundary of purple and blue – red represents maximum strain)

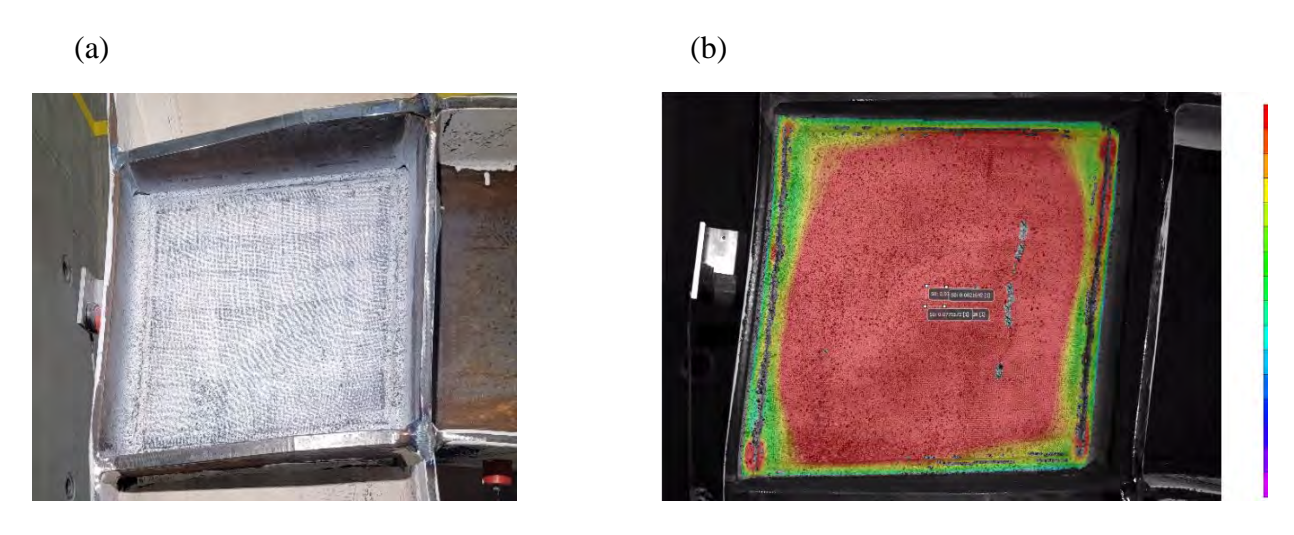


Figure 5.11: W410-RDP1A at the end of the test at 0.12 shear strain: (a) Deformed shape, (b) DIC shear strain contour (yielding $\gamma_y = 0.008$ is shown by the green areas – red represents maximum strain)





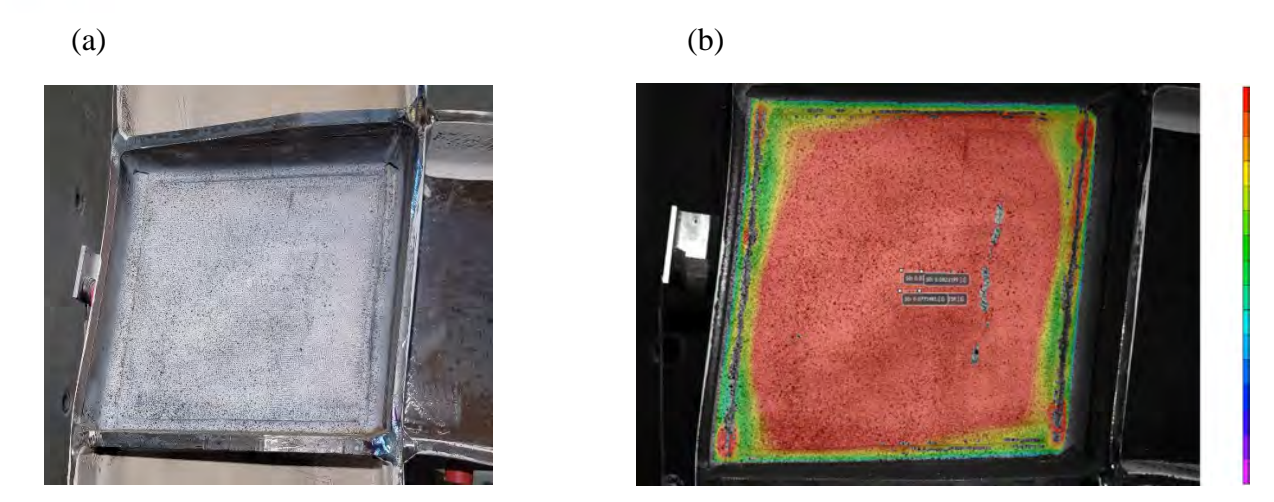


Figure 5.12: W410-RDP1B at the end of the test at 0.12 shear strain: (a) Deformed shape, (b) DIC shear strain contour (yielding $\gamma_y = 0.008$ is shown by the green areas – red represents maximum strain)

Figures 5.13a and 5.13b show, respectively, the deformed panel zone and shear strain response of the double plate for W250-RDP2A after testing. The same set of results are presented in Figure 5.14 for W250-RDP2B. Yielding in the panel zone in W250-RDP2A and W250-RDP2B occurred at 0.008 shear strain.





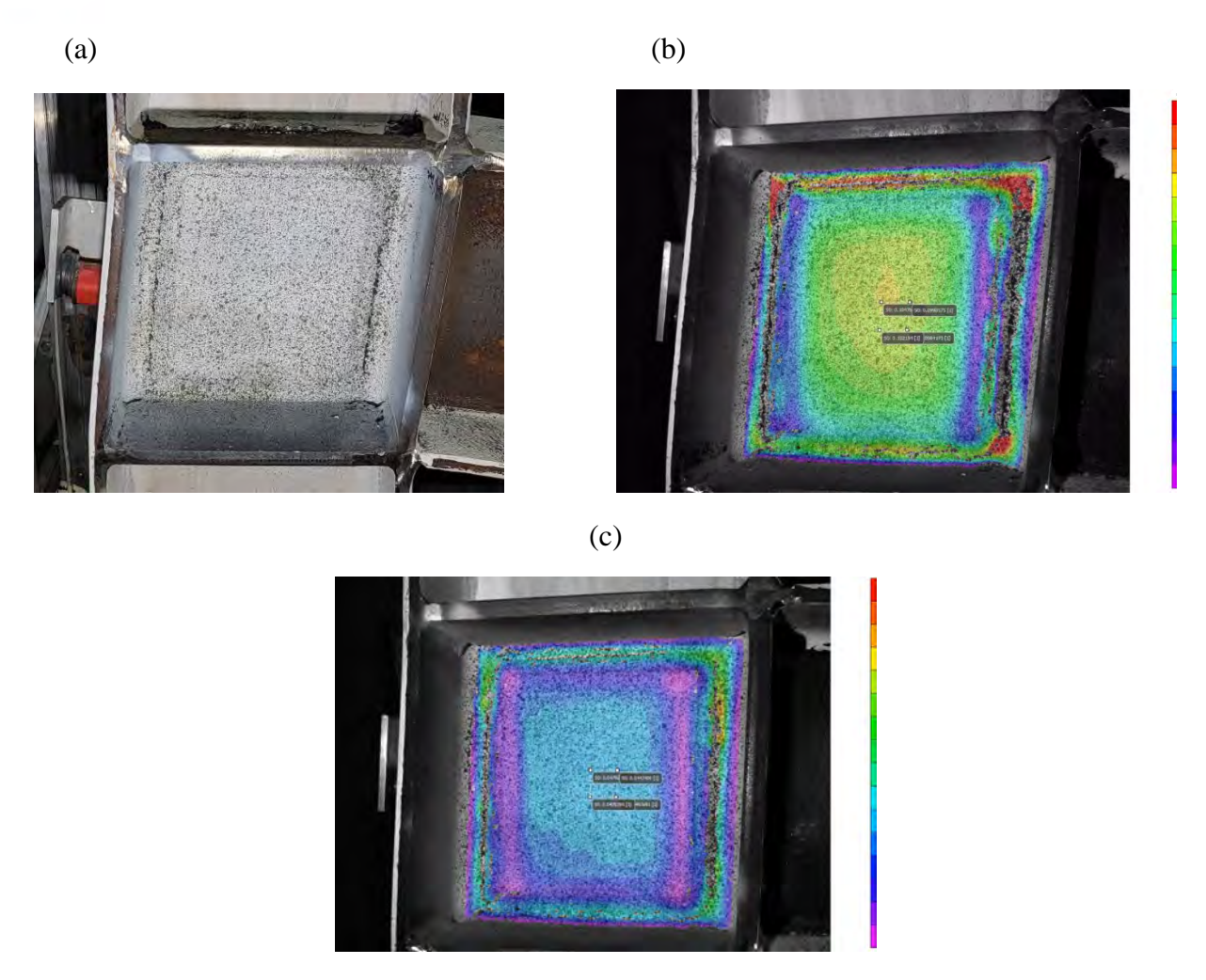


Figure 5.13: W250-RDP2A: (a) Deformed shape at the end of the test at 0.12 shear strain, (b) DIC shear strain contour at the end of the test at 0.12 shear strain (yielding $\gamma_y = 0.008$ is shown by the boundary of purple and blue – red represents maximum strain), (c) DIC shear strain contour at an average shear strain of 0.008





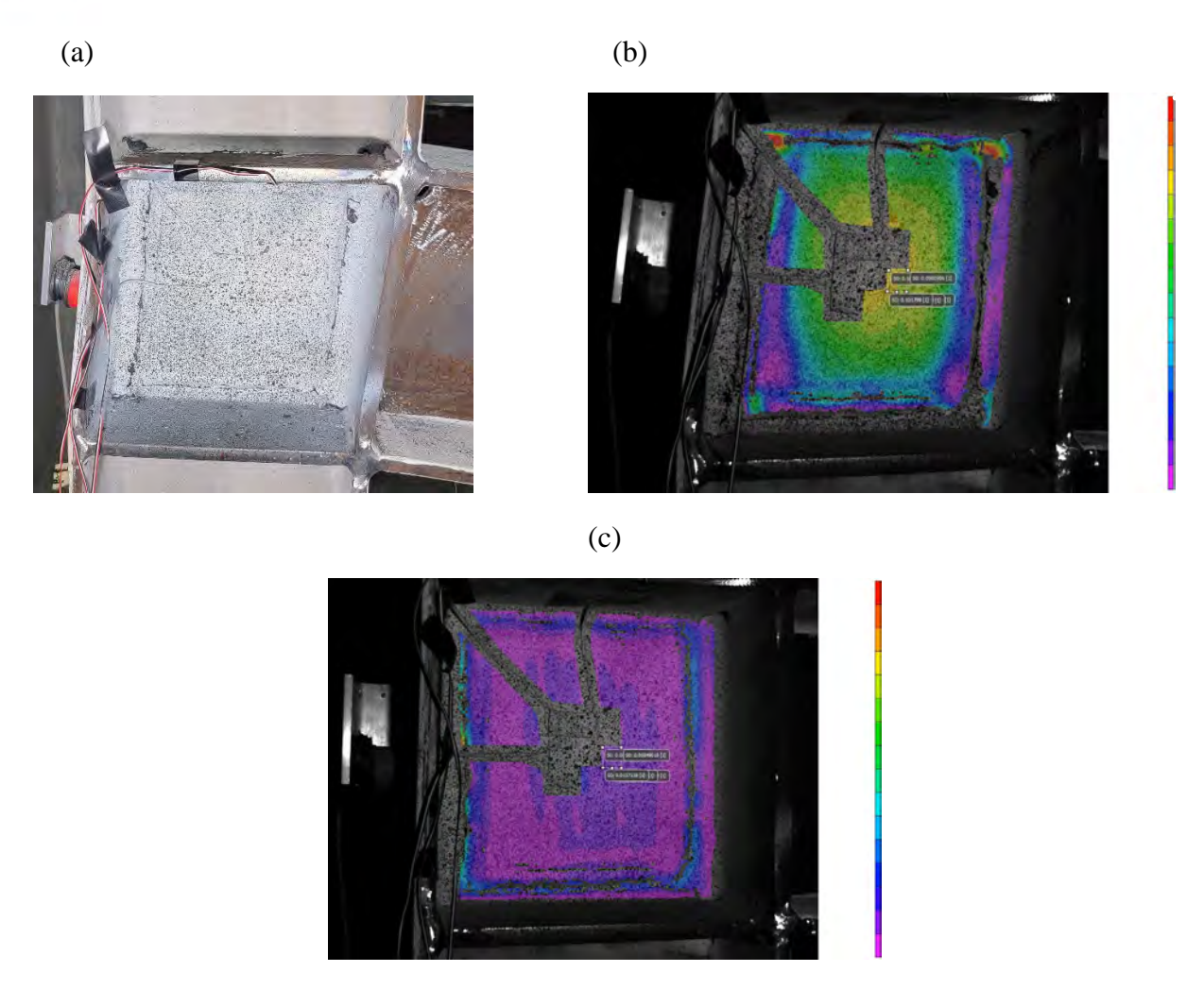


Figure 5.14: W250-RDP2B: (a) Deformed shape at the end of the test at test at 0.12 shear strain, (b) DIC shear strain contour at the end of the test at 0.12 shear strain (yielding $\gamma_y = 0.008$ is shown by the boundary of purple and blue – red represents maximum strain), (c) DIC shear strain contour at an average shear strain of 0.008

For W410-RDP2A and W410-RDP2B, the deformed panel zone and the shear distribution in the panel zone are given in Figures 5.15a, 5.15b, 5.16a, and 5.16b. For these specimens, shear buckling at approximately 0.040 strain accompanied by fracture in the doubler plate fillet weld. Fracture in the weld finally led to a complete separation of the doubler plate along its two edges.





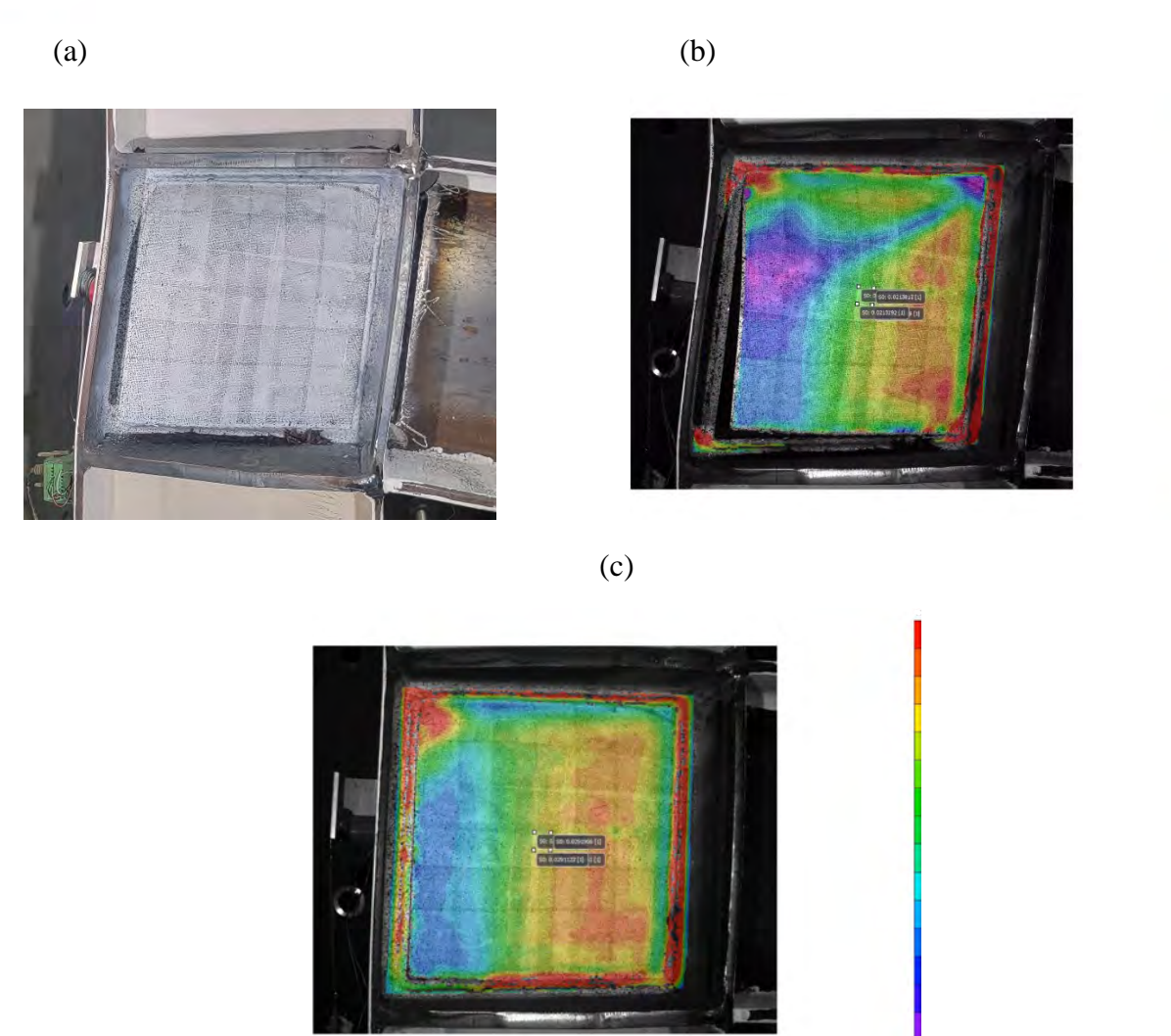


Figure 5.15: W410-RDP2A: (a) Deformed shape at the end of the test at shear strain 0.10, (b) DIC shear strain contour at the end of the test at shear strain 0.10 (yielding $\gamma_y = 0.009$ is shown by the boundary of cyan and green – red represents maximum strain), (c) DIC shear strain contour at an average shear strain of 0.009





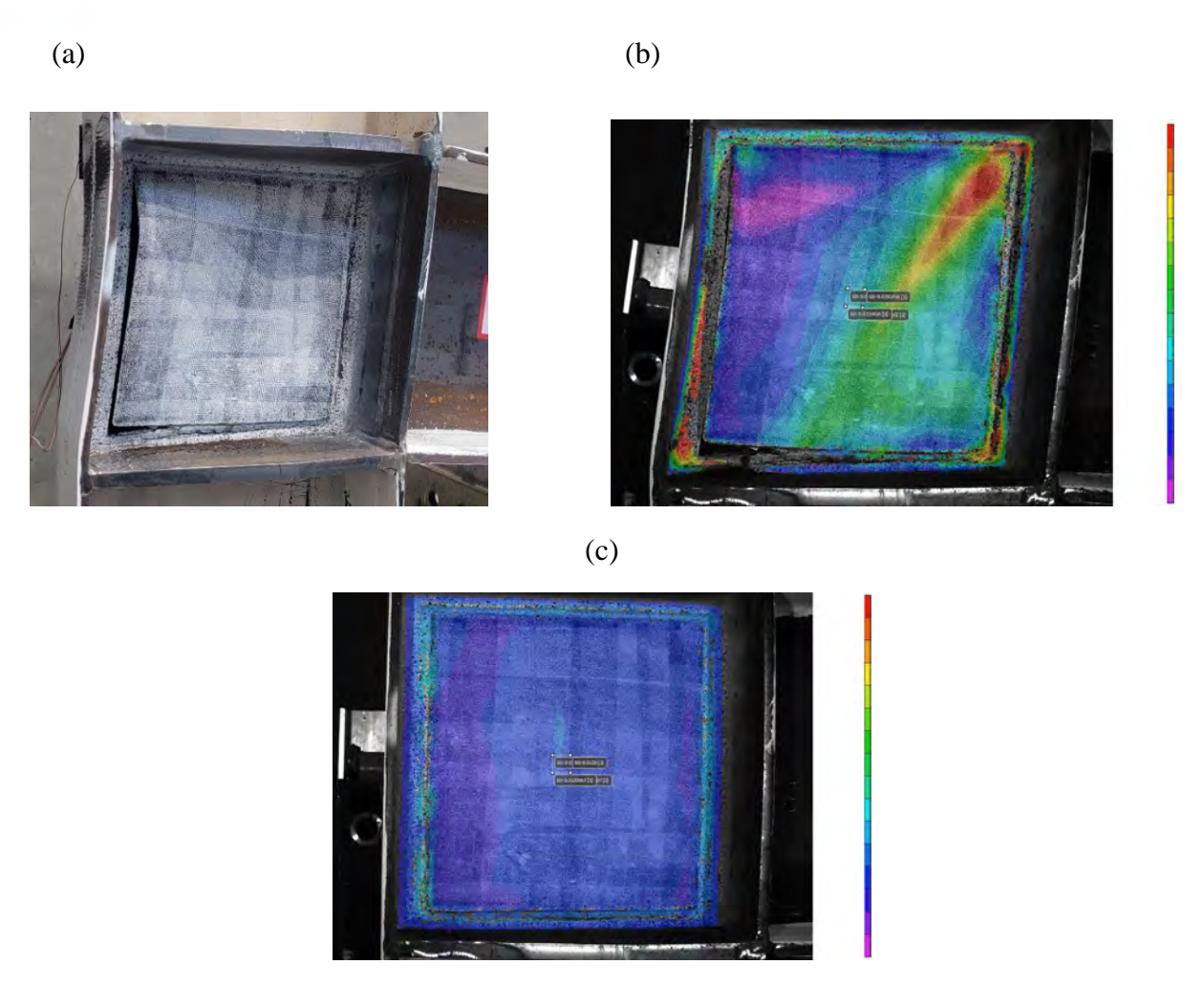


Figure 5.16: W410-RDP2B: (a) Deformed shape at the end of the test at shear strain 0.10, (b) DIC shear strain contour at the end of the test at shear strain 0.10 (yielding $\gamma_y = 0.009$ is shown by the dark blue areas – red represents maximum strain), (c) DIC shear strain contour at an average shear strain of 0.009

Overall, inelastic shear buckling developed in all reduced W410 specimens, in both the doubler plate and column web, after shear yielding and strain hardening, at shear strain exceeding approximately 0.040 (see Figure 5.4).

For all the specimens, the beam and the column outside the PZ remained elastic and behaved as expected in design, promoting panel zone yielding.





5.4 Panel Zone Local Strain Response

Shear strains on both sides of the connection are measured using a strain gauge rosette (SG) on one side and the DIC system on the opposite side and are given in Figures 5.17 to 5.24 for all the specimens. The vertical axis represents local shear strain, which is the strain collected from the rosettes or DIC system whereas the horizontal axis represents the panel zone average shear strain measured by the DIC system. Note that the strain gauges malfunctioned beyond approximately 0.030 strain.

In W250-NDP, a strain gauge is placed on Face 1 and the DIC system on Face 2 (see Fig. 5.6) of the panel zone. Shear strains on either side are consistent as shown in Figure 5.17. In W410-NDP, DIC systems are used on both faces of the column web, in addition to a SG on Face 1. Figure 5.18 shows the point where shear strain diverged at $\gamma = 0.06$ mm/mm which represents the onset of shear buckling in the column web as described earlier. This divergence indicates that the localized deformations that occur in the panel zone cause some areas to experience significant shear deformation (> 0.12) following with bulging (out of plane deformation) of the column web.

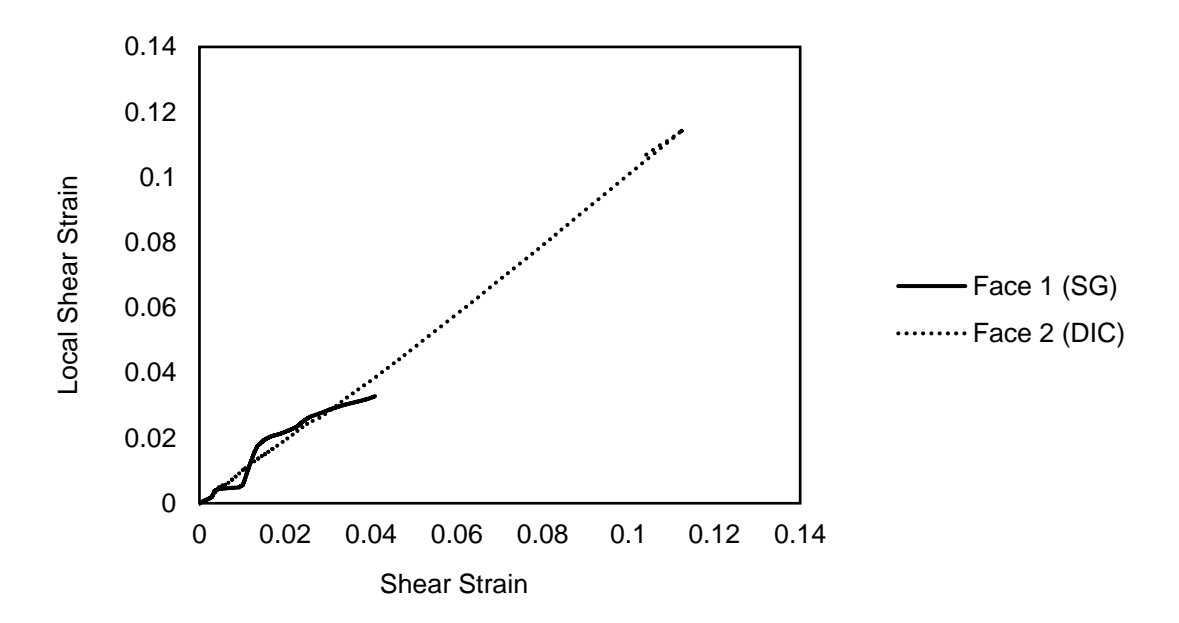


Figure 5.17: Local shear strain at the middle of the panel zone versus panel zone shear strain for W250-NDP





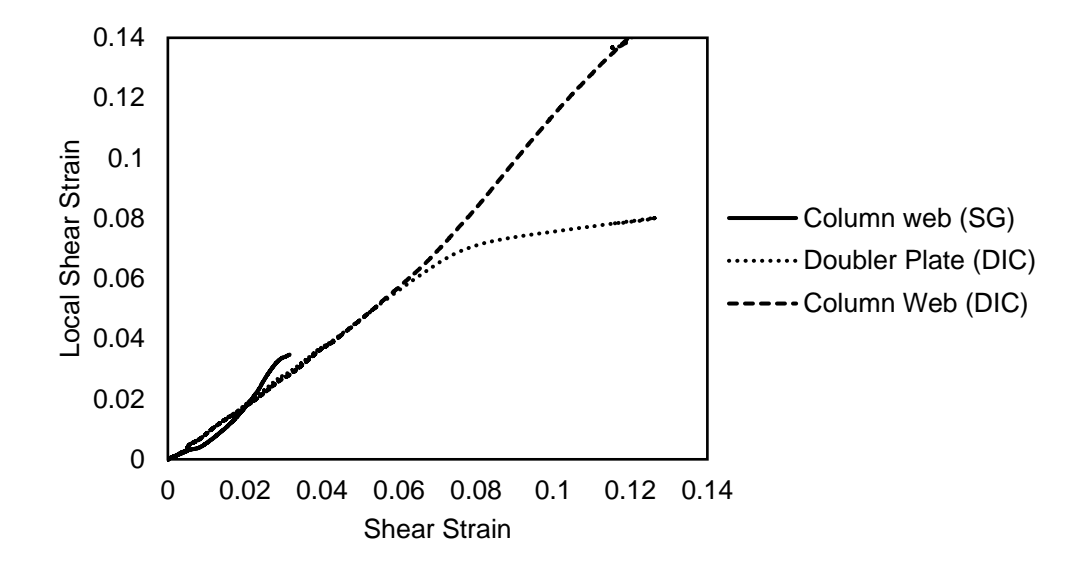


Figure 5.18: Local shear strain at the middle of the panel zone versus panel zone shear strain for W410-NDP

For W250-DP, SG on the column web and DIC system on the doubler plate were used to collect the strain data, which are shown in Figure 5.19. The results show that the strains on both sides of the panel zone were almost the same in the elastic region but they start to diverge beyond yielding, then pick up at about 0.03 shear strain.

For W410-DP, DIC system is used on the doubler plate side and a SG on the column web side. Figure 5.20 show the strain results for this specimen. Due to the sudden unloading that occurred while testing this specimen, the data from the DIC and strain gauge is not complete.





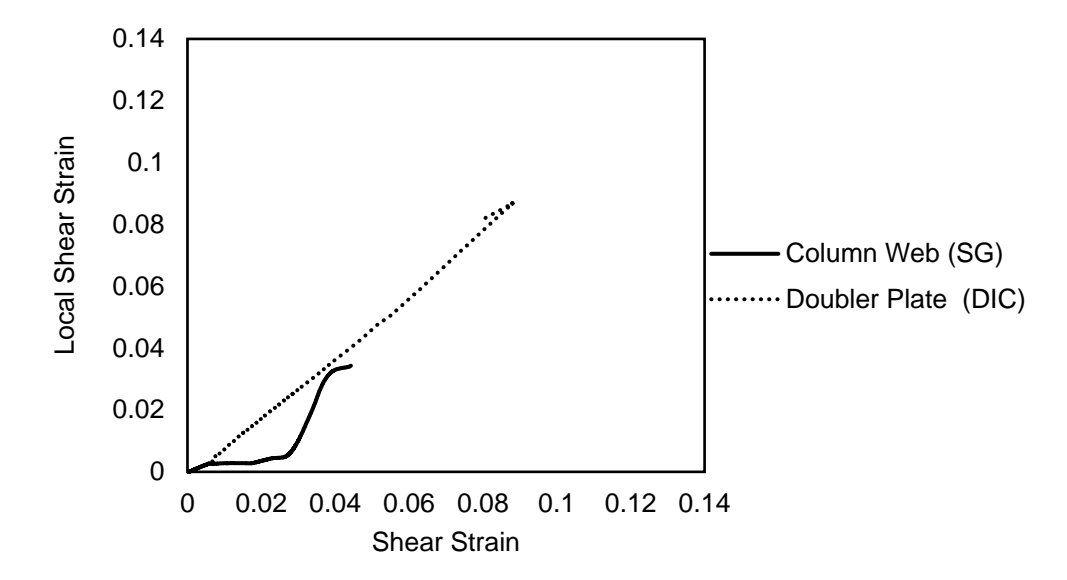


Figure 5.19: Local shear strain at the middle of the panel zone versus panel zone shear strain for W250-DP

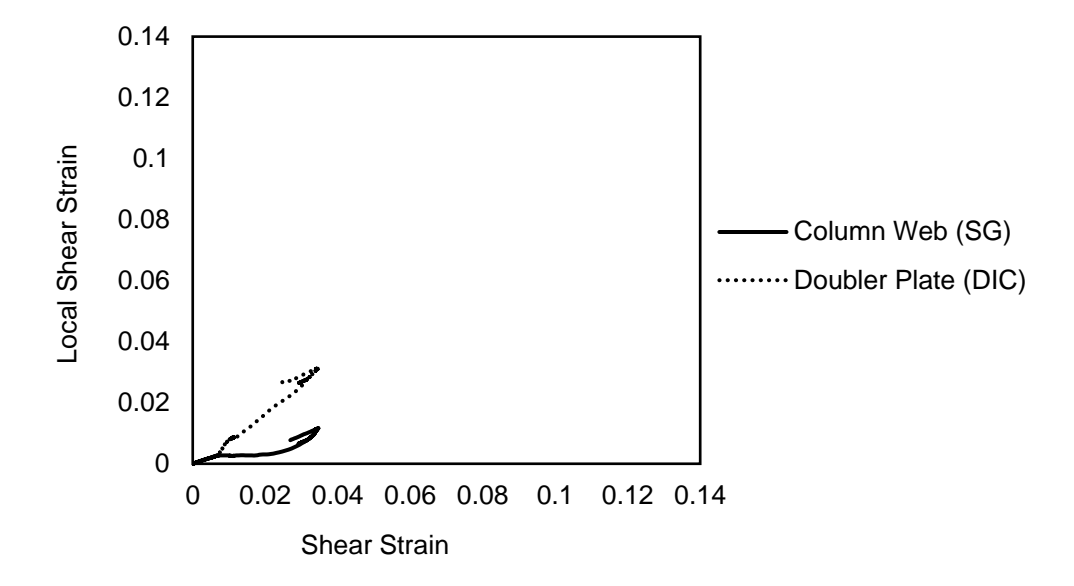


Figure 5.20: Local shear strain at the middle of the panel zone versus panel zone shear strain for W410-DP





The DIC system is used on the doubler plate side of W250-RDP1A and W250-RDP1B, whereas a strain gauge is installed on the column web to record the deformation in that area. The strain results for these specimens are shown in Figure 5.21. Similar observations as described for W250-DP were made for W250-RDP1.

For W410-RDP1A and W410-RDP1B, DIC system is used on both sides of the panel zone and an additional strain gauge is placed on the column web side. The local strain distribution on the DP side diverges from the strain gauge data on the column web side at $\gamma = 0.044$ for W410-RDP1A and $\gamma = 0.043$ for W410-RDP1B (Figure 5.22) when shear buckling starts to develop in the doubler plate and column web. The strains on both sides of the panel zone were almost the same in the elastic and post-yield regions prior to shear buckling.

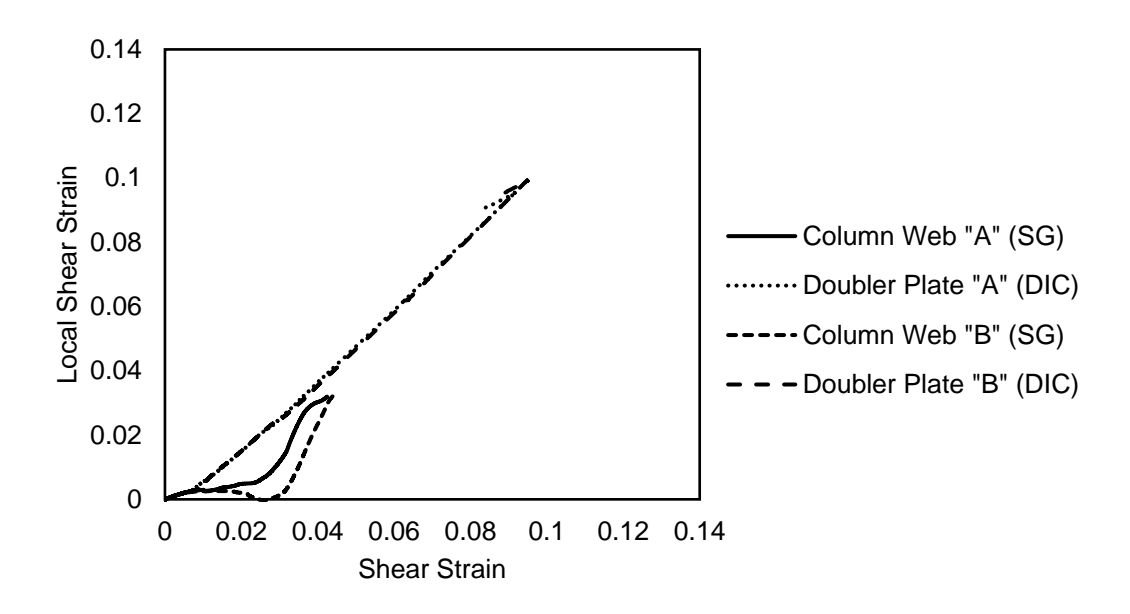


Figure 5.21: Local shear strain at the middle of the panel zone versus panel zone shear strain for W250-RDP1





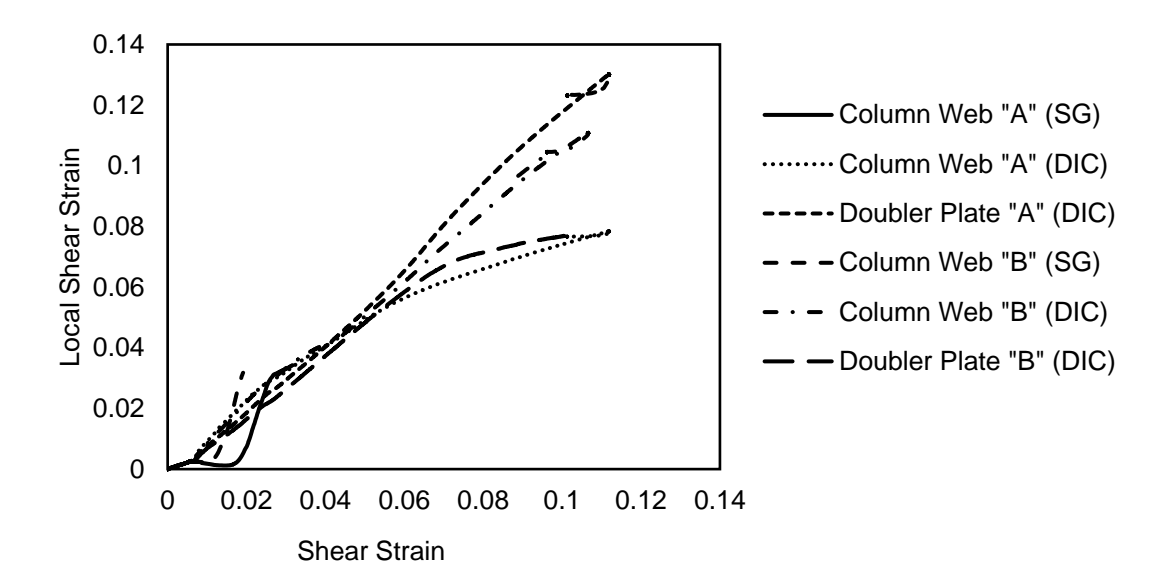


Figure 5.22: Local shear strain at the middle of the panel zone versus panel zone shear strain for W410-RDP1

For W250-RDP2A, a strain gauge and DIC system are installed on both sides of the specimen, the doubler plate and the column web. As shown in Figure 5.23, the results from the DIC system agreed with those of the strain gauge prior to yielding with a slight deviation in the post-yield region. Similar strain response as W250-RDP2A, was observed for the identical specimen, W250-RDP2B.

For W410-RDP2A and W410-RDP2B, the DIC system was installed on either side of the panel zone and a strain gauge on the column web side. Due to shear buckling accompanied by weld fracture, the doubler plate unzipped slowly away from the column web at around $\gamma = 0.05$ where the strain in the doubler plate became almost stagnant in W410-RDP2B and started to decrease in W410-RDP2A (see Figure 5.24). The shear strains on both sides of W410-RDP2A were almost the same in the elastic and post-yielding regions up until buckling whereas the strains in W410-RDP2B diverged post-yielding.





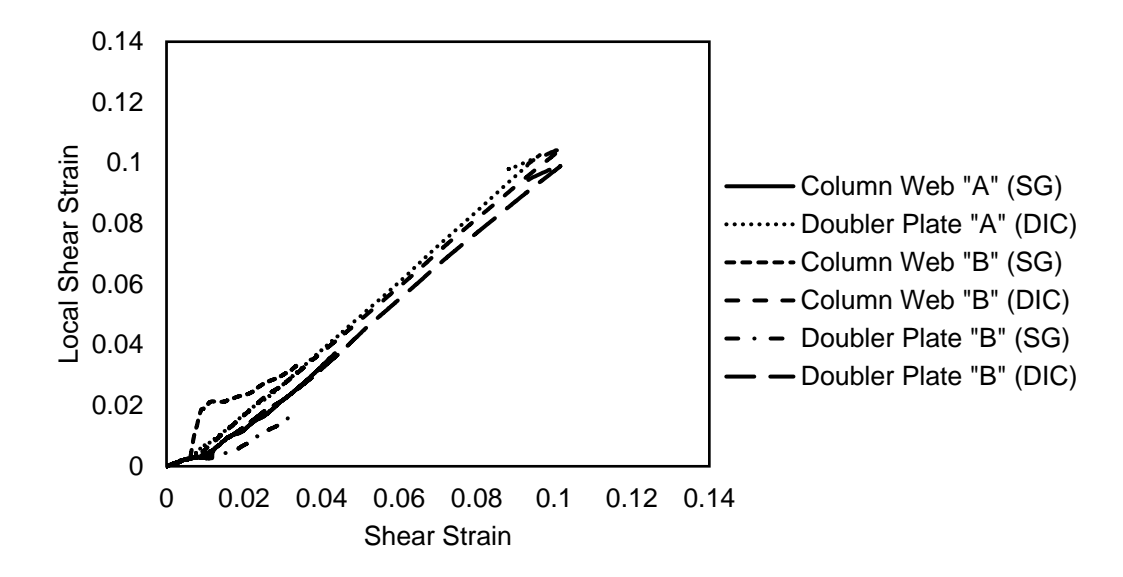


Figure 5.23: Local shear strain at the middle of the panel zone versus panel zone shear strain for W250-RDP2

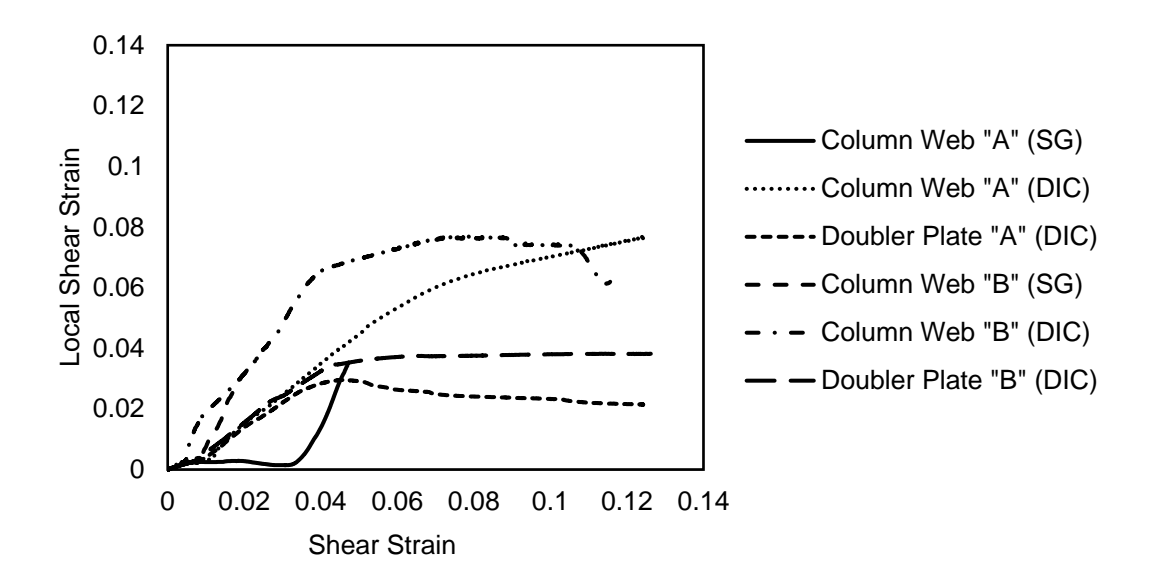


Figure 5.24: Local shear strain at the middle of the panel zone versus panel zone shear strain for W410-RDP2





In reduced doubler plate specimens, measured local strains in the doubler plate tend to lag those recorded at the column web at a given shear strain for W410-DP, W410-RDP1A, W410-RDP1B, W250-RDP2B, W410-RDP2A, and W410-RDP2B as shown Figures 5.20 to 5.24. Other researchers have observed a similar phenomenon (Bertero et al. 1973; Becker 1975; Skiadopoulos et al. 2021; Reynolds and Uang, 2022). However, the opposite was observed for W250-DP, W250RDP1A, W250-RDP1B, and W250-RDP2A (see Figures 5.19 and 5.21), which could be attributed to strain gauge data. When analyzing the strain in the elastic region, it is inferred that local strains on either side of the panel zone are nearly the same.

5.5 Discussion

5.5.1 Panel zone response and limit states

Table 5.1 lists the connection design load represented as a point load at the beam end $P_{\rm Vp-n}$, the applied load at the beam end in the experiment $P_{\rm Vp-m}$ at yielding, the predicted shear capacity of the panel zone $V_{\rm p-n}$, and the measured panel zone shear force at yielding $V_{\rm p-m}$ for the specimens. Additionally, a summary of the average strain at yielding and at maximum force is outlined in the table as well. Bilinear curves as shown in Figure 5.25 are used to obtain the measured panel zone shear force at yielding. The bilinear curves for the rest of the specimens are included in Appendix C. The bilinear curves are obtained by ensuring the elastic stiffness, the shear force at ultimate shear strain (taken as 0.025 here), and the area under the original and bi-linearized curves are the same. The test-to-predicted ratios are also presented in Table 5.1. The predicted shear capacity of the panel zone $V_{\rm p-n}$ is calculated using Equation (3-11) and the corresponding design load at the beam end $P_{\rm Vp-n}$ is back-calculated using the predicted shear capacity of the panel zone assuming shear yielding in the doubler plate as the predominant limit state. Note that the predicted shear capacity $V_{\rm p-n}$ of the specimens with the reduced details is based on the new method introduced in Chapter 6 (Equation 6-22).

Referring to Table 5.1, W410-NDP and W410-DP yielded slightly later than expected with test-to-predicted ratios of 1.07 and 1.20, respectively. Residual stresses, which could delay the onset of yielding, and uncertainties associated with doubler plate welds are the potential reasons for these discrepancies. The applied load at the beam end for W250-DP, W410-RDP1, and W410-RDP2 is almost the same as the predicted values with test-to-predicted ratios between 0.95 and 1.00,





whereas W250-NDP and W250-RDP1 showed a test-to-predicted ratio that was lower by 9% and 6%, respectively.

Table 5.1: Design load versus applied load at the beam end, and predicted shear capacity of the panel zone versus measured panel zone shear force at yielding

Specimen ID	P_{Vp-m}	P_{Vp-n}	Test	$V_{\rm p-m}$	$V_{\rm p-n}$	Test	Average	Average
	(kN)	(kN)	Predicted	(kN)	(kN)	Predicted	strain at	strain at
							shear	maximum
							yielding	force
							(rad.)	(rad.)
W250-NDP	97	107	0.91	487	537	0.91	0.007	0.110
W250-DP	176	176	1.00	880	887	0.99	0.009	0.088
W250-RDP1A	149	161	0.93	748	809	0.92	0.008	0.091
W250-RDP1B	153	161	0.95	766	809	0.95	0.008	0.095
W250-RDP2A	143	150	0.95	715	756	0.94	0.008	0.096
W250-RDP2B	143	150	0.95	715	756	0.94	0.008	0.101
W410-NDP	268	253	1.06	818	766	1.07	0.008	0.108
W410-DP	471	394	1.20	1437	1190	1.21	0.011	0.088
W410-RDP1A	406	407	1.00	1240	1229	1.00	0.008	0.105
W410-RDP1B	407	407	1.00	1241	1229	1.01	0.008	0.070
W410-RDP2A	375	397	0.94	1144	1200	0.95	0.009	0.044
W410-RDP2B	408	397	1.03	1245	1200	1.04	0.009	0.041





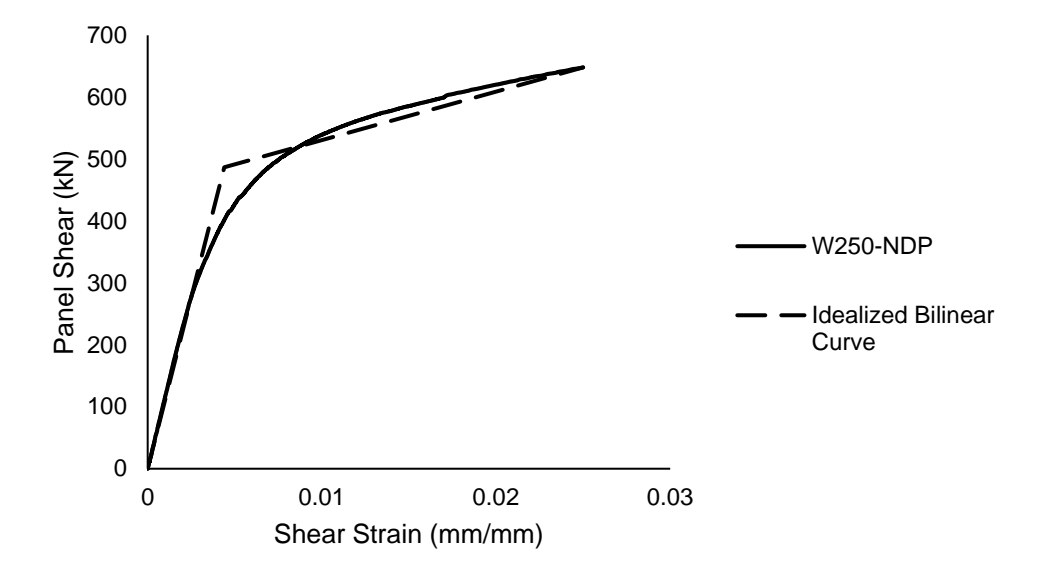


Figure 5.25: Panel shear force versus panel shear strain for W250-NDP

5.5.2 Effect of column section size

The deeper column tested in this research has a web slenderness ratio of $\frac{h}{t_{cw}} = 46.3$ (where h is the clear depth of the column web w is the column web thickness only), making the specimens more susceptible to shear bucking. The threshold for web shear buckling based on CSA S16 is:

$$\frac{h}{t_{cw}} \le 439 \sqrt{\frac{k_v}{F_{y-m}}} \tag{5-1}$$

where $k_{\rm v} = 4 + \frac{5.34}{\left(\frac{a}{h}\right)^2} = 9.64$ (shear buckling coefficient), $\frac{a}{h} = 0.97$ is the ratio of the distance

between the stiffeners to the web depth, and F_{y-m} is the measured yield strength. The slenderness ratio limit for shear buckling is calculated as 68.9, which is higher than that of the W410×60 specimens tested here, reducing the potential for shear buckling before shear yielding as confirmed by the test results.

5.5.3 Effect of doubler plate geometry (reduced vs. standard)

Referring to Figure 5.3 and Table 5.1, reducing the doubler plate size in W250 specimens, decreased $P_{\rm Vp-m}$ from 176 kN for W250-DP to an average of 151 kN for W250-RDP1A and W250-RDP1B. Further reducing the doubler plate in W250 specimens, led to a decrease in





 $P_{\rm Vp-m}$ to an average of 143 kN for W250-RDP2A and W250-RDP2B. As shown in Table 5.1, reducing the doubler plate size in W410 specimens, decreased $P_{\rm Vp-m}$ from 479 kN (W410-DP) to 406 kN (W410-RDP1A and W410-RDP1B) and further reducing the doubler plate diminished the force to an average of 393 kN in W410-RDP2A and W410-RDP2B. The average $P_{\rm Vp-m}$ of specimens A and B is used. These observations are in agreement with those reported by Shirsat (2011), i.e., narrower doubler plate leads to a reduction in stiffness and strength of the connection. Test results confirmed the potential for the application of reduced doubler plates with fillet welds in design of pipe rack structures provided that a limit on the doubler plate reduction is set to avoid significantly small doubler plates, which may promote shear buckling in the reduced areas. The results also confirmed the contributions from column flanges in resisting the applied shear in the connection (Krawinkler 1978).





6 DESIGN RECOMMENDATIONS

This chapter presents a design method for the proposed reduced-size doubler plate detail. Two working examples, including the one originally presented in Chapter 3 and the test specimen W250-RDP1, are presented to demonstrate the proposed design method.

6.1 Design Method

6.1.1 Doubler plate interface weld

The first step of the design method includes a check to ensure the fillet weld used to connect the doubler plate to the column web is sufficient to carry the weld interface load. Equilibrium is used to calculate shear forces induced in the panel zone (PZ), column web and doubler plate. Figure 6.1 depicts the panel zone area of the beam-to-column connection, including the column panel zone and a reduced doubler plate, by $2L_1$ in the horizontal direction and $2H_1$ in the vertical direction. L_{DP} and H_{DP} represent the doubler plate's length and height, respectively, whereas $L_{PZ} = d_c - 2t_{cf}$ and $H_{PZ} = d_b - 2t_{bf}$ are the panel zone's length and height. The doubler plate is assumed to be centred in the panel zone.

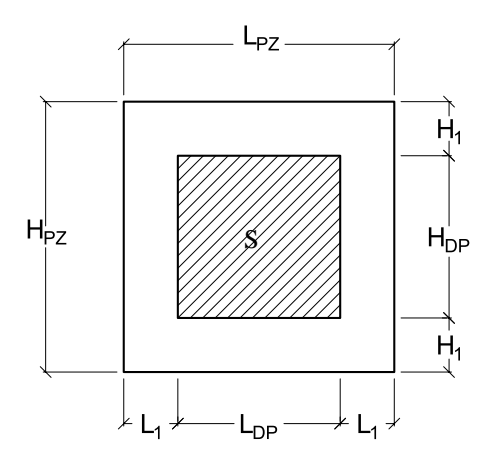


Figure 6.1: Panel zone layout and dimensions

When shear is induced in the panel zone area, the internal shear forces in each segment of the panel zone plates can be calculated using the free-body diagrams outlined in Figure 6.2. The horizontal shear demand of the panel zone, $V_{\rm PZH,d}$ (Figure 6.3) is calculated as follows:

$$V_{\text{PZH,d}} = max\left(\left|\left(V_{\text{PZH,d}}\right)_{\text{T}}\right|,\left|\left(V_{\text{PZH,d}}\right)_{\text{B}}\right|\right)$$
(6-1a)





$$(V_{PZH,d})_T = -\frac{M_{b-R}}{d_{b-R} - t_{fb-R}} + \frac{M_{b-L}}{d_{b-L} - t_{fb-L}} - V_{col-T}$$
 (6-1b)

$$(V_{\text{PZH,d}})_{\text{B}} = -\frac{M_{\text{b-R}}}{d_{\text{b-R}} - t_{\text{fb-R}}} + \frac{M_{\text{b-L}}}{d_{\text{b-L}} - t_{\text{fb-L}}} - V_{\text{col-B}}$$
(6-1c)

where $M_{\rm b-R}$ and $M_{\rm b-L}$ are the moment in the right and left beams at the column face, $d_{\rm b-R}$ and $d_{\rm b-L}$ are the depths of the right and left beams, $t_{\rm fb-R}$ and $t_{\rm fb-L}$ are the beam flange thicknesses, $V_{\rm col-T}$ and $V_{\rm col-B}$ are the column shear forces above and below the connection.

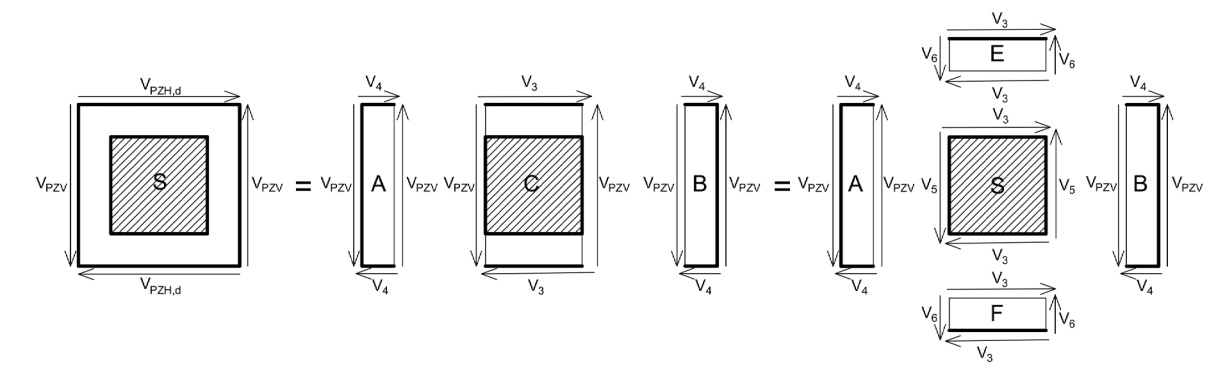


Figure 6.2: Panel zone and panel zone components free-body diagrams (force vectors are defined in their respective equations)

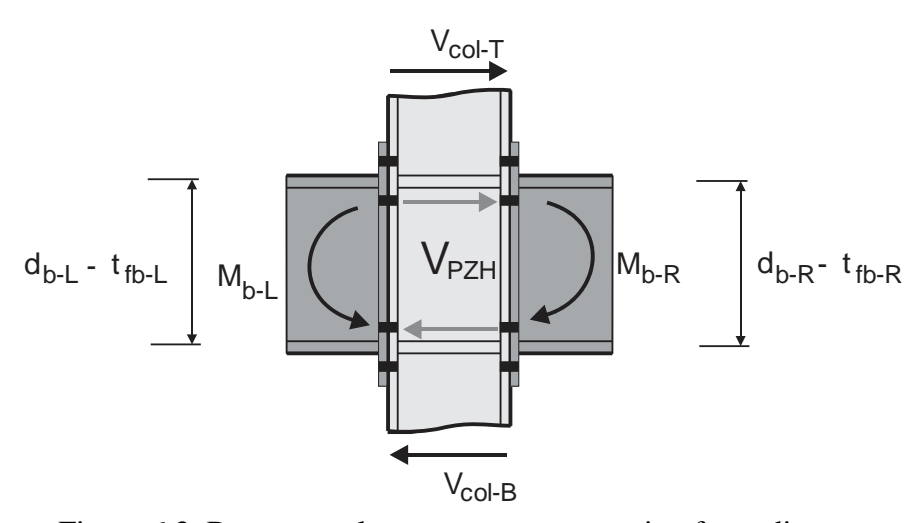


Figure 6.3: Beam-to-column moment connection force diagram

Based on the force/moment equilibrium, the vertical shear in the panel zone, $V_{\rm PZV}$, is calculated as follows:

$$V_{\rm PZV} = \left(\frac{2H_1 + H_{DP}}{2L_1 + L_{DP}}\right) V_{PZH,d} \tag{6-2}$$





The panel zone is first sectioned into three parts A, B, and C as shown in Figure 6.2. The vertical shear force in A, B, and C equals V_{PZV} . In part C, the horizontal shear force, V_3 , is calculated as:

$$V_3 = \left(\frac{L_{DP}}{2L_1 + L_{DP}}\right) V_{PZH,d} \tag{6-3}$$

Part C is further sectioned into three parts S, E, and F as shown in Figure 6.2. To satisfy the force/moment equilibrium, the horizontal shear in parts E and F along S equals V_3 . Hence, the vertical shear imposed on S, V_5 , is calculated as follows:

$$V_5 = \left(\frac{H_{DP}}{L_{DP}}\right) V_3 = \left(\frac{H_{DP}}{2L_1 + L_{DP}}\right) V_{PZH,d}$$
 (6-4)

 V_4 and V_6 from Figure 6.2 are horizontal and vertical shear forces, respectively, induced in the unreinforced areas A, B, E, and F.

The dimensions of the doubler plate should be selected such that the force V_3 does not cause failure in the fillet weld connecting DP to the column web. The resistance of the fillet weld is calculated as:

$$V_{\rm r-w} = 0.67 \phi_w A_w X_u \tag{6-5}$$

where X_u is the nominal strength of the weld metal and $\phi_w = 0.67$ is the weld resistance factor, A_w is the effective area of the weld, which is equal to $0.707Dl_w$, where D and l_w are the size and length of the doubler plate fillet weld, respectively.

Since the doubler plate and the column web in S (Figure 6.1), are welded, it can be assumed that their shear deformations are the same, which means they can be considered as two parallel shear springs. Given that their contribution to the applied shear is proportional to their thickness, the horizontal shear force acting on the doubler plate, $V_{\rm DPH}$, is calculated as follows:

$$V_{\rm DPH} = \left(\frac{t_{DP}}{t_{DP} + t_{cw}}\right) V_3 \tag{6-6}$$

where $t_{\rm DP}$ and $t_{\rm cw}$ are the thicknesses of the doubler plate and column web, respectively. A minimum plate thickness of 10 mm is recommended for the doubler plate to achieve a more practical and economical design.





The horizontal shear force acting on the doubler plate, V_{DPH} , should be transferred from the column web to the doubler plate through the fillet welds. Therefore, the horizontal welds are subjected to V_{DPH} . Combining Equations (6-3) and (6-6), $V_{DPH} = V_{f-w}$:

$$V_{\text{f-w}} = \left(\frac{t_{DP}}{t_{DP} + t_{cw}}\right) \left(\frac{L_{DP}}{L_{PZ}}\right) V_{PZH,d}$$
(6-7)

To prevent weld fracture, V_{f-w} (Eq. 6-7) is limited to the strength of the fillet weld (Eq. 6-5) as follows:

$$V_{f-w} \le 0.67(0.67X_{\rm u})(0.707Dl_w) \tag{6-8}$$

If this criterion is not met, the dimensions of the reduced DP should be adjusted, or the designer should opt for a different doubler plate detail. A typical weld size of 6 mm recommended to achieve an practical and economical design provided that the required strength is obtained (see Eq. 6-8), as this weld size can often be completed in a single pass. However, practices and preferences may vary among steel fabricators. When selecting the fillet weld size, it is recommended to keep the weld size 2 mm smaller than the doubler plate thickness to avoid melting the corners of the plate, which may result in smaller weld than specified. It is important to note that this recommendation was neglected in the specimens designed in this study to ensure weld fracture is delayed before yielding and buckling of the column panel zone.

6.1.2 Doubler plate dimensions

The dimensions of the doubler plate should be chosen such that the shear deformation in the unreinforced area is limited to avoid excessive shear deformation of the panel zone due to shear yielding of the column web. The expected profiles of shear deformation along the height of the panel zone for the two cases of with and without doubler plate are shown in Figure 6.4. As shown in this diagram, in the case of the panel zone without a doubler plate, the shear deformation is distributed uniformly along the depth of the panel zone with a shear strain of γ_{ave} , whereas in the case of the panel zone with a doubler plate, the shear deformation is concentrated in the unreinforced area of the panel zone and is not distributed uniformly along its depth. The shear strain in the doubler plate and in the perimeter area are γ_1 and γ_2 , respectively.





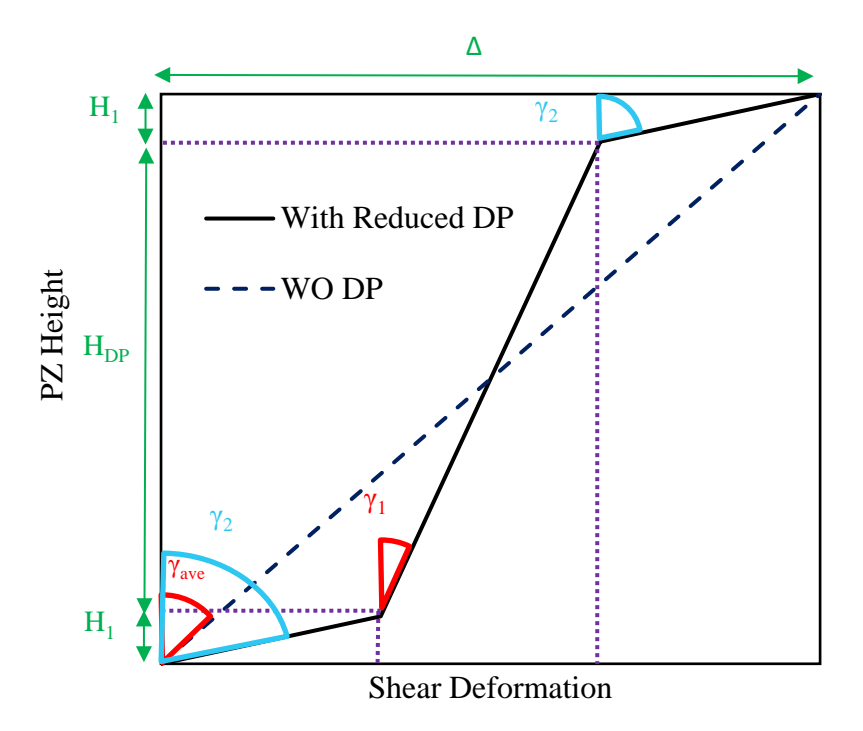


Figure 6.4: Schematic distribution of shear deformation along the panel zone height for column panel zone with reduced DP and without DP

According to Figure 6.4, in the case of the panel zone without a doubler plate, the total shear deformation of the panel zone can be calculated as follows:

$$\Delta = \gamma_{ave} H_{PZ} \tag{6-9}$$

where γ_{ave} is the critical shear strain for the case of the panel zone without a doubler plate. Assuming uniform strain, γ_{ave} , in the panel zone, Equation (6-9) can be rearranged as follows:

$$\gamma_{\text{ave}} = \frac{\Delta}{2H_1 + H_{DP}} \tag{6-10}$$

For the panel zone with a reduced doubler plate, the unreinforced area of the panel zone should be selected by limiting the total expected shear deformation of the panel zone in the unreinforced area. The shear deformation, including the deformation of the DP plus the column web behind the DP and the deformation of the unreinforced areas, is:

$$\Delta = 2\gamma_2 H_1 + \gamma_1 H_{DP} \tag{6-11}$$





Replacing Δ in Equation (6-10) with the amplitude given in Equation (6-11) and assuming that the average shear deformation in the panel zone remains below the deformation corresponding to shear yielding, the following inequality can be obtained:

$$\gamma_{\text{ave}} = \frac{2\gamma_2 H_1 + \gamma_1 H_{DP}}{H_{P7}} \le \gamma_{\text{y,web}}$$
(6-12)

To avoid excessive shear deformation in the unreinforced area of the panel zone, which experiences higher shear deformation than the interior reinforced area, the shear strain in the unreinforced region, γ_2 , is limited to $1.5\gamma_{y,web}$, a conservative value adapted from the values proposed in previous studies (Krawinkler 1978). Thus, Equation (6-12) can be rearranged to determine a limit on doubler plate reduction, H_1 :

$$H_1 \le \left(\frac{\frac{1}{1.5} - \frac{1}{\alpha}}{2 - \frac{2}{\alpha}}\right) H_{PZ}$$
 (6-13)

where $\alpha = \gamma_2/\gamma_1$ is the ratio of the shear strain in the unreinforced panel zone area, γ_2 , to the shear strain in DP area, γ_1 . Leveraging the experimental results presented in Figures 5.13c, 5.14c, 5.15c and 5.16c for both sets of specimens tested here, α can be set equal to 2.1 at 0.009 average strain for the specimens tested here, which results in an unreinforced column web of $H_1 \leq 0.18H_{PZ}$.

Once H_1 is checked against the limit, L_1 is obtained and checked as follows:

$$L_1 \le H_1 - D_s + (k - t_{cf}) \tag{6-14}$$

where D_s is the stiffener-to-column web fillet weld size and k is the distance from outer face of flange to the web toe of fillet.

To prevent shear buckling of the doubler plate, the thickness of the DP should satisfy the following requirement:

$$t_{DP} \ge \frac{L_{DP} + H_{DP}}{90} \tag{6-15}$$

This requirement has been adopted from AISC 341 (2022) for column web doubler plates.





6.1.3 Shear resistance of panel zone

The concept of plastic analysis is used to compute the shear resistance of the PZ including the reduced doubler plate assuming elastic–perfectly plastic material response for both column web and DP materials and that shear strains in the web of the column and DP are almost the same at yielding, which is confirmed by experimental testing (strain in the reduced area of the panel zone is approximately 2.1 that of the reinforced area when average strain in the panel zone approaches $\gamma_{y,web}$). Kinematic or virtual work method, which is a lower-bound method, is employed to satisfy the collapse mechanism in plastic analysis of the panel zone in pure shear. The external work done by the shear applied to the panel zone V_n is calculated as:

$$W_{\rm ext} = V_n \Delta \tag{6-16}$$

The internal work is calculated as:

$$W_{\rm int} = W_{int.web} + W_{int.DP} \tag{6-17}$$

in which $W_{\text{int,web}}$ and $W_{\text{int,DP}}$ are the internal work in the web and DP, respectively. The internal work in the web of the column is:

$$W_{\text{int,web}} = 0.66F_{y,web}d_c t_{cw} \Delta \tag{6-18}$$

The internal work in the DP is set as follows:

$$W_{\text{int,DP}} = 0.66 F_{y,DP} L_{DP} t_{DP} \left(\frac{H_{DP}}{H_{PZ}} \right) \Delta$$
 (6-19)

By equating the internal and external works:

$$W_{\rm ext} = W_{\rm int} \tag{6-20}$$

and substituting internal and external works from Equations (6-16), (6-18), and (6-19) into Equation (6-20), this equation can be rewritten as:

$$V_{\rm n}\Delta = 0.66F_{y,DP}L_{DP}t_{DP}\left(\frac{\Delta}{H_{PZ}}\right)H_{DP} + 0.66F_{y,web}d_ct_{cw}\Delta$$
 (6-21)

Thus, the shear resistance of the PZ is obtained as:

$$V_{\rm n} = 0.66F_{y,DP}L_{DP}t_{DP}\left(\frac{H_{DP}}{H_{PZ}}\right) + 0.66F_{y,web}d_ct_{cw}$$
(6-22)





The factored shear resistance of the column panel zone with a reduced doubler plate, V_r , is given as:

$$V_r = \varphi V_{\rm n}$$
 (6-23)
$$V_r = 0.9[0.66F_{y,DP}L_{DP}t_{DP}\left(\frac{H_{DP}}{H_{PZ}}\right) + 0.66F_{y,web}d_ct_{cw}]$$

where $\varphi = 0.9$ is the resistance factor for shear yielding based on CSA S16.

To account for the effect of the column axial force on the panel zone, the methodology proposed by AISC 360 Section J10.6, may be used, but further research is required to verify the influence of the column axial load on the capacity of the column web panel zone with reduced doubler plate:

For $C_f \leq 0.4C_y$,

$$V_r = 0.9[0.66F_{y,DP}L_{DP}t_{DP}\left(\frac{H_{DP}}{H_{PZ}}\right) + 0.66F_{y,web}d_ct_{cw}]$$
(6-24)

For $C_f > 0.4C_y$,

$$V_{\rm r} = 0.9 \left(1.4 - \frac{C_f}{C_v} \right) \left[0.66 F_{y,DP} L_{DP} t_{DP} \left(\frac{H_{DP}}{H_{PZ}} \right) + 0.66 F_{y,web} d_c t_{cw} \right]$$
 (6-25)

where C_f and C_y are the column axial force and the yield axial force of the column, respectively.

6.2 Design Examples

6.2.1 W250×73 beam-to-W250×73 column connection

The example presented in Chapter 3 is redesigned here using the following steps:

Step 1) Calculate the horizontal shear demand of the panel zone, $V_{\rm PZH,d}$, using Equation (6-1):

$$V_{\text{PZH,d}} = \frac{160 \text{ kNm}}{(0.254 - 0.0142)\text{m}} = 667 \text{ kN}$$

Step 2) Assume values for the reductions of the DP in vertical and horizontal directions, as well as the DP thickness and fillet weld size. Then, calculate the height and length of the doubler plate.

 $H_1 = 20$ mm, $L_1 = 20$ mm, D = 12 mm, and $t_{\rm DP} = 14$ mm. The height and length of the PZ are calculated as: $H_{\rm PZ} = d_{\rm b} - 2t_{fb} = 254 - 2 \times 14 = 226$ mm and $L_{\rm PZ} = d_c - 2t_{cf} = 254 - 2 \times 14 = 226$ mm. The doubler plate height and length are calculated as: $H_{\rm DP} = H_{\rm PZ} - 2H_1 = 226 - 2 \times 20 = 186$ mm, $L_{\rm DP} = L_{\rm PZ} - 2L_1 = 226 - 2 \times 20 = 186$ mm.





(Regular DP dimensions from Chapter 3 are 203 mm \times 201 mm)

Step 3) Verify $H_1 \le 0.18 H_{PZ}$ using Equation (6-13)

$$H_1 = 20 \text{ mm} \le 0.18 H_{PZ} = 41 \text{ mm}$$

Step 4) Verify $L_1 \le H_1 - D_s + (k - t_{cf})$ using Equation (6-14), assume $D_s = 8$ mm.

$$L_1 = 20 \text{ mm} \le H_1 - D_s + (k - t_{cf}) = 30 \text{ mm}$$

Step 5) Verify $t_{DP} \ge \frac{L_{\mathrm{DP}} + H_{\mathrm{DP}}}{90}$ using Equation (6-15).

$$t_{DP} \ge \frac{L_{DP} + H_{DP}}{90} = \frac{186 + 186}{90} = 4 \text{ mm}$$

Step 6) Calculate the horizontal shear force acting on the doubler plate, $V_{\rm DPH}$, which corresponds to the fillet weld shear demand, $V_{\rm f-w}$, using Equation (6-7)

$$V_{\text{f-w}} = \left(\frac{14}{8.6 + 14}\right) \left(\frac{186}{226}\right) \times 667 \text{ kN} = 339 \text{ kN}$$

Step 7) Calculate the capacity of the fillet weld and check against its demand using Equation (6-8)

$$V_{\rm r-w} = 0.67 \times (0.67 \times 490 \text{ MPa})(0.707 \times 14 \text{ mm} \times 186 \text{ mm}) = 346 \text{ kN}$$

$$V_{\text{f-w}} \leq V_{\text{r-w}}$$

$$339 \le 346 \text{ kN}$$

Step 8) Calculate the nominal and factored shear resistances of the panel zone using Equations (6-22) and (6-23), respectively.

$$V_{\rm n} = 0.66 \times 300 \text{ MPa} \times 186 \text{ mm} \times 14 \text{ mm} \times \left(\frac{186}{226}\right)$$

+ $(0.66 \times 350 \text{ MPa} \times 254 \text{ mm} \times 8.6 \text{ mm}) = 930 \text{ kN}$
 $V_{\rm r} = 0.9 \times 930 \text{ kN} = 837 \text{ kN}$





Step 9) If the factored shear force demand is less than or equal to the factored shear resistance, $V_{\text{PZH,d}} \leq V_{\text{r}}$, the design is considered satisfactory. Otherwise, the dimensions of the DP should be modified (Step 2). For this example,

$$V_{\rm PZHd} \leq V_{\rm r}$$

$$667 \le 837 \text{ kN}$$

which confirms that the selected reduced doubler plate dimensions 186×186×14 mm with 12 mm fillet weld can be used.

6.2.2 W250×58 beam-to-W250×58 column connection

Specimen W250-RDP1 (see Table 4.1) with $1\times D$ reduction on each side of the doubler plate is designed here based on the proposed design method under the applied panel zone shear of $V_{\rm PZH,d} = 530$ kN. The shear strength of the column web is found as 452 kN. Therefore, the shear capacity of the column web is insufficient, and a doubler plate is required to resist the applied load. The axial force in column is assumed to be less than $0.4C_y$. The measured yield stresses of 405 and 378 MPa are used for DP and column, respectively.

The design steps are summarized as follows:

- 1) Shear demand in the column panel zone, $V_{PZH,d} = 530 \text{ kN}$.
- 2) Assume values for the reductions of the DP in vertical and horizontal directions, as well as the DP thickness and fillet weld size. Then, calculate the height and length of the doubler plate. $H_1 = 17$ mm, $L_1 = 29$ mm, $H_{PZ} = 225$ mm, $L_{PZ} = 225$ mm, D = 8 mm, and $t_{DP} = 8$ mm. The doubler plate dimensions are calculated as: $H_{DP} = 191$ mm, $L_{DP} = 168$ mm.
- 3) Verify $H_1 \le 0.18 H_{PZ}$, $H_1 = 17 \text{ mm} \le 0.18 H_{PZ} = 41 \text{ mm}$.
- 4) Verify $L_1 = 29 \text{ mm} \approx H_1 D_s + (k t_{cf}) = 28 \text{ mm}$ (If this check fails, change H_1 or go back to Step 2 and change L_{DP}).
- 5) Verify $t_{DP} \ge \frac{L_{DP} + H_{DP}}{90}$, $t_{DP} = 8 \text{ mm} \ge \frac{L_{DP} + H_{DP}}{90} = 4 \text{ mm}$.
- 6) Compute shear demand on the fillet weld $V_{f-w} = 198 \text{ kN}$.
- 7) Compute shear resistance of the fillet weld $V_{r-w} = 209$ kN, and verify $V_{f-w} \le V_{r-w}$.
- 8) Compute nominal and factored shear resistance of PZ, 808 kN and 727 kN, respectively.





9) Shear demand is less than shear resistance, $V_{\text{PZH,d}} \leq V_{\text{r}}$, confirming the design is satisfactory.

Thus, an 8 mm fillet weld with a reduced doubler plate $168 \text{ mm} \times 191 \text{ mm} \times 8 \text{ mm}$ is used.

The design of the rest of the specimens (Table 4.1 and 4.2) with reduced double plate, W250-RDP2, W410-RDP1, and W410-RDP2, is shown in Table 6.1. The design indicates that a 152 mm \times 175 mm \times 8 mm doubler plate with an 8 mm fillet weld can be used in W250-RDP2. It also verifies the viability of the reduced doubler plate detail on both W410-RDP1 with a 326 mm \times 6 mm \times 348 mm doubler plate with a 6 mm fillet weld and W410-RDP2 with a 314 mm \times 6 mm \times 336 mm and a 6 mm fillet weld. For both W410-RDP1 and W410-RDP2 specimens, the measured yield stresses of 353 and 391 MPa are used for DP and column, respectively.

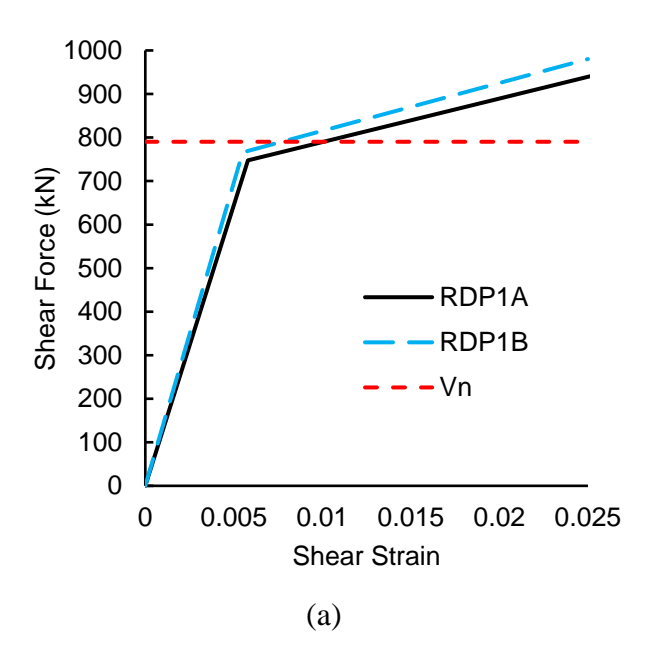
Table 6.1: Summary of proposed design for test specimens with a reduced doubler plate

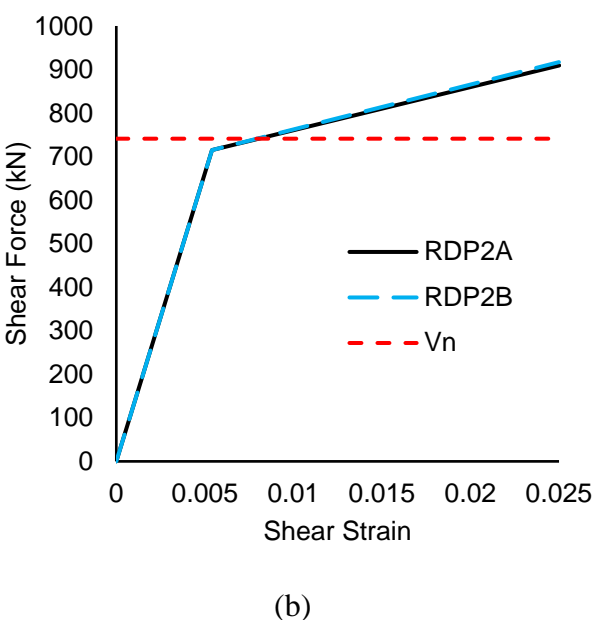
Steps	W250-RDP2	W410-RDP1	W410-RDP2	
1) Determine <i>V</i> _{PZH,d}	530 kN	830 kN	830 kN	
2) Select dimensions	PL 152×8×175 mm	PL 326×6×348 mm	PL 314×6×336 mm	
	D = 8 mm	D = 6 mm	D = 6 mm	
3) Verify	25 ≤ 41 mm	16 ≤ 68 mm	22 ≤ 68 mm	
$H_1 \le 0.18 H_{PZ}$				
4) Verify $L_1 \le H_1 -$	37 ≈ 36 mm	27 ≤ 28 mm	33 ≤ 33 mm	
$D_s + (k - t_{cf})$				
5) Verify $t_{DP} \ge$	8 ≥ 4 mm	6 ≈ 7 mm	6 ≈ 7 mm	
$\frac{L_{\rm DP} + H_{\rm DP}}{90}$				
6) Compute V_{f-w}	179 kN	311 kN	299 kN	
7) Compute V_{r-w}	189 kN	305 kN	293 kN	
and check $V_{f-w} \leq V_{r-w}$	179 ≤ 189 kN	311 ≈ 305 kN	299 ≈ 293 kN	
8) Compute V_n	756 kN	1230 kN	1200 kN	
9) Compute V_r and	680 kN	1107 kN	1080 kN	
check $V_{\rm PZH,d} \leq V_{\rm r}$	$530 \le 680 \text{ kN}$	$830 \le 1107 \text{ kN}$	$830 \le 1080 \text{ kN}$	





The proposed design method is validated by comparing the predicted shear strengths using Equation (6-22) against the results from the specimens with a reduced doubler plate (W250-RDP1A, W250-RDP1B, W250-RDP2A, W250-RDP2B, W410-RDP1A, W410-RDP1B, W410-RDP2A, W410-RDP2B). The shear force versus shear strain responses of the test specimens were idealized by bilinear curves as shown in Figure 6.5. To idealize the shear force – shear strain curves, a shear strain of 0.025 is considered as a deformation limit beyond which the connection would experience excessive shear deformation. The bilinear curves were derived so that the elastic stiffness, the shear force at the shear strain of 0.025, and the area beneath the curve, for both the actual and bilinear curves remain the same.









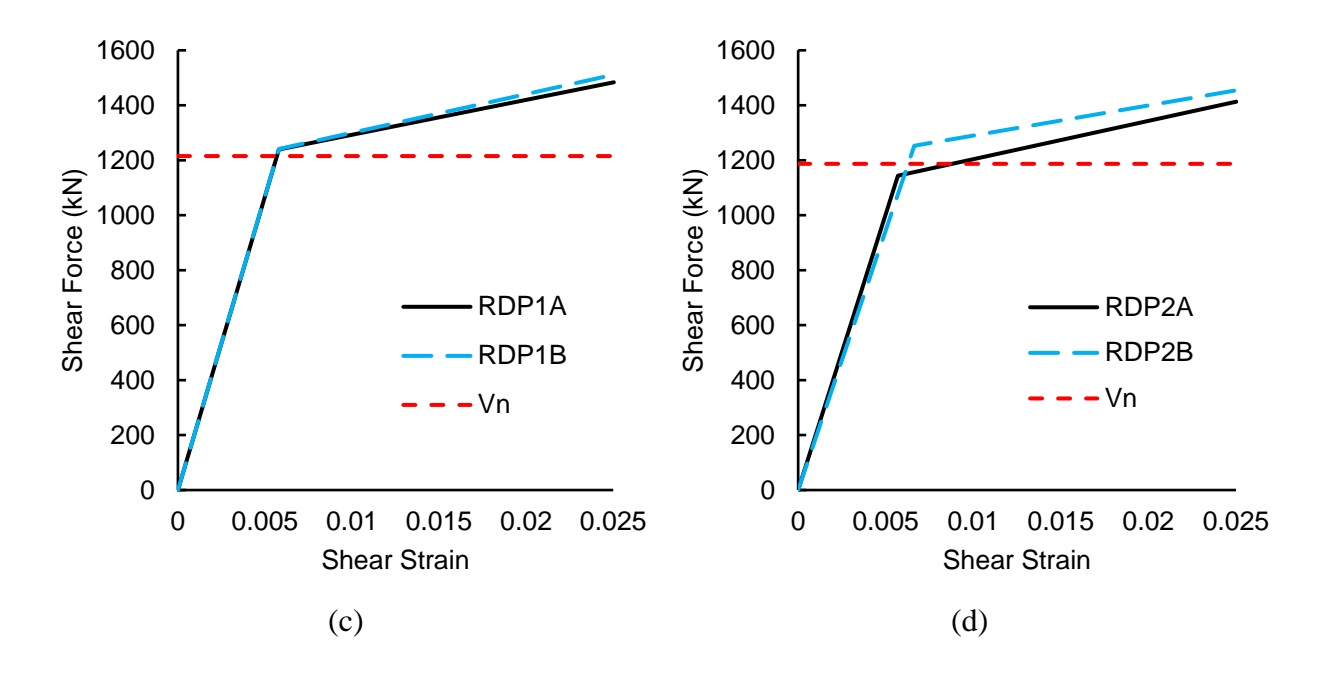


Figure 6.5: Bilinear shear force – shear strain responses of specimens against predicted shear resistance of the panel zone using proposed method: (a) W250 RDP1, (b) W250 RDP2, (c) W410 RDP1, and (d) W410 RDP2

As shown in Figure 6.5, the proposed nominal shear strength agrees well with the yield resistance obtained from the tests, which verifies the accuracy of the proposed design method. The moderate deviations of the predicted resistances stem from bilinearization of the force-deformation responses, uncertainties associated with material and geometric properties of the panel zone in the experiment, and the assumption of uniform shear strain within the depth of the panel zone at yield.





7 FINITE ELEMENT ANALYSIS

7.1 Introduction

This chapter presents the finite element modelling technique for the development of the numerical model of the beam-to-column connection and numerical simulation results used to validate the proposed design method in Chapter 6 for special loading cases, including combined biaxial moments and axial force in the beam, and axial compression force in the column.

7.2 Numerical Model

The ABAQUS finite element program was used to develop the numerical model of the beam-to-column connection including doubler plates. Figure 7.1a shows the finite element (FE) model of the connection. The connection components, including the beam, column, doubler plate (DP), and fillet welds connecting the DP to the column web, were explicitly modeled. Detailed views of the FE model for the fillet weld and DP are presented in Figure 7.1-b.

The boundary conditions of the FE model were chosen to replicate those of the test specimens. The top of the column was pinned in rotation (UR1, UR2, and UR3 \neq 0) and fixed in translation (U1 = U2 = U3 =0), while the bottom end was fixed in all degrees-of-freedom. To prevent out-of-plane deformation at the beam end, the displacement in the X-axis (see Figure 7.1a) was restrained (U1 = 0). A displacement in the Y-axis (see Figure 7.1a) was imposed at the tip of the beam. The assigned boundary conditions are shown in Figure 7.1a. 8-node linear brick elements with reduced integration and hourglass control (C3D8R) were used to construct the finite element model. Mesh sizes of 2.5 mm and 4 mm were used for the fillet welds and the DP, respectively, while a 10 mm and 15 mm mesh sizes were applied to the columns and beams, respectively. Three layers of elements were used through the thickness of the column web and flanges. A larger mesh size of 15 mm was used for the beam. These mesh sizes were selected based on a mesh sensitivity analysis to ensure a trade-off between accuracy and computational efficiency. To simulate the normal contact behaviour between the DP and the column web, a hard contact interaction was defined to prevent penetration between the two contact surfaces. For all welds, except for the DP-to-column web weld (which is explicitly modeled), a surface-based tie constraint was employed.





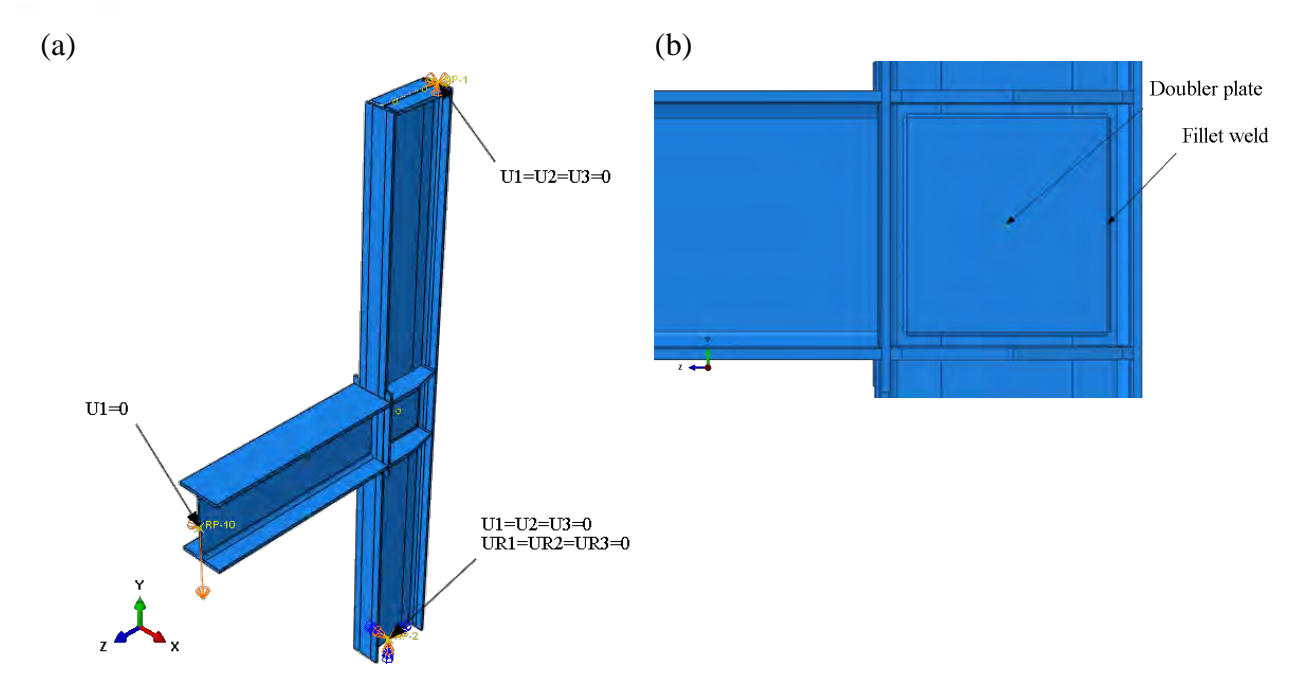


Figure 7.1: The details of the finite element model for W410-RDP1 (a) 3D view (b) DP view.

The residual stresses in the column cross-section were incorporated into the FE model following the method proposed by Rosson (2018) as shown in Figure 7.2. The amplitude of tension and compression residual stress, σ_r , was set as 60 MPa for the W250 specimen and 150 MPa for the W410 specimen.

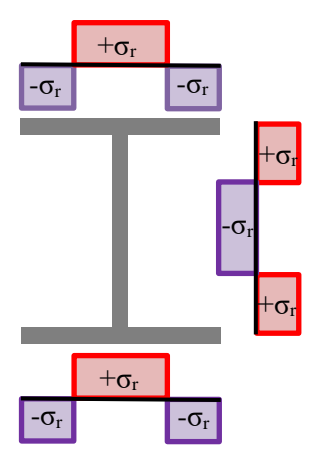


Figure 7.2 The schematic distribution of residual stresses in column cross-section.





The material properties of the steel material were based on the standard coupon tests presented in Section 4.6. The true stress—plastic strain relationships assigned to the elements of the DP, flange, and web of the W250 and W410 beams and columns are shown in Figure 7.3a and 7.3b, respectively.

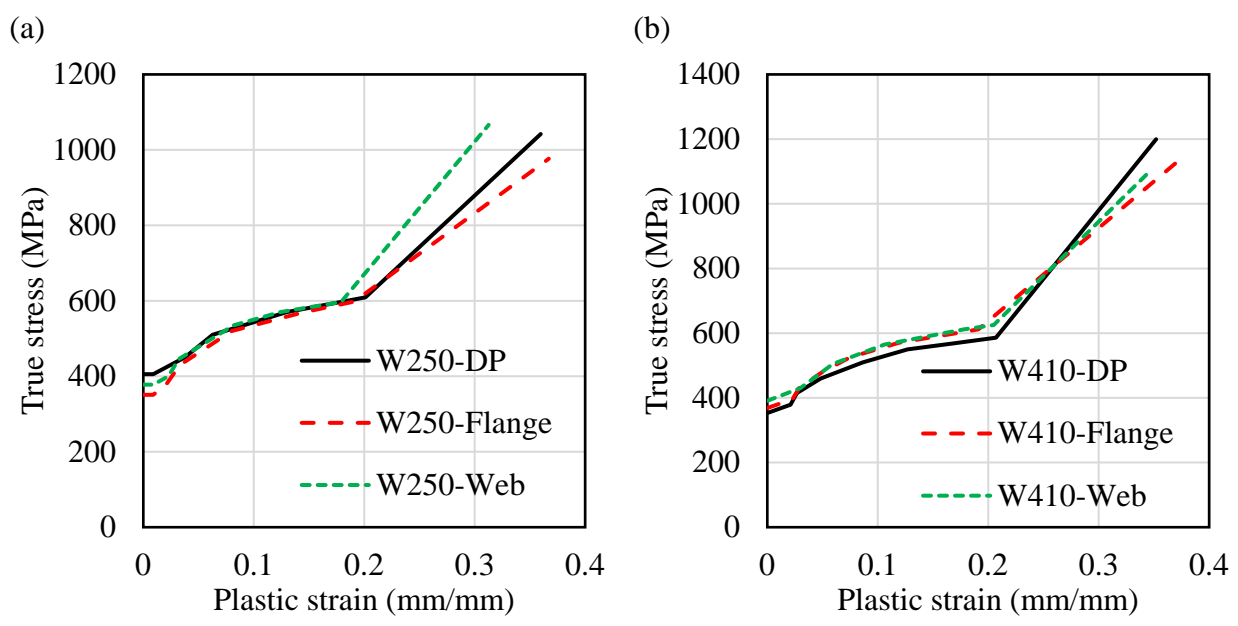


Figure 7.3: True stress–plastic strain curves (a) W250 specimens and (b) W410 specimens.

7.3 Validation of the Finite Element Model

Figure 7.4 and Figure 7.5 compare force – displacement responses at the end of the beam obtained from the tests with those calculated by finite element analysis (FEA) for the W250 and W410 specimens, respectively. As shown, the numerical results closely match the test data, confirming the accuracy of the numerical model developed here.





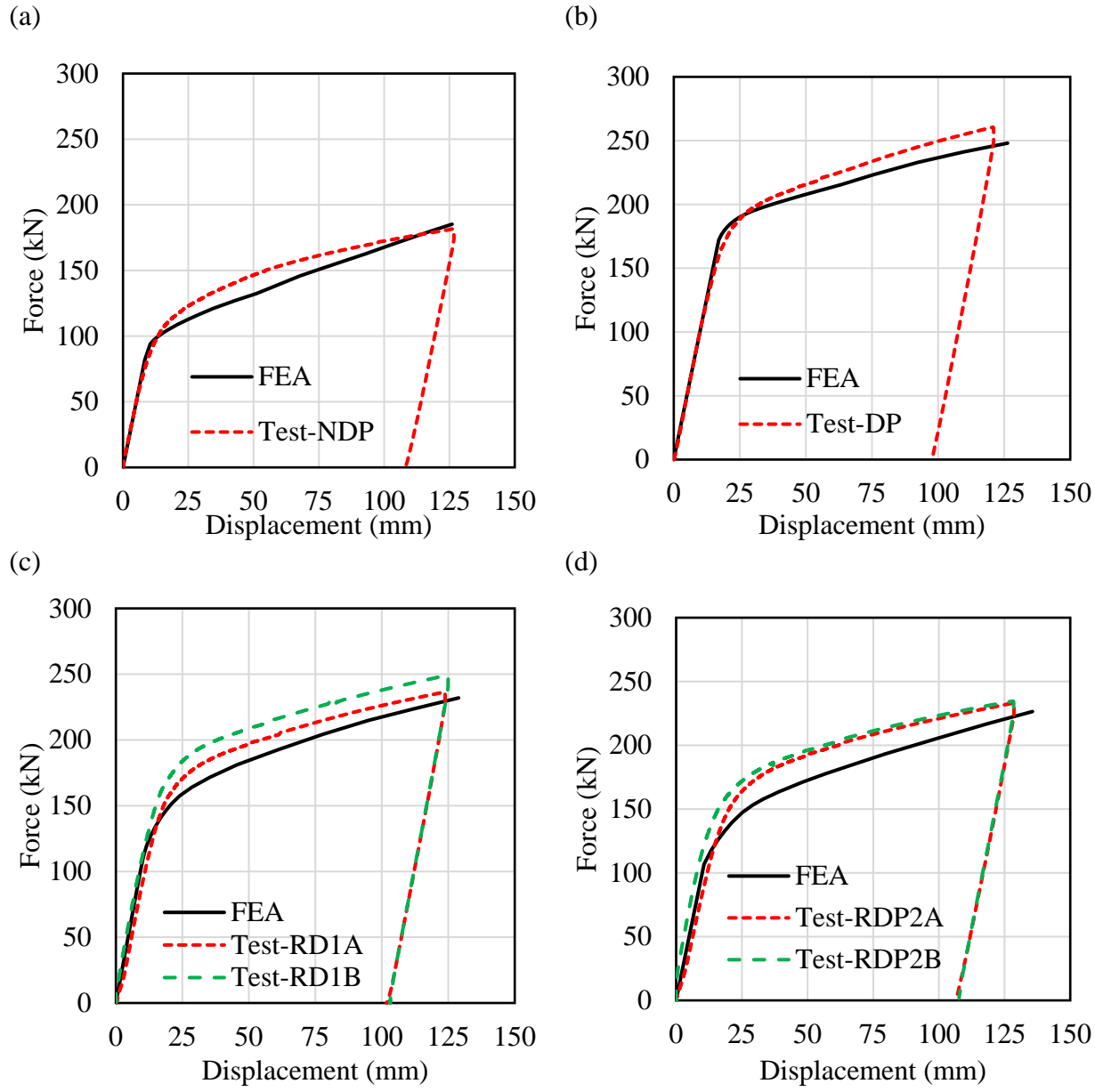


Figure 7.4: Comparison of the force-displacement responses from FEA and tests (a) W250-NDP, (b) W250-DP, (c) W250-RD1, and (d) W250-RDP2.

For W410-RDP2 specimens, the force – displacement responses predicted by FEA match with the test data up until the onset of fillet weld fracture. Beyond the fracture point, the DP no longer contributes to the shear capacity of the PZ, causing a sudden drop in force at the beam's end. In the FE model, fillet weld fracture was not explicitly modelled, as it occurs well beyond a shear strain anticipated in design, e.g., > 0.025 mm/mm. This explains the divergence between the predicted force – displacement curve and the test data beyond weld fracture.





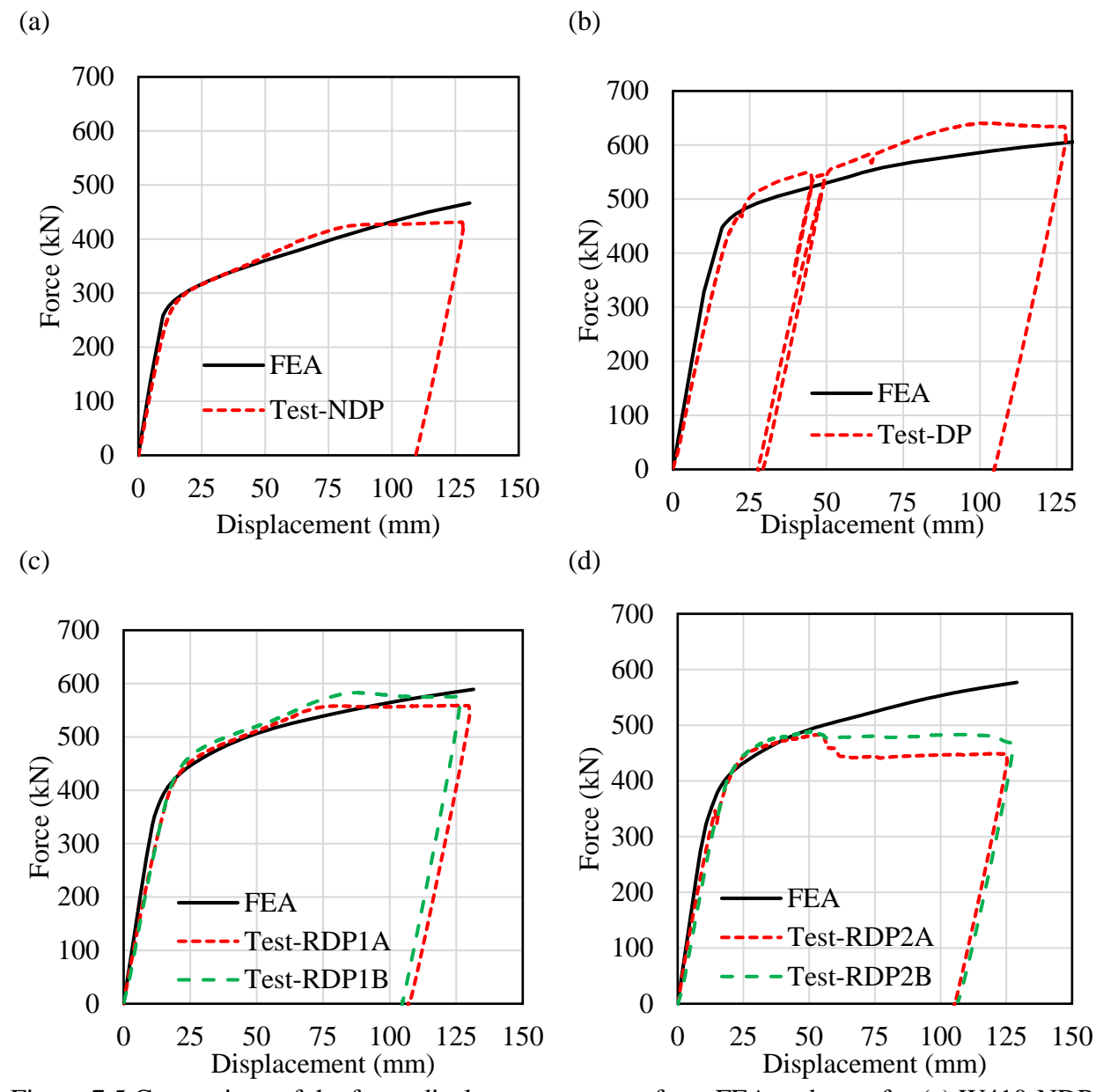


Figure 7.5 Comparison of the force-displacement curves from FEA and tests for (a) W410-NDP, (b) W410-DP, (c) W410-RD1, and (d) W410-RDP2.

7.4 Evaluation of the Proposed Design Method

A numerical parametric study was conducted to evaluate the influence of various loading scenarios, involving 1) combined axial force, weak-axis and strong-axis bending in the beam, 2) axial force in the column, on the shear stress developed in the DP and the adequacy of the proposed design method introduced in Chapter 6.





7.4.1 Effect of combined axial force and bending in the beam

Steel pipe rack module moment connections are typically subjected to a combination of weak-axis moment, strong-axis moment, and axial force arising in the beam framing into the column flange. To evaluate the simultaneous effects of these actions, a typical steel pipe rack moment connection, designed in Chapter 3, was analyzed in this section. As shown in Figure 7.6, this connection consists of a W250×73 profile for both beam and column sections, conforming to CSA G40.21 350W steel (CSA, 2018). The detailed design of this connection is presented in Chapter 3.

The validated FE model described earlier was adjusted to assess the effects of different beam loading cases on the shear response of the DP. The column length was reduced to 0.5 m, and both the top and bottom ends of the column were constrained against translation and rotation degrees-of-freedom to minimize the contribution of column deformation to the overall connection response.

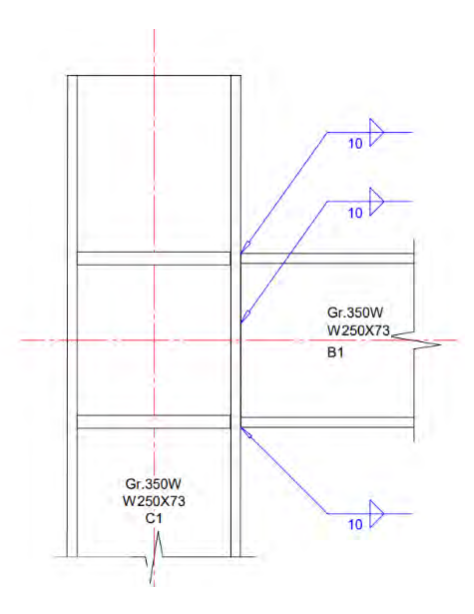


Figure 7.6: The prototype moment connection used for numerical response evaluation.

Four design load cases were considered to evaluate the effects of different combinations of strong-axis moment (M_{fx-b}), weak-axis moment (M_{fy-b}), and axial force (N_{f-b}) in the beam. The details of these loading cases are provided in Table 7.1. The maximum amplitudes of these loads were





selected to achieve an axial force-moment interaction ratio of 0.65 in the beam. In Load Case 1, the strong-axis moment is the dominant loading action, whereas in Load Cases 2 and 3, the weak-axis moments are higher. In Load Case 4, the beam axial force is the primary loading action.

Table 7.1: Selected beam load cases.

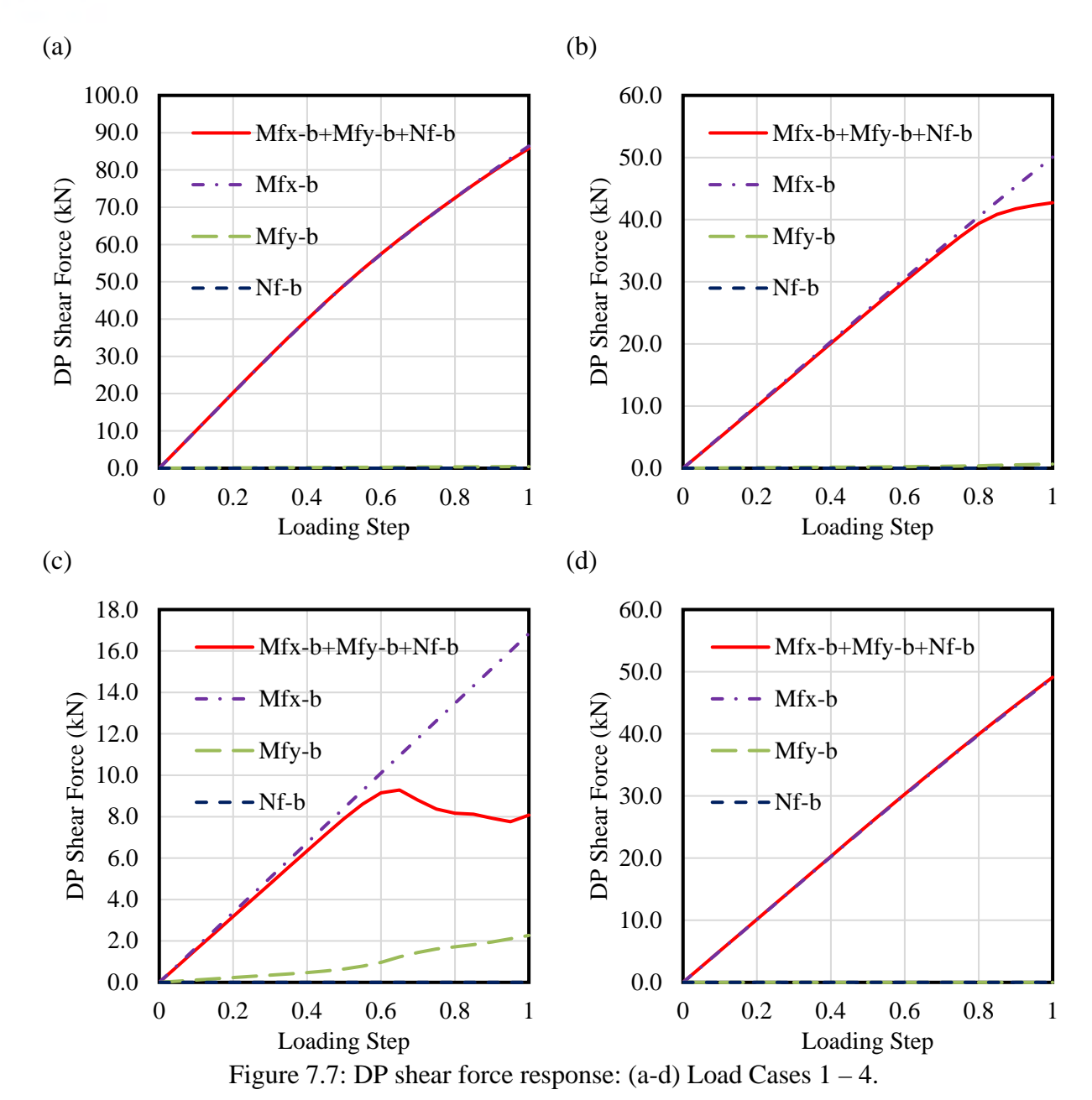
	$N_{\text{f-b}}(kN)$	$M_{\text{fx-b}}$ (kN.m)	$M_{\text{fy-b}}$ (kN.m)
Load Case 1	100	150	50
Load Case 2	100	75	100
Load Case 3	100	25	135
Load Case 4	1000	75	25

The moments and axial force were gradually applied to the beam by exerting forces at its end in the X, Y, and Z directions (see Figure 7.1a), and the resulting shear force in the DP was monitored. The shear stress in the elements located at the center of the DP was extracted and averaged at each time step, then multiplied by the product of thickness and length of the DP ($t_{DP} \times L_{DP}$) to compute the resulting shear force in the DP.

Figure 7.7a to 7.7d present the shear force in the DP versus loading steps for Load Cases 1 to 4 (Table 7.1), respectively. In these figures, $M_{fx-b} + M_{fy-b} + N_{f-b}$ represents the shear force in the DP induced by the combination of three loading components. As shown, the contributions of the weak-axis moment and axial force to the shear force in the DP are negligible, with the shear force primarily induced by strong-axis bending in the beam. Although the load cases were designed to keep the connection elastic, stress concentrations led to localized yielding in certain regions of the DP.







analyses for Load Cases 1 to 4 (Table 7.1). In Load Cases 1 and 4, where the strong-axis moment exceeds the weak-axis moment, the shear stress distribution follows a similar pattern, with the maximum shear stress occurring at the center of the DP. Conversely, in Load Cases 2 and 3, where the weak-axis moment is greater than the strong-axis moment, the shear stress distribution follows

Figure 7.8a to 7.8d illustrate the distribution of in-plane shear stress in the DP at the end of the

a different pattern, reaching its maximum and minimum values at the lower and upper parts of the DP while remaining minimal at the center. As previously noted, the contribution of the beam axial





force to the DP shear force is negligible, suggesting that the axial force does not significantly influence the shear stress distribution in the DP.

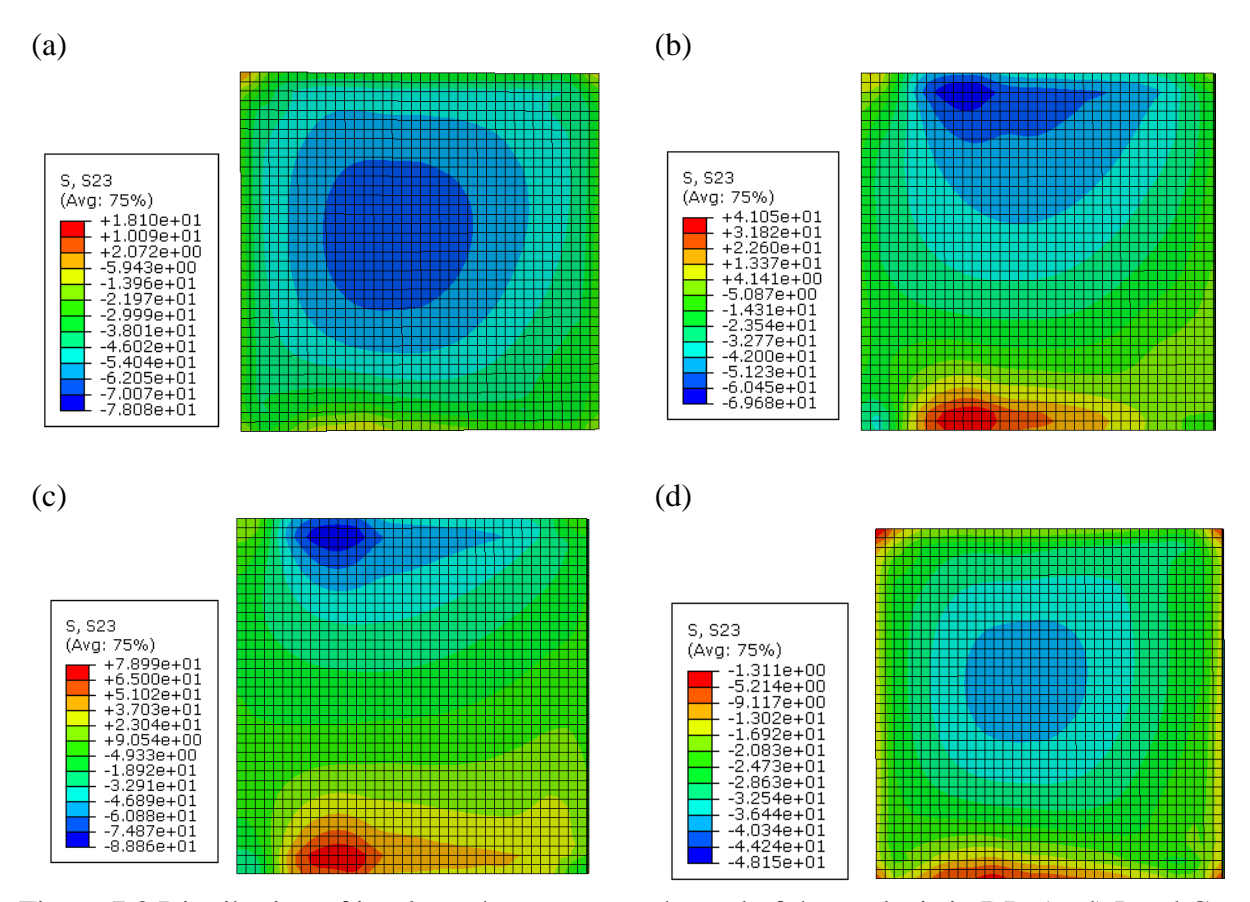


Figure 7.8 Distribution of in-plane shear stress at the end of the analysis in DP: (a–d) Load Cases 1–4 (stress values in MPa).

7.4.2 Effect of column axial force

The effect of column axial force on the behaviour of PZ is evaluated by varying axial force levels in the column: 0.0, 0.4, and 0.6 $F_{yc}A_{col}$, where A_{col} and F_{yc} are the cross-sectional area and minimum specified yield stress of the column, respectively. To prevent out-of-plane buckling of the column, out-of-plane deformation in the X-axis (see Figure 7.1a) was constrained. Although this constraint prevents global out-of-plane buckling, it does not restrict shear buckling of the column web. The axial force was first applied to the column along the Y-axis (see Figure 7.1a) using a load-controlled analysis. Subsequently, a vertical displacement was imposed at the tip of the beam along the Y-axis (see Figure 7.1a) using in a displacement-controlled mode.

Figure 7.9a, 7.10a, 7.11a, and 7.12a illustrate the shear force – shear strain responses of the PZ for W250-RDP1, W250-RDP2, W410-RDP1, and W410-RDP2, respectively. For W250-RDP1 and





W250-RDP2, the influence of the column axial force in the linear phase of response is minimal. However, the curves diverge in the nonlinear range, with the post-yield stiffness of the DP decreasing as the axial force increases. For W410-RDP1 and W410-RDP2, the shear force – shear strain responses exhibit higher discrepancies in both the linear and hardening phases under different column axial forces. The stiffness in the linear phase gradually decreases as the column axial force increases from 0.0 to $0.6 \, F_{yc} A_{col}$ due to the geometric nonlinearity effect (P- Δ), which induces additional deflection in the Z-direction. For instance, in W410-RDP2, the deflection in the Z-direction at the top of the panel zone (PZ) at a PZ shear strain of 0.025 is 8.61 mm for a column axial force of 0.0 and 10.64 mm for 0.6. This confirms the influence of column axial force on the lateral deformation of the column in the Z-direction and the resulting reduction in connection flexural stiffness.

Figures 7.8b, 7.9b, 7.10b, and 7.11b present the average shear stress in the DP versus the average shear strain of the PZ for specimens W250-RDP1, W250-RDP2, W410-RDP1, and W410-RDP2, respectively. To calculate the average shear stress, the shear stress in the elements located at the center of the DP was extracted and averaged at each time step. The average shear strain was determined by measuring the relative displacement in the Z-direction at the top and bottom of the PZ and dividing it by the height of the PZ. This average shear strain is the same as that presented in Chapter 6. For W250-RDP1 and W250-RDP2, the shear stress – shear strain responses are not affected noticeably by column axial force. The curves remain elastic and linear up to a shear strain of 0.005, where yielding begins in the perimeter area. At a shear strain of 0.01, yielding initiates in the DP and progresses such that at approximately 0.015 shear strain, the DP has fully yielded reaching a stress value of 229 MPa.

The shear stresses in the DP of the W250 specimen under all column axial forces, as well as in the W410 specimens under no axial force, do not decrease after yielding. This indicates that shear buckling does not occur in the PZ for these cases up to a shear strain of 0.025. For W410-RDP1 and W410-RDP2, subjected to a column axial force of $0.6F_{yc}A_{col}$, the shear stress – shear strain curves reach their peak at shear strains of 0.01 and 0.013, respectively. Following shear yielding in the DP, shear buckling of the column web took place, which resulted in a reduction in shear stress in both specimens. When the column axial force was reduced to $0.4F_{yc}A_{col}$, shear buckling occurred at shear strains of 0.015 and 0.018 for W410-RDP1 and W410-RDP2, respectively.





Figure 7.13a and 7.13b show the shear strain distribution in the PZ at the onset of shear buckling for W410-RDP1 under column axial loads of $0.4 F_{yc}A_{col}$ and $0.6 F_{yc}A_{col}$, respectively. Similarly, Figure 7.13c and 7.13d present the shear strain distribution for W410-RDP2 under the same axial loads. As shown, the shear strain follows a consistent pattern in both cases, with the maximum values occurring in the perimeter area. Within the DP, shear strain is highest at the center and decreases toward the edges. In both W410-RDP1 and W410-RDP2 specimens, increasing the column axial force leads to earlier shear buckling. Additionally, greater DP reduction further accelerates shear buckling.

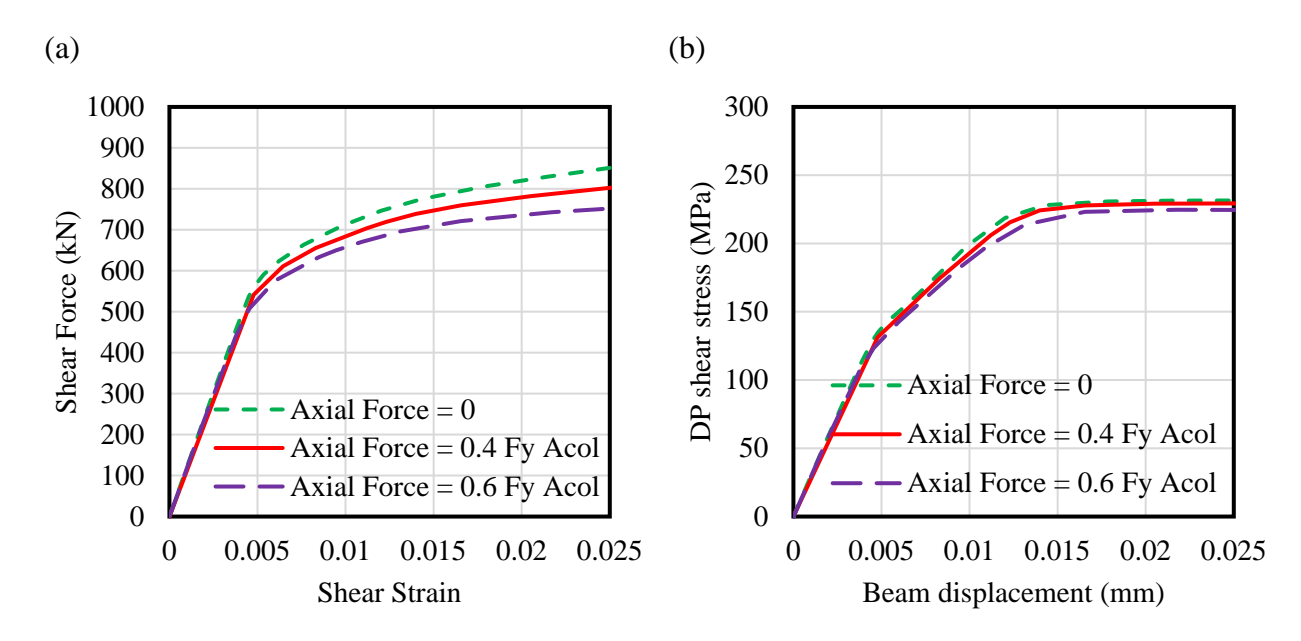


Figure 7.9: (a) PZ shear force versus PZ shear strain, and (b) DP shear stress versus PZ shear strain for W250-RDP1 under column axial force.





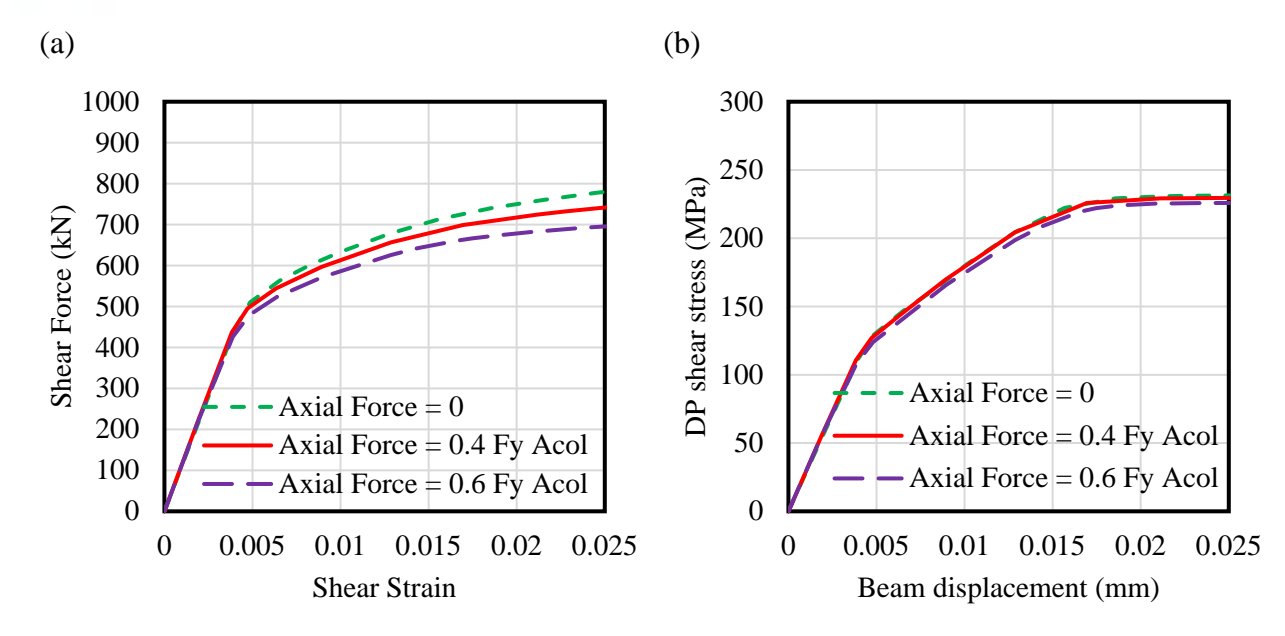


Figure 7.10 (a) Shear force versus shear strain of the PZ, and (b) shear stress in the DP versus the PZ shear strain for the W250-RDP2 specimen under various column axial force.

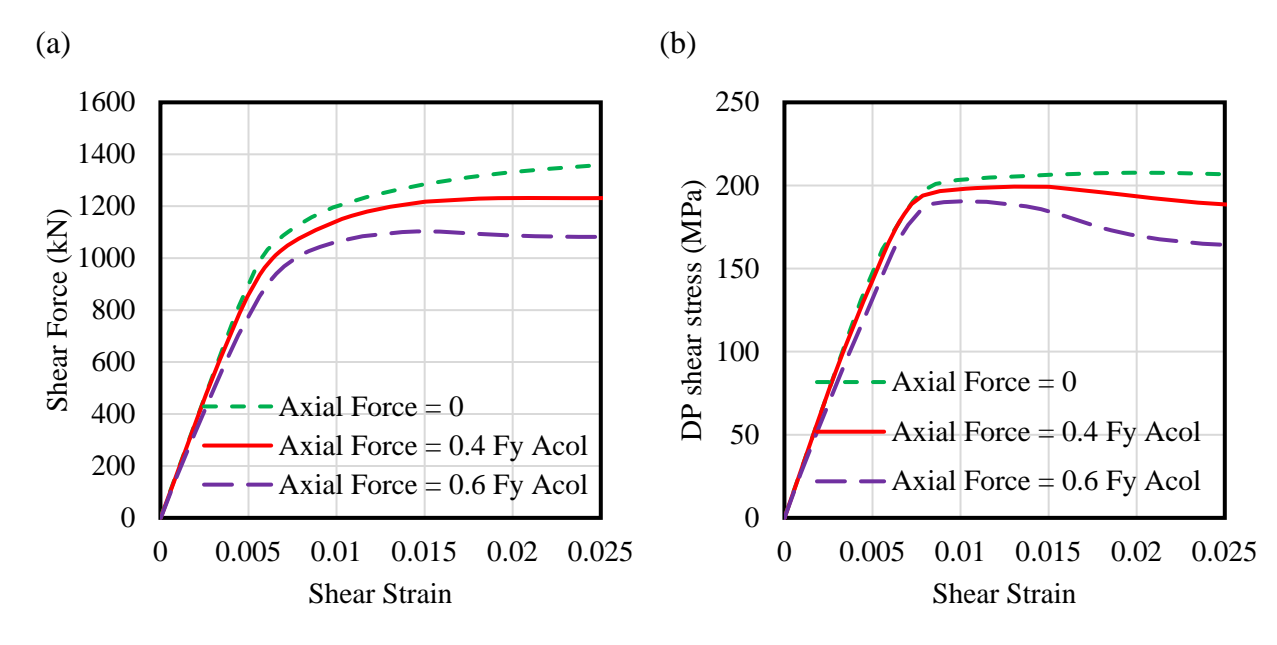


Figure 7.11 (a) Shear force versus shear strain of the PZ, and (b) shear stress in the DP versus the PZ shear strain for the W410-RDP1 specimen under various column axial force.





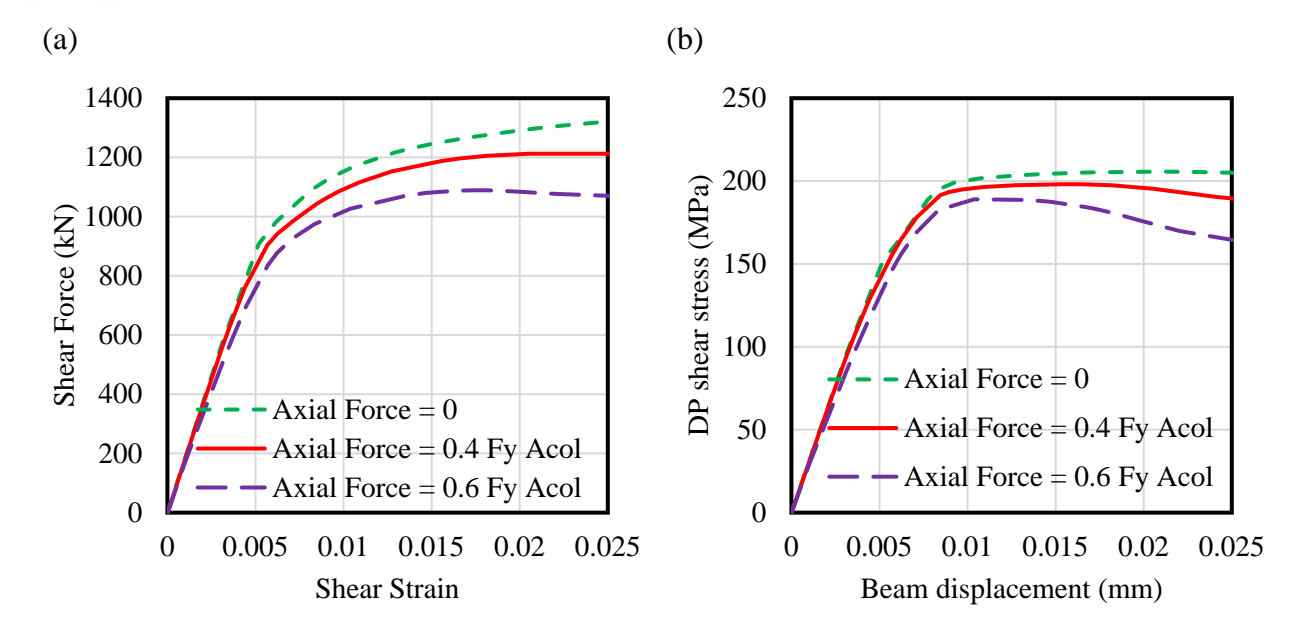


Figure 7.12 (a) Shear force versus shear strain of the PZ, and (b) shear stress in the DP versus the PZ shear strain for the W410-RDP2 specimen under various column axial force.

The shear force – shear strain responses were idealized as bilinear curves by setting the area under the original and bilinear curves the same when a target shear strain of 0.025 is attained. The resulting bilinear curves were also adjusted by multiplying them by the respective error obtained as the test-to-predicted ratio at yielding, which are 1.09, 1.23, 1.07, and 1.07 for W250-RDP1, W250-RDP2, W410-RDP1, and W410-RDP2, respectively. The bilinear shear force – shear strain curves for W250-RDP1, W250-RDP2, W410-RDP1, and W410-RDP2 are shown in Figures 7.12a to 7.12d, respectively.

The shear strength of the PZ was then calculated using Equations (6-23) and (6-24). No reduction is needed for the case without axial force and that under $0.4F_{yc}A_{col}$. However, for the case under a column axial force of $0.6F_{yc}A_{col}$, a reduction factor of 0.8 is computed using Equations (6-23) and (6-24). These shear capacities are given on the bilinear shear force – shear strain curves associated with W250-RDP1, W250-RDP2, W410-RDP1, and W410-RDP2 in Figures 7.12a to 7.12d, respectively.





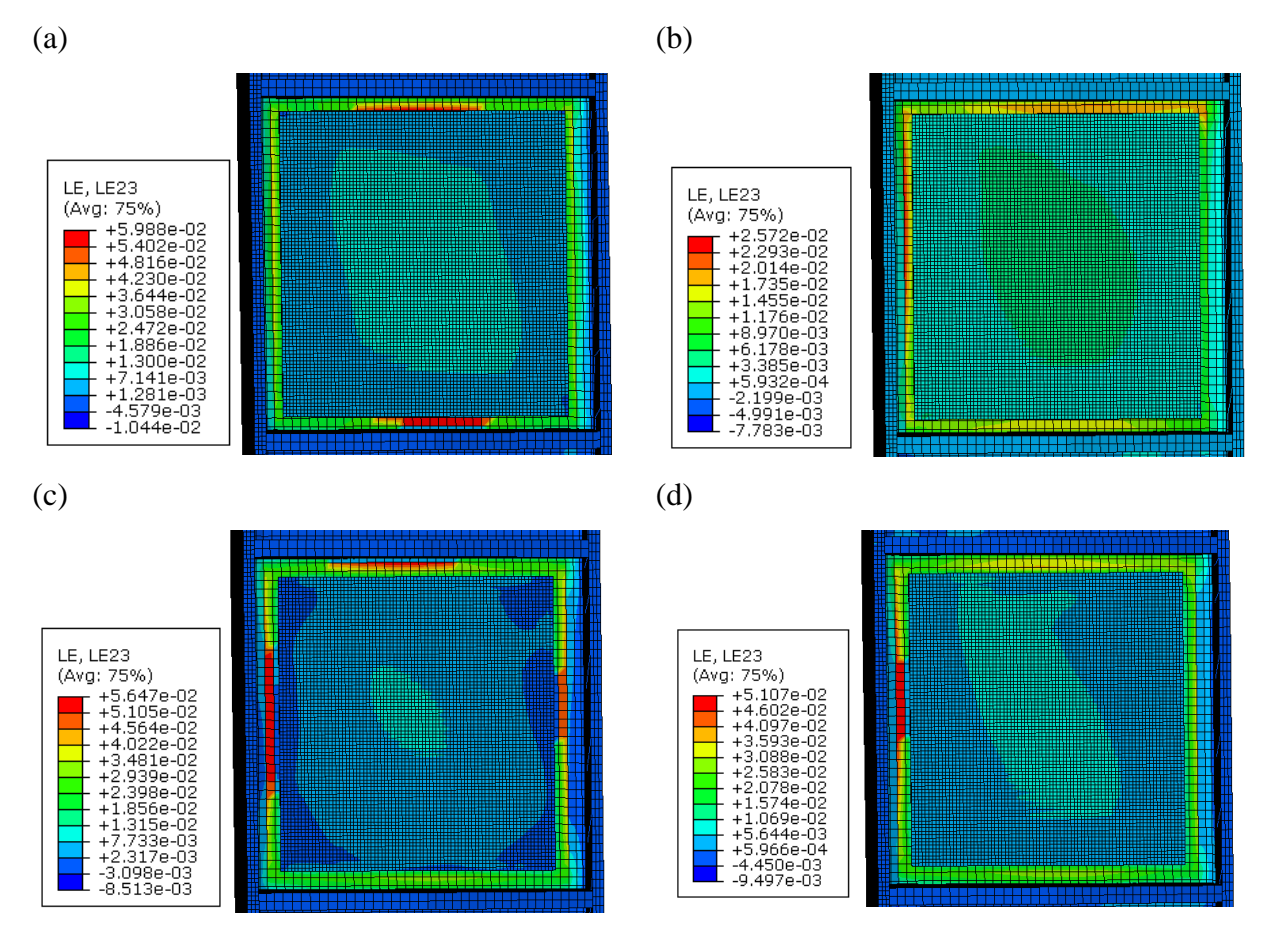


Figure 7.13 Distribution of in-plane shear strain at the onset of shear buckling: (a) W410-RDP1, Axial Force = $0.4 F_{yc}A_{col}$ (b) W410-RDP1, Axial Force = $0.6 F_{yc}A_{col}$ (c) W410-RDP2, Axial Force = $0.6 F_{yc}A_{col}$.

As shown in Figure 7.12a, for W250-RDP1 under no axial force and an axial force of $0.4F_{yc}A_{col}$, the shear force at yield is 748 kN, which is 8% higher than the predicted PZ capacity using Equation (6-23) 809 kN. The reason for this overestimation by the design equation is that the original AISC 360 equation neglects the limited detrimental effect of column axial load on shear capacity of the column PZ when the column axial force is below 40% of its squash load, $0.4F_{yc}A_{col}$ here. Although this method may slightly over predict the shear strength of the panel zone, it is deemed acceptable in the framework of design. For W250-RDP1 under an axial load of $0.6F_{yc}A_{col}$, the predicted shear strength using Equation (6-24) is found to be 647 kN, which is slightly (in the





order of 10%) lower than the numerical simulation results, 713 kN. A similar pattern is observed for W250-RDP2, as shown in Figure 7.12b.

For W410-RDP1, the yielding shear forces for column axial forces of 0.0, 0.4, and 0.6 $F_{yc}A_{col}$ are 1241 kN, 1200 kN, and 1120 kN, respectively, with corresponding calculated shear strengths of 1229 kN, 1229 kN, and 983 kN. Compared to the yielding shear forces, the calculated strengths are 0.9% lower, 2.4% higher, and 12.2% lower, respectively. For W410-RDP2, the yielding shear forces for the three column axial forces are 1117 kN, 1061 kN, and 1014 kN, with corresponding calculated shear strengths of 1200 kN, 1200 kN, and 960 kN, respectively. The calculated shear strengths are 7.4% higher, 13.1% higher, and 5.4% lower than the yielding shear forces. Similar to W250 cases, the AISC 360 equation neglects the effect of column axial load on shear capacity when the column axial force is below $0.4F_{yc}A_{col}$, therefore the predicted shear strength of the PZ for this column axial load is slightly unconservative, which is acceptable in the design framework.

Table 7.2 compares the actual yielding shear force and predicted shear strength calculated using Eq 6-23 and Eq 6-24 for W250-RDP1, W250-RDP2, W410-RDP1, and W410-RDP2 under various column axial forces. In this table, the error of the prediction, defined as the difference of predicted shear strength and actual yielding shear force divided by the actual shear force, are also presented. The results indicate that the predicted shear strengths in presence of column axial force using Equations (6-23) and (6-24) are slightly unconservative (in the order of 6.1 % on average) when the column axial force is below $0.4F_{yc}A_{col}$, and relatively conservative (in the order of 9.4% on average) when the column axial force reaches $0.6F_{yc}A_{col}$. One can attribute the former to the axial force cutoff proposed by AISC 360, below which the potential reduction in shear capacity of the DP in the presence of axial force is neglected.





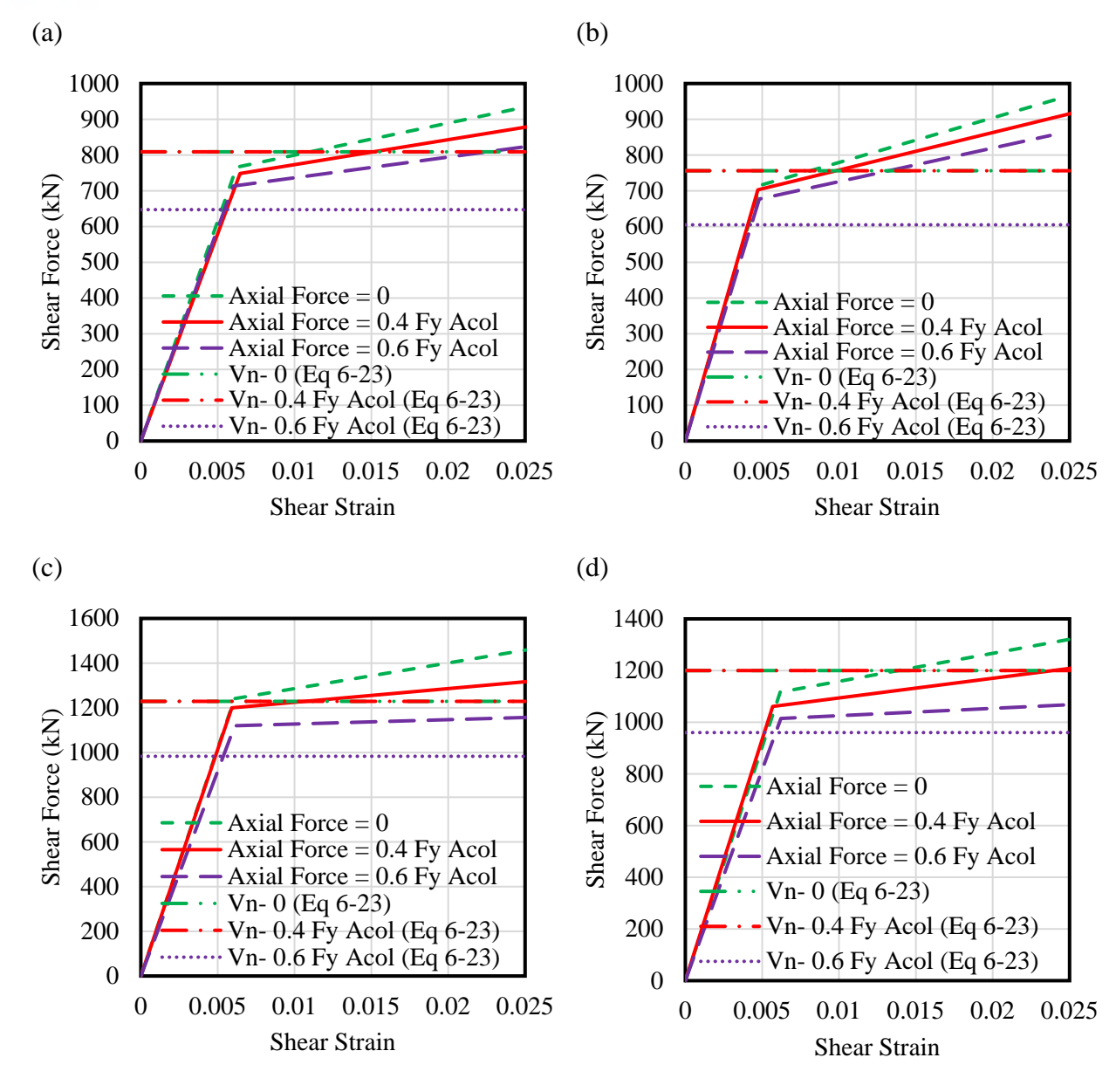


Figure 7.14: Idealized PZ shear force – PZ shear strain responses and predicted shear strength values using Equations (6-23) and (6-24) under column axial force: (a) W250-RDP1, (b) W250-RDP2, (c) W410-RDP1, and (d) W410-RDP2.





Table 7.2 Actual and predicted yielding shear forces.

Specimens	Column axial force / (FyAcol)	Predicted shear strength values (kN)	Actual yielding shear force (kN)	Error (%)
W250-RDP1	0.0	809	766	5.6
	0.4	809	748.4	8.1
	0.6	647.2	713.3	-9.3
W250-RDP2	0.0	756	715	5.7
	0.4	756	702.7	7.6
	0.6	604.8	676.7	-10.6
W410-RDP1	0.0	1229	1241	-1.0
	0.4	1229	1200.2	2.4
	0.6	983.2	1120.2	-12.2
W410-RDP2	0.0	1200	1117	7.4
	0.4	1200	1061	13.1
	0.6	960	1014.5	-5.4





8 CONCLUSIONS AND RECOMMENDATIONS

8.1 Summary

Steel moment connections in pipe rack modules are designed to transfer bending moments, shear forces, and axial forces, which produce a complex stress condition in the column web and often result in an expensive detail that makes the connection fabrication a labor-intensive task in the shop. The use of doubler plates and stiffeners is often required in such connections to improve panel zone strength and stability. This research project aimed at 1) proposing a new doubler plate detail for steel moment connections, 2) performing twelve full scale experimental tests, and 3) proposing a design method to size column web doubler plates with the reduced configuration. To investigate the effect of reducing the doubler plate and using fillet welds in pipe rack module connections, a full-scale experimental test setup was developed. The experimental study consisted of twelve moment connections, where each six specimens represented a different beam-to-column W-section. Six used W250x58 beams and columns and the rest used W410x60 columns and W410x100 beams. Instrumentation was used to collect data throughout the experiments. Residual stress measurements and coupon tests were performed for the columns and doubler plates of the specimens, then used in the numerical model to improve the accuracy of the results. A new design method was developed to size doubler plate dimensions taking into account potential limit states and limiting shear deformation in the panel zone beyond yielding. The test program designed to verify this detail included beam-to-column connection subassemblies with column panel zone involving the standard DP detail, reduced DP details and no doubler plate. Finally, a numerical parametric study was performed to evaluate the influence of beam design loads and column axial force on the response of the reduced DP and further validate the proposed design method for special loading scenarios.

8.2 Conclusions

The main findings of this study are as follows:

- A new doubler plate detail is proposed by reducing the doubler plate size and using fillet welds to attach the doubler plate to the column web in the panel zone area.
- When reducing the doubler plate size, the strength of the connection tends to reduce. This
 reduction is more prominent in W250×58 columns, with 15% and 19% reduction for
 standard doubler plate and further reduced doubler plate, respectively.





- The first mode of failure observed is shear yielding of the doubler plate and column web. On average, shear yielding in the panel zone, including column web and doubler plate, takes place at 0.007-0.011 shear strain.
- Shear yielding was accompanied by shear buckling in the specimens with deep W410 column, with web slenderness ratio of 46.3, when reduced/further reduced doubler plate and no doubler plate are used. Shear buckling occurred after significant shear yielding and strain hardening at 0.04 0.06 shear strain.
- A mechanics-based design method was developed in the framework of the Canadian steel design standard to size reduced doubler plates in beam-to-column moment connections under demands arising from monotonic loading. The method involves verifying doubler plate interface weld resistance, shear resistance of the doubler plate, and a limit on the depth of the reduced area of the panel zone to avoid excessive shear deformation.
- The design method was demonstrated using two working examples, W250×73 beam-to-W250×73 column connection and W250×58 beam-to-W250×58 column connection (i.e., Specimen W250-RDP1).
- The design method is validated based on experimental data, which confirmed its sufficient accuracy.
- The results of numerical simulations showed that shear stress in the DP is primarily induced by the strong-axis moment and respective shear transferred by the beam, with the effects of beam axial force and weak-axis bending on the response of DP being negligible.
- The proposed design equations to compute shear capacity of the column panel zone in the presence of column axial force (adapted from AISC 360) can predict the shear strength of the panel with sufficient accuracy.

8.3 Limitations and Recommendations

While this research provides a design method and a doubler plate detail that facilitates the fabrication process of these connections, further research can be conducted on connections under cyclic loads and under different doubler plate reduction details. A parametric study using finite element modeling and the experimental results collected could also be conducted in order to apply the new method over a variety of beam-to-column combinations. The limitations of the design method include:





- The design method should only be applied to a maximum doubler plate reduction of 2D on all sides of the doubler plate, since the design method includes a threshold for H_1 based on the reductions tested in this research. The limit proposed to reduce the doubler plate should be further validated for cases exceeding a 2D reduction.
- The design method should only be applied in the case of monotonic loading (no seismic application). The influence of cyclic loading should be evaluated in the future.
- The reduction of the doubler plate dimensions leads to a lower lateral stiffness of the beam-to-column connection, which in turn, can increase lateral deformation of the frame under applied lateral loads. However, this increased deformation is deemed negligible given the proposed reduction for the doubler plate. Future studies should investigate this aspect of the frame design.
- The design method proposed is for pipe rack beam-to-column moment connections but could potentially be used in building applications with further research on deeper columns.





REFERENCES

Abaqus/CAE User's Manual, 2023. Dassault Systèmes Simulia Corp., Providence, RI.

American Institute of Steel Construction. ANSI/AISC 360-1973. Specification for the Design, Fabrication and Erection of Structural Steel for Buildings, Chicago, IL.

American Institute of Steel Construction. 2022. ANSI/AISC 360-22, Specification for Structural Steel Buildings, Chicago, IL.

American Institute of Steel Construction. 2022. Seismic provisions for structural steel buildings, ANSI/AISC 341-22. Chicago, IL.

Australian Steel Institute (ASI). 2009. Design Guide 11: Welded beam-to-column moment connections.

American Welding Society. 2016. AWS, Structural welding code-seismic supplement. Available from https://www.scribd.com/document/534851590/aws-d18-2016.

Becker, R. 1975. "Panel zone effect on the strength and stiffness of steel rigid frames." Eng. J. 12 (1): 19–29.

Bedair, O. 2015. Rational Design of Pipe Racks Used for Oil Sands and Petrochemical Facilities. Practice Periodical on Structural Design and Construction, 20(2): 04014029. American Society of Civil Engineers. doi:10.1061/(ASCE)SC.1943-5576.0000224.

Bertero, V. V., H. Krawinkler, and E. P. Popov. 1973. Further studies on seismic behavior of steel beam-column subassemblages. Rep. No. EERC-73-27. Berkeley, CA: Earthquake Engineering Research Center.

Canadian Institute of Steel Construction (CISC). 2021. Handbook of Steel Construction - 12th Edition. Available from https://steelstore.cisc-icca.ca/products/handbook-of-steel-construction-12th-edition-2021.

Canadian Standards Association. 2019. CSA S16-19, Design of Steel Structures. Mississauga, ON.

Canadian Standards Association. 2018. G40.20-13/G40.21-13 (R2018): General requirements for rolled or welded structural quality steel / Structural quality steel, 350WT. CSA Group.





Ciutina, A.L., and Dubina, D. 2008. Column Web Stiffening of Steel Beam-to-Column Joints Subjected to Seismic Actions. Journal of Structural Engineering, 134(3): 505–510. American Society of Civil Engineers. doi:10.1061/(ASCE)0733-9445(2008)134:3(505).

Drake, R.M., and Walter, R.J. 2010. Design of Structural Steel Pipe Racks.

Engineering Fundamentals (efunda). 2024. Rosette strain gauges. Available from: https://www.efunda.com/formulae/solid_mechanics/mat_mechanics/strain_gage_rosette.cfm

Gupta, U. 2013. Cyclic loading analysis of doubler plate attachment details for steel moment resisting frames.

Krawinkler, H. 1978. Shear in Beam-Column Joints in Seismic Design of Steel Frames, n.d.

Lee, D., Cotton, S., Hajjar, J., Dexter, R., and Ye, Y. 2005. Cyclic Behavior of Steel Moment-Resisting Connections Reinforced by Alternative Column Stiffener Details I. Connection Performance and Continuity Plate Detailing. Engineering Journal, 42.

LIMCON V3 User's Manual, 2006. Engineering Systems Pty Limited, Turramura, Australia.

Morgan, B. 2021. Personal communication. WF Steel and Crane, Nisku, AB

Reynolds, M., and Uang, C.-M. 2019. Alternative Weld Details and Design for Continuity Plates and Doubler Plates for Applications in Special and Intermediate Moment Frames: 514.

Reynolds, M., and Uang, C.-M. 2021. Economical Weld Details and Design for Continuity and Doubler Plates in Steel Special Moment Frames. Journal of Structural Engineering, 148(1): 04021246. doi:10.1061/(ASCE)ST.1943-541X.0003203.

Rosson B. T. 2018. Modeling the influence of residual stress on the ultimate load conditions of steel frames, in: Proceedings of the 2018 SSRC Annual Stability Conference.

Shirsat, P.S. 2011. Preliminary analysis of doubler plate attachment details for steel moment resisting frames. MSc thesis, University of Texas at Austin.





Skiadopoulos, A., Elkady, A., and Lignos, D.G. 2021. Proposed Panel Zone Model for Seismic Design of Steel Moment-Resisting Frames. Journal of Structural Engineering, 147(4): 04021006. American Society of Civil Engineers. doi:10.1061/(ASCE)ST.1943-541X.0002935.

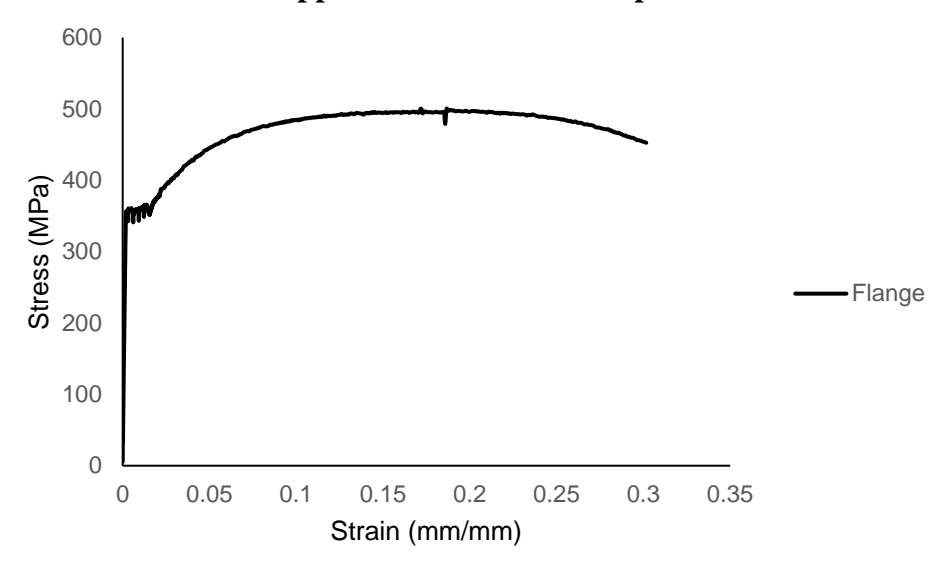
WF Steel and Crane, wfsteelandcrane. "Well Pair Modules". Instagram, 2021.

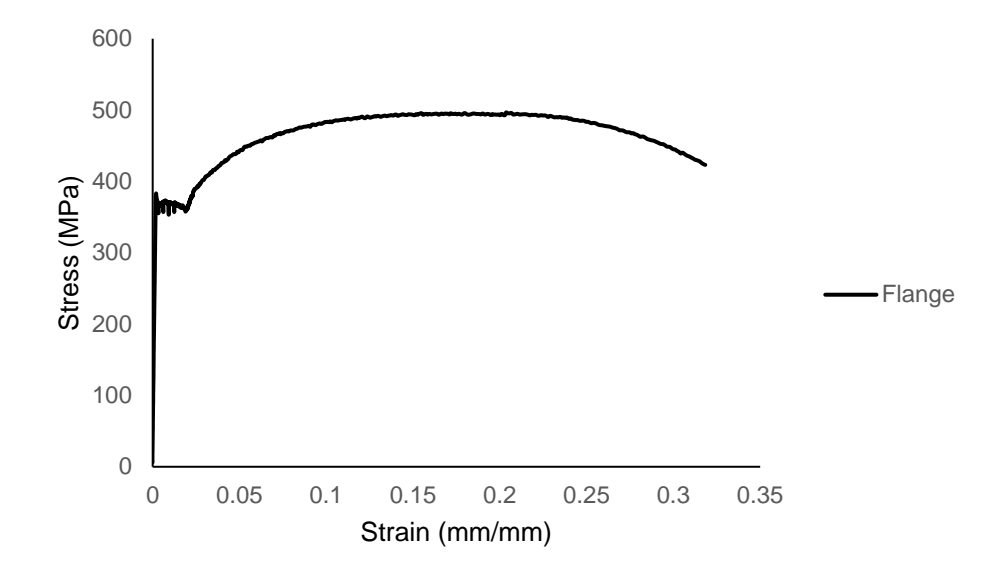
Ziemian, R.D. 2010. Guide to Stability Design Criteria for Metal Structures. 6th Ed., John Wiley & Sons, Inc., Hoboken, NJ.





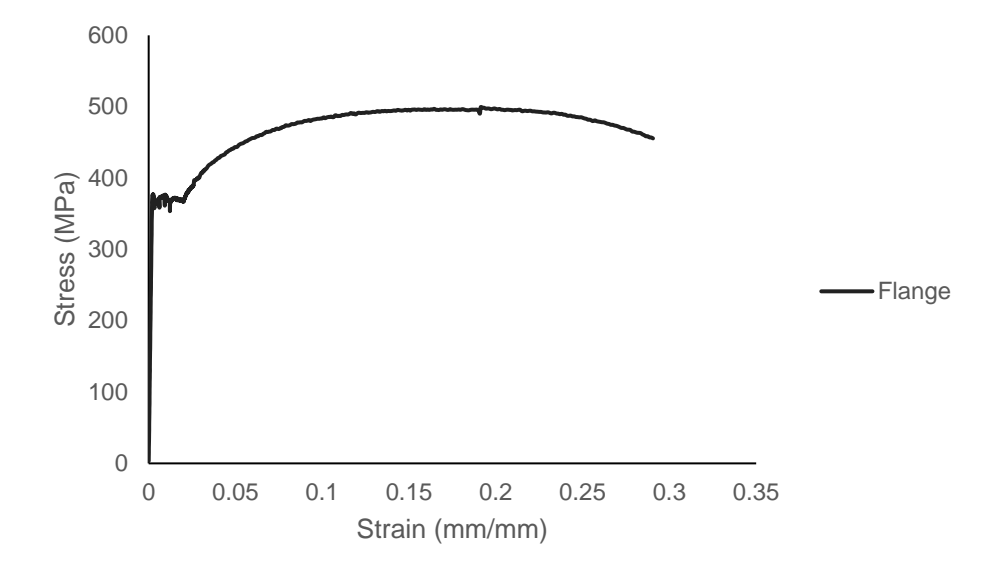
Appendix A: Material Properties

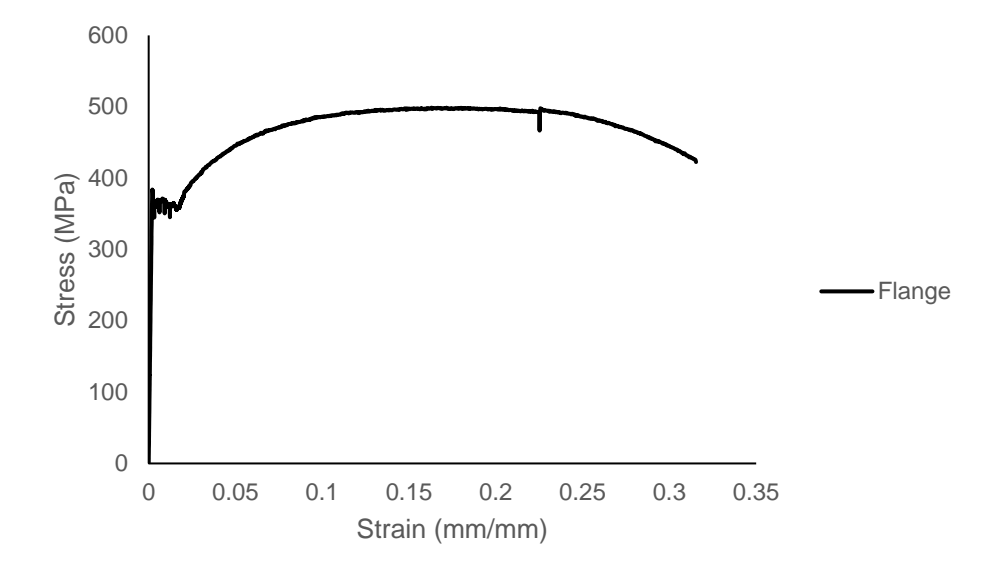






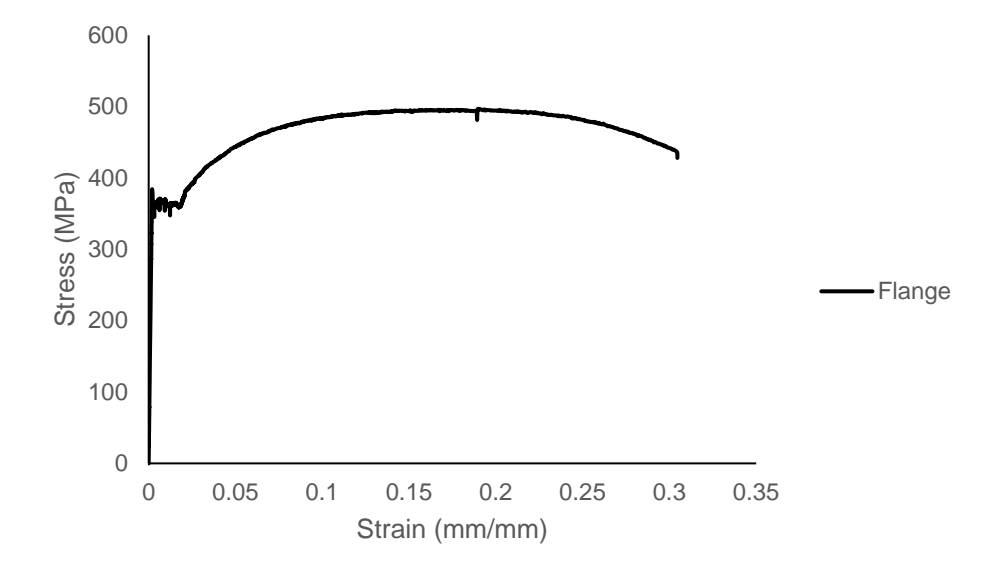


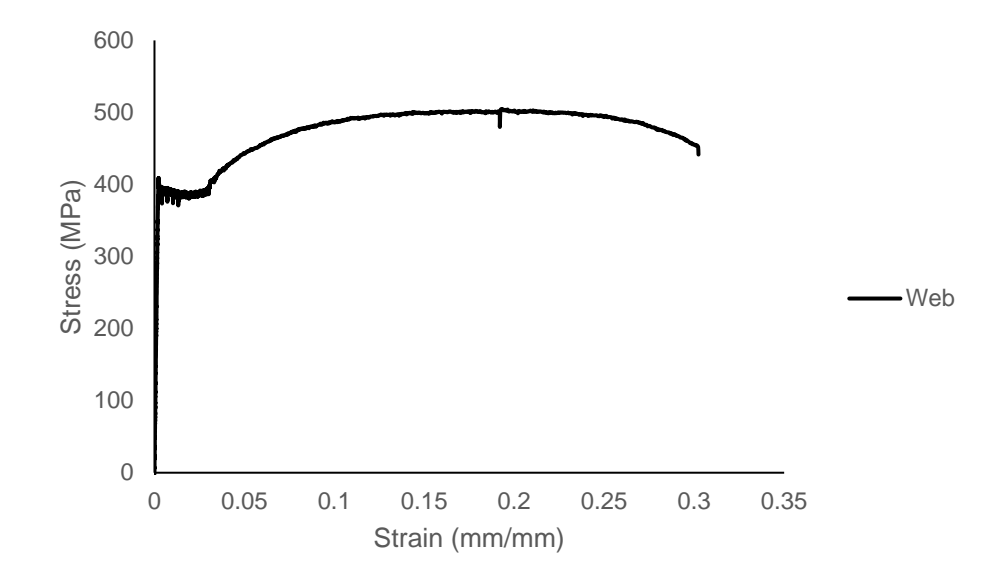






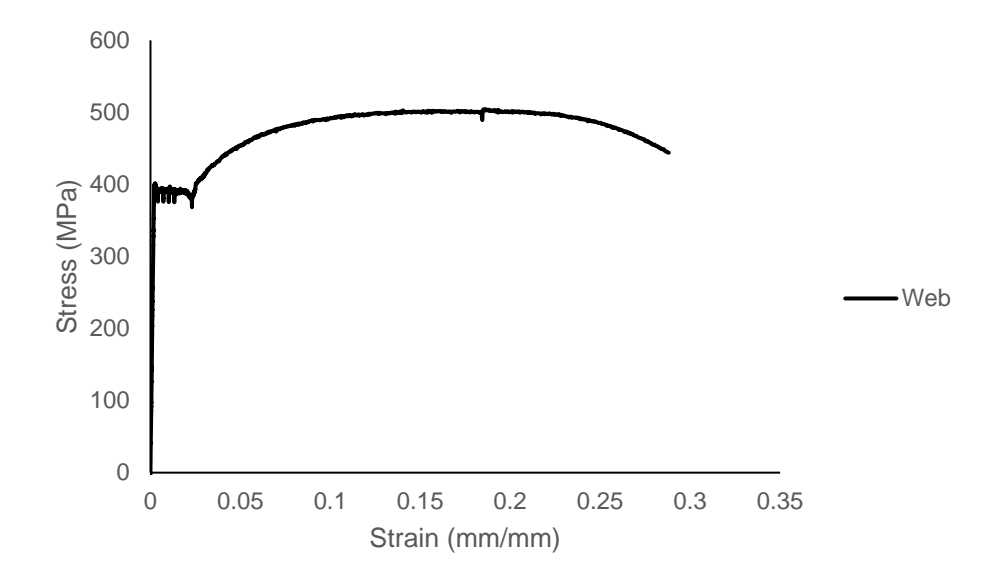


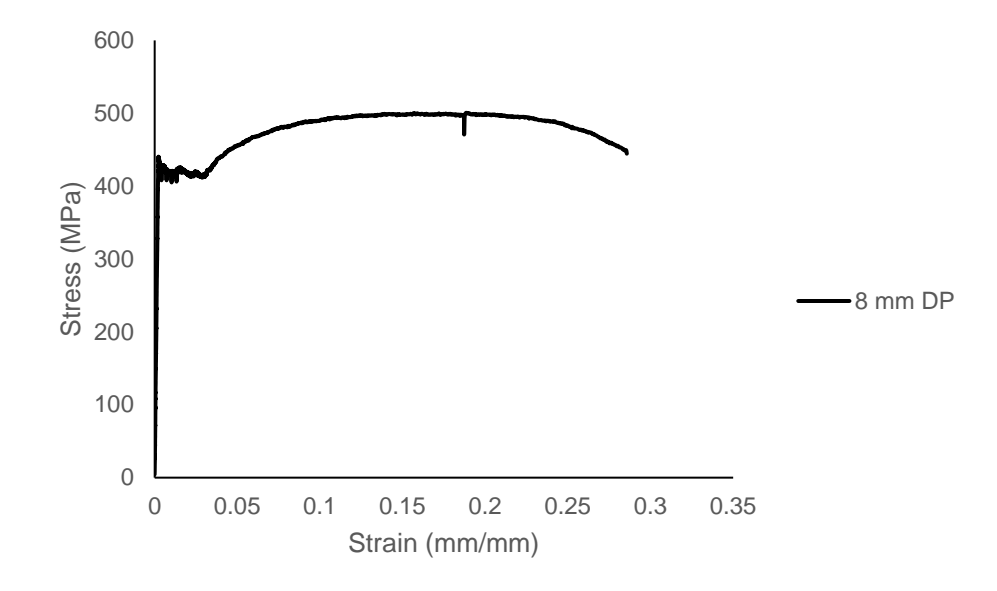
















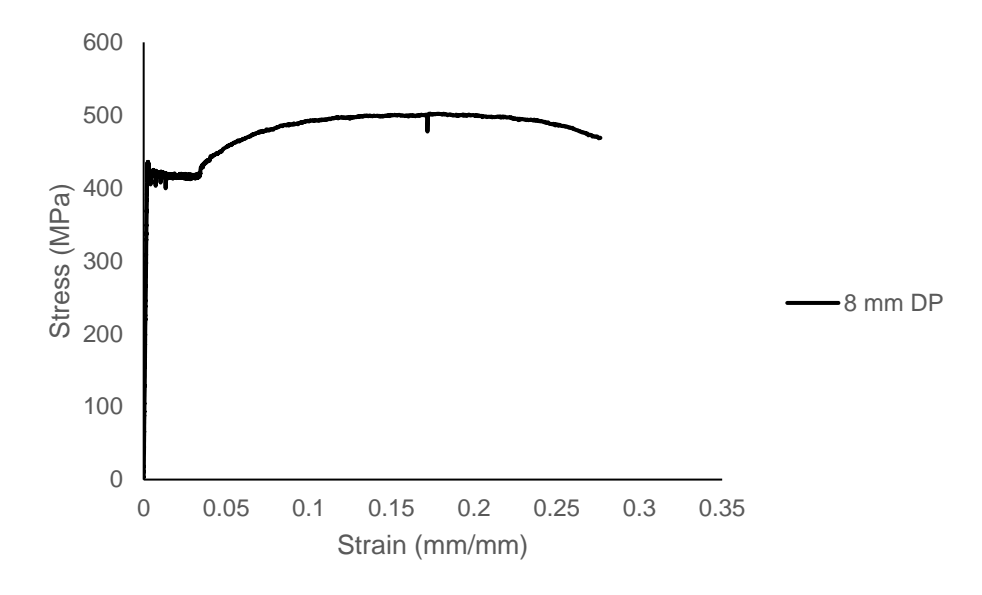
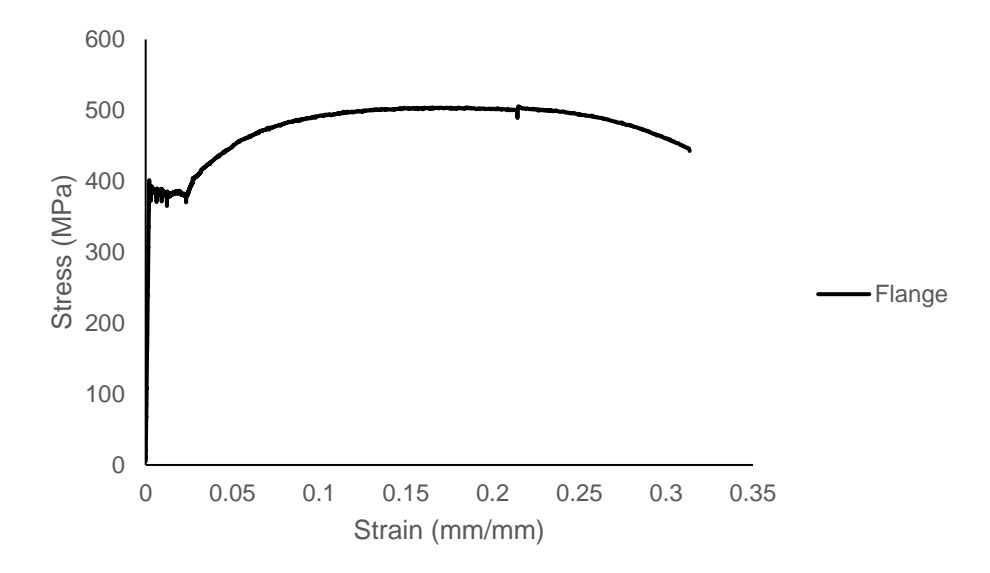
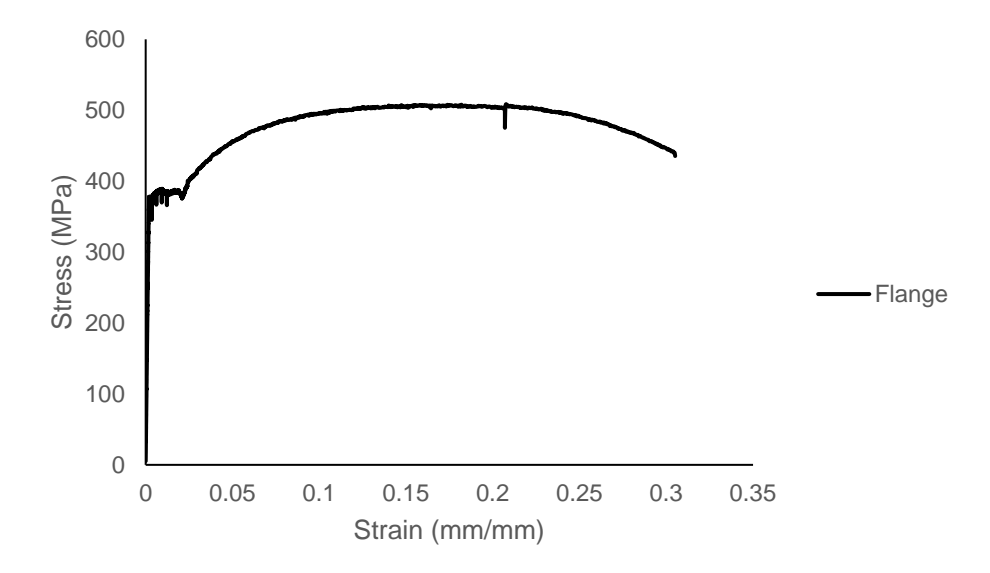


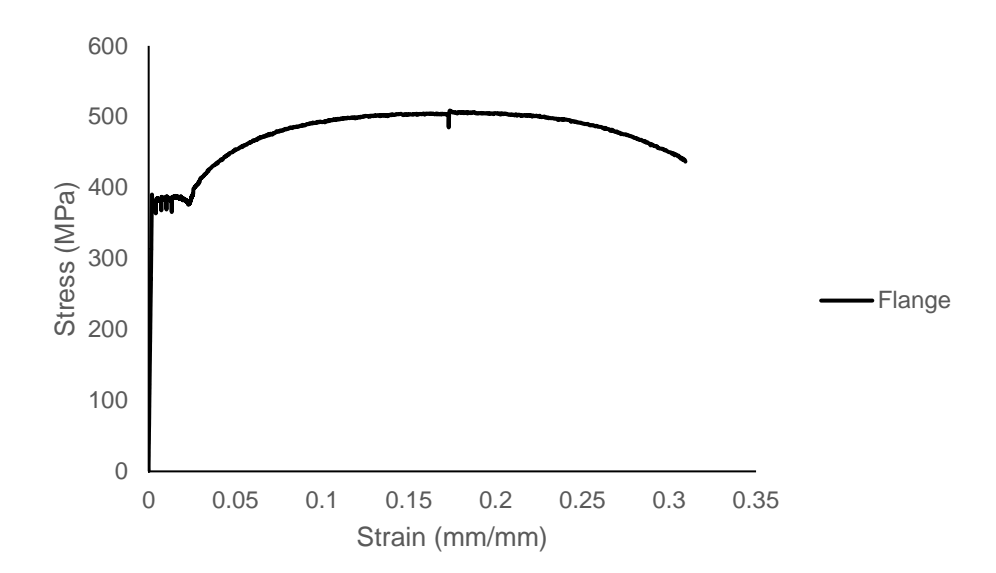
Figure A.1: Engineering stress-strain results for W250 specimens





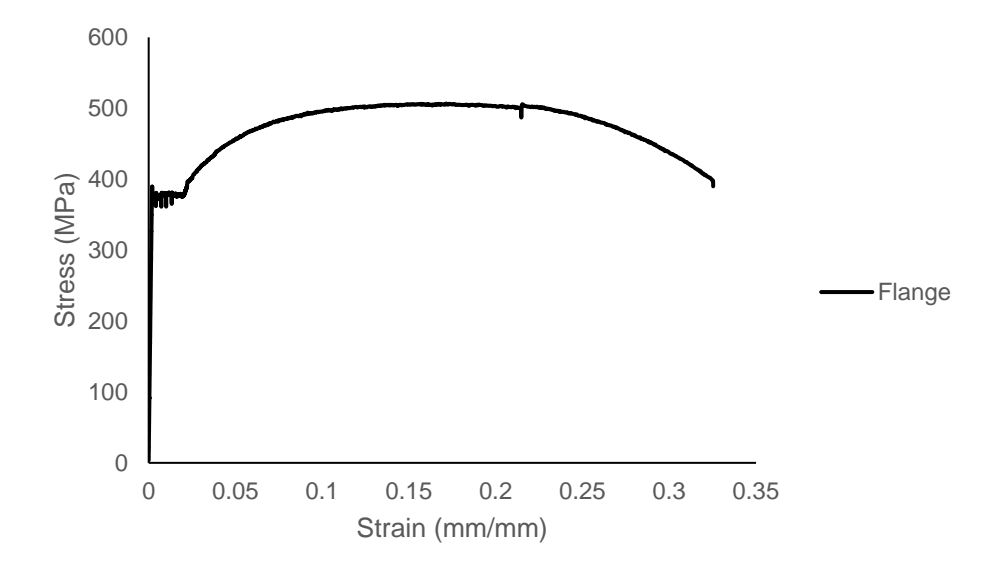


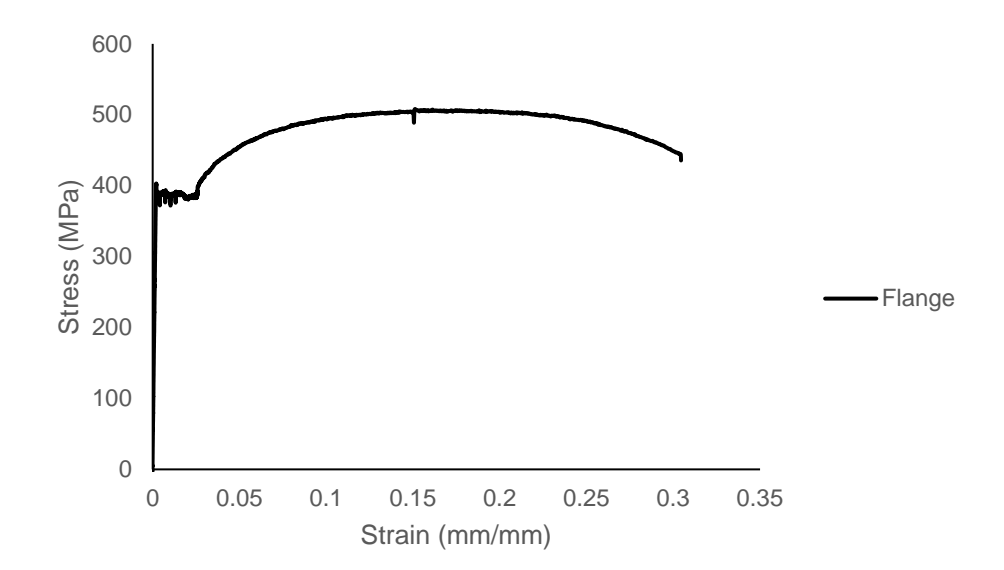






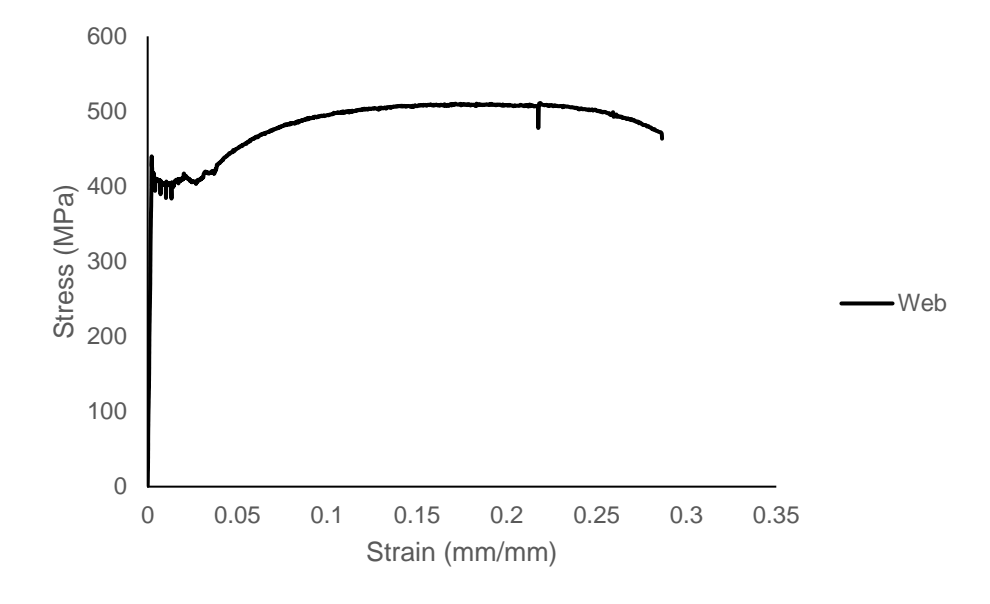


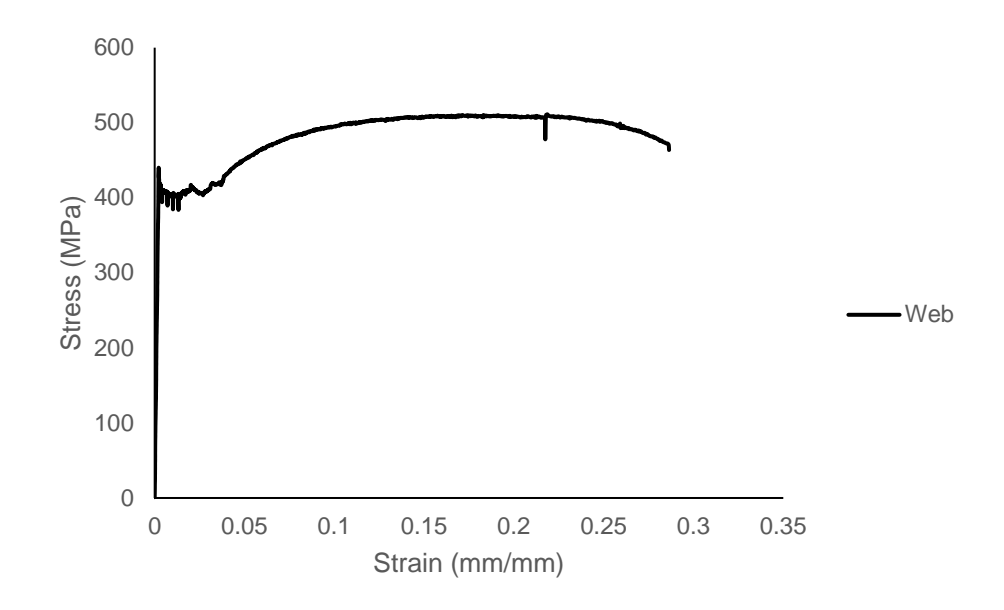






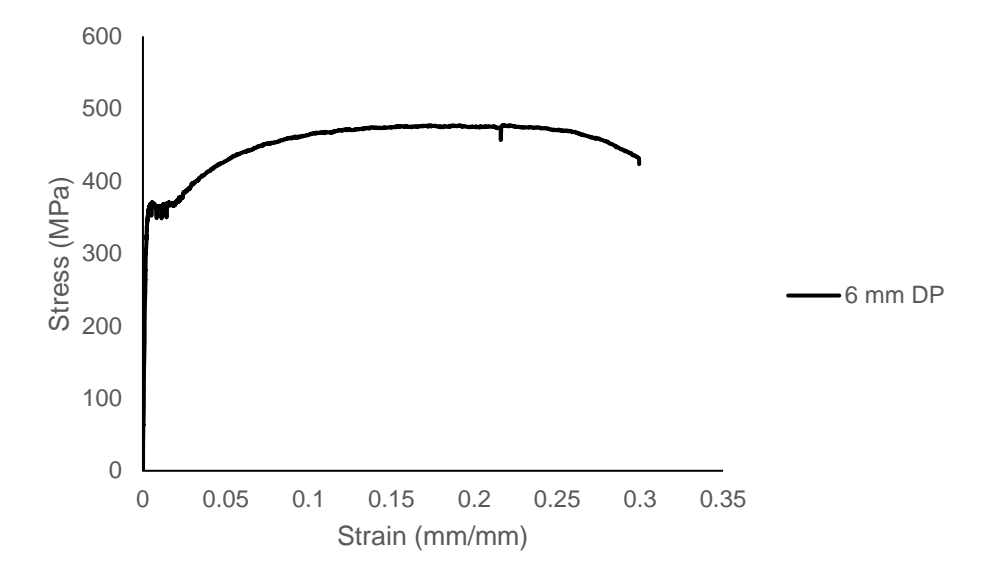












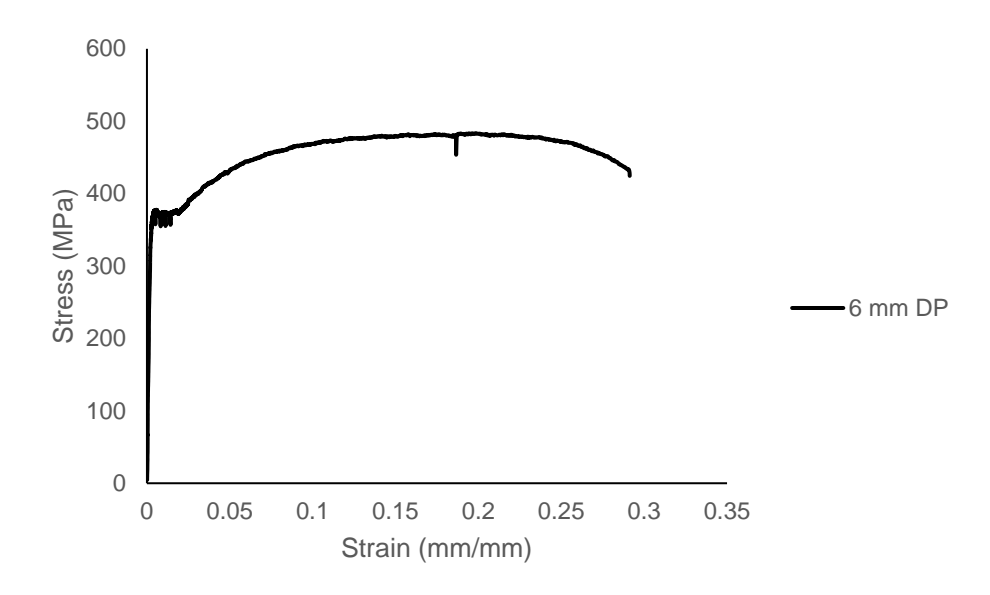


Figure A.2: Engineering stress-strain results for W410 specimens



Appendix B: Residual Stress Measurements

	After	Ref. Bar	200 mm Gage Length Avg. of 3 Reading Length wrt After Ref. Bar	-	0.333 0.329 0.329 0.372 -0.043	0.200 0.202 0.199 0.200 -0.001	0.109 0.108 0.108 0.159 -0.051	0.250 0.252 0.252 0.261 -0.009	0.014 0.016 0.014 -0.021 0.035	0.045 0.040 0.044 0.080 -0.036	0.061 0.064 0.063 0.073 -0.010	0.149 0.148 0.148 0.000		0.079 0.076 0.077 0.083 -0.006	0.047 0.042 0.045 0.032 0.013	-0.074 -0.073 -0.074 -0.103 0.029	-0.025 -0.026 -0.024 -0.052 0.028	0.037 0.039 0.038 -0.076 0.114	0.081 0.080 0.081 0.012 0.069	0.494 0.495 0.494 0.515 -0.021	0.519 0.521 0.520 0.561 -0.041		0.050 0.054 0.052 -0.164 0.216	-0.195 -0.195 -0.130 -0.065	-0.587 -0.587 -0.585 -0.460 -0.125	0.294 0.291 0.292 0.442 -0.150	-0.272 -0.277 -0.276 -0.151 -0.125	-0.029 -0.029 -0.029 0.105 -0.134	
			200 mm		0.326	0.195	0.106	0.254	0.013	0.048	0.063	0.148		0.076	0.047	-0.075	-0.020	0.039	0.081	0.492	0.521		0.052	-0.194	-0.582	0.290	-0.278	-0.028	000
	Before	Ref. Bar	Reading Before		0.000	0.000	0.000	0.000	0.000	0.000	0.000	0.000		0.000	0.000	0.000	0.000	0.000	0.000	0.000	0.000		0.000	0.000	0.000	0.000	0.000	0.000	000
Side A		Uncorrected	Length wrt Ref. Bar	Flange 1	-0.031	-0.001	-0.002	-0.025	-0.005	0.015	-0.008	0.005	Flange 2	-0.181	0.084	-0.132	-0.301	0.809	0.039	0.415	0.327	Web	0.066	-0.005	-0.053	-0.014	-0.050	-0.051	0.00
	After		Reading After		-0.237	0.220	-0.849	-0.051	0.297	-0.144	-0.225	0.160		0.258	-0.039	0.058	0.277	-0.771	0.042	0.079	0.193		0.200	0.333	0.408	0.434	0.755	0.366	010
	4		of 3		-0.268	0.219	-0.851	-0.076	0.292	-0.129	-0.233	0.165		0.077	0.045	-0.074	-0.024	0.038	0.081	0.494	0.520		0.266	0.328	0.355	0.420	0.705	0.315	7 70 0
			ingth Avg. of 3		-0.269	0.217	-0.851	-0.077	0.293	-0.130	-0.238	0.164		-0.235	-0.030	0.080	0.320	-0.713	0.070	0.089	0.188		0.267	0.328	0.358	0.418	0.704	0.314	010
			100 mm Gage Length		-0.268	0.220	-0.847	-0.075	0.292	-0.130	-0.230	0.162		-0.236	-0.033	0.080	0.321	-0.718	0.074	0.085	0.191		0.267	0.328	0.355	0.421	0.706	0.314	2100
			100 m		-0.266	0.220	-0.855	-0.076	0.291	-0.128	-0.231	0.168		-0.234	-0.033	0.076	0.324	-0.715	0.073	0.085	0.190		0.265	0.328	0.353	0.421	0.705	0.317	7 10 0
	Before	Ref. Bar	Reading Before		0000	0000	0.000	000'0	000'0	000'0	0.000	000'0		000'0	0.000	0.000	000'0	000'0	000'0	0.000	0000		000'0	000'0	0.000	0.000	0.000	0.000	000
		!	Slice ID		1F1A	1F2A	1F3A	1F4A	1F5A	1F6A	1F7A	1F8A		2F1A	2F2A	2F3A	2F4A	2F5A	2F6A	2F7A	2F8A		W1A	W2A	W3A	W4A	W5A	W6A	V / / V /





							Side B							
	Before					After		Before					After	
	Ref. Bar					Ref. Bar	Uncorrect	Ref. Bar					Ref. Bar	Uncorrec ted
Slice ID	Reading Before	100	mm Gage l	100 mm Gage Length Avg. of 3	of 3	Reading After	ed Lengun wrt Ref.	Reading Before	200 n	nm Gage Le	200 mm Gage Length Avg. of 3	of 3	Reading After	Length wrt Ref.
							Bar							Bar
							Flange 1							
1F1B	0.000	0.320	0.325	0.321	0.322	0.272	0:020	0.000	-0.233	-0.237	-0.239	-0.236	-0.290	0.054
1F2B	0.000	-1.428	-1.430	-1.431	-1.430	-1.441	0.011	0.000	0.165	0.163	0.165	0.164	0.190	-0.026
1F3B	0.000	-0.279	-0.282	-0.280	-0.280	-0.263	-0.017	0.000	-0.760	-0.761	-0.762	-0.761	-0.692	-0.069
1F4B	0.000	-0.558	-0.557	-0.560	-0.558	-0.544	-0.014	0.000	-0.134	-0.134	-0.131	-0.133	-0.118	-0.015
1F5B	0.000	0.730	0.729	0.735	0.731	0.700	0.031	0.000	0.195	0.199	0.195	0.196	0.124	0.072
1F6B	0.000	0.536	0.529	0.534	0.533	0.437	0.096	0.000	0.541	0.540	0.541	0.541	0.526	0.015
1F7B	0.000	0.092	0.090	0.089	0.090	0.104	-0.014	0.000	0.321	0.324	0.326	0.324	0.370	-0.046
1F8B	0.000	-0.372	-0.368	-0.373	-0.371	-0.416	0.045	0.000	0.108	0.106	0.106	0.107	0.176	-0.069
							Flange 2							
2F1B	0.000	-0.087	-0.087	-0.085	-0.086	-0.104	0.018	0.000	0.071	0.074	0.077	0.074	0.034	0.040
2F2B	0.000	0.769	0.768	0.769	0.769	0.765	0.004	0.000	0.225	0.227	0.226	0.226	0.224	0.002
2F3B	0.000	0.575	0.574	0.573	0.574	0.587	-0.013	0.000	0.047	0.048	0.045	0.047	0.026	0.021
2F4B	0.000	-0.115	-0.116	-0.120	-0.117	-0.151	0.034	0.000	0.165	0.164	0.166	0.165	0.071	0.094
2F5B	0.000	0.466	0.477	0.467	0.470	0.438	0.032	0.000	0.469	0.460	0.462	0.464	0.391	0.073
2F6B	0.000	0.449	0.440	0.444	0.444	0.406	0.038	0.000	0.094	0.095	0.093	0.094	0.010	0.084
2F7B	0.000	0.690	0.697	0.701	0.696	0.682	0.014	0.000	0.015	0.018	0.014	0.016	-0.040	0.056
2F8B	0.000	0.225	0.222	0.221	0.223	0.205	0.018	0.000	0.031	0.033	0.031	0.032	0.056	-0.024
							Web							
W1B	0.000	0.009	0.013	0.013	0.012	0.036	-0.024	000'0	-0.250	-0.252	-0.250	-0.251	-0.171	-0.080
W2B	0.000	0.074	0.067	0.072	0.071	0.112	-0.041	000'0	0.139	0.141	0.144	0.141	0.207	-0.066
W3B	0.000	0.162	0.162	0.163	0.162	0.211	-0.049	000'0	0.073	0.073	0.075	0.074	0.194	-0.120
W4B	0.000	0.085	0.083	0.085	0.084	0.128	-0.044	000'0	-0.045	-0.052	-0.053	-0.050	0.084	-0.134
W5B	0.000	1.627	1.630	1.630	1.629	1.642	-0.013	0.000	-0.199	-0.199	-0.198	-0.199	-0.126	-0.073
W6B	0.000	-0.323	-0.318	-0.320	-0.320	-0.275	-0.045	0.000	-0.018	-0.018	-0.016	-0.017	0.098	-0.115
W7B	0.000	-0.808	-0.800	-0.810	-0.806	-0.794	-0.012	0.000	0.107	0.109	0.107	0.108	0.163	-0.055
W8B	0.000	-0.211	-0.213	-0.214	-0.213	-0.179	-0.034	0.000	-0.101	-0.094	-0.097	-0.097	0.037	-0.134





Table B.1: Residual stress measurements of W250×58 section

							Side A					:		
	Before					After		Before					After	
	Ref. Bar					Ref. Bar	Uncorrected	Ref. Bar					Ref. Bar	Uncorrected
Slice ID	Reading Before	100 r	100 mm Gage Length Avg. of 3	ength Avg.	of 3	Reading After	Length wrt Ref. Bar	Reading Before	200 m	200 mm Gage Length Avg. of 3	ngth Avg.	of 3	Reading After	Length wrt Ref. Bar
							Flange 1							
1F1A	0.000	-0.063	-0.066	-0.065	-0.065	-0.091	0.026	0.000	0.119	0.121	0.121	0.120	0.019	0.101
1F2A	0.000	0.134	0.129	0.131	0.131	0.104	0.027	0.000	-0.003	-0.004	-0.005	-0.004	-0.079	0.075
1F3A	0.000	0.044	0.044	0.049	0.046	0.004	0.042	0.000	-0.024	-0.025	-0.026	-0.025	-0.160	0.135
1F4A	0.000	-0.075	-0.076	-0.076	-0.076	-0.126	0.050	0.000	-0.053	-0.050	-0.051	-0.051	-0.198	0.147
1F5A	0.000	-0.112	-0.110	-0.107	-0.110	-0.108	-0.002	0.000	0.433	0.434	0.430	0.432	0.360	0.072
1F6A	0.000	0.313	0.313	0.314	0.313	0.331	-0.018	0.000	0.287	0.285	0.286	0.286	0.253	0.033
							Flange 2							
2F1A	0.000	-1.359	-1.360	-1.361	-1.360	-1.321	-0.039	0.000	-0.093	-0.094	-0.091	-0.093	-0.072	-0.021
2F2A	0.000	0.034	0.034	0.033	0.034	0.036	-0.002	0.000	0.015	0.015	0.016	0.015	0.044	-0.029
2F3A	0.000	-0.349	-0.349	-0.348	-0.349	-0.404	0.055	0.000	-0.262	-0.261	-0.264	-0.262	-0.368	0.106
2F4A	0.000	-0.087	-0.088	-0.090	-0.088	-0.105	0.017	0.000	0.099	0.098	0.096	0.098	0.035	0.063
2F5A	0.000	-0.250	-0.247	-0.247	-0.248	-0.296	0.048	0.000	0.149	0.148	0.147	0.148	0.128	0.020
2F6A	0.000	0.204	0.204	0.206	0.205	0.195	0.010	0.000	-0.393	-0.399	-0.397	-0.396	-0.425	0.029
							Web							
W1A	0.000	-1.095	-1.106	-1.101	-1.101	-0.978	-0.123	0.000	0.028	0.029	0.029	0.029	0.272	-0.243
W2A	0.000	-0.211	-0.211	-0.213	-0.212	-0.182	-0.030	0.000	0.762	0.766	0.763	0.764	0.865	-0.101
W3A	0.000	-0.231	-0.232	-0.234	-0.232	-0.165	-0.067	0.000	0.256	0.257	0.258	0.257	0.590	-0.333
W4A	0.000	-0.015	-0.014	-0.013	-0.014	0.042	-0.056	0.000	-0.020	-0.019	-0.020	-0.020	0.177	-0.197
W5A	0.000	-0.192	-0.190	-0.197	-0.193	-0.013	-0.180	0.000	-0.253	-0.253	-0.251	-0.252	-0.030	-0.222
W6A	0.000	-0.348	-0.345	-0.350	-0.348	-0.222	-0.126	0.000	-0.114	-0.114	-0.115	-0.114	0.116	-0.230
W7A	0.000	-0.298	-0.297	-0.301	-0.299	-0.201	-0.098	0.000	0.098	0.096	0.097	0.097	0.359	-0.262
W8A	0.000	-0.116	-0.116	-0.116	-0.116	-0.031	-0.085	0.000	-0.106	-0.105	-0.107	-0.106	0.191	-0.297
W9A	0.000	-0.040	-0.038	-0.040	-0.039	0.048	-0.087	0.000	-0.204	-0.205	-0.205	-0.205	0.061	-0.266
W10A	0.000	-0.047	-0.044	-0.042	-0.044	0.106	-0.150	0.000	0.273	0.272	0.271	0.272	0.530	-0.258
W11A	0.000	-0.024	0.024	0.028	0.009	0.091	-0.082	0.000	-0.150	-0.152	-0.152	-0.151	0.110	-0.261
W12A	0.000	0.197	0.197	0.200	0.198	0.283	-0.085	0.000	0.195	0.197	0.198	0.197	0.421	-0.224
W13A	0.000	-0.418	-0.417	-0.417	-0.417	-0.351	-0.066	0.000	0.072	0.073	0.076	0.074	0.252	-0.178
W14A	0.000	-0.310	-0.309	-0.311	-0.310	-0.269	-0.041		0.351	0.351	0.355	0.352	0.480	-0.128
W15A	0.000	0.201	0.202	0.207	0.203	0.194	0.009	0.000	1.176	1.177	1.177	1.177	1.183	-0.006
W16A	0.000	0.856	0.852	0.850	0.853	0.788	0.065	0.000	-0.184	-0.185	-0.186	-0.185	-0.303	0.118





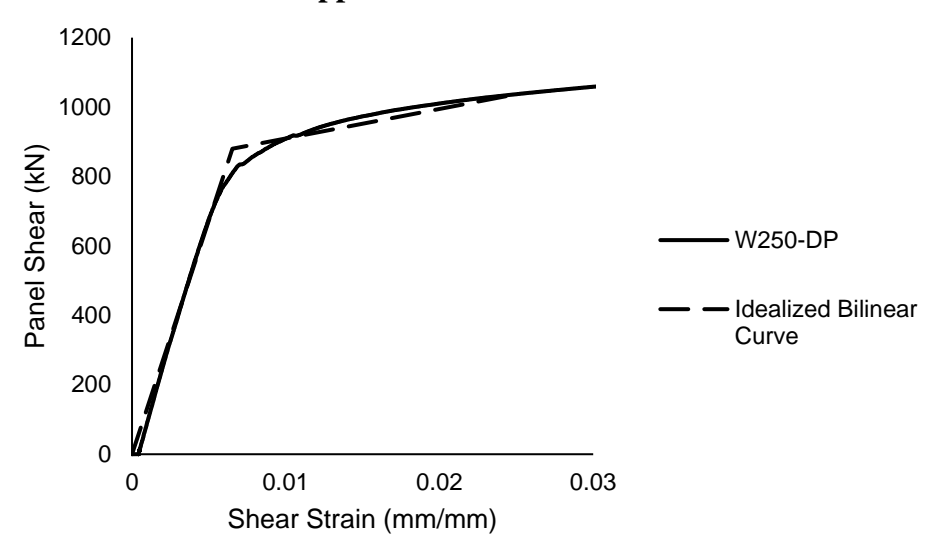
							Side B							
	Before					After		Before					After	
Slice ID	Ref. Bar Reading Before	100 n	nm Gage L	100 mm Gage Length Avg. of 3)f3	Ref. Bar Reading After	Uncorrect ed Length wrt Ref. Bar	Ref. Bar Reading Before	200 m	ım Gage Le	200 mm Gage Length Avg. of	of 3	Ref. Bar Reading After	Uncorrec ted Length wrt Ref. Bar
							Flange 1							
1F1B	0.000	0.162	0.169	0.163	0.165	0.173	-0.008	0.000	0.050	0.053	0.054	0.052	0.064	-0.012
1F2B	0.000	0.422	0.428	0.416	0.422	0.261	0.161	0000	0.210	0.209	0.208	0.209	0.069	0.140
1F3B	0.000	0.227	0.228	0.227	0.227	0.288	-0.061	0.000	-0.129	-0.129	-0.131	-0.130	-0.335	0.205
1F4B	0.000	-0.146	-0.148	-0.141	-0.145	-0.204	0.059	0000	0.160	0.164	0.166	0.163	-0.014	0.177
1F5B	0.000	-0.156	-0.156	-0.158	-0.157	-0.171	0.014	0.000	-0.045	-0.045	-0.043	-0.044	-0.056	0.012
1F6B	0.000	0.307	0.310	0.312	0.310	0.306	0.004	0000	0.027	0.024	0.022	0.024	-0.005	0.029
							Flange 2							
2F1B	0.000	-0.276	-0.276	-0.278	-0.277	-0.300	0.023	0000	0.050	0.049	0.048	0.049	0.058	-0.009
2F2B	0.000	0.415	0.417	0.417	0.416	0.356	0.060	0.000	-0.113	-0.112	-0.112	-0.112	-0.219	0.107
2F3B	0.000	0.383	0.384	0.382	0.383	0.295	0.088	0.000	-0.050	-0.053	-0.051	-0.051	-0.239	0.188
2F4B	0.000	0.421	0.422	0.425	0.423	0.331	0.092	0.000	-0.011	-0.011	-0.009	-0.010	-0.192	0.182
2F5B	0.000	0.248	0.249	0.248	0.248	0.188	090'0	0.000	0.038	0.035	0.032	0.035	-0.118	0.153
2F6B	0.000	-0.291	-0.291	-0.290	-0.291	-0.295	0.004	0.000	0.355	0.355	0.354	0.355	0.358	-0.003
							Web							
W1B	0.000	-0.442	-0.442	-0.445	-0.443	-0.515	0.072	0.000	-0.034	-0.036	-0.039	-0.080	-0.189	0.109
W2B	0.000	-0.022	-0.020	-0.026	-0.023	-0.011	-0.012	0.000	-0.081	-0.074	-0.086	-0.082	0.036	-0.118
W3B	0.000	-0.424	-0.436	-0.434	-0.431	-0.374	-0.057	0.000	-0.081	-0.082	-0.083	-0.082	0.076	-0.158
W4B	0.000	-0.051	-0.059	-0.057	-0.056	0.026	-0.082	0.000	0.203	0.207	0.208	0.206	0.401	-0.195
W5B	0.000	-0.714	-0.709	-0.714	-0.712	-0.646	-0.066	0.000	-0.026	-0.025	-0.023	-0.025	0.197	-0.222
W6B	0.000	0.357	0.357	0.358	0.357	0.440	-0.083	0.000	0.027	0.029	0.028	0.028	0.320	-0.292
W7B	0.000	-0.598	-0.591	-0.591	-0.593	-0.495	-0.098	0.000	0.127	0.125	0.125	0.126	0.380	-0.254
W8B	0.000	-0.637	-0.639	-0.639	-0.638	-0.537	-0.101	0.000	-0.192	-0.196	-0.196	-0.195	0.058	-0.253
W9B	0.000	-0.147	-0.133	-0.136	-0.139	-0.073	-0.066	0.000	-0.019	-0.020	-0.020	-0.020	0.219	-0.239
W10B	0.000	-0.650	-0.646	-0.649	-0.648	-0.542	-0.106	0.000	0.139	0.139	0.137	0.138	0.391	-0.253
W11B	0.000	-0.096	-0.091	-0.089	-0.092	0.001	-0.093	0.000	0.107	0.108	0.104	0.106	0.329	-0.223
W12B	0.000	-0.483	-0.488	-0.480	-0.484	-0.409	-0.075	0.000	0.055	0.052	0.052	0.053	0.256	-0.203
W13B	0.000	-0.086	-0.077	-0.082	-0.082	-0.034	-0.048	0.000	0.165	0.166	0.167	0.166	0.349	-0.183
W14B	0.000	-0.038	-0.033	-0.035	-0.035	0.016	-0.051		0.265	0.265	0.268	0.266	0.403	-0.137
W15B	0.000	-0.155	-0.152	-0.167	-0.158	-0.138	-0.020	0.000	0.149	0.150	0.149	0.149	0.237	-0.088
W16B	0.000	-0.098	-0.095	-0.094	-0.096	-0.089	-0.007	0.000	0.281	0.282	0.286	0.283	0.309	-0.026

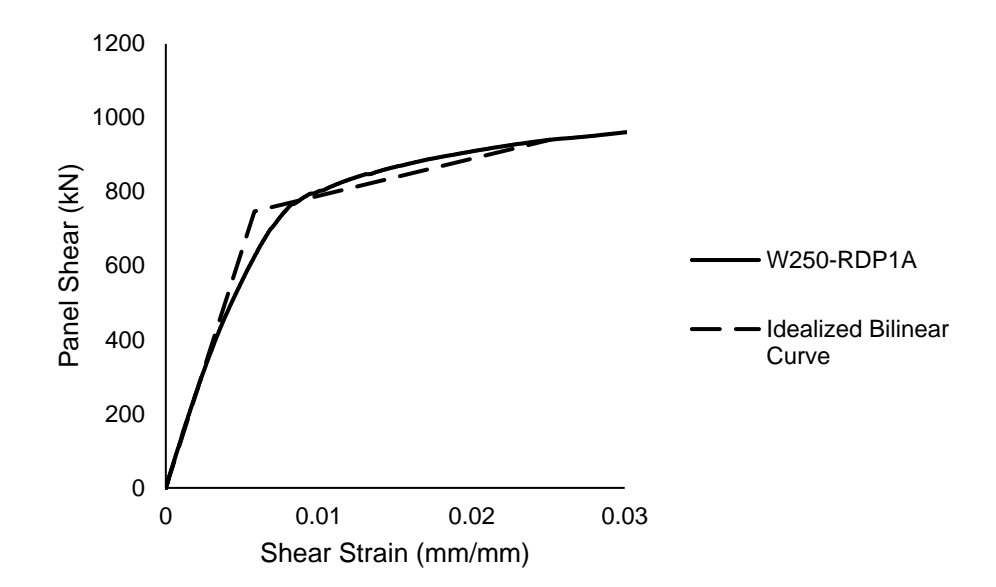
Table B.2: Residual stress measurements of W410×60 section





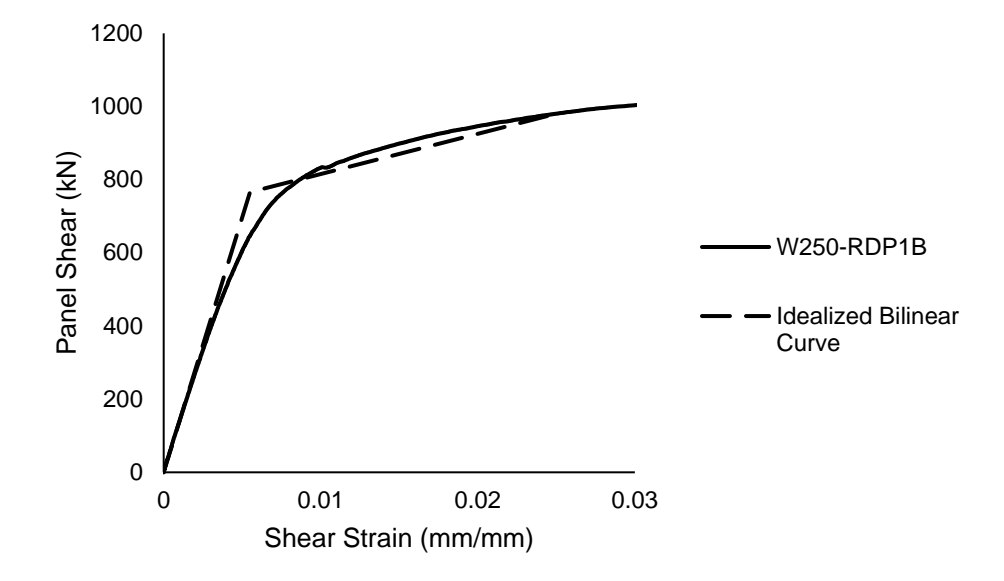
Appendix C: Bilinear Curves

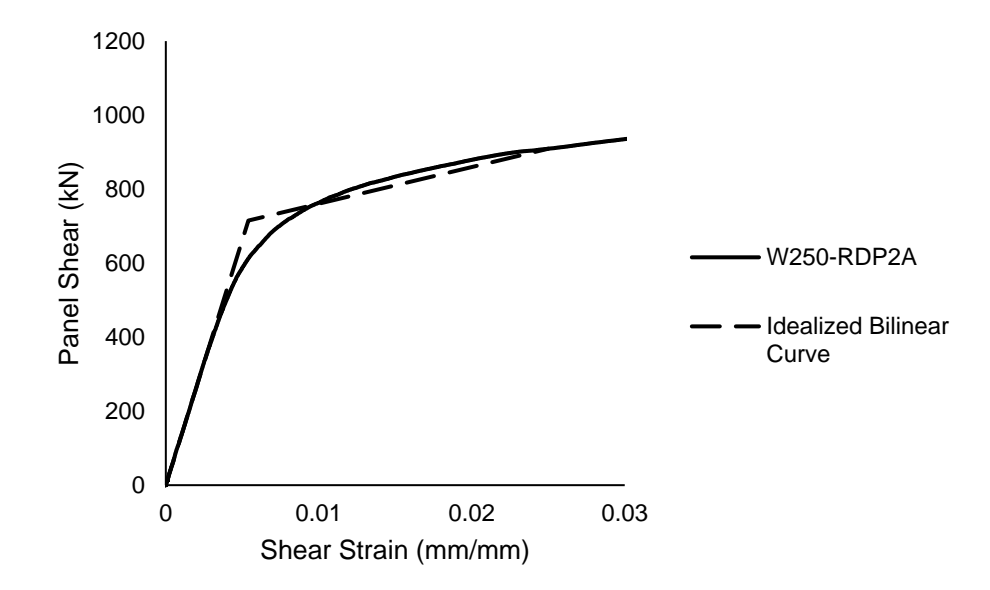
















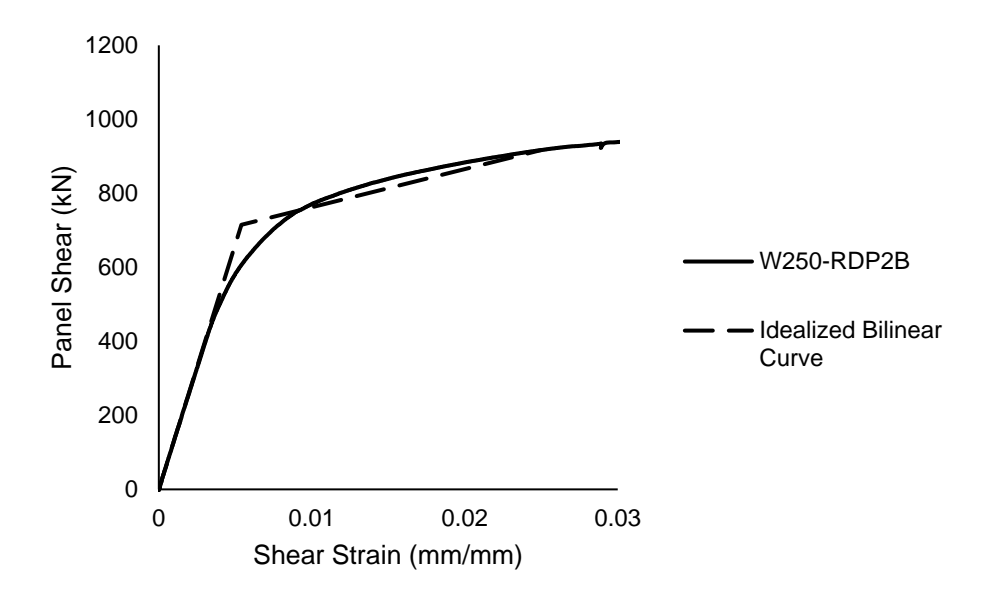
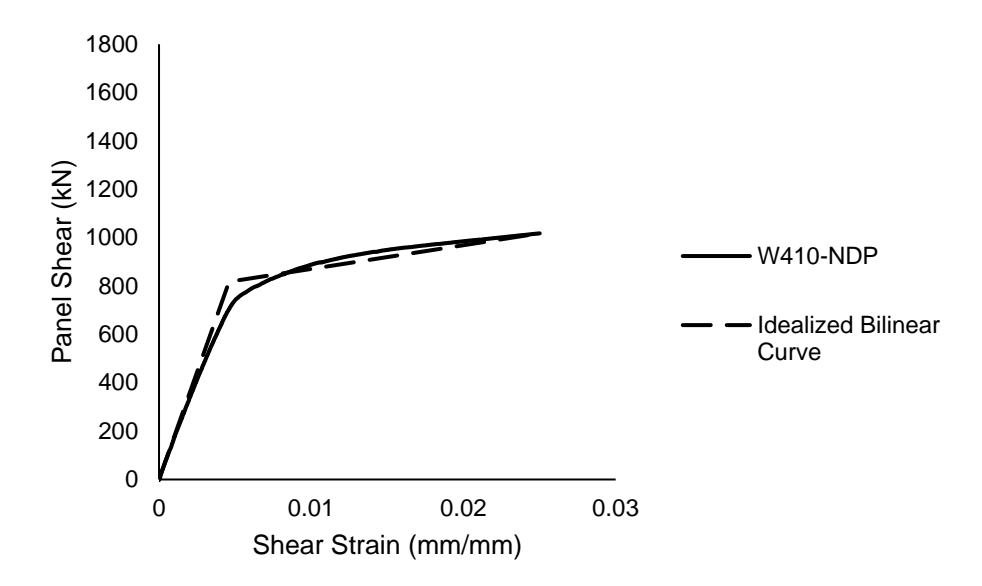
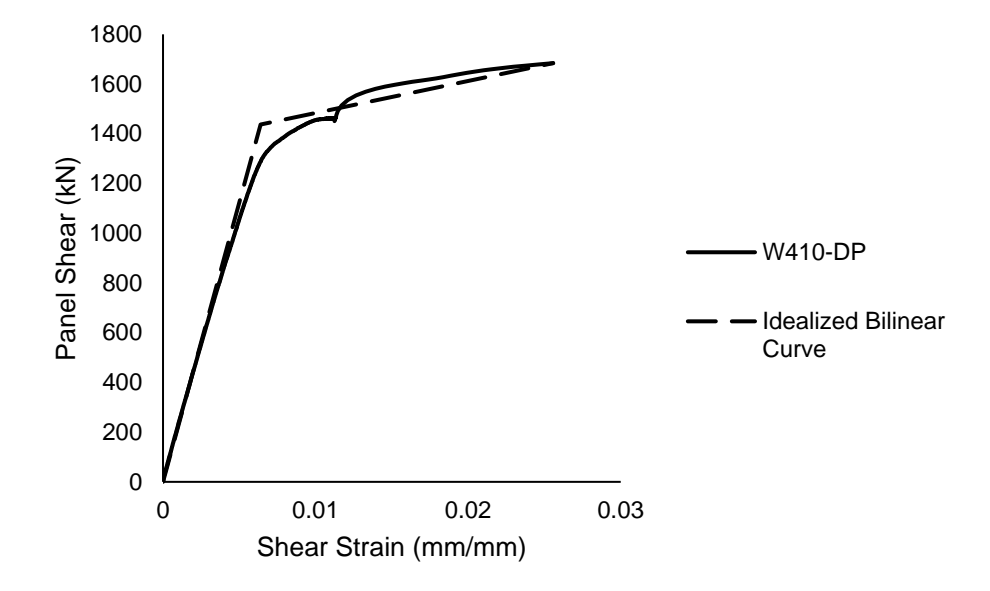


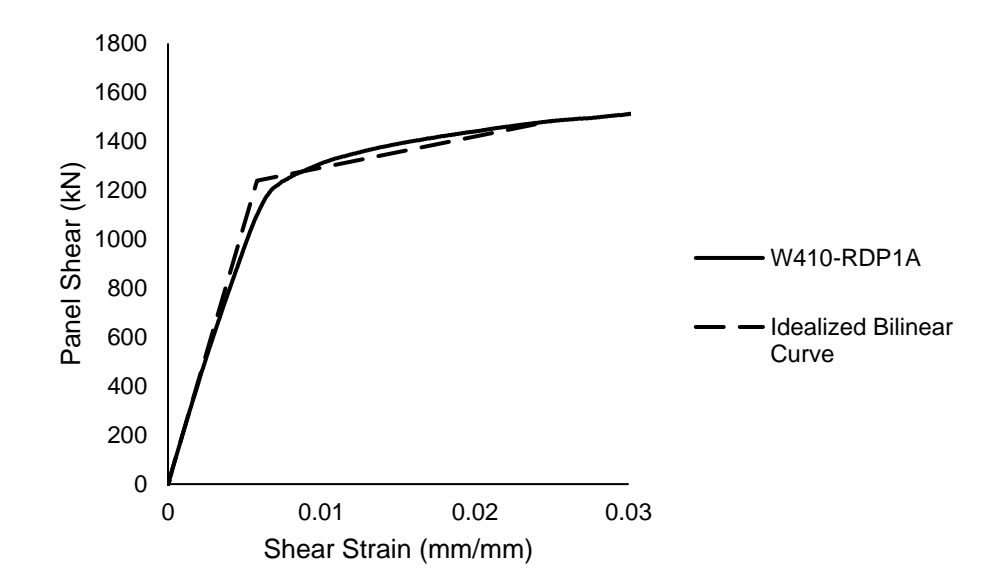
Figure C.1: Panel shear force versus panel shear strain for W250 specimens





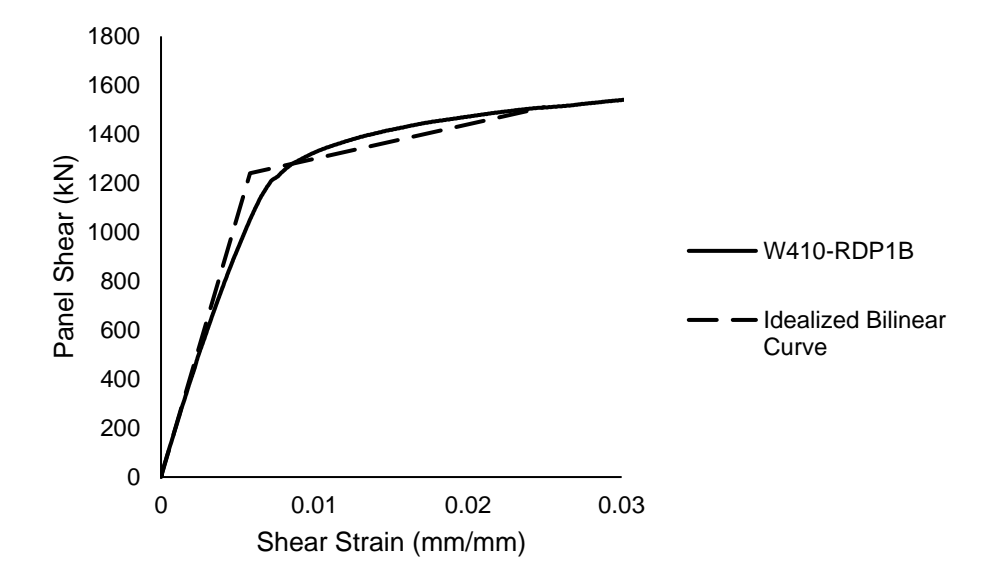


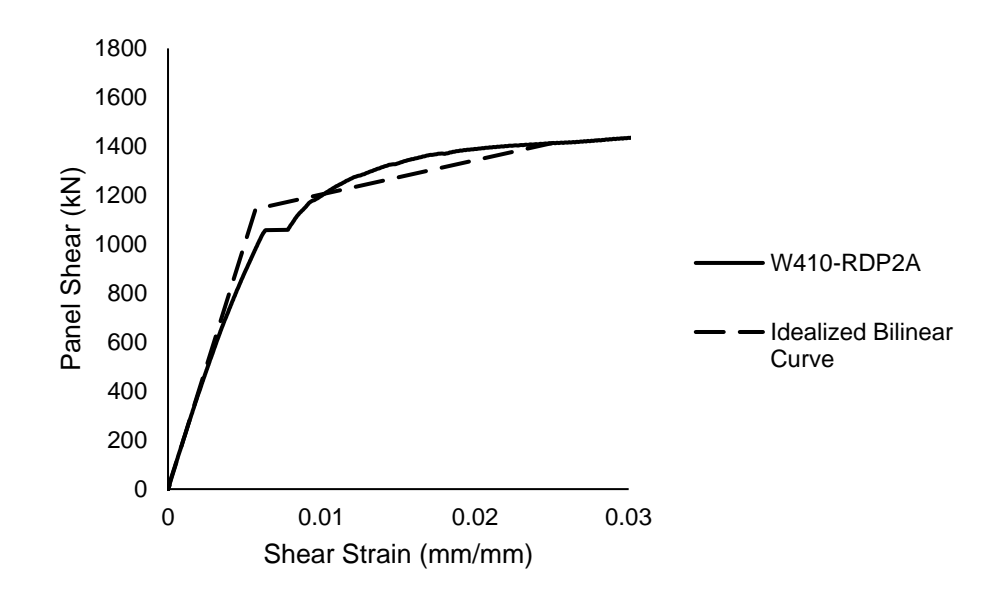
















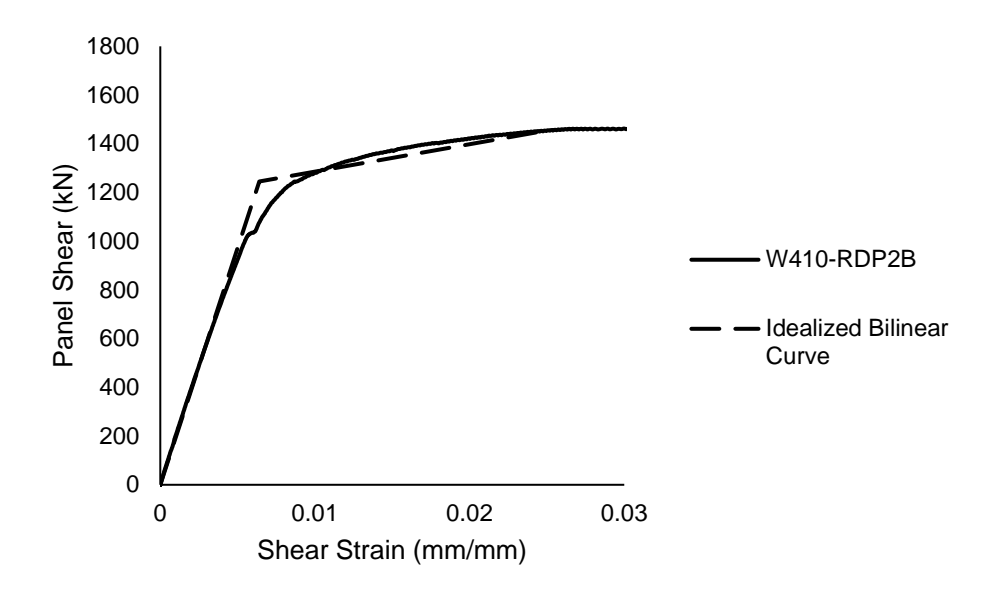


Figure C.2: Panel shear force versus panel shear strain for W410 specimens





Appendix D: Specimen Drawings

GENERAL NOTES: 1. ALL DIMENSIONS ARE IN MILLIMETERS UNLESS OTHERWISE SPECIFIED

- DO NOT SCALE DRAWINGS
 CONTINUITY PLATE: CP
- 4. DOUBLER PLATE: DP
- 5. PLATE: PL
- HOLE DIAMETER: Ø
 CROSS-SECTIONAL DIMENSIONS OF STANDARD STEEL SHAPES ARE NOMINAL VALUES AND ARE SHOWN FOR REFERENCE ONLY
- 8. FOR ANY CLARIFICATIONS, CONTACT HANA CHAYA AT HCHAYA@UALBERTA.CA OR (780) 729 5490

SCOPE:

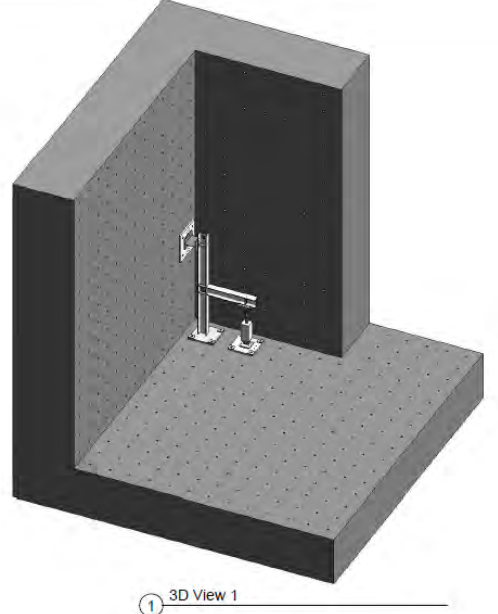
- 1. SIX SPECIMENS USED TO ANALYZE THE PANEL ZONE BEHAVIOUR IN PIPE RACK MOMENT CONNECTIONS
- 2. FOUR DETAILS ARE OUTLINED IN THESE DRAWINGS
- 3. TWO SETS OF S.2.3 AND S.2.4 ARE REQUIRED
- 4. PJPGW OF DP IN S.2.2 TO BE MANUFACTURED FOLLOWING WF CURRENT PRACTICE
- 5. NEED 2" THICK BASEPLATES FOR COLUMN
- 5. NEED 2 THICK BASEPLATES FOR COLUNG
 6. ACTUATOR BASEPLATE HAS EIGHT
 THREADED HOLES WITH A 1" DIAMETER
 7. SPECIFIC TO S.7 AND S.8:

 ALL TOLERANCES ARE +/- 0.8 MM
- - BLIND THREADED HOLES ON TOP AND RIGHT ONLY

MATERIALS OF STEEL:

- 1. COLUMNS: CSA G40.21 350W OR ASTM A992

- 2. BEAMS: CSA G40.21 350W OR ASTM A992
 3. CONTINUITY PLATES: CSA G40.21 350W
 4. DOUBLER PLATES: CSA G40.21 300W
 5. ADAPTER PLATE: ASTM A514 (PRINCIPAL
- FRONT VIEW TO BE MILLED)
 6. ACTUATOR FIXTURE: CSA G40.21 350W OR ASTM A572 GR.50
- WELD ELECTRODE: E70XX
- 8. COLUMNS CUT FROM THE SAME HEAT



LIST OF DRAWINGS:

- S.1 GENERAL
 S.2 COLUMN SECTION DETAIL
 - S.2.1 CONNECTION DETAIL 1 S.2.2 CONNECTION DETAIL 2
 - S.2.3 CONNECTION DETAIL 3
- S.2.4 CONNECTION DETAIL 4
 S.3 BEAM SECTION DETAILS
- S.4 ACTUATOR BASEPLATE
- S.5 SPACER
- S.6 COLUMN BASEPLATE
- S.7 ADAPTER PLATE S.8 ACTUATOR FIXTURE

LAST SHEET REPRESNTS THE MATERIAL REQUESTED FOR ALL 12 SPECIMENS



ALBERTA

WF Steel & Crane Alternative DP Details

General

REVIEWED: JUNE 13/2023

PLANNED START OF FABRICATION: AUG 2023

Hana Chaya

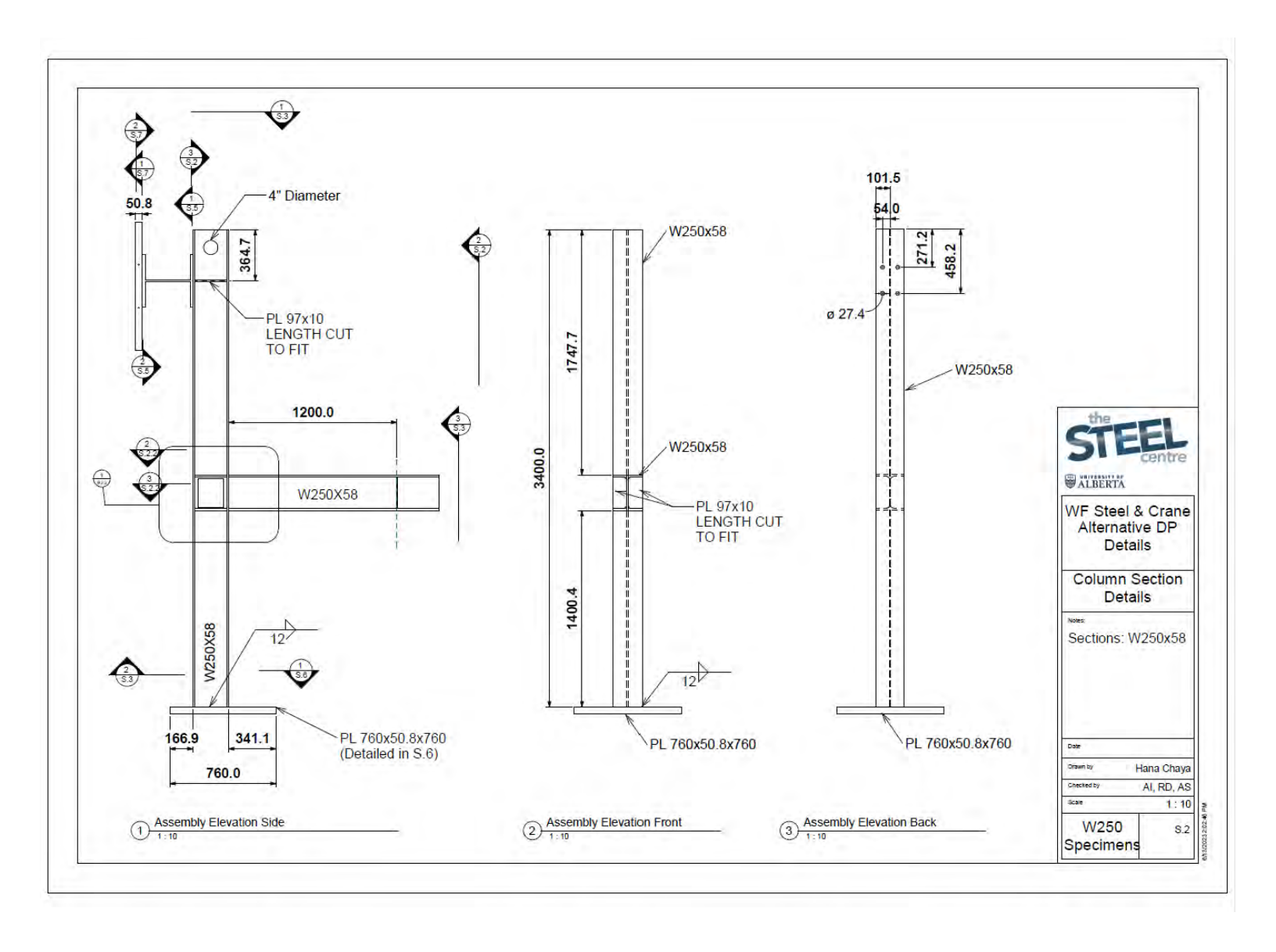
AI, RD, AS

S.1

W250 Specimens

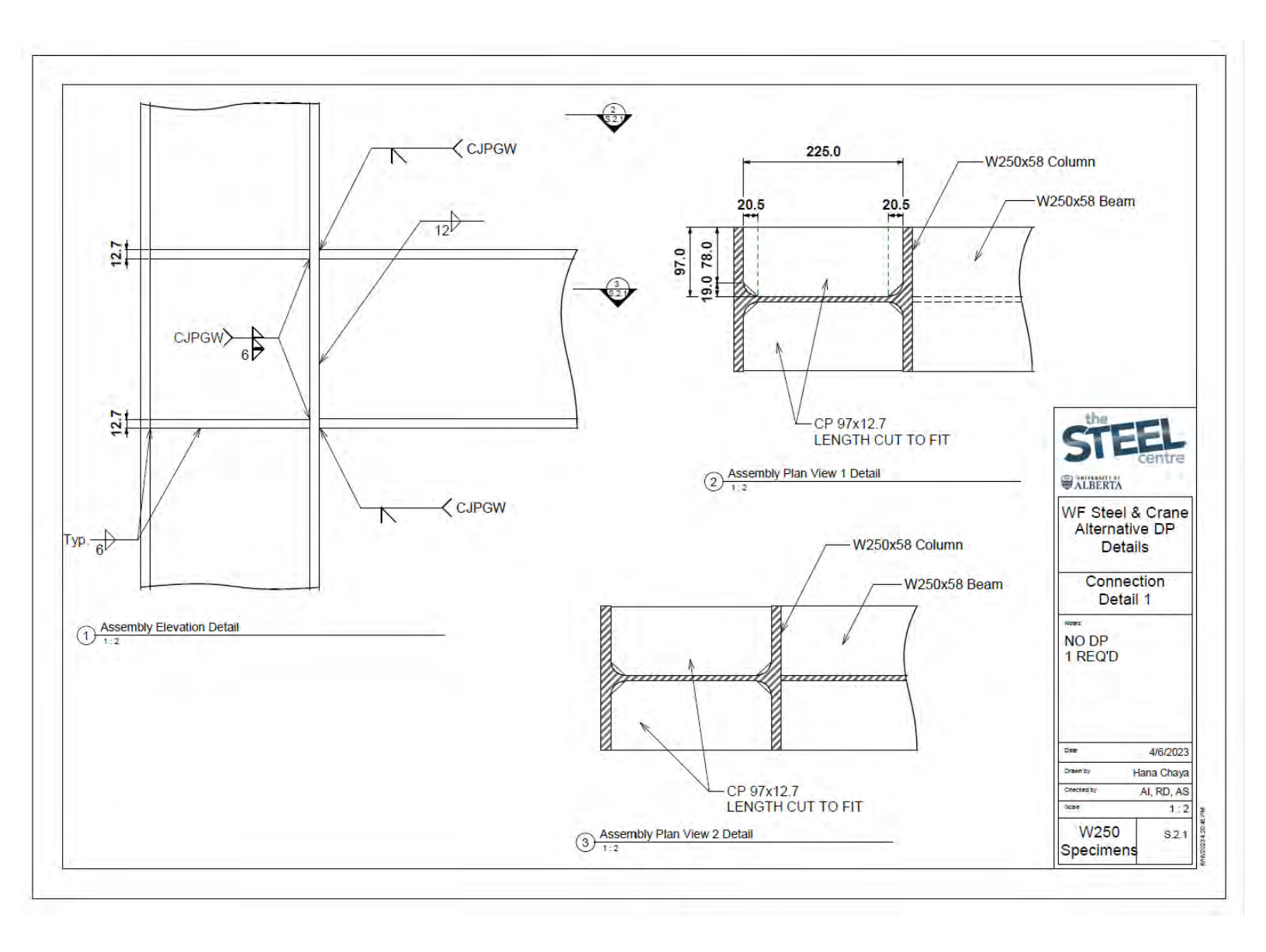






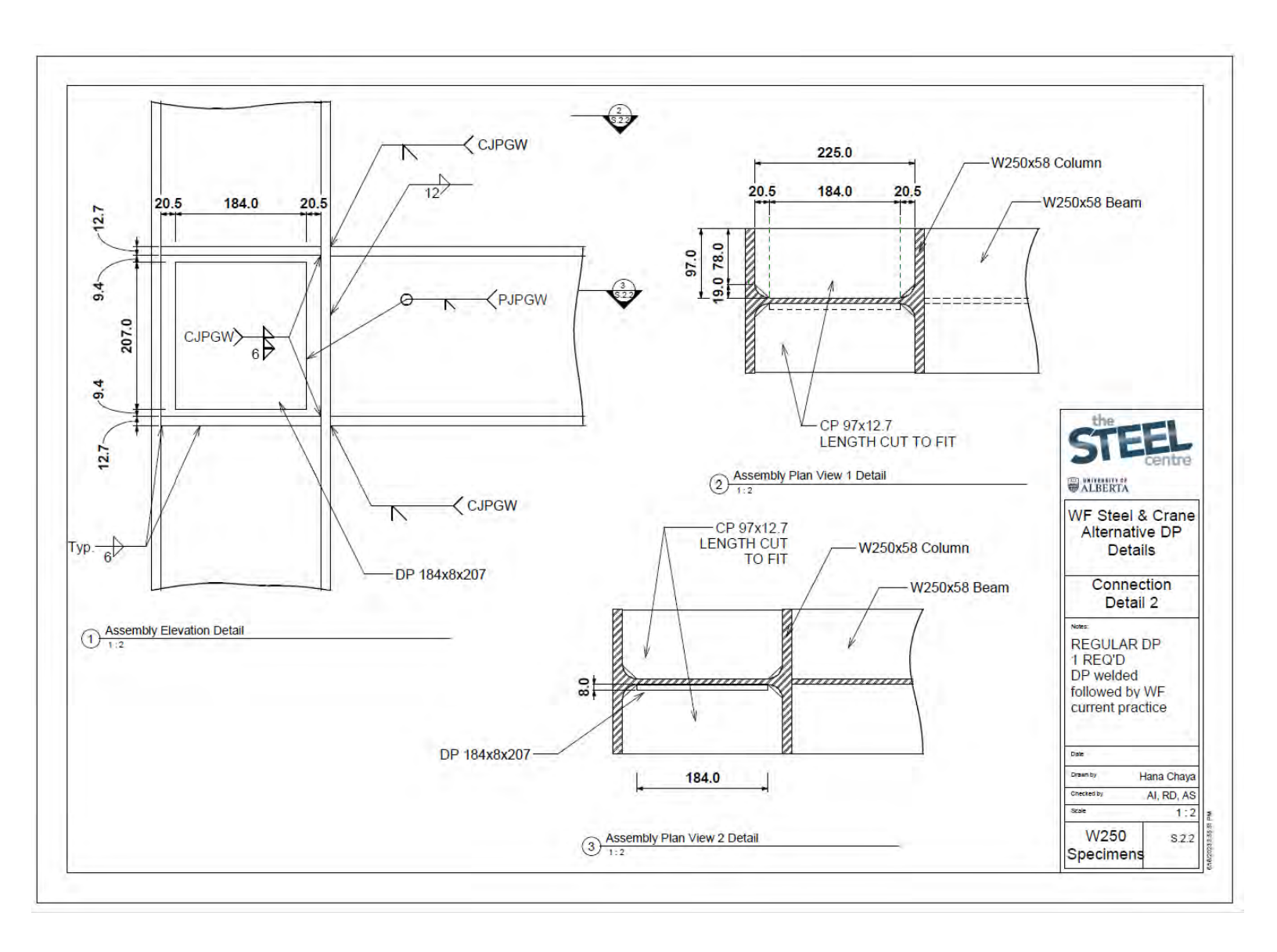






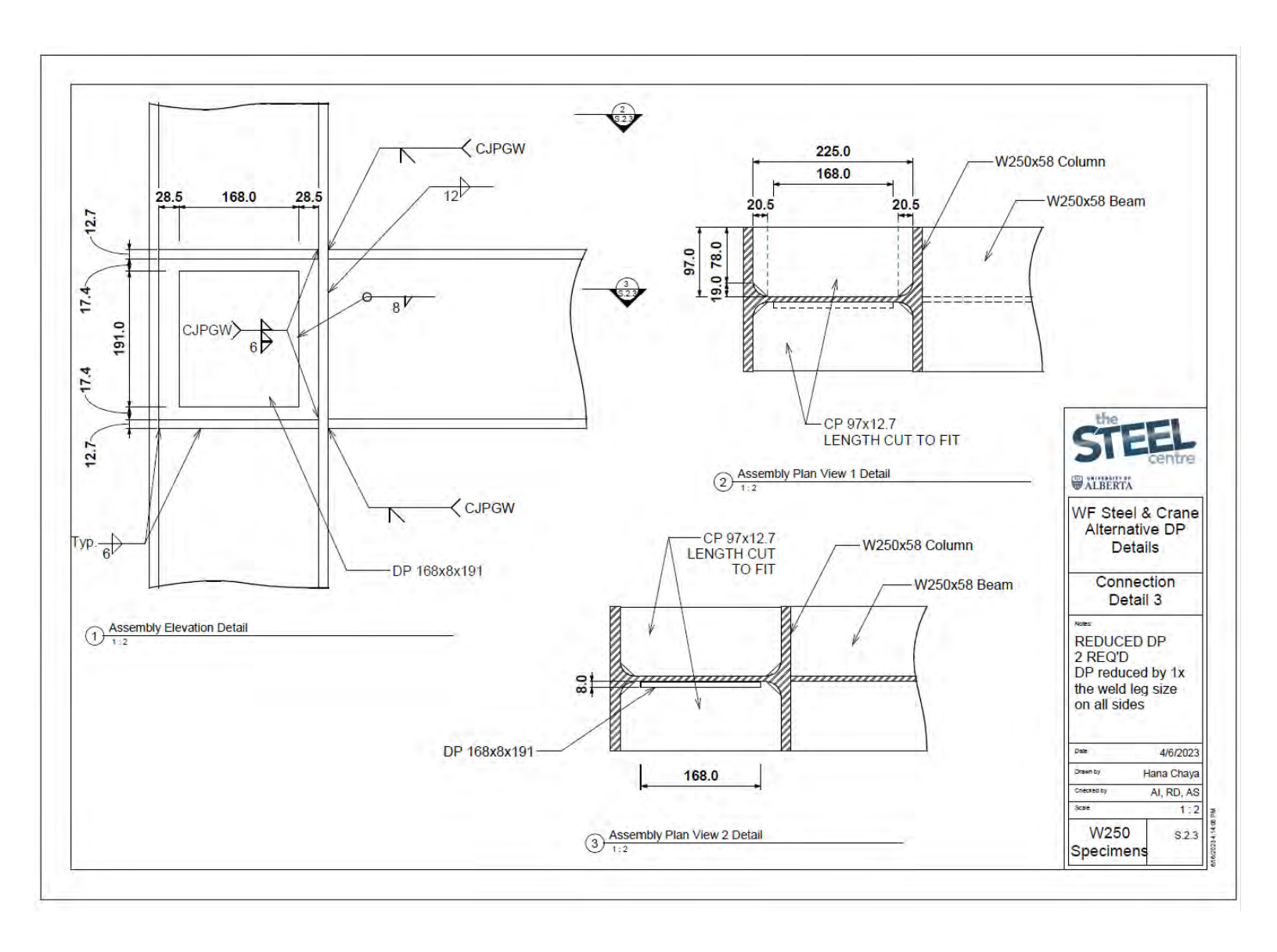






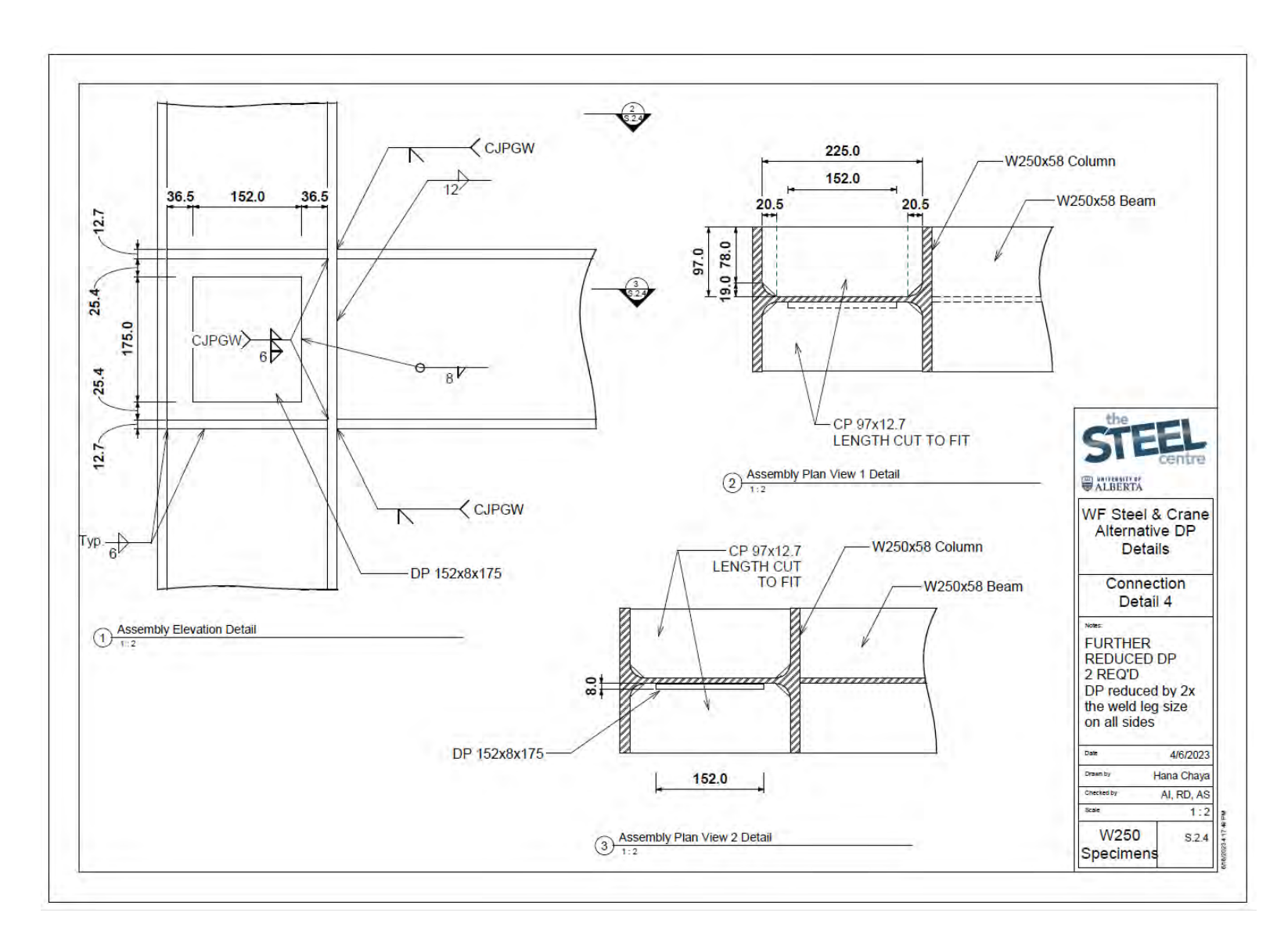






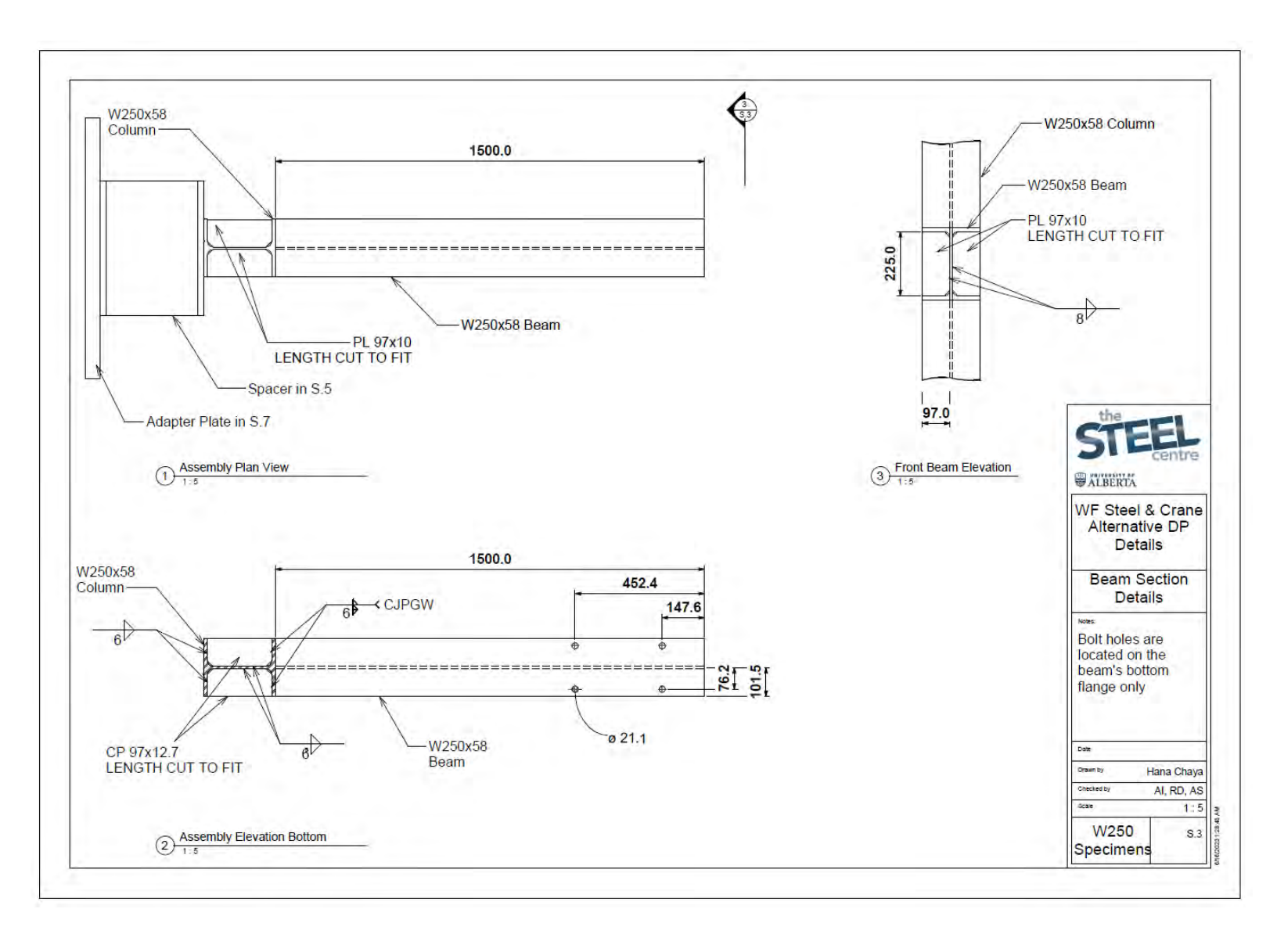






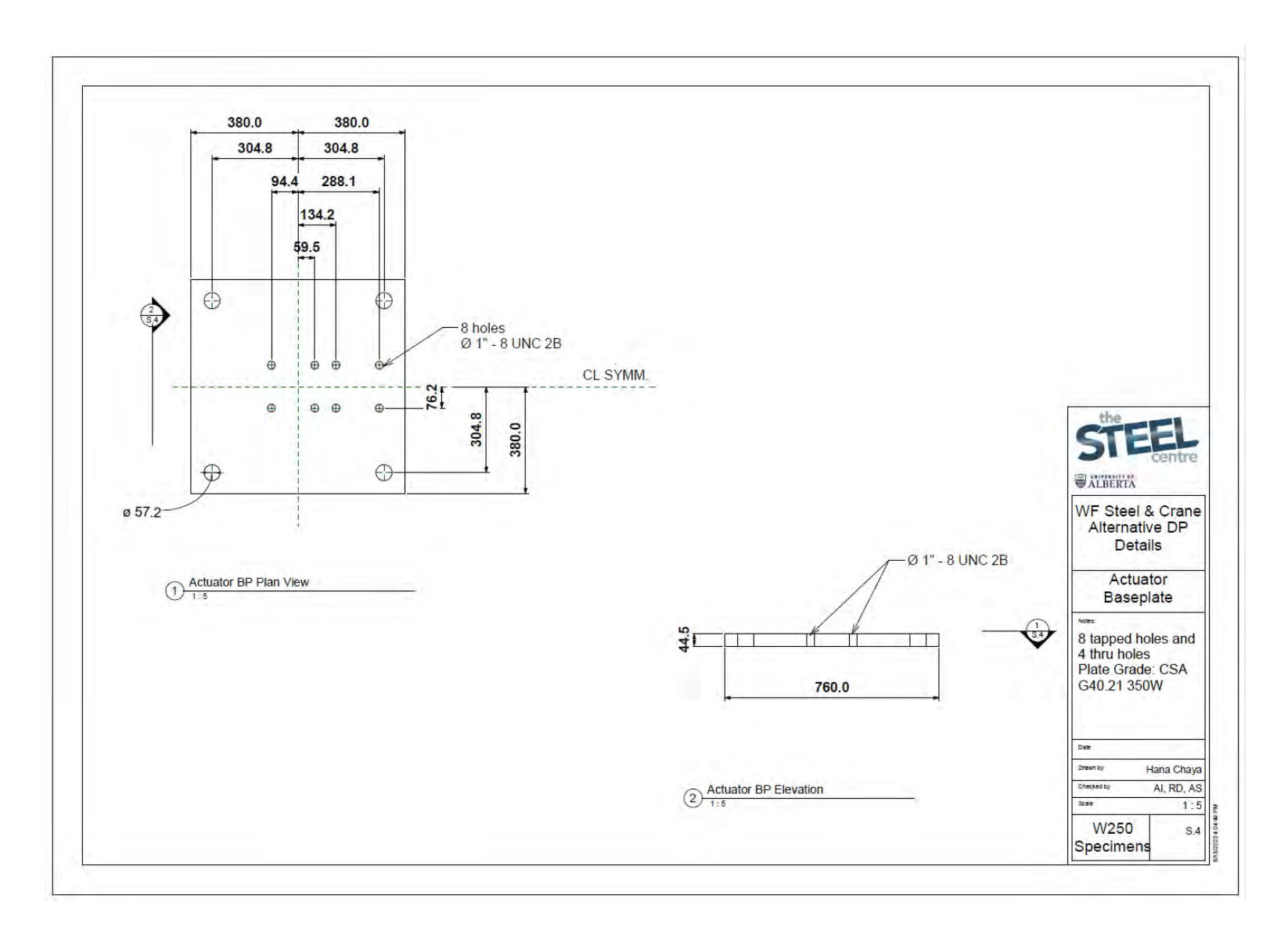






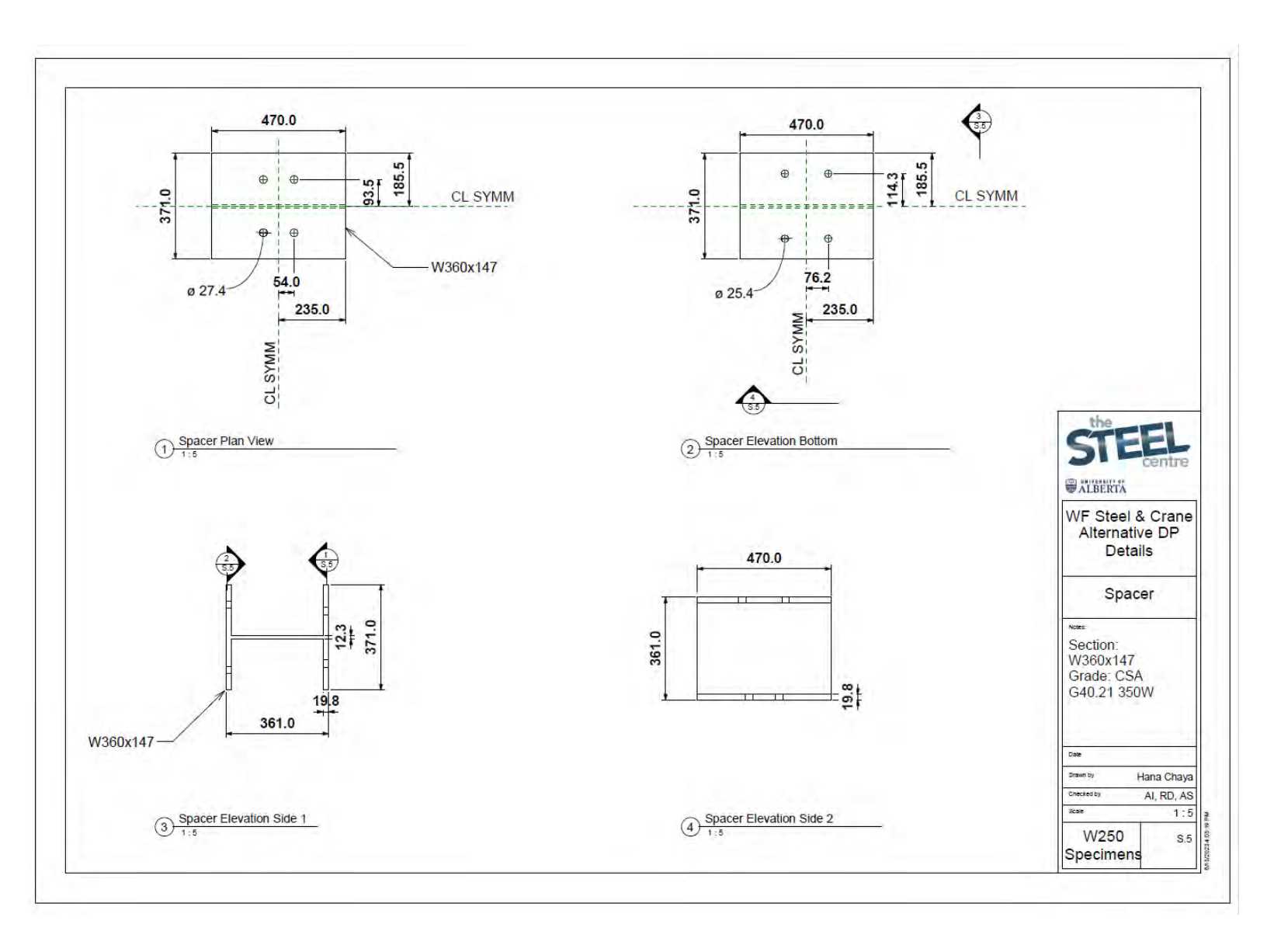




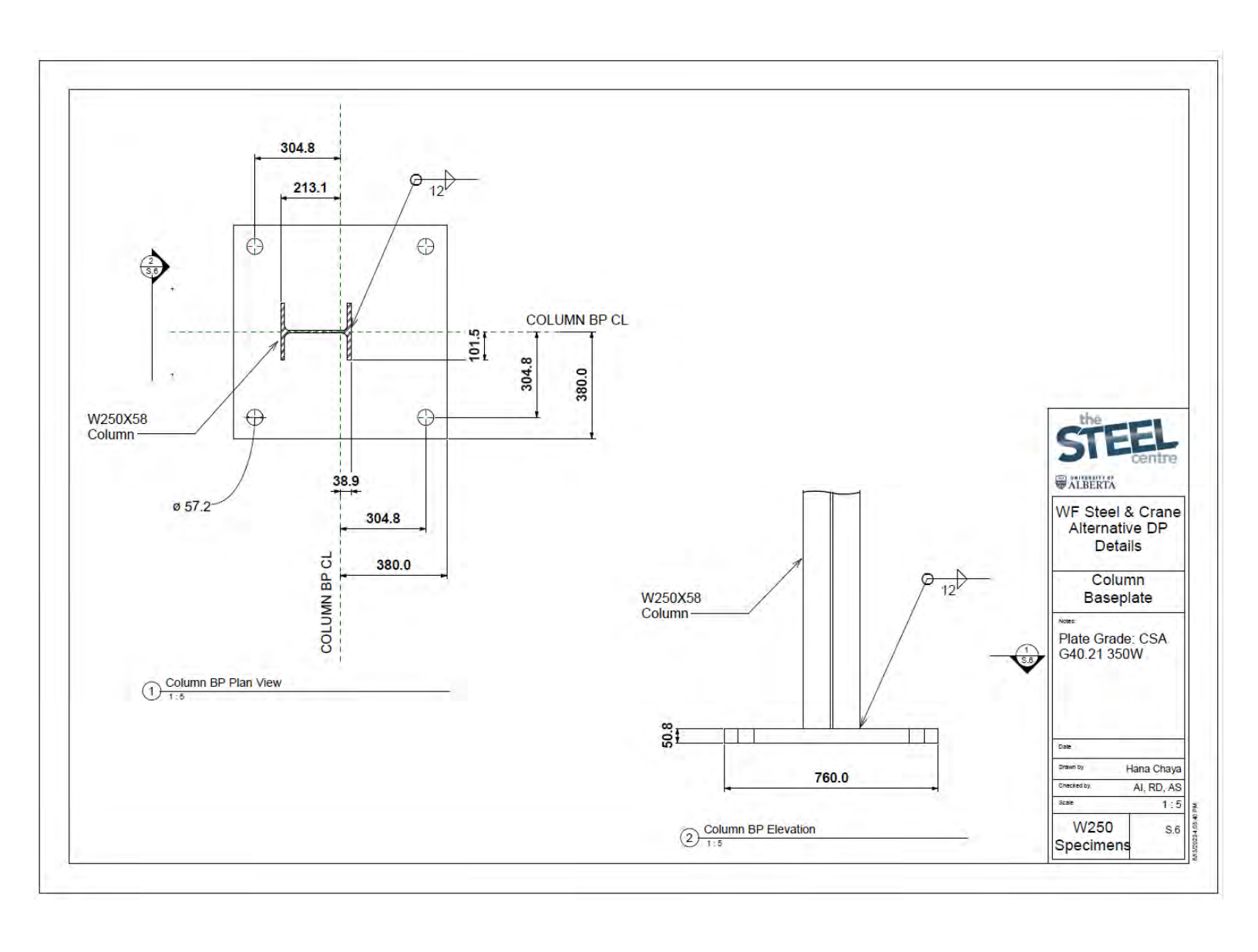






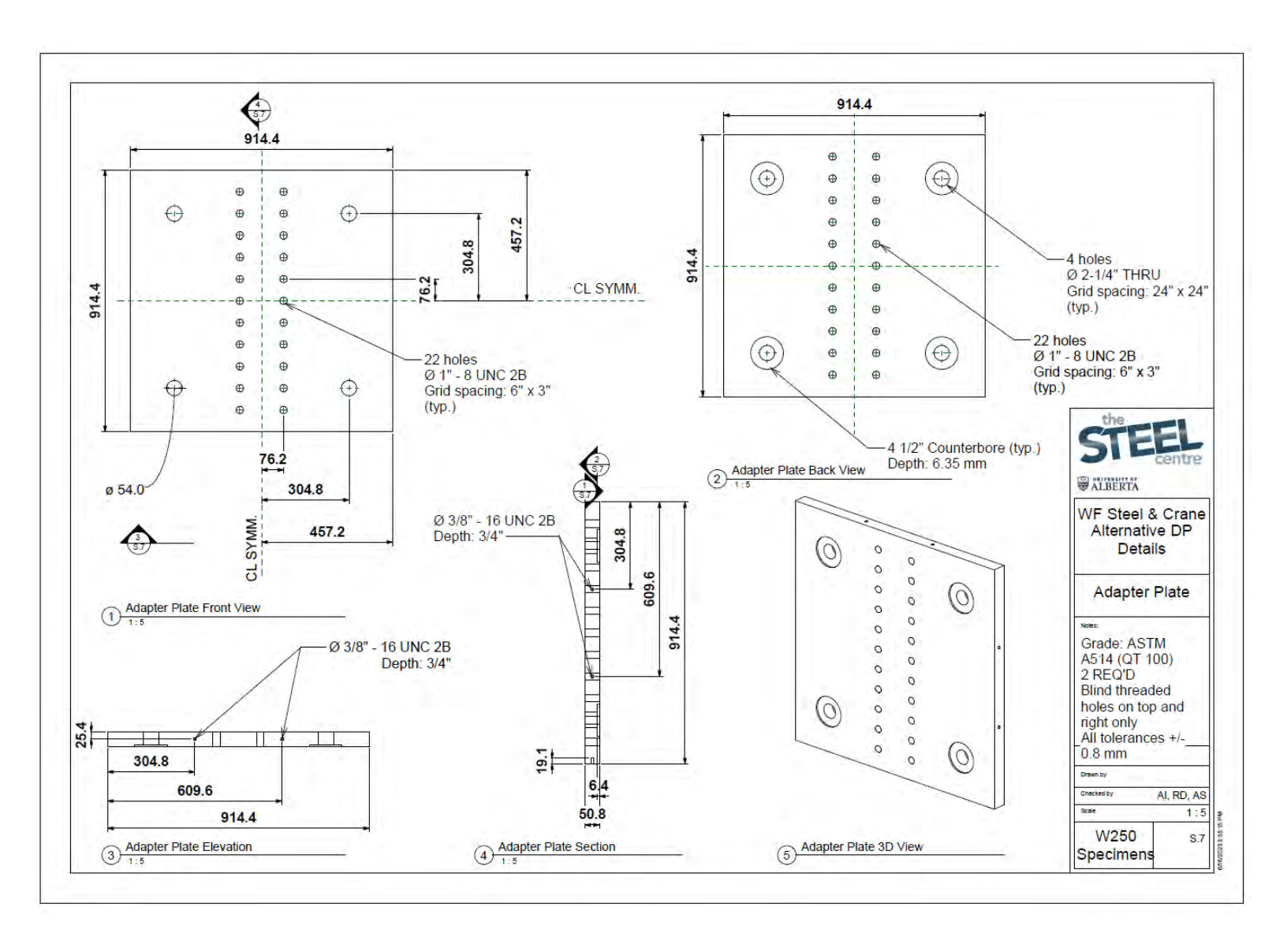






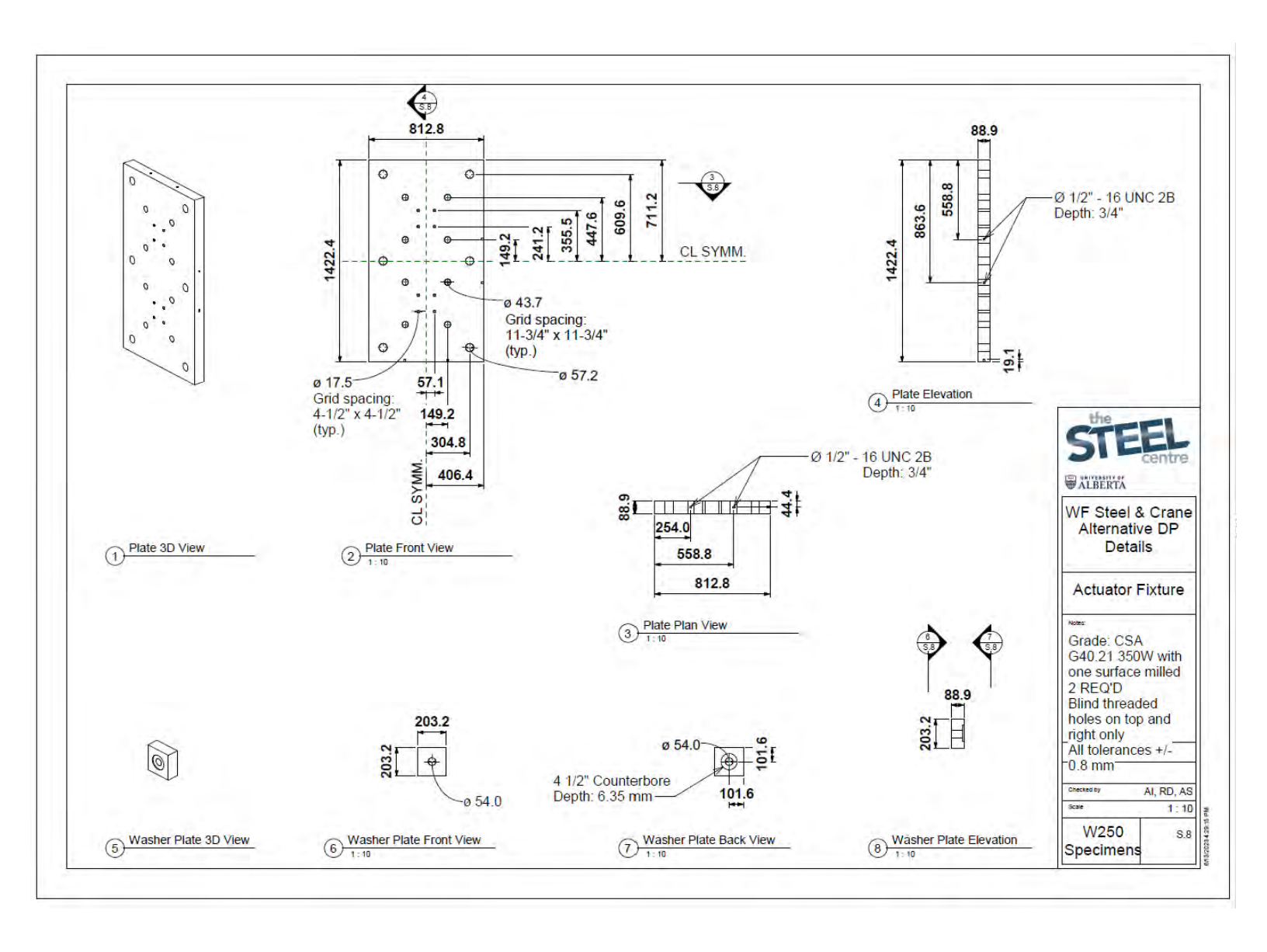
















List of materials requested for 12 specimens

2	0	n	ti	n	u	İ	ty	P	la	te	25
			-1		٠.		CE				

W250 Specimens

Location	Thickness	Thickness (mm)	Grade	Number
Column panel zone	1/2"	12.7	350W	24
Column top	3/8"	10	300W	12
Beam loading	3/8"	10	300W	12

Refer to drawings: Sheet S.2.1

Sheet S.3 (3)

Sheet S.2.2

Sheet S.2.3 Sheet S.2.4

W410 Specimens Sheet S.3 (1)

3/4" 19.05 350W 24 panel zone Column 3/8" 300W 12 top Beam loading 3/8" 10 12 300W

Refer to: Sheet S.2.1 Sheet S.3 (1)

Sheet S.3 (3)

Sheet S.2.2

Sheet S.2.3

Sheet S.2.4

Doubler Plates

W250 Specimens

Regular DP	3/8"	8	300W	1
Reduced DP (2T)	3/8"	8	300W	2
Reduced DP (4T)	3/8"	8	300W	2

W410

Regular DP	15	6	300W	1
Reduced DP (2T)	(7-1	6	300W	2
Reduced DP (4T)	re l	6	300W	2

Specimens

			5

Actuator Baseplate	1 3/4"	44.45	350W	1
Spacer	W36	0x147	350W	1
Column Baseplate	2"	50.8	350W	12
Adapter plate	2 ⁿ	50.8	A514 (QT 100)	2
Actuator Fixture	3 1/2"	88.9	350W	2
Washer Plates	3 1/2"	88.9	350W	12

Sheet S.4 Sheet S.5 Sheet S.6

Sheet S.7

Sheet S.8 (1) Sheet S.8 (5)



GENERAL NOTES:

- ENERAL NOTES:

 1. ALL DIMENSIONS ARE IN MILLIMETERS UNLESS OTHERWISE SPECIFIED

 2. DO NOT SCALE DRAWINGS

 3. CONTINUITY PLATE: CP

- DOUBLER PLATE: DP
- PLATE: PL
- CROSS-SECTIONAL DIMENSIONS OF STANDARD STEEL SHAPES ARE NOMINAL VALUES AND ARE SHOWN FOR REFERENCE ONLY
- 8. FOR ANY CLARIFICATIONS, CONTACT HANA CHAYA AT HCHAYA@UALBERTA.CA OR (780) 729 5490

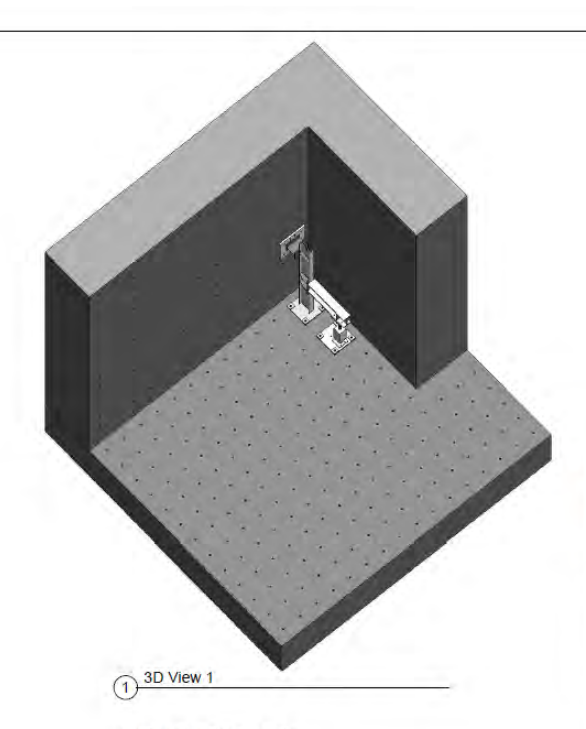
SCOPE:

- SIX SPECIMENS USED TO ANALYZE THE PANEL ZONE BEHAVIOUR IN PIPE RACK MOMENT CONNECTIONS
- 2. FOUR OUT OF SIX DIFFERENT DETAILS ARE OUTLINED IN THESE DRAWINGS
- TWO SETS OF S.2.3 AND S.2.4 ARE REQUIRED
- PJPGW OF DP IN S.2.2 TO BE MANUFACTURED FOLLOWING WF

CURRENT PRACTICE

- MATERIALS OF STEEL: 1. COLUMNS: CSA G40.21 350W OR ASTM
 - 2. BEAMS: CSA G40.21 350W OR ASTM A992
 - CONTINUITY PLATES: CSA G40.21 350W
 - 4. DOUBLER PLATES: CSA G40.21 300W 5. WELD ELECTRODE: E70XX

 - 6. COLUMNS CUT FROM THE SAME HEAT



LIST OF DRAWINGS:

- S.1 GENERAL
- S.2 COLUMN SECTION DETAIL

 - S.2.1 CONNECTION DETAIL 1
 S.2.2 CONNECTION DETAIL 2
 - S.2.3 CONNECTION DETAIL 3 S.2.4 CONNECTION DETAIL 4
- S.3 BEAM SECTION DETAILS
- S.4 COLUMN BASEPLATE



Alternative DP Details

General

REVIEWED: JUNE 13/2023 PLANNED START OF FABRICATION: AUGUST 2023

ate	May 3/2023
rawn by	Hana Chaya
thecked by	AI, RD, AS
icale	
W410 Specimen	S.1





